GEOLOGY AND ORIGINS OF THE MIKE LAKE (SKARN RIDGE)

GOLD-COPPER SKARN DEPOSIT, YUKON TERRITORY, CANADA

By

Stephanie Anne Mrozek

RECOMMENDED:

Advisory Committee Chair

Chair, Department of Geology and Geophysics

APPROVED:

Dean, College of Natural Sciences and Mathematics

Dean of the Graduate School

August 13, 2012

Date

GEOLOGY AND ORIGINS OF THE MIKE LAKE (SKARN RIDGE) GOLD-COPPER SKARN DEPOSIT, YUKON TERRITORY, CANADA

A

THESIS

Presented to the Faculty

of the University of Alaska Fairbanks

in Partial Fulfillment of the Requirements

for the Degree of

MASTER OF SCIENCE

By

Stephanie Anne Mrozek, B.S.

Fairbanks, Alaska

August 2012

Abstract

The Mike Lake (Skarn Ridge) deposit has an elemental suite of Cu-Au-Bi-As-Sn and a mineralogy dominated by scapolite, clinopyroxene, and pyrrhotite, with lesser garnet and Fe-axinite (a Ca-borosilicate). This study is the first published description of the deposit. The deposit was studied with techniques including drill core logging and detailed surface mapping (1:5,000 scale), combined with petrographic examination of polished thin sections, X-ray fluorescence and X-ray diffraction analyses, electron microprobe analysis of major minerals, and $^{40}Ar/^{39}Ar$ dating. Ore mineralization styles include vein-controlled, disseminated, and net-textured replacements of clinopyroxene and calcite by electrum, chalcopyrite, pyrrhotite, and arsenopyrite, with variable native bismuth and bismuth tellurides. A strong Au:Bi correlation ($R^2 = 0.74$) indicates the two elements were transported and deposited together; however a poor Au:Cu correlation ($R^2 = 0.23$) suggests different mineralization events or different modes of Au-Cu transport. The virtual absence of retrograde alteration provides an ideal opportunity to examine metal- and silicate-zoning patterns apparently associated with prograde alteration. Using the $^{40}Ar/^{39}Ar$ dating method, I have determined that the adjacent Mike Lake pluton is younger than the skarn, and hence, genetically unrelated. Through analysis of samples from surface and 72 drill holes, I show systematic zoning in skarn mineralogy and mineral compositions suggesting deposit derivation from an unknown pluton to the southeast at depth.

Table of Contents

List of Figures

Page

List of Tables

Page

Acknowledgements

For the last four years I have devoted a disproportionate majority of my time, energy, and sanity to two men in my life: Mike (Lake) and Rainer (Newberry). I am especially grateful for the patience of my family and friends who have supported me from start to finish, put up with my tendency take on way too many things at once, and tolerated my absence in their lives for so long. I am proud to finally celebrate this accomplishment with you.

I have many people to acknowledge, and I apologize if I forget to mention anyone specifically. Foremost I thank my advisor, Rainer, for taking me on as a student in the first place, and then being completely accessible any day of the year (and any hour of the day) for moral support and technical help, even beyond the scope of this project. Rainer's enthusiasm for teaching and everything geology is contagious and will inspire me throughout the rest of my life and career. My committee members Paul Layer and Ken Severin kept me moving forward in between working hiatuses. I really appreciate their availability and willingness to work with my self-imposed crazy schedule to help me get this done!

To John, for enticing this heat-seeker to take the leap and move to frozen Alaska; it has proven to be a place full of unexpected warmth, rewards, and opportunities that I would not have ventured to discover on my own. Peers, officemates, and friends, especially Dave (aka Dav), Brian, and Bonnie; you each challenged me in different ways

that helped me grow personally, academically and professionally – I thank you for your unique roles in my success. To my students, for teaching me so much! To Ryan, for supporting me in my life, career, and school decisions, and also for inspiration in food, music, travel, scrabble, and life after thesis – you are Great. To the Mike Lake crew, especially Julia for her sunny disposition (you are awesome!), Kat for being a shamelessly devious femme crew leader, Dan for carrying my giant rock up and then down a mountain all for the sake of science, and all of the UBC Engineers; thanks for keeping it interesting, it was a memorable summer. To Archer Cathro & Associates, especially President Bill Wengzynowski, for bringing me on-board the Mike Lake project.

For financial support, I sincerely thank UAF (multiple teaching assistantships), Dynamite Resources (analytical support), the Society of Economic Geologists (Barrick Fellowship and SEG Foundation-Canada research grant), the Association of Environmental and Engineering Geologists (Marliave Award), the Alaska Geological Society (scholarship), and Alaska Women in Mining (scholarship). Kinross Gold Corporation (Fort Knox Mine) provided tuition assistance during the years leading up to my full-time graduate studies. Free Vulcan™ lessons from Maptek™ really helped me put my ideas together into a 3D model that became an integral part of this thesis – I can't begin to put a price on that. A final thanks goes out to Joe Bartolino of Newmont Mining Corporation for giving me the flexibility to finish this project while navigating the terrain of my new job.

1. General Introduction

My involvement in the Mike Lake project began in May of 2008 when I was hired as a seasonal employee of the Vancouver BC based consulting firm, Archer Cathro & Associates (contractor for the mineral claims holder, Dynamite Resources). I worked as a geologist in their remote exploration camp for one field season (June-August, 2008), with the added bonus of being able to collect an unlimited number of samples for my thesis. Unfortunately, by the time I had to return to school at the end of August we had completed just 27 out of 68 planned drill holes. As a result, I was only able to collect samples from the first 27 holes drilled in 2008 plus 3 holes drilled in previous years (2005, 2007). The samples I collected represent approximately 40% of the total drilling on Skarn Ridge, however I was able to obtain 100% of the drill core assay data for analysis.

There were four geologists on the crew (including myself), plus two senior geologists. While my primary duty was to log core from two (and eventually three) drills, I was able to spend a week assisting the senior geology staff with creating a geological map of the study area. Therefore, the geologic map presented in this thesis is a compilation of work by Bill Wengzynowski, Robin Tolbert, and myself.

Due to the scale and pace of the drill program, core-logging responsibilities were also shared. This resulted in varied observations and interpretations that sometimes needed to be reconciled before I could effectively model the data. By reviewing assays, core photos, and core logs I was able to resolve most of the inconsistencies on a case-by-case basis and come up with a more complete picture of the Mike Lake subsurface.

Original geological interpretations were honored whenever possible, and also in cases where my reconciliation efforts produced ambiguous results.

A confidentiality agreement restricts the disclosure of certain data in this report. In most cases gold values are reported as "high/medium/low" instead of as exact values.

No exploration follow-up has taken place at Mike Lake since the summer of 2008. However, Inform Resources (a Vancouver BC based company) recently acquired the property and has planned a reconnaissance program for summer 2012.

2. Introduction to the Mike Lake (Skarn Ridge) Au-Cu Skarn Deposit

2.1. Introduction to Skarns

Skarn deposits are an important class of ore deposit characterized by high grades and low tonnages, variable ore mineralogy (Au, Cu, Fe, W, Zn, Pb, and others), and Ca-Mg silicate gangue (grandite garnet, clinopyroxene, wollastonite, Ca-amphibole, etc.). The term 'skarn' is often used interchangeably to describe both the contact metamorphic rock type and the deposit. Hydrothermal in origin, skarns form where high temperature, element-laden fluids interact with favorable host rocks (usually calcite or dolomitic marble), resulting in an overall addition of exotic elements by way of a process called "metasomatism". Skarn formation is largely controlled by fluid pH changes, however, fluid temperature, volume, duration of the hydrothermal system, and bulk composition (e.g., SiO_2 content), coupled with the reactivity of the host rocks are factors that determine the overall size and endowment of each deposit.

A conceptual model for skarn formation involves three events: (1) contact metamorphism (isochemical mineralogical changes ultimately caused by plutonic heating but most likely catalyzed by hot water); (2) 'prograde' high temperature, hydrothermal-metasomatic formation of anhydrous Ca-Mg silicates; and (3) 'retrograde' breakdown of the prograde assemblage to form hydrous silicates, such as epidote, hornblende, actinolite, and tremolite.

At any point in space or time, 'metamorphism' precedes 'prograde metasomatism', but the two processes occur regionally at the same time. Isochemical contact metamorphism can be viewed as an 'outer front' to prograde metasomatism,

which occurs when element-depleted hot water passes through rocks containing lower-temperature mineral assemblages. In contrast, the entire system must cool down before retrograde metamorphism and metasomatism take place. Thus, 'contact metamorphism' and 'prograde' alteration take place at an earlier time than 'retrograde' alteration in the cooling history of a deposit.

All skarns possess inherent mineralogical and geochemical zoning patterns that are related to the source and pathways of hydrothermal fluids during deposit formation. Zoning patterns are generally complex due to the variety of geological controls that can be present, but an understanding of these patterns (and the fluid-flow directions they indicate) is of paramount importance for exploration and mining success.

Broadly speaking, skarns are a 'system' that can be described as two parts: endoskarn (intrusive protolith) and exoskarn (calcareous sedimentary protolith). For clarity, in this thesis the term 'skarn' will replace 'exoskarn' unless otherwise specified. Both may be mineralized. However, due to the easily replaceable nature of the protolith, 'exoskarn' tends to host the highest ore grades in the skarn system. In both the exoskarn and endoskarn, metasomatic processes produce a silicate mineral zonation that changes with distance from the fluid source. Endoskarn is essentially an alteration zone consisting of Ca-rich metasomatic minerals that have replaced the original mineralogy of an igneous rock; the reaction is driven by hydrothermal fluids and the availability of Ca from the adjacent sedimentary rock. Endoskarn may be garnet rich (proximal), or more typically an assemblage of clinopyroxene + calcic plagioclase (where clinopyroxene has replaced igneous biotite and amphibole, and calcic plagioclase has replaced other

feldspars). For a 'pure' marble protolith, the exoskarn assemblage is typically dominated by garnet (proximal) and clinopyroxene (distal). The maximum extent of the skarn is controlled by the outer limits of metasomatism and is marked by a feature called the 'marble front' (a metasomatic contact between clinopyroxene-dominated skarn and unaltered marble). Fluid continues beyond this point and causes metamorphism of rocks it passes through, but no longer adds components (metasomatism). Much of the 'isochemical metamorphism' that occurs in a skarn is probably due to such 'spent' fluids. Ore distribution in skarns is dependent on the element of interest. In gold skarns, however, the highest gold concentrations are typically found in the most distal portions of the exoskarn, adjacent to the marble front (Meinert, 1989).

Due to their genetic relationship with plutonic-hydrothermal systems, skarns typically occur above and along the margins of plutons (either barren or mineralized). This noted occurrence has contributed to successful exploration strategies throughout a variety of tectonic settings. However, the pluton adjacent to a given skarn is not always the fluid source or the mineralizer; sometimes the pluton-country rock contact simply provides a conduit for rising hydrothermal fluids, and other times there is no relationship between the pluton and adjacent skarn (e.g., faulted contact). These different scenarios demonstrate the need for early, detailed documentation of zoning patterns in every skarn system in order to determine the fluid source, and hence the most likely vectors to ore within each system.

2.2. Location and Access

The Mike Lake Au-Cu skarn deposit (a.k.a. "Skarn Ridge") is a remote exploration property located approximately 85 km ENE of Dawson City, Yukon Territory, Canada. The closest road access is from the Brewery Creek Mine at the end of the North Fork Road, via the Dempster Highway, 8 km from the Dempster-Klondike junction (Figure 2.1). The mine site served as a staging area for supplies to support the 2008 exploration program. At the time of this study (2008) the property consisted of 353 contiguous mineral claims that could only be accessed by helicopter. Helicopter time from the Brewery Creek mine is approximately 20 minutes (25 km) over the rugged Ogilvie Mountains. The Mike Lake property comprises a variety of intrusion-related deposit types associated with mid- to Late-Cretaceous plutons. The Skarn Ridge deposit, located 1.5 km west-northwest of the exploration camp (centered at 64°15' N, 137°54' W) is the focus of this study.

2.3. Physiography, Vegetation, and Climate

The property is situated in the Ogilvie Mountains, an east-west trending mountain range of sharp ridges typical of alpine glaciated terrain. North-facing slopes are steep to vertical, while south facing slopes are more moderate (~30° or less), often covered by talus and flanked by talus aprons. The Mike Lake property is almost entirely above the tree line; sparse, permafrost-tolerant vegetation consists of sub-arctic grasses, sedges, and lichen on slopes, with patchy buckbrush and black spruce stands on the valley floor.

Local elevations range from 1,070 to 2,100 m. The sub-arctic latitude results in a short summer (June-August) with long sunny days, generally light rain showers and

temperatures as high as 20°C/68°F. However, mountain weather can be unpredictable any time of year, producing summer storms that can leave behind several centimeters of snow, as I experienced on July 1, 2008.

2.4. Geological Framework

The Mike Lake property lies within the so-called Tintina Gold Belt (TGB); the informal name given to a broad zone of mid- and late-Cretaceous intrusion-related gold deposits that occur across the central portions of Alaska and the Yukon Territory (Figure 2.2). A variety of gold showings and deposit types exist within this belt, including skarns, replacements, mantos, veins, porphyry-style stockworks, polymetallic lodes, and placers. This metallogenic diversity has contributed to the region's global notoriety for gold and mineral exploration potential. Mining in the TGB has been conducted since the late 1800's, beginning with the gold rushes of the Klondike and interior Alaska.

Broadly defined, the TGB is an arc-shaped metallogenic province that spans over 2,000 km from west-central Alaska to northern British Columbia (Till et al., 2007). In Alaska, it is roughly bounded – but not entirely – by two steeply dipping, active right-lateral strike-slip faults: the Tintina Fault in the north, and the Denali Fault approximately 250 km to the south. On the Yukon side of the TGB, the northern extent is expanded to include several plutonic suites that occur roughly within the Selwyn Basin (a late Precambrian-Devonian sedimentary basin that occupies the central Yukon; it is truncated by the Tintina fault to the southwest). Classification schemes for plutonic suites in the TGB differ in Alaska and the Yukon, and several classification schemes have been proposed (Anderson, 1985; Mortensen et al., 1995; Mortensen et al., 2000; Hart et al.,

2004). For simplicity and consistency with other Yukon publications, the scheme presented here is modified from Hart et al., 2004. Each suite is defined by distinguishing characteristics that are based largely on age and location, as compositions alone are not a reliable differentiator (Figure 2.3).

Previous workers have assigned the undated Mike Lake pluton (also called the Rubble Lake pluton) to the Tombstone Plutonic Suite on the basis of geographic location (Bordin et al., 1998; Hart, 2007; Wengzynowski, 2009). The Tombstone Plutonic Suite is described as the youngest suite in the TGB, comprising an approximately 800 km long, 50 km wide belt of mid-Cretaceous quartz-alkalic plutons. This suite is offset by approximately 400 km of dextral displacement along the Tintina Fault, resulting in an eastern segment in the west-central Yukon and a western segment in central Alaska (Figure 2.2). The Alaskan segment contains the 16.5 Moz Livengood gold deposit.

Regional geologic mapping (1:250,000 scale) completed by the Geological Survey of Canada (Green and Roddick, 1971; Green, 1972; Templeman-Kluit, 1980), places Mike Lake in an upper plate block of the Selwyn Basin, surrounded by a complex fold-and-thrust belt in the central Yukon Territory. North-directed thrusting of Precambrian and Paleozoic rocks resulted in low-grade metamorphic fabrics and mineralogies on a regional to local scale (Figure 2.4). In the immediate Skarn Ridge area, Bordin et al. (1998) document tight E-W trending fold axes (Figure 2.5), presumably associated with the thrust event(s).

Bordin et al. (1998) also mapped a gabbroic unit near the southwest base of Skarn Ridge. Mafic intrusions have been identified at several sites within 50 km of Mike Lake,

including Antimony Mountain, Keno Hill, and the Marn prospect (Gordey and Makepeace, 1999). Several authors classify this unit as "Galena Suite", and assign a *likely* age of Triassic (Don Murphy, Yukon Geological Survey, writ. comm., 2010). Mortensen and Thompson (1990) dated a mafic sill from the Tombstone area of the Ogilvie Mountains using U-Pb zircon-baddeleyite and found an age of 232 ± 1.5 Ma (latest Middle Triassic). Extension-related mafic sills and dikes occur sporadically throughout the central Yukon with an uncertain timing relative to thrusting. Clusters of post-thrusting Cretaceous intrusions caused contact metamorphism; coalescing halos produced regional-scale contact effects. Sixty kilometers south of Mike Lake, the tectonically active Tintina fault juxtaposes Selwyn Basin sedimentary rocks against regionally metamorphosed pelitic rocks of the Yukon-Tanana terrane.

The following stratigraphic summary (this and following paragraph) has been modified after the original work of Green and Roddick (1971) and Green (1972), unless otherwise referenced. The Selwyn Basin contains marine sedimentary rocks that range from Late Proterozoic to early Mesozoic. Regionally, several stratigraphic units are continuous throughout the Selwyn Basin, including (from oldest to youngest) the Late Proterozoic Hyland Group, the Lower Cambrian Gull Lake Formation, the Upper Cambrian-Middle Ordovician Rabbitkettle Formation, the Ordovician to Lower Devonian Road River Group, and the Lower Devonian to Mississippian Earn Group.

Rocks mapped as Rabbitkettle Formation are the dominant rock type on Skarn Ridge (Figure 2.5). A distinctive stratigraphic unit within the Selwyn Basin, the Rabbitkettle Formation has a characteristic composition, weathering appearance, and

stratigraphic position that distinguish it from the dominantly argillaceous sediments above and below it. At its type locality, the formation consists of limestone, silty limestone, calcareous siltstone, and siltstone (Dénise Hèon, Yukon Geological Survey, writ. comm., 2012). Elsewhere in the basin, other facies include thinly laminated argillaceous limestone, sandy dolostone, quartz sandstone, conglomerate, and green volcanic ash. Bedding characteristics vary from massive to recessive, platy/thin-bedded to wavy-bedded, and sometimes nodular. Typical weathering colors are light grey to tan, with occasional orange to brick red. Across the central Yukon, the Rabbitkettle Formation is observed to unconformably overlie the gently folded shales and siltstones of the Cambrian Narchilla, Gull Lake, and Vampire formations (Dénise Hèon, Yukon Geological Survey, writ. comm., 2012). This unconformity is referred to as the sub-Late Cambrian unconformity (or sub-Rabbitkettle unconformity), and is an important stratigraphic marker throughout the Selwyn Basin.

Locally, carbonate rocks of the Selwyn Basin can be an ideal host for skarn and replacement-style mineralization, while simultaneous metamorphism and alteration of pelitic rocks resulted in weak to non-mineralized hornfelses. Granitic plutons of the Selwyn Basin are often rimmed by contact metamorphic aureoles, and numerous dikes and sills (ranging from Triassic to Cretaceous) cut across the host rocks. In a regional context, these granitic intrusions are contemporaneous with other mid-Cretaceous intrusion-related gold deposits of the TGB, including Fort Knox, Pogo, and Dublin Gulch (Newberry, 2000).

2.5. Previous Work

The Mike Lake property has changed ownership at least a dozen times since the first claims were staked in the early 1960's. Early drilling (3 diamond drill holes in 1975) in the Mike Lake and Anvil Lake intrusions focused on high-grade stockwork veins and disseminated gold. Sampling was limited to these large Cretaceous stocks and associated dikes. Several prospective areas were identified, including a quartz-arsenopyrite vein anomaly in the Mike Lake pluton that became known as the Spartan Vein. From 1975 to 1998 at least five different exploration companies worked the property by collecting geochemical samples and digging shallow hand trenches. Additional claims were staked, but no new targets were identified.

In 1997, Homestake Canada took over the property and compiled results from over 1,200 rock, soil, and silt samples collected in the early 1990's. Several new targets were identified (Bordin et al., 1998), and their exploration strategy for the 1998 field season focused on eight of these targets, including Skarn Ridge. Homestake carried out prospecting, mapping, trenching (Figure 2.6), and geophysical surveys with the goal of identifying "…a large, bulk tonnage contact skarn or high grade, metasomatized replacement zones within reactive calcareous grit or limestone conglomerate strata" (Bordin et al., 1998). Their work during the 1998 field season resulted in the discovery of a metasomatized body of undetermined dimensions from which rock and chip samples returned values of up to 0.109 ounces per ton (3.4 grams per tonne) on Skarn Ridge. In 1999 Homestake was taken over by Barrick Gold Corporation and no follow up work was done until 2004 when Dynamite Resources acquired the property.

In 2004, Dynamite Resources conducted additional prospecting, mapping, and soil geochemical surveys. Diamond drilling began in 2005 with two drill holes near the southeast base of Skarn Ridge, SK05-01 and SK05-02. Drilling was focused elsewhere on the property in 2006, but in 2007 a single hole, SK07-01, was drilled on upper Skarn Ridge in line with the previously drilled SK05-01 and SK05-02 (Figure 2.6). Dynamite Resources announced this as their "Discovery Hole" for the Skarn Ridge target: an 89.3 meter section of near-surface skarn grading 0.61% Cu, 1.38 g/t Au, and 13.6 g/t Ag. As a result, the focus of the 2008 drill program became a 1500 x 700 meter area of anomalously high gold and copper in soil mostly east of the 2007 Discovery Hole. Sixty-eight holes were drilled from May to October 2008, resulting in 10,004 meters of drill core for the 2008 season and an overall total of 72 drill holes on Skarn Ridge.

In this study, I describe the geology of Skarn Ridge in detail using all of the drill hole data from the 2008 exploration program (and earlier). I document silicate zoning and its relationship to mineralization. By combining $^{40}Ar/^{39}Ar$ geochronology ages with geochemical data and cross-cutting relationships, I present a model for the timing and formation of the Skarn Ridge deposit, and propose a deep source for the skarn-forming fluids that is unrelated to the Mike Lake pluton as well as the numerous dikes and sills that are exposed on Skarn Ridge.

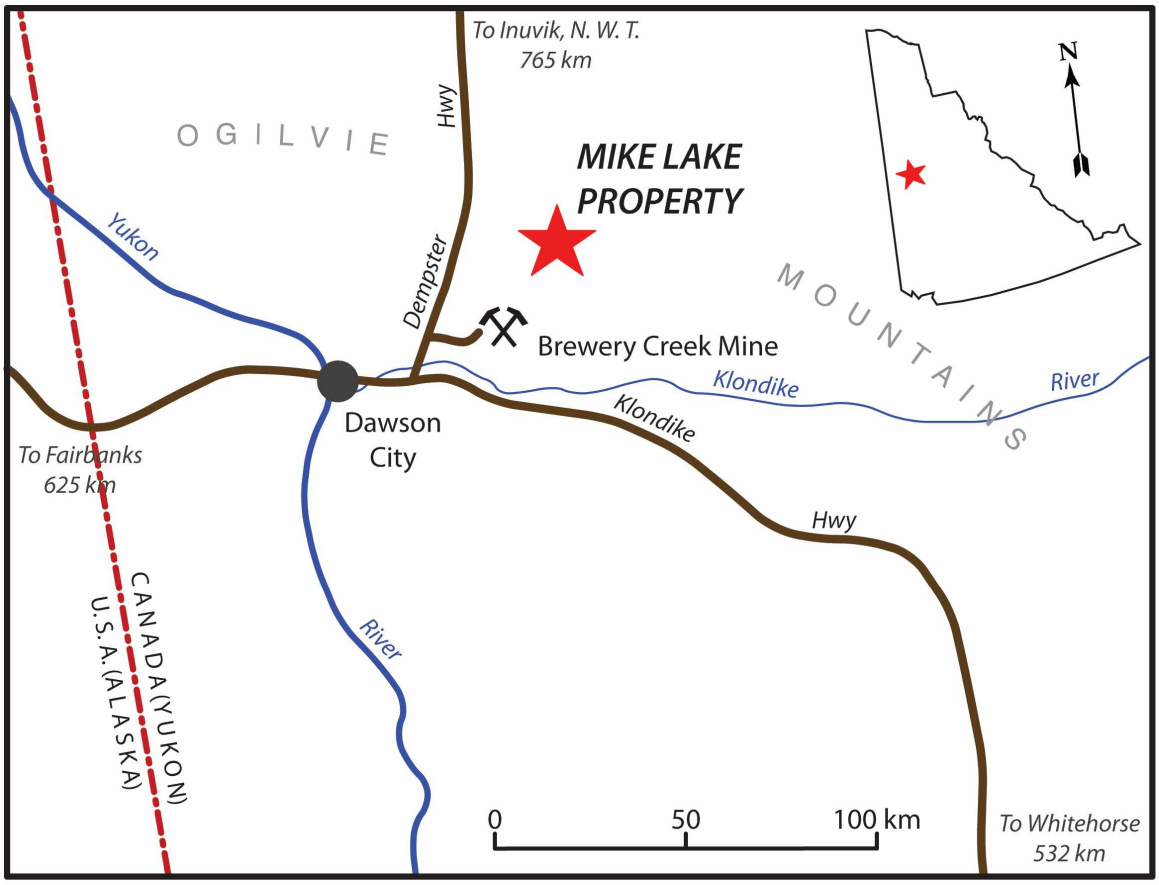

Figure 2.1 Location of and access to the Mike Lake property.

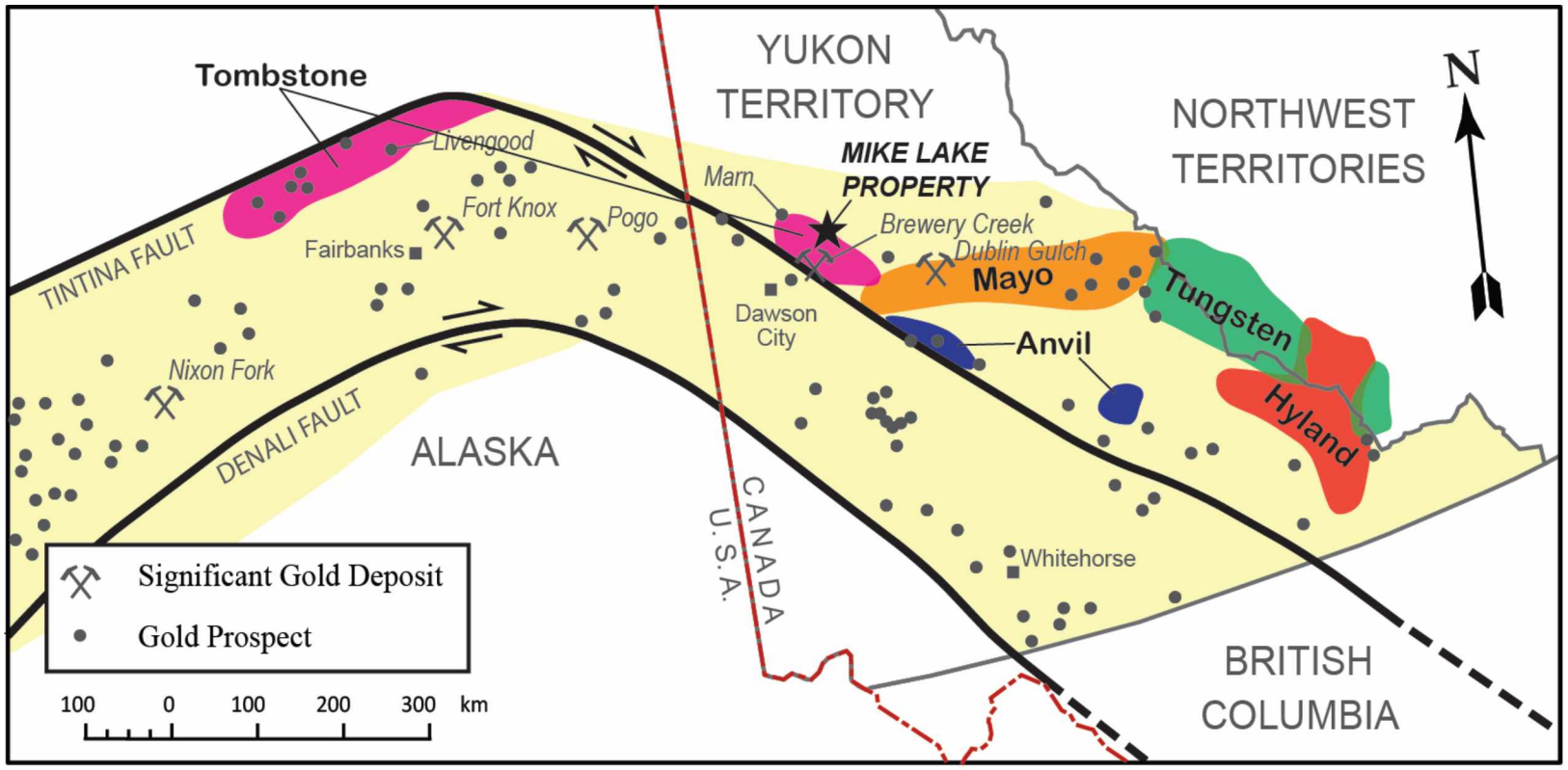

Figure 2.2. Plutonic suites of the "Tintina Gold Belt".
Note that the Tombstone Suite is present in both Alaska and the Yukon Territory. The extent and location of each plutonic suite is based on its classification by the Yukon Geological Survey, (2012).

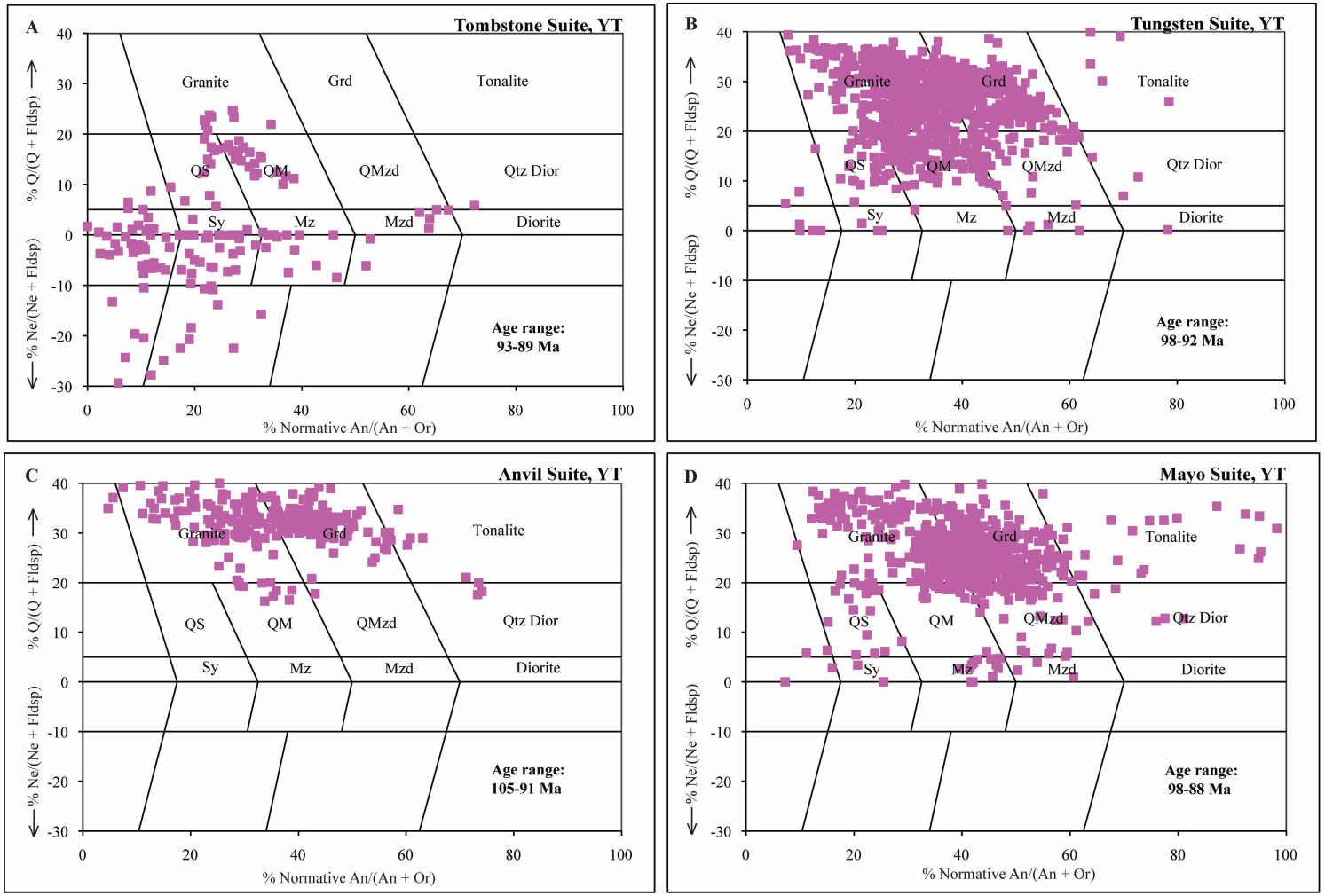

Figure 2.3. Age and normative mineralogy for selected Selwyn Basin plutonic suites. Data from Yukon Geological Survey, (2012).

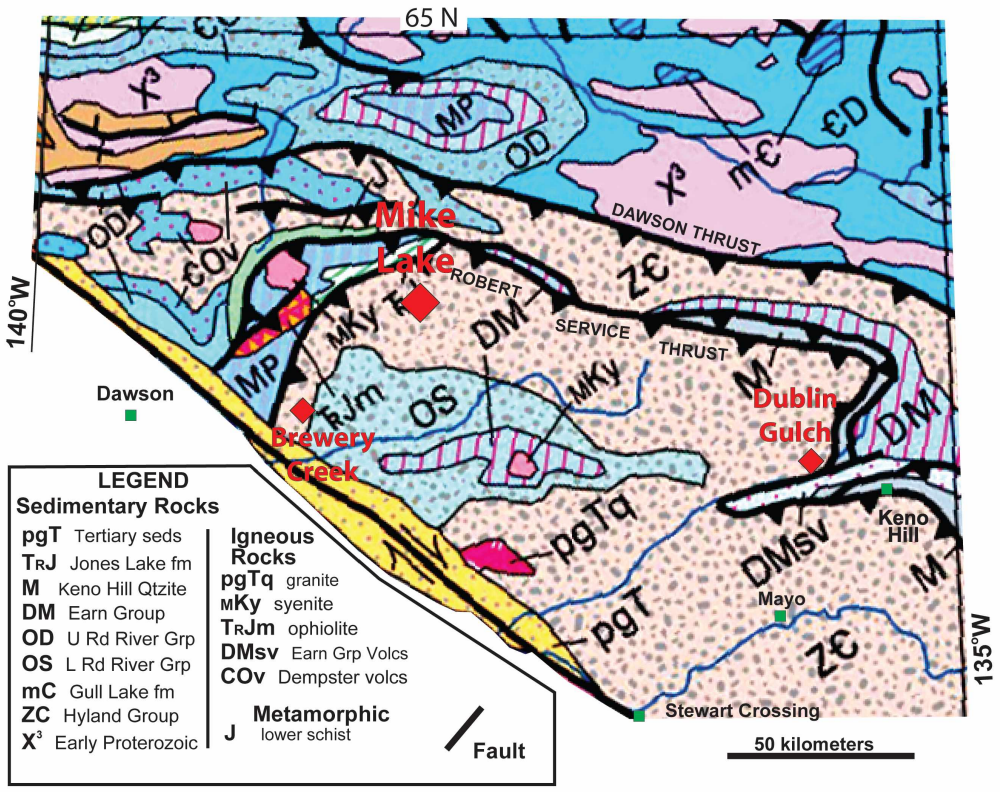

Figure 2.4. Simplified geologic map of the west-central Yukon, north of the Tintina Fault. Modified after Reed et al., (2005).

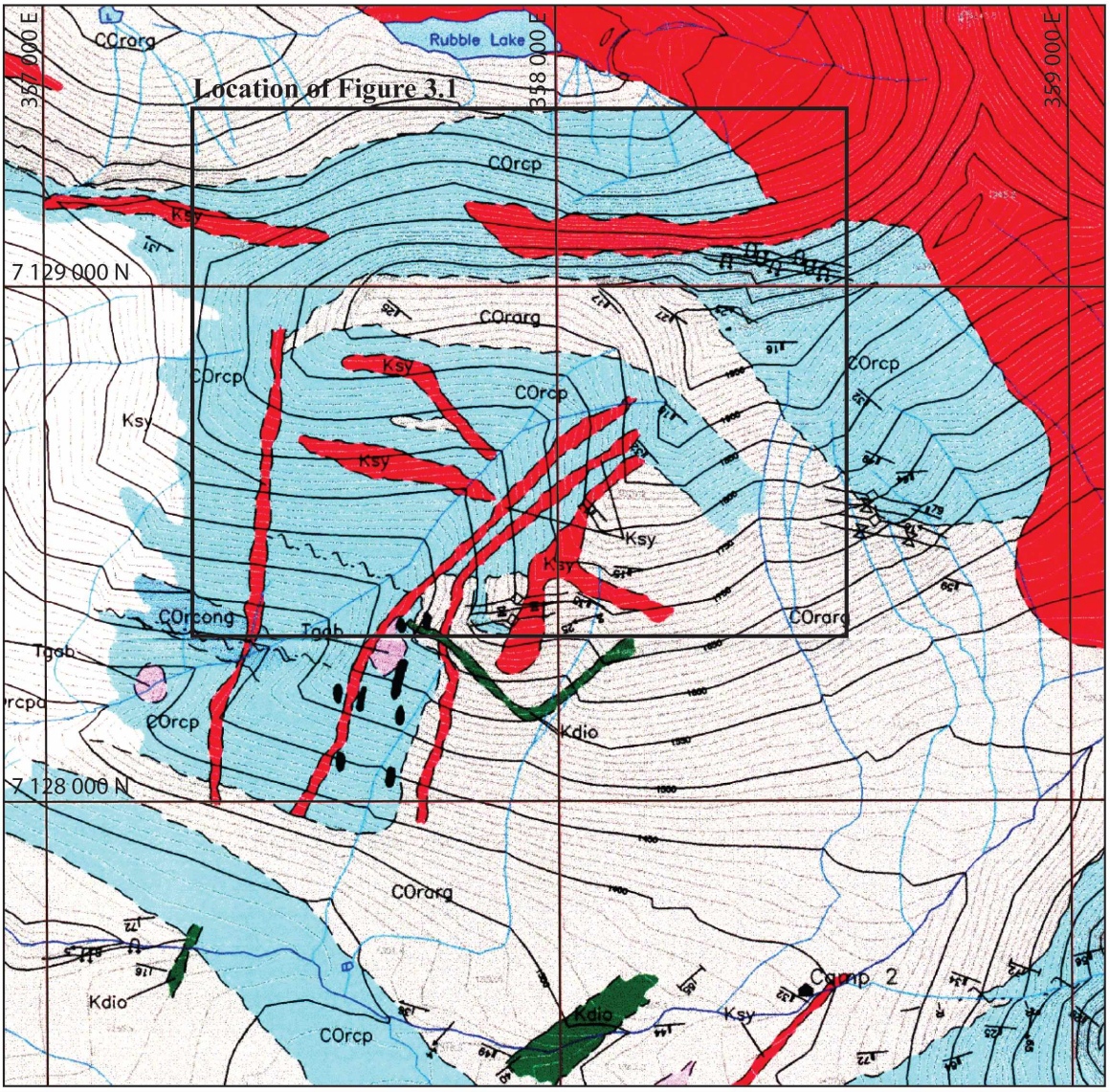

LEGEND

Late Cretaceous

Kdio Biotite-hornblende diorite

Ksy Syenite

Triassic

Tgab Pyroxene-hornblende gabbro

Cambro-Ordovician (Rabbitkettle Formation)

COrcp Calcareous phyllite

COrcong Calcareous phyllite with limestone conglomerate

COrarg Argillite

Figure 2.5. Pre-2008 Skarn Ridge area geology.
Modified after Bordin et al., (1998).

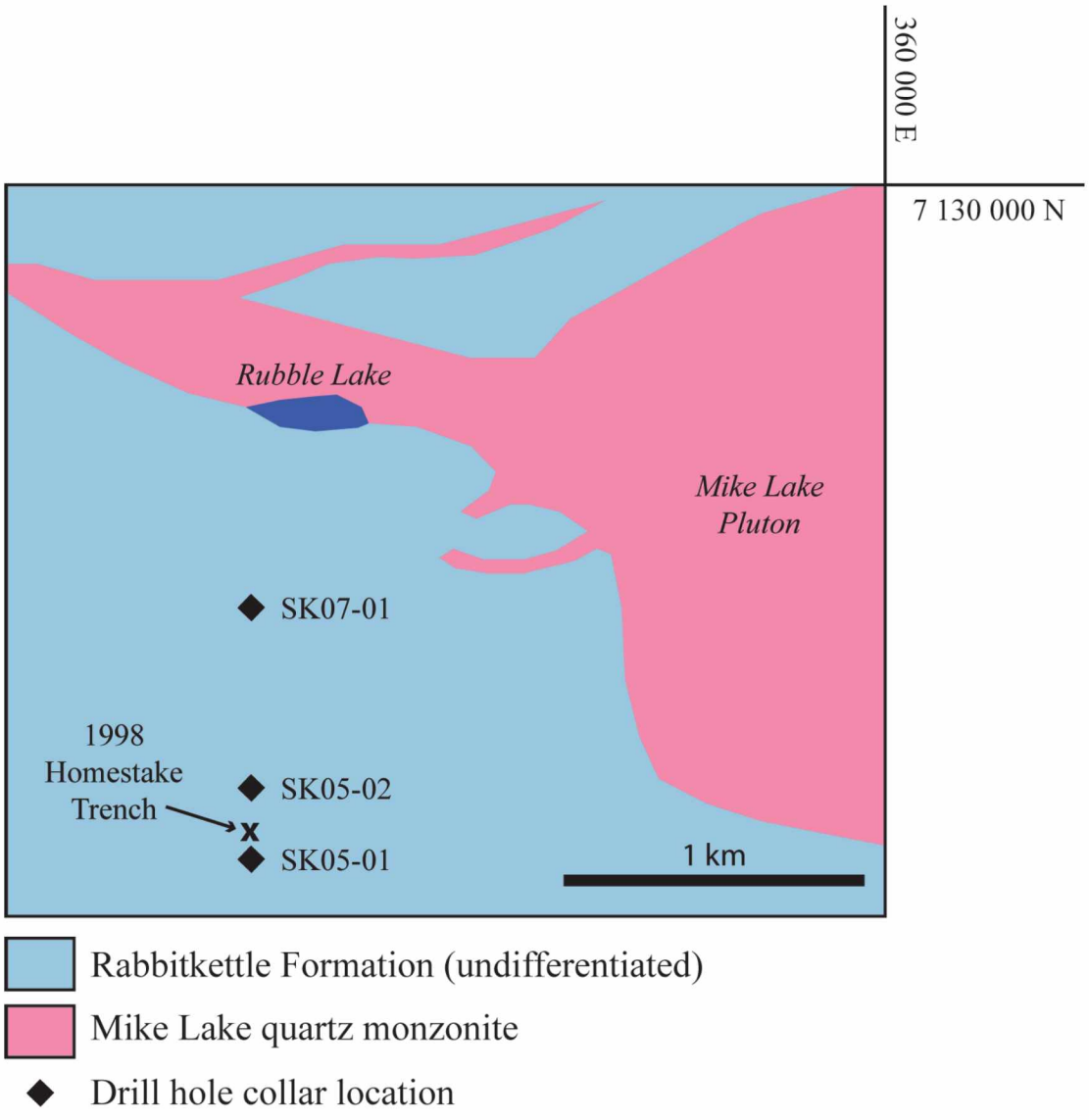

Figure 2.6. Sketch map showing pre-2008 drilling and trenching on Skarn Ridge.

2.6. References

Anderson, R.G., 1985, An overview of some Mesozoic and Tertiary plutonic suites and their associated mineralization in the northern Canadian Cordillera *in* Taylor, R.P., and Strong, D.F., eds., Recent Advances in the Geology of Granite-Related Mineral Deposits: Canadian Institute of Mining and Metallurgy Special Volume 39, p. 96-113.

Bordin, D., Papageorge, M., and Kuran, D.L., 1998, Geological, Geochemical, and Geophysical Program on the Mike Lake Property: private report for Homestake Canada Inc.

Gordey, S.P., and Makepeace, A.J., 1999, Yukon bedrock geology in Yukon digital geology, S.P. Gordey and A.J. Makepeace (comps.) *in* Geological Survey of Canada Open File D3826 and Exploration and Geological Services Division: Yukon, Indian, and Northern Affairs Canada, Open File 1999-1(D).

Green, L.H., 1972, Geology of the Nash Creek, Larsen Creek, and Dawson map areas, Yukon Territory: Geological Survey of Canada, Memoir 364.

Green L.H., and Roddick, J.A., 1971, Geology of Larsen Creek, Yukon Territory: Geological Survey of Canada, Map 1283A, scale 1:250,000.

Hart, C.J.R., 2007, Reduced Intrusion-Related Gold Systems *in* Goodfellow, W.D., ed, Mineral Deposits of Canada: A Synthesis of Major Deposit Types, District Metallogeny, the Evolution of Geological Provinces, and Exploration Methods: Geological Association of Canada, Mineral Deposits Division, Special Publication No. 5, p. 95-112.

Hart, C.J.R., Goldfarb, R.J., Lewis, L.L., and Mair, J.L., 2004, The Northern Cordilleran mid-Cretaceous Plutonic Province: Ilmenite/magnetite-series granitoids and intrusion-related mineralization, Resource Geology, v. 54, p. 253-280.

Meinert, L.D., 1989, Gold Skarn Deposits – Geology and exploration criteria *in* Groves, D., Keays, R., and Ramsay, R., eds., Proceedings of Gold '88: Economic Geology Monograph #6, p.537-552.

Mortensen J.K., and Thompson, R.I., 1990, A U-Pb zircon-baddeleyite age for a differentiated mafic sill in the Ogilvie Mountains, west-central Yukon Territory *in* Radiogenic Age and Isotopic Studies: Report 3, Geological Survey of Canada, Paper 89-2, p. 23-38.

Mortensen, J.K., Murphy, D.C., Hart, C.J.R., and Anderson, R.G., 1995, Timing, tectonic setting, and metallogeny of Early and mid-Cretaceous magmatism in Yukon Territory: Geological Society of America, Abstracts with Programs, v. 27, p. 65.

Mortensen J.K., Hart, C.J.R., Murphy, D.C., and Heffernan, S., 2000, Temporal evolution of early and mid-Cretaceous magmatism in the Tintina Gold Belt *in* The Tintina Gold Belt: Concepts, Exploration, and Discoveries, British Columbia and Yukon Chamber of Mines Special Volume 2, p. 49-57.

Newberry R.J., 2000, Mineral Deposits and associated Mesozoic and tertiary igneous rocks within the Interior Alaska and adjacent Yukon portions of the 'Tintina Gold Belt': a progress report *in* The Tintina Gold Belt: Concepts, exploration, and discoveries, Special Volume 2, p. 59-88.

Reed, J.C. Jr., Wheeler, J.O., and Tucholke, B.E., 2005, Geologic Map of North America: Geological Society of America, 1:5,000,000 scale.

Templeman-Kluit, D.J., 1980, Geology and Mineral Deposits of Southern Yukon *in* Yukon Geology and Exploration, 1979-80: Department of Indian and Northern Affairs, p. 7-31.

Till, A.B., Roeske, S.M., Bradley, D.C., Friedman, R., and Layer, P.W., 2007, Early Tertiary transtension-related deformation and magmatism along the Tintina fault system, Alaska *in* Till, A.B., Roeske, S.M., Sample, J.C., and Foster, D.A., eds., Exhumation Associated with Continental Strike-Slip Fault Systems: Geological Society of America, Special Paper 434, p. 233-264.

Wengzynowski, W.A., 2009, Assessment report describing geology, mineralization, and diamond drilling at the Mike Lake property: Archer Cathro & Associates (1981) Limited, 1844 p.

Yukon Geological Survey, Igneous Database, (http://servlet.gov.yk.ca/ygsis/index.do).

3. Rock Types and Alteration

3.1. Introduction

A variety of igneous and metamorphic rocks are present on Skarn Ridge (Figures 3.1. to 3.3.). Field classification yielded inconsistent results, however distinguishing them on the basis of immobile trace and major element geochemistry simplifies their classification.

I have determined that there are four major types of igneous rocks on Skarn Ridge: (1) quartz monzonite of the Mike Lake pluton; (2) felsic porphyritic dikes; (3) intermediate "green" dikes; and (4) mafic sills (Figures 3.3 and 3.4). The Mike Lake pluton, felsic porphyritic dikes, and green dikes were observed on the surface (Figure 3.1); mafic sills were only identified in drill core. Average compositions (by XRF) are presented in Table 3.1; compositions of all igneous samples are presented in Tables 3.A-1 to 3.A-5. All igneous units intrude contact metamorphosed and variably metasomatized rocks of inferred Rabbitkettle Formation, Gull Lake Formation, and Hyland Group protoliths.

Metamorphic rocks are classified as one of six major types, based on texture, grain size, and composition determined by XRF (Tables 3.A-6 to 3.A-7): (1) skarn; (2) calc-silicate hornfels; (3) marble; (4) grit; (5) black hornfels; and (6) mixed hornfels. Together, these comprise a stratigraphic section that ranges from uppermost skarn with interbedded calc-silicate hornfels, grit, and marble, to basal black hornfels ± quartz grit ±

mixed hornfels. Marble occurs as unmetasomatized lenses within the skarn and is a prominent map feature on the west side of Skarn Ridge.

With few exceptions, all rocks on Skarn Ridge are hydrothermally altered. Alteration is of two types: (1) higher temperature ('prograde') including skarn, endoskarn and potassic alteration in intrusive rocks; and (2) lower temperature ('retrograde'), which commonly appears as an amphibole + axinite overprint on many rock types; or as a propylitic (chlorite ± calcite ± epidote) overprint on post-skarn rocks. To understand the ore deposit, it is necessary to understand the rocks and their alteration.

3.2. Methods

All core was logged, sampled for assay, and stored on site at the Mike Lake drill camp. A quality assurance/quality control (QA/QC) protocol was in place to ensure that handling, sampling, and assaying procedures were adhered to (Wengzynowski, 2009). Core was transported by helicopter twice per day from the drill site to the core processing facility in camp. There, the core was subjected to geotechnical logging (% recovery and rock quality designation, "RQD") and geological logging (lithology, alteration, structure, mineralization), photographed, and marked for sampling and assay. Core was sawn on site, longitudinally, with one half returned to the core box for an archive and the other half sealed in a plastic sample bag labeled with a unique assay number. Field duplicates (quartered core), blanks, and certified standards were added to each sample batch on a pre-determined insertion schedule. Samples were shipped to ALS Chemex assay lab in North Vancouver, BC, where they were dried, crushed, pulverized, and split to ~250 g,

then subjected to a four-acid (nitric, perchloric, hydrofluoric, and hydrochloric acid) "near total" digestion and analyzed for 33 elements using ALS Chemex method ME-ICP61a. All samples were analyzed for gold using traditional fire assay techniques and an atomic absorption (AA) finish (ALS Chemex method Au-AA25).

Analytical work was conducted from September 2009 – May 2010, and included polished thin section petrography (reflected and transmitted light) of 78 slides, X-ray fluorescence (XRF) of 18 whole rock pressed pellets, X-ray diffraction (XRD) of 10 powder mounts and polished rock slabs, and electron microprobe analysis (EMPA) of major minerals.

Silicate (clinopyroxene, garnet, scapolite, amphiboles, biotite), sulfide (arsenopyrite, sphalerite, galena, etc.), and native metal minerals (Au, Bi, Ag, Te, etc.) were analyzed by electron microprobe using quantitative routines calibrated with natural mineral standards. Semi-quantitative analyses were performed with the same instrument using energy dispersive spectrometry (EDS).

I performed all quantitative microprobe analyses with a Cameca SX-50 microprobe equipped with four wavelength dispersive spectrometers (WDS). I used 10 second peak and background counting times and beam conditions of 15 kV and 20 nA with a 5 micron diameter beam. All data were collected in three separate batches over a two-year period, and at least one secondary standard was employed for each analytical session to ensure consistency of the data. In particular, for all silicate analytical sessions I used the secondary standards augite (USNM 122142), garnet (USNM 87375), and

hornblende (USNM 143965) and averaged the results of 5 sequential analyses. Average concentrations of all oxide components greater than 1 wt% (in all analytical sessions) deviated from the official values by less than 6 relative percent. Further, percent Fe/(Fe+Mg) for the three standards deviated from those calculated from official values by less than 1%. (For example, atomic Fe/Fe+Mg for hornblende USNM 143965 should be 33%; I measured values of 32-34% in all sessions). Based on this precision, measured % hedenbergite (%Hd) component in clinopyroxene for the Skarn Ridge data set should be well within 2% of the true value. Complete microprobe data is given in Appendix 3.A-8.

I analyzed 44 samples (34 igneous, 10 metamorphic) for major and trace elements using XRF. I pulverized and prepared samples as standard pressed-powder pellets, followed by analysis with a Panalytical Axios 4 kW wavelength dispersive spectometer (WDS) in the UAF Advanced Instrumentation Laboratory. Instrument conditions included count times of 10 seconds for major elements and 40-100 seconds for trace elements, accelerating voltage of 32 kV for light elements/60 kV for heavy elements, and tube current of 66 mA for light elements/125 mA for heavy elements. I also performed semi-quantitative analyses of fine-grained, polished, 40 mm diameter rock surfaces using these same conditions. Calibrations were performed on internationally certified, natural rock standards, including AGV-1, AL-1, BCR-1, BHVO-1, BR, DR-N, GA, GH, GS-N, GSP-1, JA-1, JB-2, JF-1, JG-1, JG-2, JGb-1, JR-1, MA-N, MRG-1, NIM-G, NIM-L, NIM-N, NIM-S, QLO-1, RGM-1, STM-1, SY-2, and W-2. Precision, based on replicate analyses, is $< 1\%$ of the amount present. Accuracy is approximately $\pm$ 5% for

concentrations > 20 ppm, and ± 1-2% for concentrations > 0.5% (Lough et al., 2012). XRD analyses were conducted on a Rigaku MiniFlexII desktop X-ray diffractometer at a scan speed of 0.5 degrees per second, through the range of 5.00-50.00 degrees, with measurements taken at every 0.05 degrees. X-rays were produced from a copper source tube at 30 kV and 15 mA.

Potassium feldspar staining was used to assist with modal mineral estimations in felsic igneous rocks. The method (Lyons, 1971) requires several steps. Rocks with a smooth surface (e.g., sawn) are subjected to a 10 second etch in concentrated hydrofluoric acid, rinsed in deionized water, dried, then placed in a supersaturated solution of sodium cobaltinitrite (stain) for 45 seconds. The sample is then removed from the stain, rinsed again in deionized water and then dried. Potassium feldspars absorb the yellow stain and can easily be distinguished from plagioclase and other similarly colored minerals.

3.3. Igneous Rocks

3.3.1. Mafic Sills (Gb)

Bordin et al. (1998), identified a small body of mafic rock approximately 1.5 km south of Skarn Ridge, which they mapped as Triassic Galena Suite (Figure 2.5). This mafic body was outside of the 2008 map area; however, within the map area altered mafic rocks were identified in drill core. Based on structural reconstructions (Chapter 4), this unit has a sill-like shape.

The mafic rocks are the most inconsistently identified igneous unit on Skarn Ridge. Difficulty in recognizing this unit stems largely from its pervasive alteration, structural discontinuities, and seemingly gradational contacts with skarn. Numerous drill log entries incorrectly document this lithology as "garnet skarn", "brown hornfels", "clinopyroxene skarn with an axinite overprint", "grit with an axinite overprint", and as "other intrusives", which made for obvious difficulties in creating cross sections. Following a meticulous reexamination of all core logs, photos, and assays (Figure 3.5), I identified this unit in several locations where it was not previously recognized. I confirmed all logged occurrences (for which I had samples) with immobile trace element discrimination by XRF and then plotted all confirmed occurrences in the Vulcan™ database and noted any discontinuities in the triangulation solid. I scrutinized these 'missing' intercepts using the drill core assays, noting intercepts with elevated Ti, V, P, and Cr (all characteristic of the mafic sills and largely resistant to compositional changes during hydrothermal alteration; c.f., Table 3.2. I checked the core photos and geologist descriptions to ensure that the rock appearances were compatible with altered mafic rock (brown or "bleached" brown, igneous texture, and diffuse contacts) and (if so) I added the confirmed occurrences to my 3D model. I addressed ambiguous cases using all of the available information (Figure 3.5). In doing so, the mafic sill 'grew' from approximately 12 original and discontinuous intercepts to 38 intercepts defining nearly continuous sheets with gently undulating "folds" that mimic the stratigraphy. The mafic unit is indeed sill-form, approximately 5-10 meters thick, is stacked ("upper" and "lower" sills),

and can be traced for > 300 meters along strike without structural interruption (Chapter 4).

Due to extensive alteration, neither modal nor normative classification schemes can be applied to the mafic sill. Based on petrographic observations and XRF immobile element data for eight variably altered samples, it must be a mafic alkali igneous rock (Figure 3.4). The composition – based on least mobile trace element data – is alkalic basalt, which is consistent with its tectonic discrimination (Figure 3.6). Its original mineralogy is largely destroyed and only relict plagioclase boxes and fragments of primary biotite remain near the core of the sill (Figure 3.7). The present (alteration) mineralogy consists of approximately 45% biotite (~30% secondary and ~15% original igneous, both variably chloritized), 20% remnant (albitized) plagioclase, 10% scapolite, 10% actinolite, 5% axinite, up to 5% skeletal ilmenite and magnetite, minor pyrrhotite, chalcopyrite, and arsenopyrite, and trace amounts of sphene, zircon, apatite, and rutile (Figure 3.3 A and 3.7).

At least three different types of alteration are present in this unit. From oldest to youngest (based on petrographic relationships), they are: (1) secondary biotite (potassic alteration); (2) scapolite-amphibole-pyrrhotite (endoskarn alteration); and (3) late axinite-calcite-actinolite overprint (retrograde alteration). In general, the sills are most altered along their margins and become less altered towards their centers.

Secondary biotite alteration is a high-temperature replacement of original igneous biotite and amphibole by hydrothermal biotite. It is pervasive throughout the unit, except

in the cores of the thickest sills, where minor amounts of primary biotite occur. Primary biotite may be distinguished from secondary biotite by its coarse-grained (>200 μm) subhedral sheets, which contrast with the very fine-grained, mottled texture of its "shreddy" secondary counterpart with ubiquitous associated fine-grained rutile (Figure 3.7 C).

Scapolite-amphibole-pyrrhotite alteration comingles with secondary biotite alteration. Texturally and mineralogically, the conversion of biotite to amphibole (and plaglioclase to scapolite) is a completely different reaction than the formation of secondary biotite. The former is a Ca-addition (especially biotite to amphibole) that is characteristic of endoskarn. The latter is 'potassic alteration', commonly seen in porphyry-related hydrothermal systems at temperatures of about 400°C (Beane, 1974). A significant enrichment of K_2O and Cl in the mafic sills relative to unaltered alkalic mafic rocks (Figure 3.8) indicates that both secondary biotite and scapolite are variably present throughout the unit. The nearly inverse relationship between K_2O (anomalously enriched in secondary biotite) and Cl (a major constituent of scapolite) indicates that the two occurred independently.

Axinite-calcite-actinolite alteration overprints all other alteration assemblages in the mafic sills and appears to be late based on its presence in almost all rock types on Skarn Ridge except for the Mike Lake pluton.

Mafic sills are cut by all other igneous rocks and are consequently the oldest igneous unit. This is also the only igneous unit that is mineralized (contains anomalous

Cu, S, Cl, Au); all other igneous units cut across mineralized rocks and are not anomalous in these ore-related elements (Table 3.A-1).

3.3.2. Porphyritic Dikes (Fpd) and Green Dikes (IntG)

These two sets of dikes are practically indistinguishable based on their mineralogy and alteration alone. However in hand specimen they display distinct colors, textures, and grain sizes that set them apart during core logging. Higher concentrations of TiO_2, MnO, CaO, MgO, FeO, and P_2O_5 in the green dikes differentiates them from the more felsic porphyritic dikes (Tables 3.A-2 and 3.A-3). The low Cl contents of both dike types (Tables 3.A-2 and 3.A-3) indicate that scapolite (endoskarn alteration) is not present in either. The low Na_2O and anomalous As and W, however, indicate that some alteration is present.

Less common than porphyritic dikes are "green" dikes of intermediate composition. Although they have a subtle porphyritic texture, they may be distinguished from the porphyritic dikes by their overall finer grain size (phenocrysts 0.5-1 cm, matrix <0.1 mm) and pale greenish groundmass (Figure 3.3 B). They are also more mafic and narrower than the porphyry dikes, with thickness rarely exceeding 1 meter. With the exception of the "Bueno dike", a green dike mapped in a drainage southeast of Skarn Ridge (Figure 3.1), this unit was not observed on the surface, although it was locally identified in drill core. A green dike sample from drill hole SK08-012 (17.75 m) displays a sharp, chilled contact with the mafic sill, indicating that mafic sill is older. Compositions (Table 3.A-2) and modal mineral estimates in feldspar-stained, least-

altered samples indicate that the green dikes are quartz-poor; they plot as monzonite (Figure 3.9) to syenite (Figure 3.10). Immobile element classification for the clearly altered varieties (Figure 3.4) also indicates these dikes were originally monzonite.

The most abundant igneous rocks on Skarn Ridge are porphyritic dikes. They form the prominent ridges and spurs of Skarn Ridge and are exposed discontinuously in valleys and saddles. They are steeply dipping (approaching 90°), up to 12 meters thick, and strike in two main orientations: approximately 030° and 090°. Based on normative analysis these dikes plot as quartz syenite (Figure 3.10); estimated mineral abundance of feldspar-stained slabs show they are quartz monzonite (Figure 3.9). Compositions measured by XRF are given in Table 3.A-3. The distinctive texture of these dikes consists of large alkali feldspar phenocrysts (0.5-2 cm long) suspended in a grey matrix of fine-grained (0.5-1 mm) plagioclase, alkali feldspar, hornblende, and 5-10% quartz (Figure 3.3 C).

Both green and porphyritic dikes display varying degrees of alteration, from apparently unaltered to patchy and pervasive propylitic alteration. Axinite-calcite-actinolite alteration is common: it appears as partially to completely replaced plagioclase phenocrysts (pseudomorphs), as well as patches, pegmatitic aggregates, and veins throughout each unit (Figure 3.11). Axinite is a Ca-borosilicate mineral that is easily recognizable due to its lilac-brown color and bladed crystal habit. Locally, axinite-replaced plagioclase feldspars contain quartz + calcite + clinozoisite, with proximal

hornblende. Other minerals less commonly associated with axinite-calcite-actinolite alteration include scheelite and arsenopyrite.

Porphyritic dikes contain two types of xenoliths: one set is compositionally indistinguishable from intermediate green dikes and the other indistinguishable from mafic sills (Figure 3.4 A). Further, a mafic sill xenolith contains 0.8% Cl, whereas the enclosing porphyritic dike contains 0.3% Cl (Tables 3.A-4 and 3.A-1, respectively). These relations indicate that porphyritic dikes are younger than both green dikes and mafic sills, and that gold-related alteration occurred before porphyritic dike emplacement.

3.3.3. Mike Lake Pluton (Qm)

The Mike Lake pluton is a body of largely unaltered hornblende-biotite granite. Least altered samples are composed of approximately 30% plagioclase, 30% alkali feldspar, 15-20% quartz and up to 25% biotite and hornblende. Pinkish-beige phenocrysts of alkali feldspar up to 1.5 cm long occupy up to 10% of the rock, giving the rock a porphyritic texture (Figure 3.3 D). The subequigranular matrix is light grey and composed of fine-medium grained ($\leq$ 3 mm) plagioglase + alkali feldspar. Quartz is subhedral, transparent, clear to smoky and individual grains do not exceed 2 mm in diameter. Hornblende and biotite often occur as intergrown aggregates (up to 3 mm) and sometimes show minor chloritization. Primary pale green clinopyroxene (augite?) crystals can be seen in thin section; they account for <1% of the mafics (<0.25% of the rock). Mineral estimation from feldspar-stained slabs indicates it contains enough quartz to be a granite (Figure 3.9); normative analyses suggest it is a quartz monzonite (Figure

3.10). It has been historically identified as quartz monzonite because the quartz is not obvious, especially in unstained samples. XRF compositions are presented in Table 3.A-5.

Samples from the Rubble Lake cirque (north of Skarn Ridge) show very weak non-pervasive propylitic alteration, but have substantial arsenic anomalies (up to 350 pm). On average, about 20-40% of the biotite and hornblende are partially converted to chlorite ± calcite. The Mike Lake Pluton does not display endoskarn, potassic, or axinite alteration within 1 km of Skarn Ridge. Industry reports claim it is unaltered (Bordin et al., 1998; Wengzynowski, 2009).

Although this unit does not crop out on Skarn Ridge, it occupies the largest areal extent of any other igneous rock within 10 km of Skarn Ridge; it dominates the northeast quadrant of the mapped area (Figure 3.1). Exposures are steep and contacts are typically obscured by talus. The Mike Lake quartz monzonite weathers to a buff-beige color with typical granitic exfoliation.

3.4. Metamorphic Rocks

3.4.1. Skarn (Sk)

Skarn is the dominant rock type present on the aptly named Skarn Ridge. This unit (together with calc-silicate hornfels) comprises the uppermost portion of the local stratigraphy, and due to its original marble composition it is also the most favorable host for gold mineralization in the stratigraphic package. Clinopyroxene skarn ranges in color from medium to dark green; however, color-based zoning patterns could not be discerned

in the field. Garnet is rare, but where present it forms small isolated bands or clusters (up to several mm wide) in or near calcite clots and veinlets. Crystals are euhedral, up to 3 mm in diameter, and pink to brownish-pink in color. Compositions determined by microprobe analysis show a range of Hd_{14}-Hd_{87} for clinopyroxene (Figure 3.12 A, Table 3.A-8) and Ad_8-Ad_{98} for garnet (Figure 3.12 B, Table 3.A-9).

Scapolite is an abundant accessory mineral that occurs variably throughout the skarn (0-60%), with occasional coarse-grained/massive amalgamations of sheath-like elongate clusters. Compositions are Me_{28}-Me_{59} (Table 3.A-10), where Me represents the end member meionite (Ca) in the marialite-meionite ($Na_4Al_3Si_9O_{24}Cl$ - $Ca_4Al_6Si_6O_{24}CO_3$), solid solution (Figure 3.13).

Little retrograde alteration is present in the skarn and calc-silicate package; what exists is present as coarse-grained amphibole + calcite ± axinite ± arsenopyrite ± scheelite. Grain sizes rarely exceed 1 cm, and average $\leq$ 3 mm. All amphiboles display the typical elongate, bladed to needle-like habit and commonly occur in felted intergrowths with other retrograde minerals in veins, vein envelopes, and irregular patches in skarn. Based on XRF analyses, axinite contains up to 500 ppm tin.

Two types of amphiboles are present: low-Cl ferro-actinolite – ferrohornblende and high-Cl ferro-edenite – ferropargasite (Figure 3.14, Table 3.A-11). Atomic Cl is clearly proportional to atomic Na + K; for amphiboles with maximum Na + K approaching 1.0, the atomic Cl approaches 0.8, with a formula total of 2.0 OH^- + F^- + Cl^-; Figure 3.15. The iron-rich amphiboles impart a dark green color to the skarn, which was

noted descriptively in some core logs where retrograde alteration was not specifically indicated. In thin section, some amphiboles display an intense bluish-green color in plane-polarized light; reasonable behavior given their high iron contents. I occasionally saw pale green to colorless tremolite-actinolite (?) in core, although never in thin section.

3.4.2. Calc-Silicate Hornfels (Csh)

Calc-silicate hornfels (csh) is the second most abundant rock type on Skarn Ridge and is presumed to be an altered part of the Rabbitkettle Formation. Csh is commonly interbedded with skarn and black hornfels in thin (mm-scale) laminations to thick (several meters) layers. Metasomatism of the compositionally heterogeneous protolith (Figure 3.16) produced a lithologic package with variable color patterns that include green hornfels, banded "zebra" hornfels (green and white), skarn-hornfels (light and dark green), and mixed hornfels (green, cream, and purple). During the 2008 field season these variations were treated as separate core logging and surface map units; I treat them as one unit because of the difficulty I encountered when attempting to correlate them from one drill hole to another.

Based on X-ray diffraction (XRD) analyses, these rocks are composed of quartz, feldspar (plagioclase > alkali feldspar), and calcite, with lesser and variable amounts of diopside, biotite, Ca-amphibole, clinozoisite, and scapolite. Some representative XRF analyses are presented in Appendix 3.A-6. Axinite + calcite + actinolite alteration is present as a late, preferential overprint on some compositional layers in calc-silicate hornfels, and less frequently as cross-cutting veinlets (Figure 3.17).

3.4.3. Marble (Mbl)

Marble of the Rabbitkettle Formation is present on the far western edge of Skarn Ridge and also as unmetasomatized lenses within the calc-silicate package. The unit ranges in color from buff-white to pale grey and contains variable amounts of metamorphic scapolite present as round nodules up to 5 mm in diameter. The abundance of scapolite is loosely controlled in "layers"; however, the abundances estimated are highly variable. Scapolite abundance estimations were recorded in drill logs, but the results were not sufficiently consistent to delineate stratigraphic horizons. In addition to scapolitic layers, the unit also contains layers and lenses of hornfelsed silty and sandy meta-sedimentary rocks, also referred to as "grit" (see ahead, 3.4.4.) in core logs.

Map relationships show an approximately located contact between skarn and marble in the western portion of the field area. A clear metasomatic front was not revealed in drill core and the surface contact is obscured by talus. More information is needed in this area to determine the actual nature of this contact.

3.4.4. Grit

A quartz grit unit occurs as minor interlayers in skarn, calc-silicate hornfels, and black hornfels in drill core, and also as lenses and thin layers in marble outcrops west of the main map area. Thickness varies between <1 cm and 10 cm and color ranges from medium grey to pale purple. Rare surface exposures appear as semi-resistant beds with a coarse sandpaper-like texture on weathered surfaces. Mineralogically, the unit is dominated by rounded quartz grains up to 1 mm in diameter in a matrix of finer-grained

quartz ± calcite, with minor feldspar, clinozoisite, and undifferentiated micas identified by XRD. Compositions are listed in Table 3.A-7. Rare, late actinolite veins (≤ 5 mm thick) cut these rocks.

3.4.5. Black Hornfels (Blh)

Black hornfels comprises the basal Skarn Ridge stratigraphic section, marking the lower limit of significant mineralization. The deepest drill holes on Skarn Ridge in 2008 were terminated in this unit. Some interlayering with calc-silicate hornfels and skarn was observed at the upper contact of this unit in drill core, but otherwise this contact is relatively sharp and can be traced throughout most subsurface drill intercepts. In outcrop, this unit is a recessive slope-former that weathers into small blocks and plates. It is dark brown to black in color, except where bleaching along fractures and veins imparts a pale purple hue. This unit is dominated by very fine-grained quartz and biotite with lesser feldspar, chlorite, and micas. XRF analyses are provided in Table 3.A-7.

3.4.6. Mixed Hornfels (Mxh)

Mixed hornfels is a map unit (Figure 3.1) that is basically an undifferentiated hornfels consisting of black, white, and brown layers. This unit lies entirely outside of the drilled area. Not much is known about this unit; I do not have any surface samples and it was not encountered in drill core. It is possible that the mixed hornfels is actually a continuation of the black hornfels representing a slight facies change. The color variation may also be the result of hydrothermal alteration.

3.5. Discussion

The data presented show that the porphyritic dikes are younger than the green dikes, which are younger than the mafic sills. Although no cross-cutting relationships between the porphyritic dikes and the Mike Lake pluton are known, the lack of high-temperature alteration and mineralization indicated that the latter is likely the youngest intrusion in the study area. Modal and normative classification schemes distinguish between the Mike Lake pluton and porphyritic dikes. However, immobile element classification shows some overlap between the two rock types (Figure 3.4). This overlap could indicate that these are different manifestations of the same magmatic episode. Alternatively, the rocks could represent different degrees of evolution of a single magmatic parent. Given the wide range in compositions seein in the individual Yukon magmatic suites and their considerable degree of overlap (Figure 2.2), either seems perfectly likely.

The historic classification of the Mike Lake pluton as Tombstone Suite (Bordin et al., 1998; Hart, 2007; Wengzynowski, 2009) is problematic given the actual rock types (granite and quartz monzonite) observed. Tombstone Suite compositions range widely, but only about one quarter of the normative data fit into the granite and quartz monzonite categories (Figure 2.3 A). The next closest (geographically) plutonic suite is the Mayo Suite, which is predominantly granite and quartz monzonite (Figure 2.2), so it is possible that the Mike Lake pluton is actually part of the Mayo Suite, but that it has been mis-classified as Tombstone Suite.

Regardless of which plutonic suite the Mike Lake pluton is classified as, it post-dates skarn formation and mineralization. Unmineralized porphyritic dikes display sharp contacts with mineralized skarn, so they also post-date skarn formation and mineralization. Green dikes show less distinct contacts due to alteration, and generally do not appear mineralized in hand specimen. The green dikes have ambiguous timing with respect to skarn formation and mineralization – that is, they were most certainly in place during the waning stages of mineralization, but it is unclear if they were contemporaneous with either event. Mafic sills are the most intensely altered igneous rock and they contain abundant pyrrhotite and occasional chalcopyrite. Based on cross-cutting relationships with other intrusives and mineralization, and the intensity of alteration, these sills pre-date skarn formation and may have formed part of the plumbing system for skarn-forming fluids.

The metamorphic host rocks are similarly difficult to classify. Based on descriptions of the Rabbitkettle Formation from throughout the Selwyn Basin (Templemen-Kluit, 1980; Gordey, et al., 1981; Abbot, 1993; and Gordey and Anderson, 1993), this unit was the skarn protolith. Stratigraphic classification of hornfels units is more problematic due to the degree of folding, faulting, hornfelsing, alteration, and general uncertainty in correlation between the local and regional stratigraphy. Descriptions of the Rabbitkettle Formation typically include 'argillite laminations and layers'; however, thicknesses are not specifically mentioned and are likely variable across the basin. If the bedding on Skarn Ridge is not overturned, it is possible that the black

hornfels is actually Gull Lake Formation or Hyland Group, both unconformable with the overlying Rabbitkettle Formation. Both are dominated by argillaceous sediments and may contain grit layers; that is, are likely protoliths for the non-calcareous rocks at Skarn Ridge. Although truncated beds were not recorded in the black hornfels, the (typically) sharp contact between skarn and black hornfels leads me to conclude that this contact represents an abrupt change in lithology, and therefore is not as likely to be an argillaceous member of the Rabbitkettle Formation as it is likely to be Gull Lake Formation or Hyland Group. Without further drilling beneath the unmineralized hornfels unit (highly unlikely) to establish if calcareous rocks reappear at depth, it is impossible to say with certainty whether the lower hornfels is simply an interbedded argillaceous layer in the Rabbitkettle Formation, versus a completely different unit.

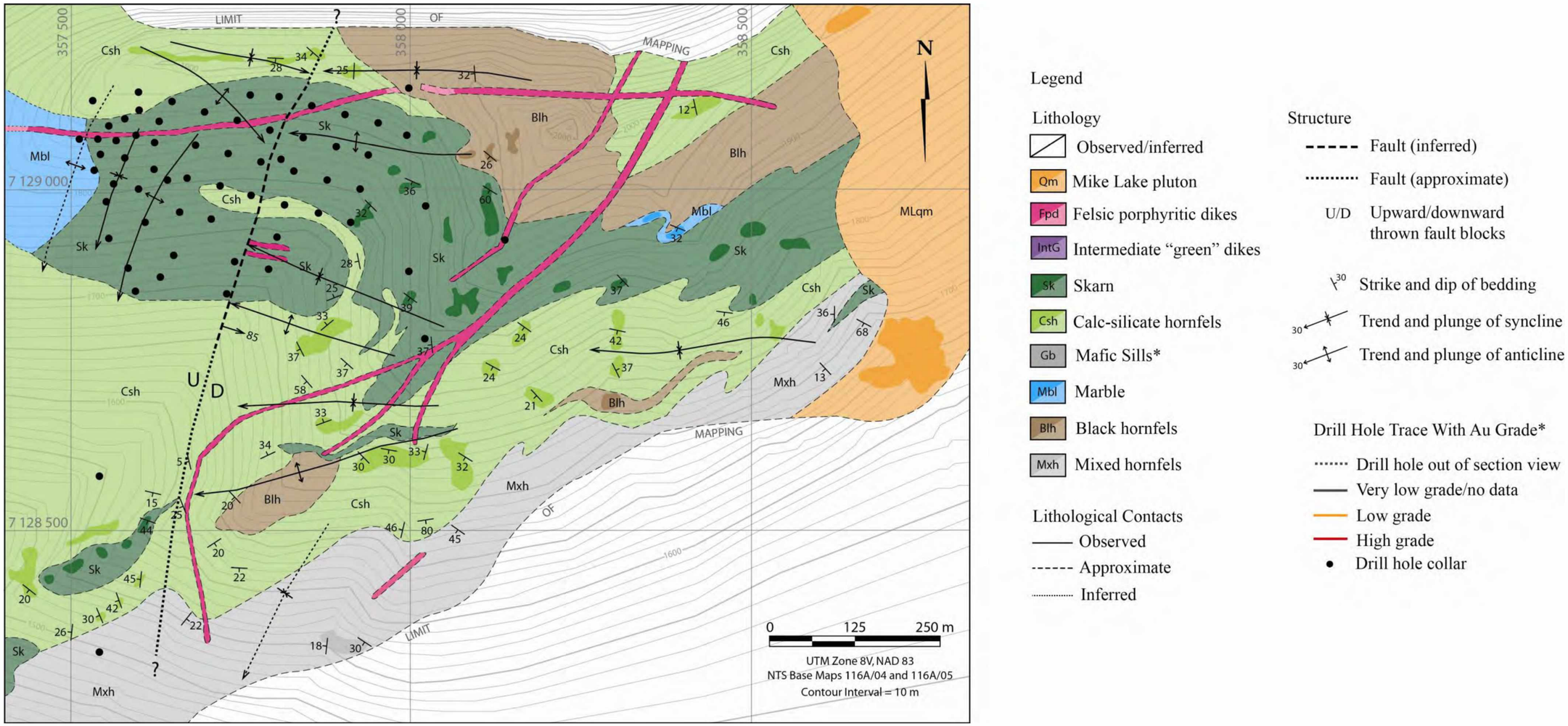

Figure 3.1. Geologic map of Skarn Ridge.
Geology by W. Wengzynowski, R. Tolbert, and S. Mrozek (this study).

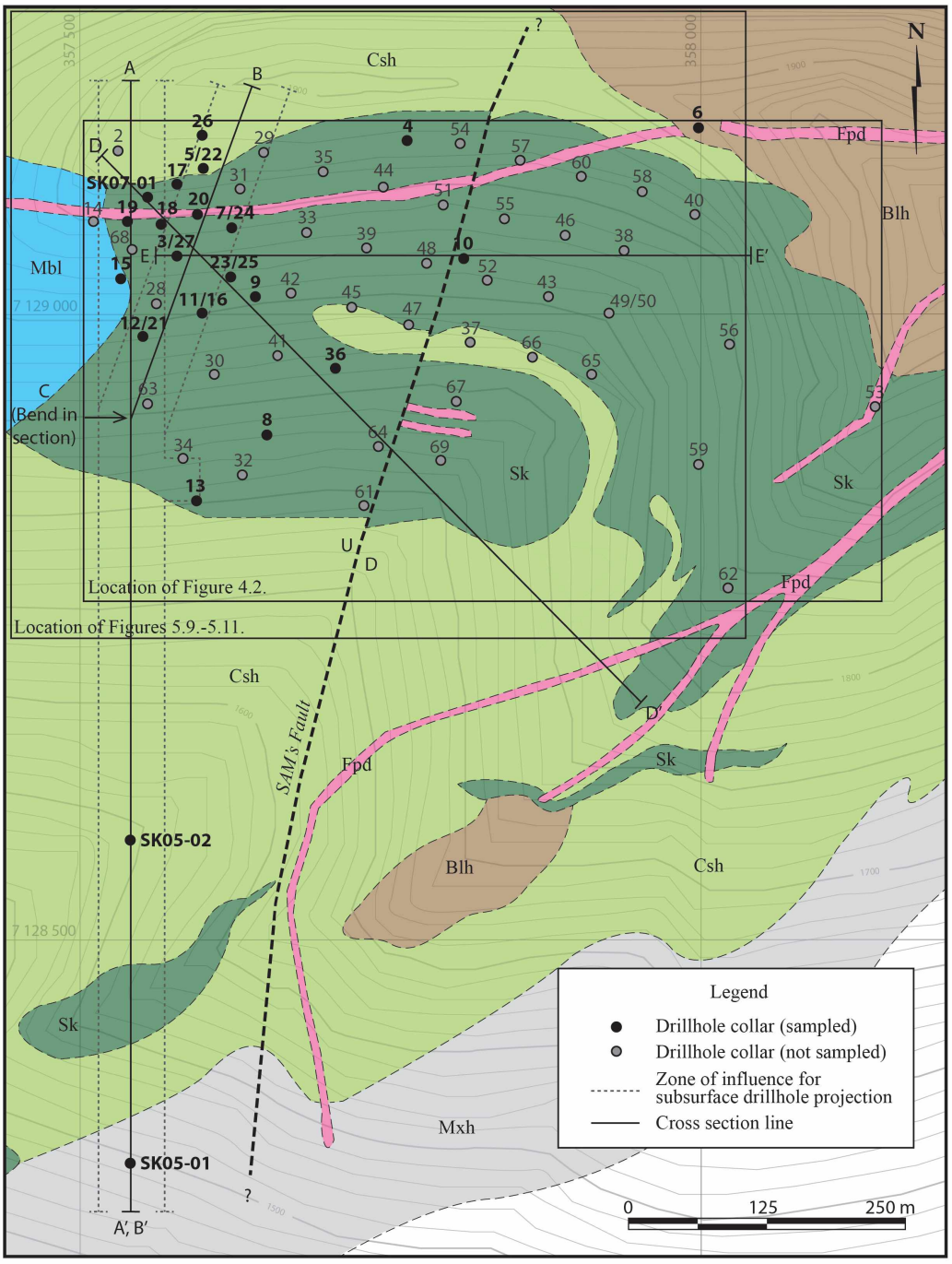

Figure 3.2. Location of geologic cross-sections A-A' to E-E' and selected figures. Numbers denote 2008 drill hole collar identifiers with prefix 'SK08-'. Master legend accompanies Figure 3.1.

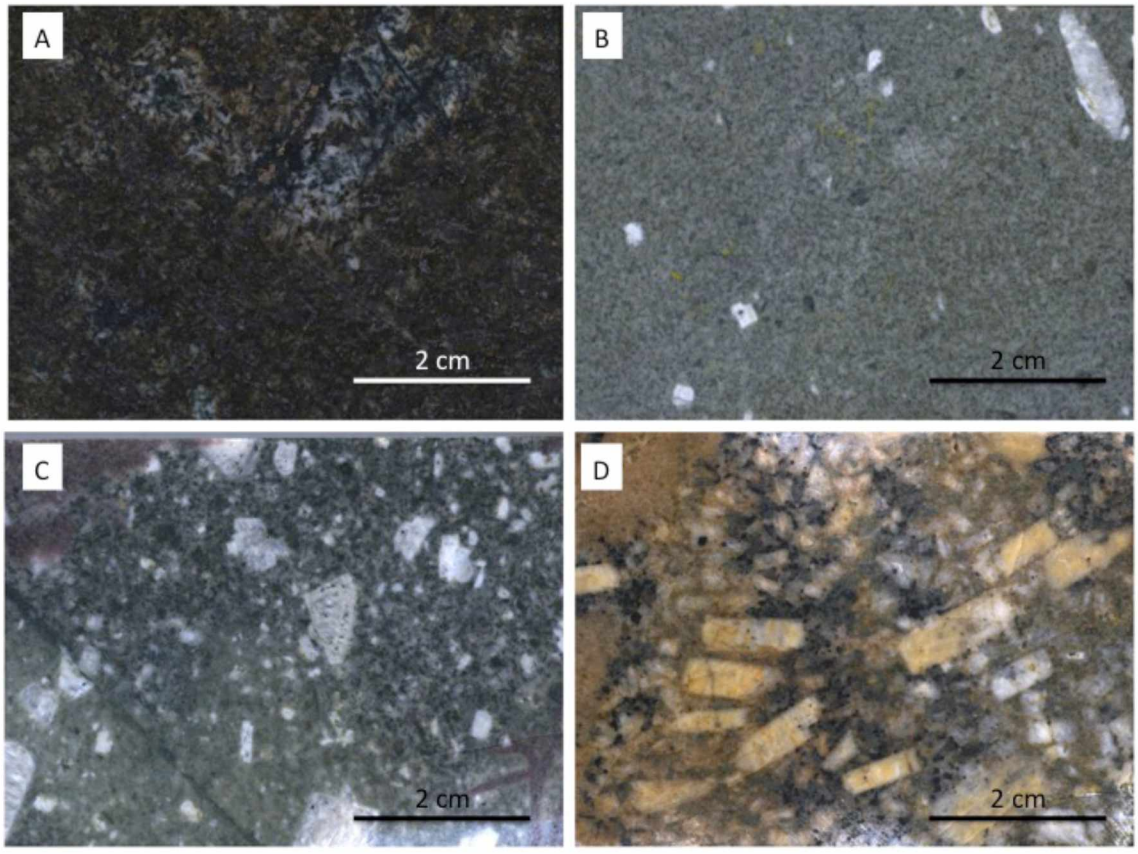

Figure 3.3. Igneous rock types on Skarn Ridge.
A: mafic sill. B: green dike. C: felsic porphyritic dike (with axinite alteration). D: Mike Lake pluton showing minor oxidation. See text for unit descriptions.

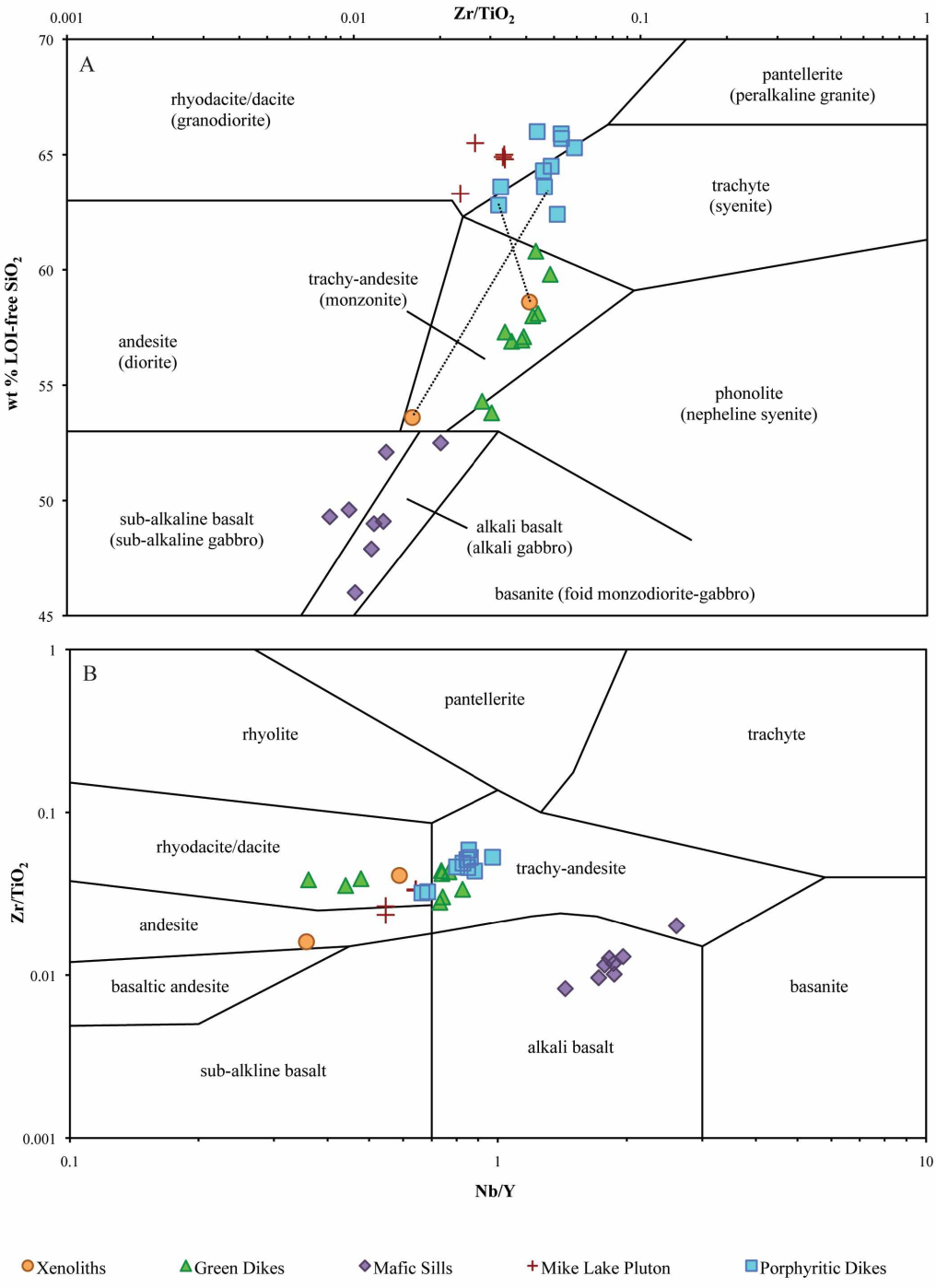

Figure 3.4. Igneous rock classification by immobile trace elements.
Xenoliths in A and B are hosted in porphyritic dikes. Data are based on quantitative XRF analyses. Intrusive equivalent names are given in parentheses. Both diagrams are modified from Winchester and Floyd (1977) using data from this study (Tables 3.A-1 to 3.A-5).

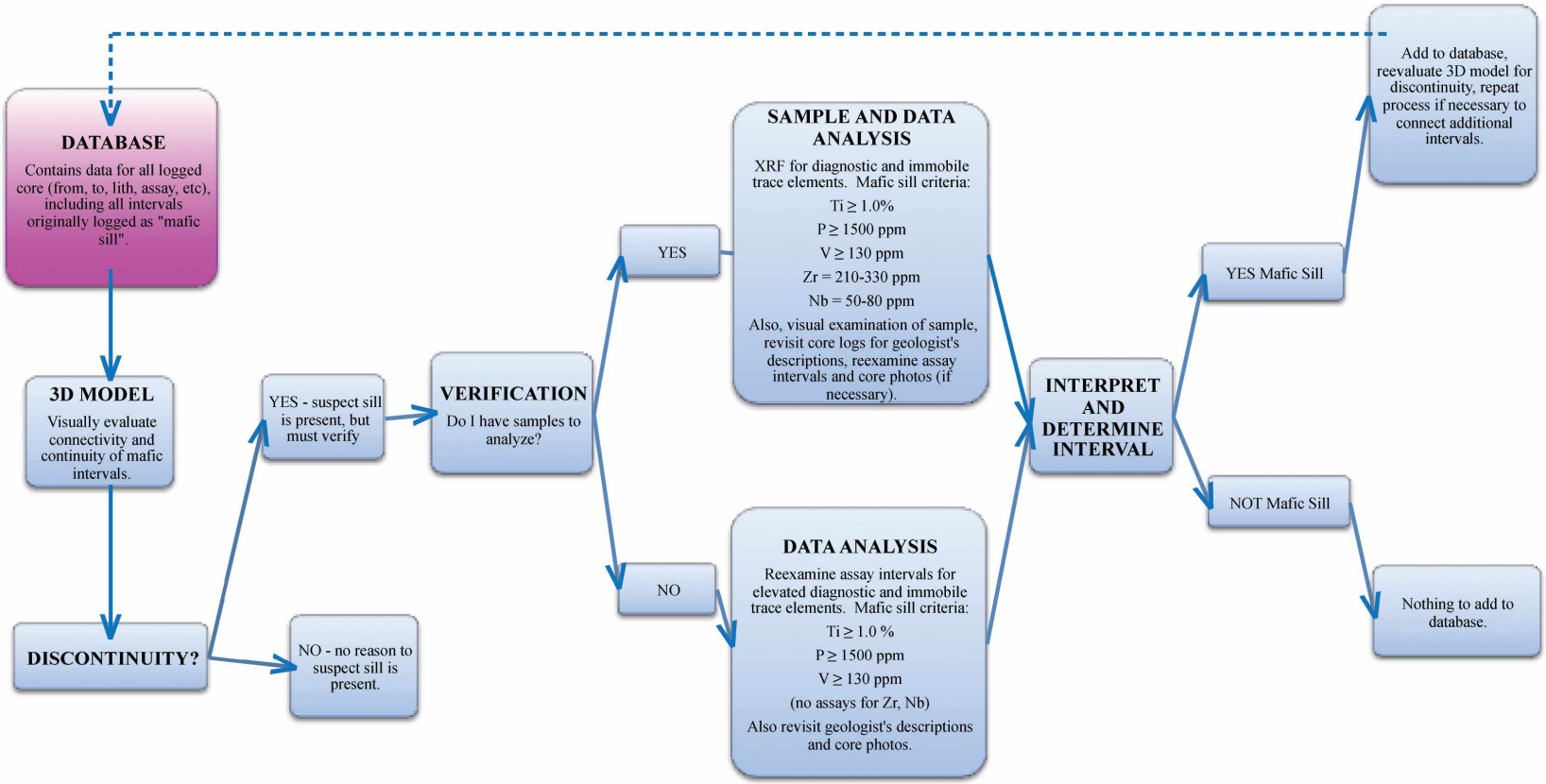

Figure 3.5. Workflow for evaluating and determining mafic rock drill intercepts.
Model by S. Mrozek (created for this study).

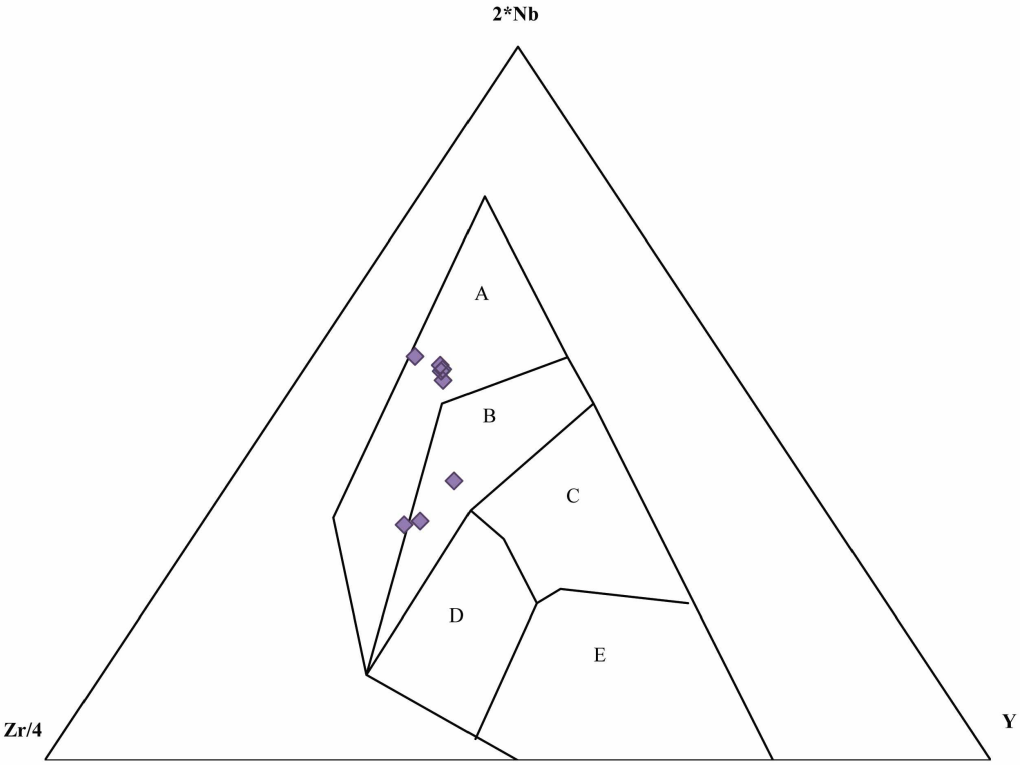

Figure 3.6. Tectonic discrimination of basalts using immobile trace elements.
A = within-plate alkali basalts, B = within-plate alkali basalts and within-plate tholeiites, C = E-type MORB, D = within-plate tholeites and volcanic arc basalts, E = N-type mid-ocean ridge basalts and volcanic arc basalts. Diagram modified after Meschede (1986) with data from this study (Table 3.A-1).

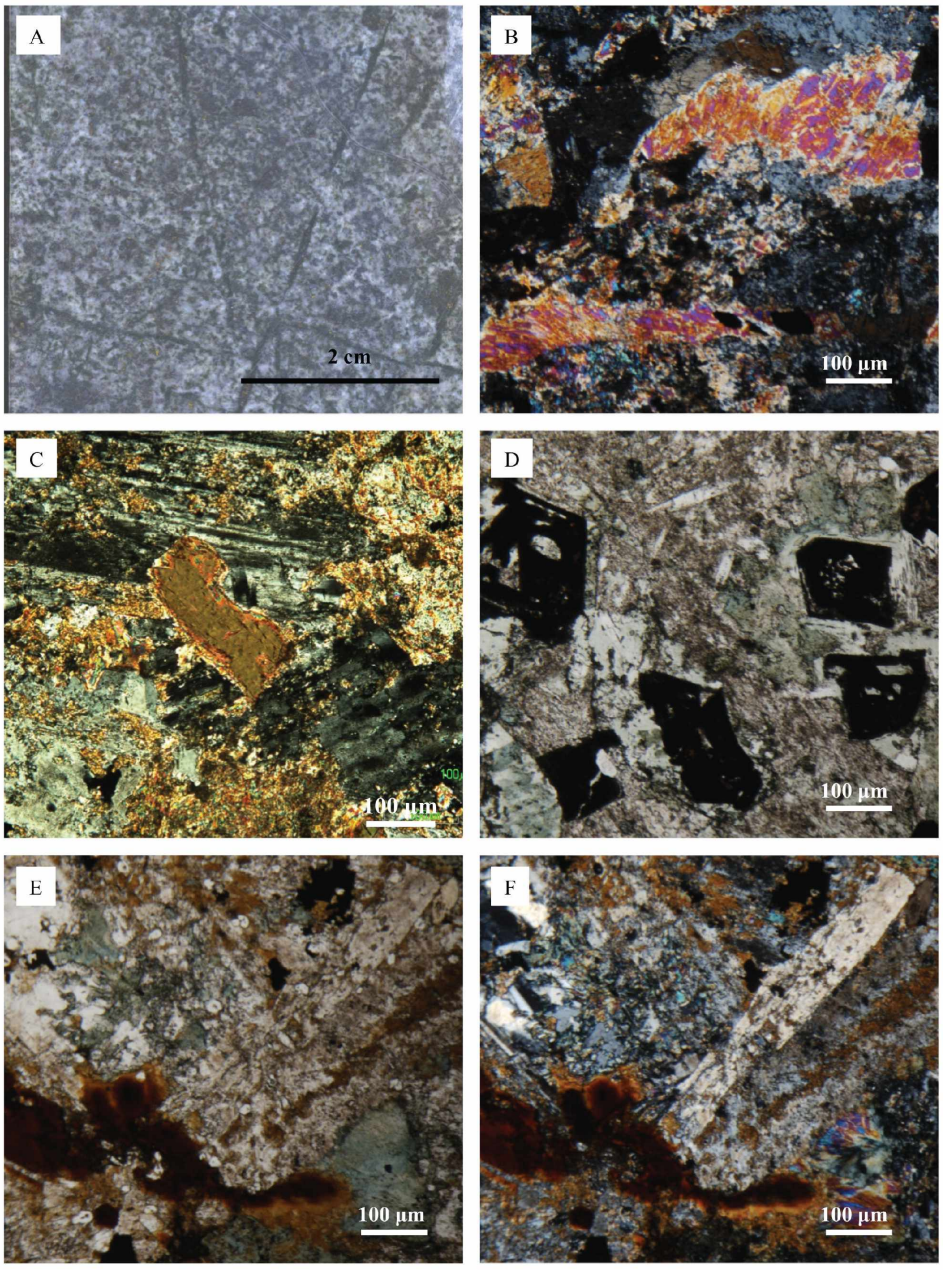

Figure 3.7. Mafic sill alteration mineralogy.
A: 'bleached' hand specimen of mafic sill from drill core. B: scapolite alteration. C: least-altered mafic sill sample showing primary biotite sheet (center) surrounded by relict plagioclase and secondary biotite. D: skeletal magnetite in altered groundmass, including minor amphibole and apatite. E: relict plagioclase, secondary biotite, amphibole, and apatite in plane polarized light. F: same as E, crossed polars.

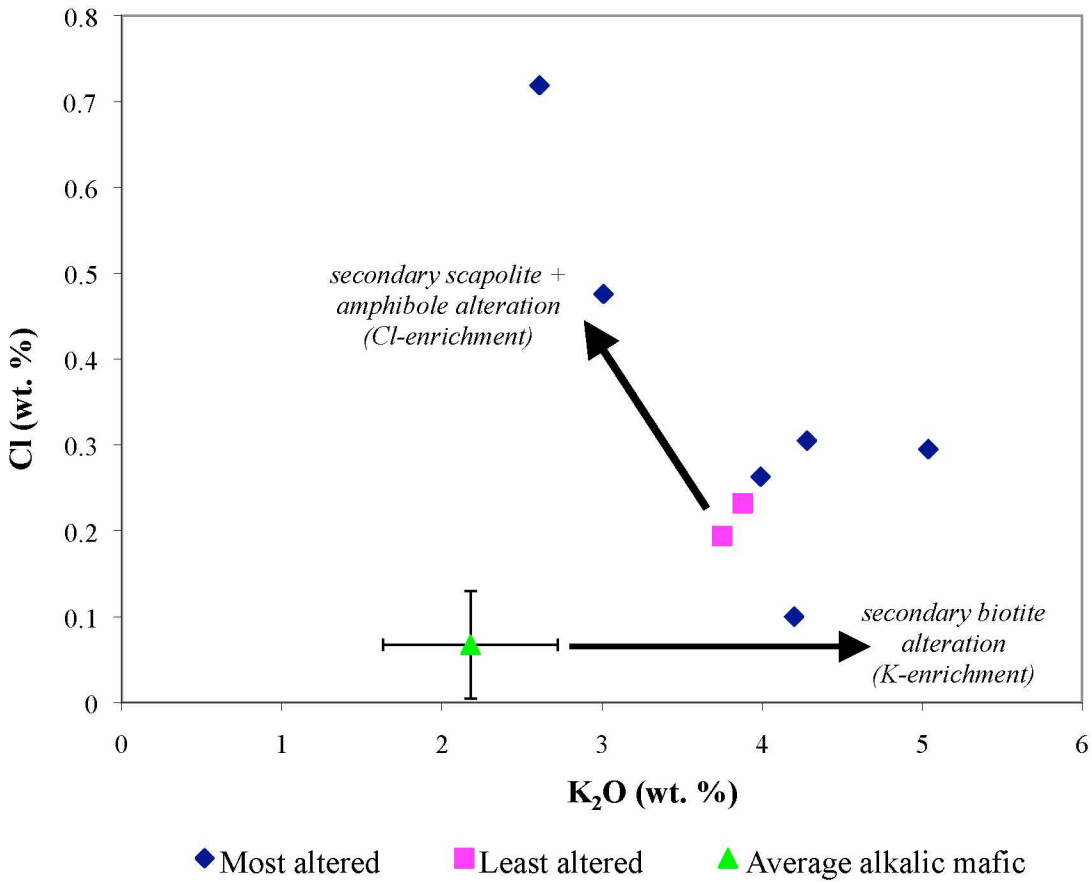

Figure 3.8. Average alkalic basalt plotted with K_2O vs. Cl for mafic sill samples. Excess K_2O is from replacement of hornblende by biotite; loss of K_2O and gain in Cl is from replacement of plagioclase and biotite by scapolite and actinolite. Average alkali mafic rock point and error bars (1 standard deviation) based on data in Mutschler et al. (1981).

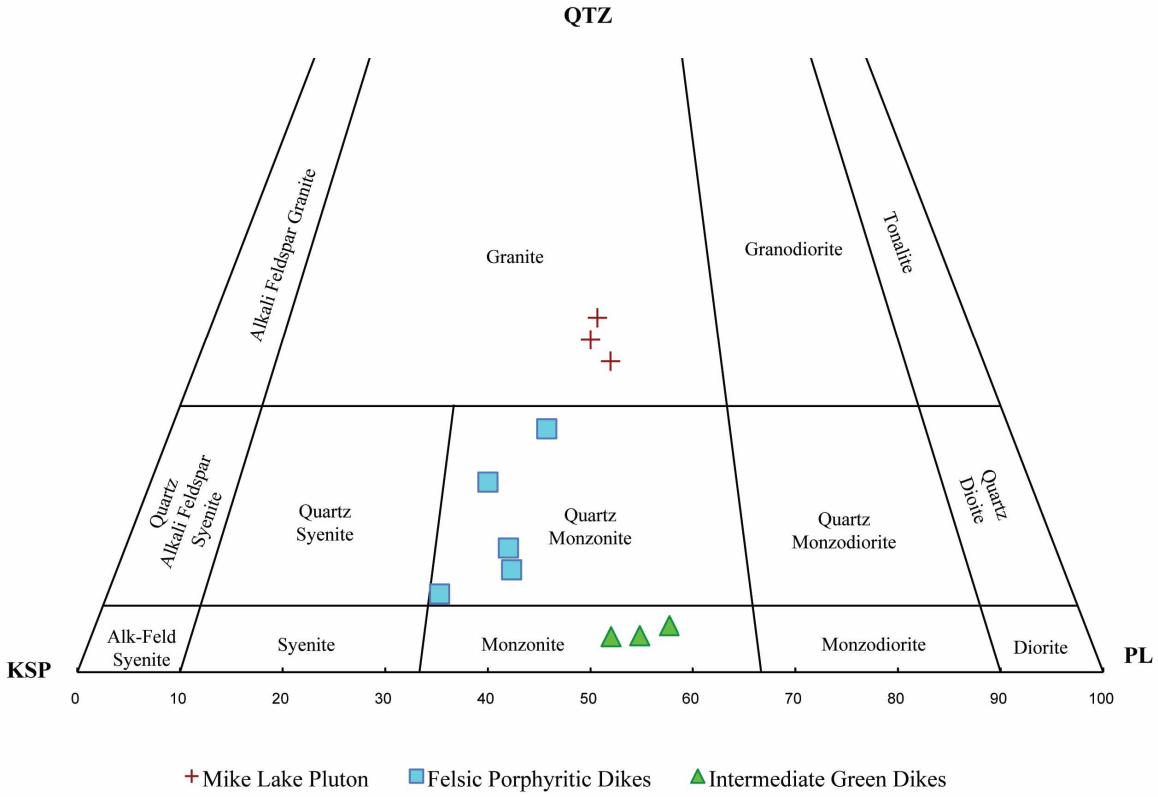

Figure 3.9. Modal mineralogy of representative least-altered igneous rock samples. Felsic and intermediate samples are plotted on the IUGS rock classification diagram (Streckeisen, 1974). Mafic sill samples are too altered to include in this scheme. Axes: QTZ = quartz; KSP = alkali feldspar; PL = plagioclase feldspar. AFSy = alkali feldspar syenite (field on chart).

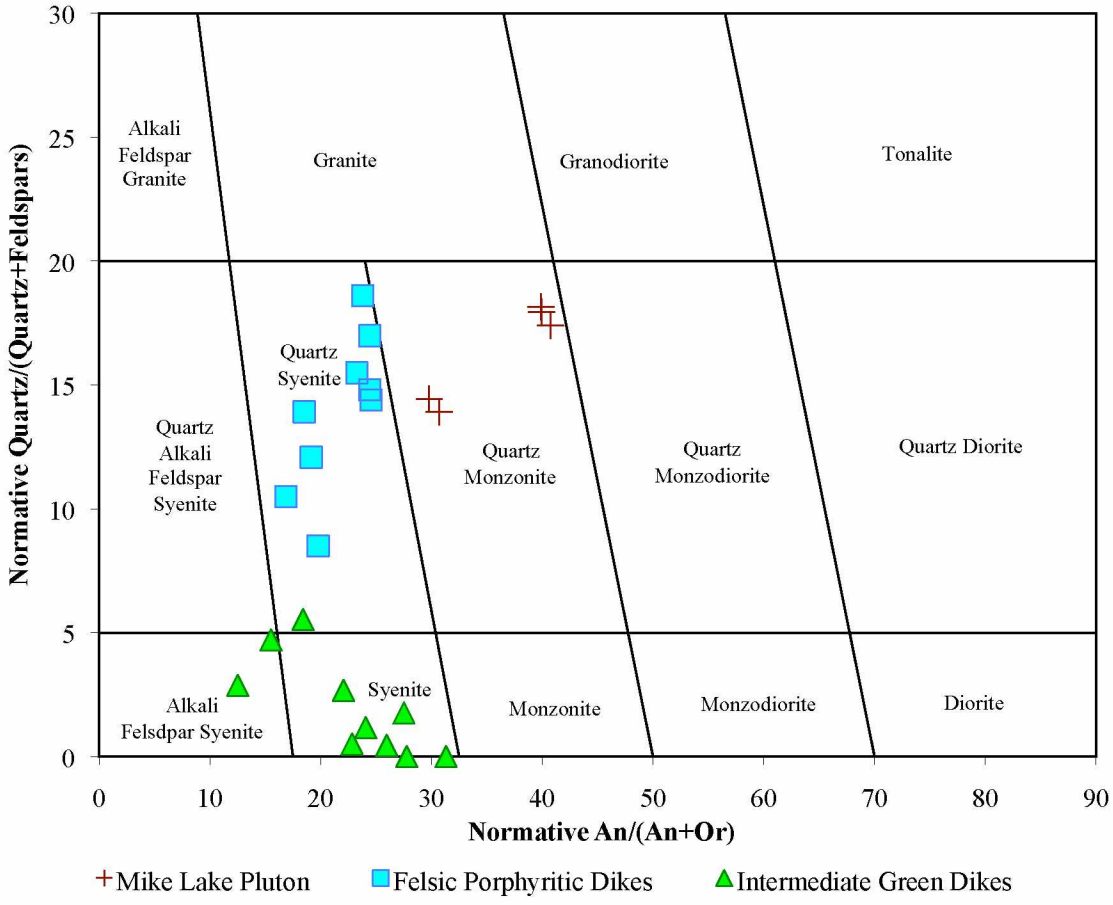

Figure 3.10. CIPW normative classification of least-altered igneous rocks.
Scheme based on the method of Strekeisen and LeMaitre (1979). Mafic sill samples were too altered to be included on this figure. An = anorthite, Or = orthoclase.

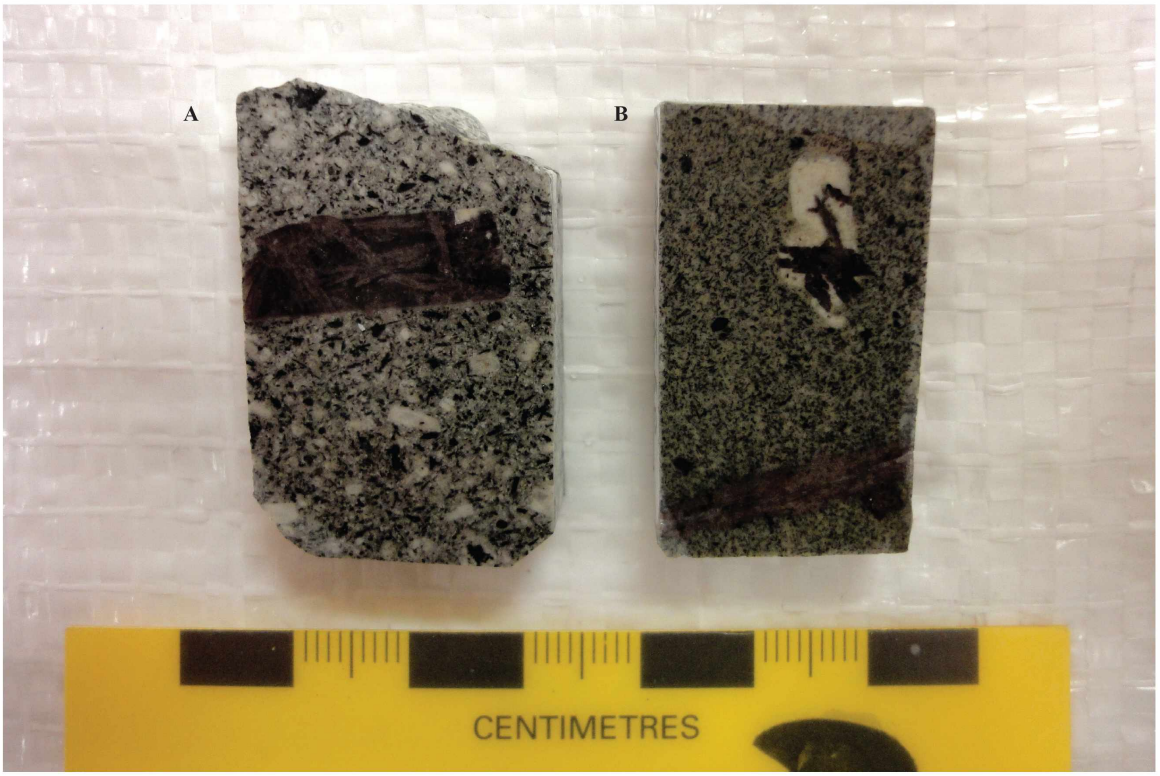

Figure 3.11. Axinite alteration in dikes.
A: complete replacement (pseudomorphism) of a feldspar in a felsic porphyritic dike. B: partial replacement of a feldspar and an axinite vein in an intermediate "green" dike sample.

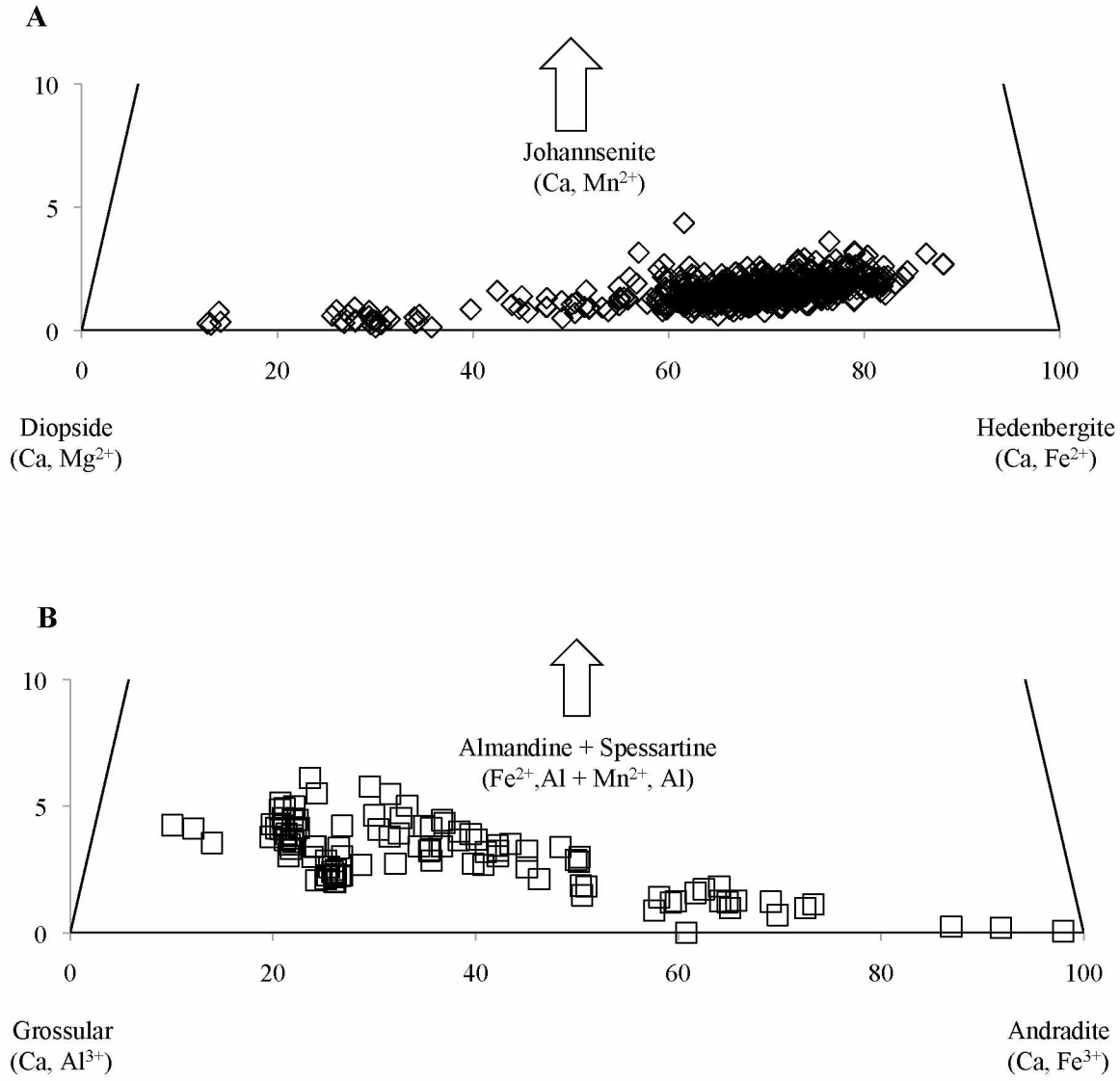

Figure 3.12. Skarn Ridge clinopyroxene and garnet compositions.
A: Clinopyroxene compositions expressed in terms of the end members diopside, hedenbergite, and johannseite, based on 504 microprobe analyses (this study). The compositional range Hd_{14}-Hd_{87}, with Hd_{60}-Hd_{80} most common. B: Skarn garnet compositions in terms of the end-members grossularite, andradite and almandine + spessartine, based on 107 microprobe analyses. Compositions range from Ad_8 to Ad_{98}.

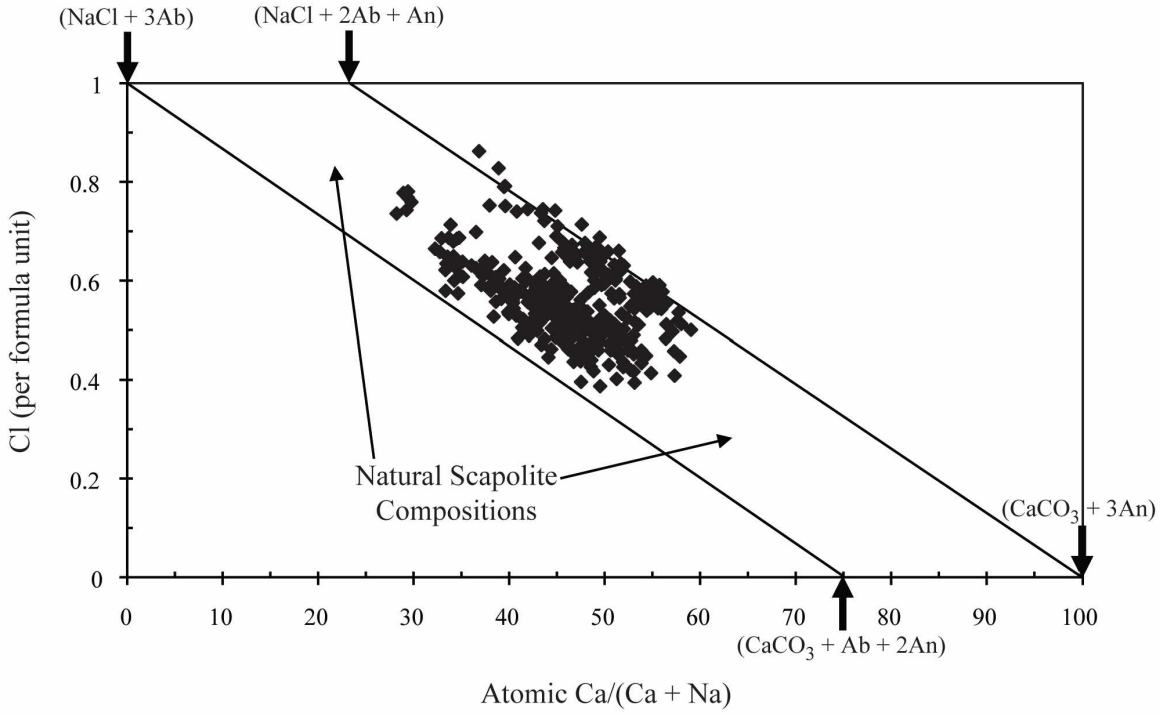

Figure 3.13. Skarn Ridge scapolite compositions.
Scapolite compositions are plotted within the limits of natural scapolite compositions, from Teertstra and Sherriff, (1997). Mineralogy is expressed in terms of the end members marialite (NaCl + 3Ab) and meionite ($CaCO_3$ + 3An).

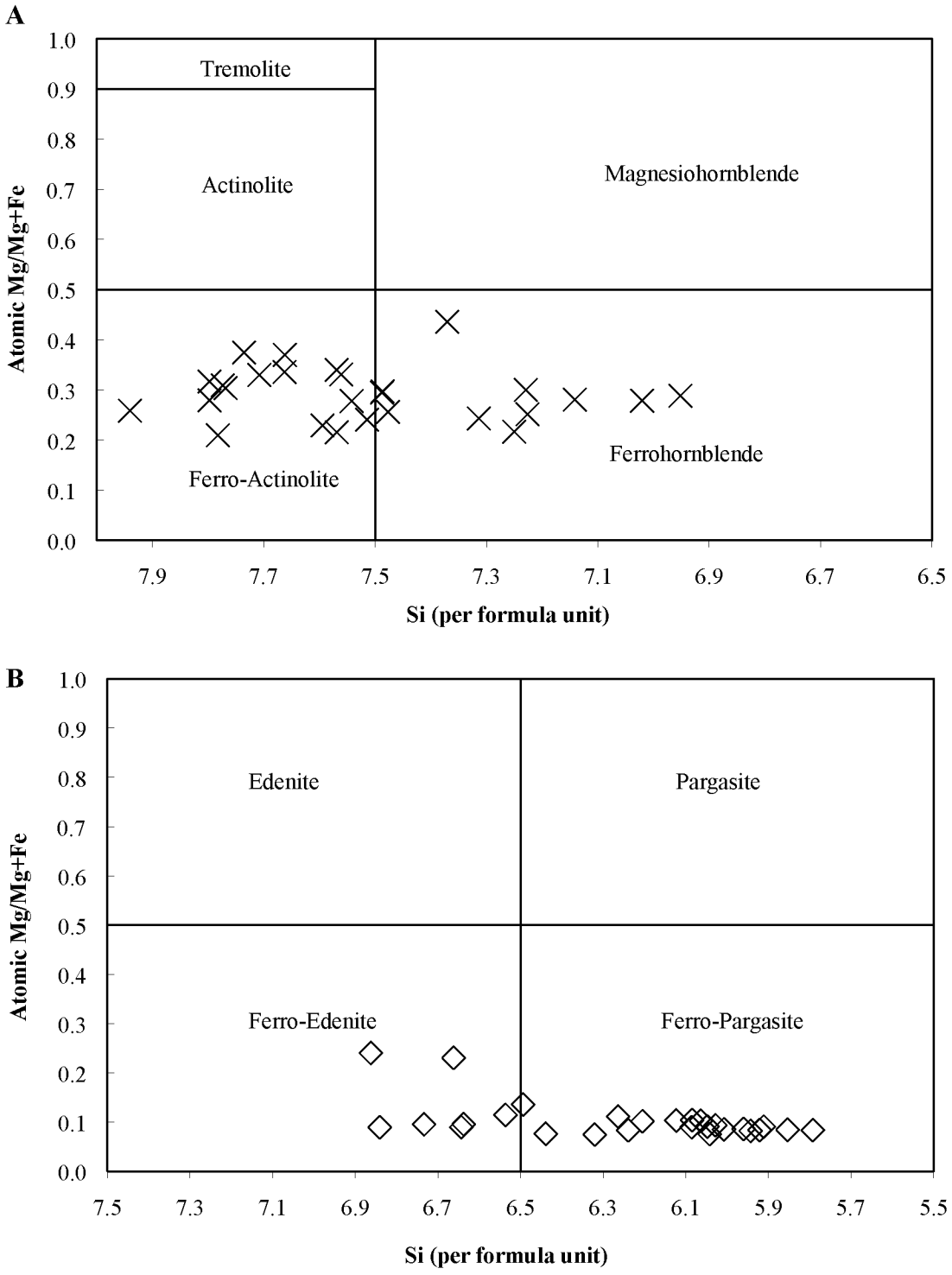

Figure 3.14. Amphibole compositions using the nomenclature of Leake et al. (1997). Parameters for A: Ca > 1.5 and (Na+K) < 0.5 per formula unit (pfu). Parameters for B: Ca > 1.5, (Na+K) > 0.5 pfu, and $^{VI}Al > Fe^{3+}$.

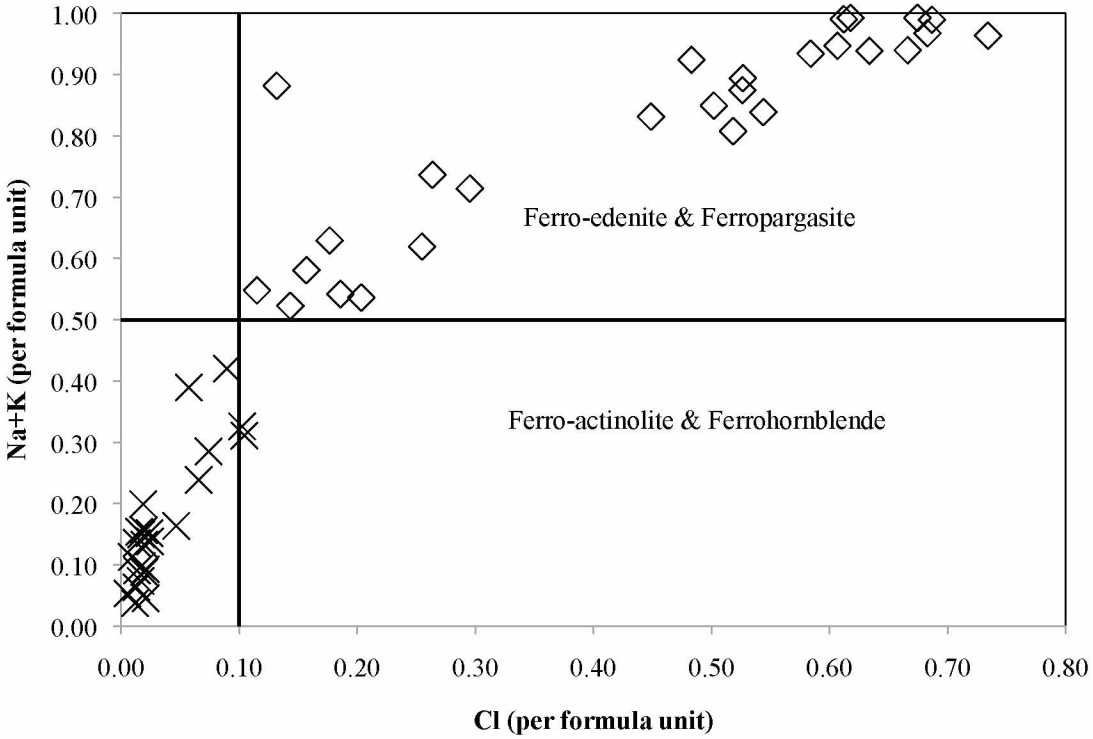

Figure 3.15. Cl vs. Na+K per formula unit for Mike Lake skarn amphiboles. Atomic Cl and Na+K are clearly proportional to each other, although such is not required by charge balance in the amphibole (Cl^- substitutes for OH^-). Vertical line at Cl = 0.1 pfu coincidentally separates low alkali from high alkali amphiboles. Nomenclature from Leake et al. (1997).

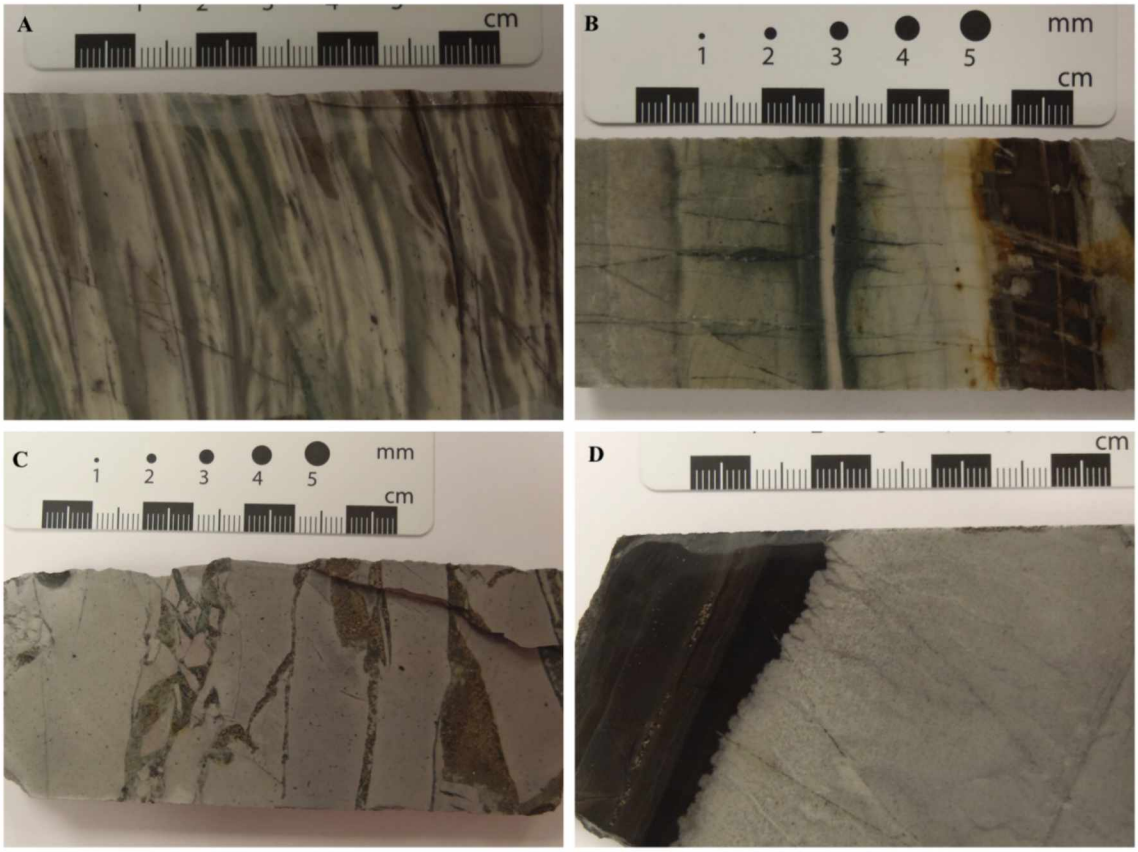

Figure 3.16. Skarn Ridge hornfelses.
A and B: typical calc-silicate hornfels showing banded appearance with alternating bands of green, cream, and purple-brown, C: gritty calc-silicate hornfels showing brittle deformation texture and pyrrhotite mineralization along fractures, D: black hornfels displaying bleaching; note how bleached hornfels can easily be confused with massive calc-silicate hornfels.

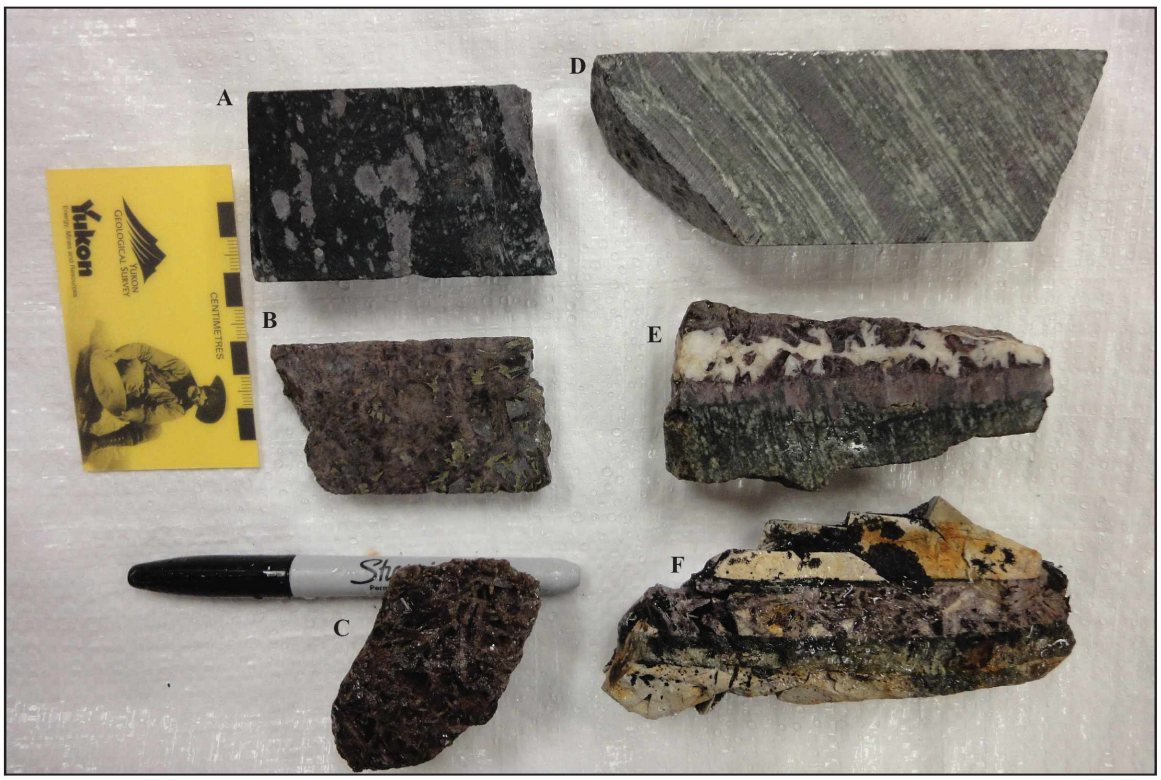

Figure 3.17. Axinite alteration in metamorphic rocks.
A: axinite "polka dots" in retrograde skarn. B and C: coarse grained, mineralized (chalcopyrite, arsenopyrite, scheelite) axinite veins intercepted in skarn. D: axinite replacement along bedding in calc-silicate hornfels. E and F: Axinite + calcite + scheelite + amphibole veins cutting across undifferentiated calc-silicate rocks. Axinite is the purple mineral.

Table 3.1 Average wt. % XRF compositions of igneous rocks from Skarn Ridge.

	Mike Lake Pluton	Porphyritic Dikes	Green Dikes	Mafic Sills
SiO_2	64.3	64.5	57.3	49.4
Al_2O_3	15.6	15.6	15.1	17.2
CaO	6.60	4.62	9.25	8.20
Na_2O	3.49	3.23	1.91	3.40
K_2O	4.32	6.03	7.04	3.85
MgO	1.81	1.40	2.66	4.65
FeO	2.45	3.26	4.72	7.36
TiO_2	0.49	0.49	0.72	2.5
MnO	0.049	0.067	0.12	0.067
P_2O_5	0.34	0.320	0.51	1.1
BaO	0.13	0.21	0.35	0.79
Cl	0.055	0.055	0.039	0.32
S	0.011	0.051	0.047	0.85
Cu	0.001	0.005	0.015	0.020
Total (%)	99.7	99.9	99.8	99.7

Table 3.2. Assay characteristics of Skarn Ridge mafic sills and adjacent rocks.

Hole ID	Depth (m)			%	Parts per Million					
(SK08-)	From	To	Lithology	Ti	Ba	Cr	Cu	Ni	P	V
003	8.00	10.00	Skarn	0.2	300	40	270	100	710	50
	10.00	12.00	Skarn	0.2	420	40	170	10	740	50
	12.00	14.00	Mafic	1.0	340	30	240	20	1600	160
	14.00	16.00	Mafic	1.7	2500	10	530	10	3180	220
	16.00	18.00	Mafic	1.6	3400	<10	260	<10	3810	180
	18.00	20.85	Mafic	1.9	2250	10	800	30	2570	330
	20.85	22.00	Skarn	0.3	270	30	1570	20	1370	60
	22.00	24.00	Skarn	0.2	770	30	1670	10	1120	40
012	5.90	8.00	Skarn & Hornfels	0.3	260	40	100	10	570	60
	8.00	9.65	Skarn & Hornfels	0.7	1280	50	10	10	1240	120
	9.65	11.58	Mafic	1.8	3310	10	90	10	2470	310
	11.58	13.00	Mafic	1.6	5800	<10	150	<10	3540	200
	13.00	14.63	Mafic	1.6	3720	40	240	80	3880	180
	14.63	16.10	Mafic	1.5	3330	<10	100	<10	3320	180
	16.10	17.11	Mafic	1.5	360	20	190	<10	3530	190
	17.11	18.32	Green Dike	1.1	3460	10	50	<10	2080	180
	18.32	20.00	Mafic	1.8	1910	10	290	10	2930	280
	20.00	22.63	Mafic	1.6	1310	20	160	10	2200	290
	22.63	24.00	Skarn & Hornfels	0.4	620	50	1550	10	910	80
	24.00	26.00	Skarn & Hornfels	0.3	390	40	4180	10	950	50
013	151.49	153.00	Skarn	0.2	<50	40	2500	20	1310	50
	153.00	155.31	Skarn	0.2	50	40	6270	30	990	50
	155.31	158.00	Mafic	0.6	140	20	760	10	1530	100
	158.00	160.63	Mafic	1.8	480	20	880	20	2700	320
	160.63	162.95	Mafic	1.7	560	40	970	30	2850	300
	162.95	165.45	Mafic	1.3	430	40	1660	30	2170	210
	165.45	167.02	Skarn & Hornfels	0.3	130	40	390	<10	790	60
	167.02	169.45	Skarn & Hornfels	0.3	160	40	300	<10	780	60
037	59.28	62.28	Skarn	0.3	<50	40	2940	10	1030	50
	62.28	64.44	Skarn	0.3	<50	40	1810	20	940	70
	64.44	67.44	Mafic	2.0	70	10	940	10	2630	270
	67.44	70.44	Mafic	2.1	240	<10	820	10	3090	280
	70.44	72.48	Mafic	2.0	160	20	990	70	2220	340
	72.48	75.48	Skarn	0.3	<50	40	560	10	920	50
	75.48	78.48	Skarn	0.3	50	40	320	20	750	50

3.6. References

Abbot, J.G., 1993, Revised stratigraphy and new exploration targets in the Hart River area, southeastern Yukon *in* Yukon Exploration and Geology, 1992: Exploration and Geological Services Division, Department of Indian and Northern Affairs Canada, p. 13-23.

Beane, R.E., 1974, Biotite stability in the porphyry copper environment: Economic Geology, v. 69, p. 241-256.

Bordin, D., Papageorge, M., and Kuran, D.L., 1998, Geological, Geochemical, and Geophysical Program on the Mike Lake Property: private report for Homestake Canada Inc.

Gordey, S.P., and Anderson, R.G., 1993. Evolution of the northern cordilleran miogeosyncline, Nahanni map area, Yukon and Northwest Territories: Geological Survey of Canada, Memoir 428.

Gordey, S.P., Wood, D., and Anderson, R.G., 1981, Stratigraphic framework of southeastern Selwyn Basin, Nahanni map area, Yukon Territory and District of Mackenzie *in* Current Research, Part A: Geological Survey of Canada, Paper 81-1A., 1981, p. 395-398.

Hart, C.J.R., 2007, Reduced Intrusion-Related Gold Systems *in* Goodfellow, W.D., ed, Mineral Deposits of Canada: A Synthesis of Major Deposit Types, District Metallogeny, the Evolution of Geological Provinces, and Exploration Methods: Geological Association of Canada, Mineral Deposits Division, Special Publication No. 5, p. 95-112.

Leake, B.E., Woolley, A.R., Arps, C.E.S., Birch, W.D., Gilbert, M.C., Grice, J.D., Hawthorne, F.C., Kato, A., Kisch, H.J., Krivovichev, V.G., Linthout, K., Laird, J., Mandarino, J.A., Maresch, W.V., Nickel, E.H., Rock, N.M.S., Schumacher, J.C., Smith, D.C., Stephenson, N.C.N., Ungaretti, L., Whittaker, E.J.W., and Youzhi, G., 1997, Nomenclature of amphiboles: Report of the Subcommittee on Amphiboles of the International Mineralogical Association, Commission on New Minerals and Mineral Names: American Mineralogist, v. 82, p. 1019–1037.

Lough, T.A., Freeman, L.K., Elliot, B.A., Griesel, G.A., Newberry, R.J., and Szumigala, D.J., 2012, Geochemical, major-oxide, minor-oxide, trace-element, and carbon data from rocks collected in 2011 in the Moran area, Tanana and Melozitna quadrangles, Alaska: Alaska Division of Geological & Geophysical Surveys Raw Data File 2011-4, v. 2, 176 p.

Lyons, P.C., 1971, Staining of feldspars on rock slab surfaces for modal analysis: Short Communications, Mineralogical Magazine, v. 38, p. 519.

Meschede, M., 1986, A method of discriminating between different types of mid-ocean ridge basalts and continental tholeiites with the Nb-Zr-Y diagram: Chemical Geology, v. 56, p. 207-218.

Mutschler, F.E., Rougon, D.J., Lavin, O.P., and Hughes, R.D., 1981, Petros – A data bank of major element chemical analyses of igneous rocks for research and teaching (Version 6.1): Boulder, Colorado, NOAA – National Geophysical and Solar-Terrestrial Data Center.

Streckeisen, A.L., 1974, Classification and Nomenclature of Plutonic Rocks, Recommendations of the IUGS Subcommission on the Systematics of Igneous Rocks: Geologische Rundschau. Internationale Zeitschrift für Geologie, Stuttgart, Germany, v. 63, p. 773-785.

Streckeisen, A.L., and Le Maitre, R.W., 1979, A chemical approximation to the modal QAPF classification of the igneous rocks: Neues Jahrbuch für Mineralogie, Abhandlungen, v. 136, p. 169-206.

Teertstra, D.K., and Sherriff, B.L., 1997, Substitutional mechanisms, compositional trends, and the end-member formulae of scapolite: Chemical Geology v. 136, p. 233-260.

Templemen-Kluit, D.J., 1980, Geology and Mineral deposits of southern Yukon *in* Yukon Geology and Exploration, 1979-80: Geology Section, Department of Indian and Northern Affairs, p. 7-31.

Wengzynowski, W.A., 2009, Assessment report describing geology, mineralization, and diamond drilling at the Mike Lake property: Archer Cathro & Associates (1981) Limited, 1844 p.

Winchester, J.A. and Floyd, P.A., 1977, Geochemical discrimination of different magma series and their differentiation products using immobile elements: Chemical Geology v. 20, p. 325-343.

3.7. Appendix

Table 3.A-1. Mafic sill compositions by XRF.

Sample ID	SK08-003	SK08-003	SK08-003	SK08-012	SK08-015	SK08-015	SK08-027	SK08-027
Depth (m)	15.50*	15.50**	16.15**	11.62**	31.40*	35.97**	12.00**	12.00**
SiO_2	49.1	52.1	52.5	49.0	47.9	46.0	49.3	49.6
Al_2O_3	16.0	17.7	17.9	17.4	16.7	17.0	17.1	17.4
CaO	10.6	9.24	10.3	4.73	5.46	7.50	8.90	8.89
Na_2O	3.67	3.16	3.08	3.75	4.80	2.90	2.95	2.85
K_2O	2.61	4.28	3.99	5.04	3.01	4.20	3.88	3.75
MgO	3.75	3.36	3.29	3.40	4.51	7.20	5.73	5.92
FeO	7.16	4.60	4.53	9.55	11.2	8.80	6.51	6.50
TiO_2	2.51	2.53	1.86	2.69	2.91	2.70	2.58	2.60
MnO	0.06	0.06	0.07	0.06	0.10	0.04	0.08	0.08
P_2O_5	1.28	1.43	0.98	1.03	1.14	0.76	1.00	0.84
BaO	0.27	0.49	0.57	2.60	1.09	0.47	0.46	0.41
Oxide Total (%)	97.0	98.9	99.1	99.3	98.8	97.6	98.5	98.8
As	0.032	-	-	-	-	-	-	-
Au	-	-	-	-	-	-	-	-
Br	0.005	0.003	0.002	-	-	-	0.002	-
Ce	0.013	-	-	-	0.012	-	-	-
Cl	0.719	0.305	0.263	0.295	0.476	0.100	0.232	0.194
Co	0.002	-	-	-	0.009	-	-	-
Cr	0.002	-	-	-	0.003	-	0.001	-
Cs	-	-	-	-	-	-	-	-
Cu	0.039	0.007	0.018	0.014	0.001	0.058	0.011	0.008
F	0.386	-	-	-	-	0.550	0.730	0.557
Ga	0.002	-	0.003	-	0.003	0.001	0.002	-
La	-	-	-	-	-	-	-	-
Mo	-	-	-	-	-	-	-	-
Nb	0.007	0.006	0.007	0.005	0.007	0.006	0.005	0.005
Ni	0.005	-	-	-	0.004	0.003	0.004	-
Pb	0.005	-	0.004	-	0.001	0.004	0.003	-
Rb	0.015	0.026	0.022	0.036	0.017	0.035	0.035	0.040
S	1.65	0.648	0.537	0.597	0.582	2.20	0.325	0.282
Sb	0.002	-	-	-	-	-	-	-
Sn	0.003	-	-	-	-	0.004	0.007	0.005
Sr	0.061	0.077	0.079	0.073	0.068	0.049	0.072	0.072
Th	-	-	-	-	-	-	-	-
U	0.001	-	-	-	-	-	-	-
V	0.029	-	-	-	0.037	0.049	0.041	-
W	0.009	-	-	-	0.001	-	-	-
Y	0.003	0.003	0.002	0.004	0.003	0.003	0.003	0.003
Zn	0.008	0.005	0.018	0.004	0.006	0.006	0.008	0.008
Zr	0.026	0.030	0.033	0.027	0.031	0.027	0.021	0.025

- element not detected.

* Pressed pellet XRF analysis

** Slab XRF analysis

Table 3.A-2. Green dike compositions by XRF.

Sample ID	SK08-008	SK08-008	SK08-008	SK08-008	SK08-008	SK08-008	SK08-008	Float-1	Bueno-1	Bueno-2
Depth (m)	12.45*	55.60**	114.80*	189.00**	192.00*	192.00**	194.16**	Surface**	Surface**	Surface**
SiO_2	57.3	59.8	60.8	58.1	54.3	53.8	58.0	56.9	57.1	57.0
Al_2O_3	14.2	15.9	15.5	16.0	14.2	14.9	16.1	14.5	14.8	14.9
CaO	9.15	7.47	6.54	9.58	10.40	11.10	8.60	8.75	10.60	10.35
Na_2O	0.59	0.96	2.65	2.34	2.38	2.49	2.35	1.11	1.99	2.23
K_2O	8.42	10.30	7.53	6.87	5.37	5.22	7.10	7.47	6.05	6.08
MgO	1.47	1.00	1.79	2.18	4.53	4.14	2.25	3.18	3.06	2.99
FeO	6.33	2.88	3.47	3.15	6.18	6.08	3.80	6.00	4.69	4.65
TiO_2	0.89	0.59	0.64	0.65	0.93	0.83	0.68	0.72	0.64	0.65
MnO	0.29	0.09	0.08	0.09	0.11	0.11	0.10	0.11	0.11	0.11
P_2O_5	0.50	0.36	0.44	0.56	0.75	0.70	0.52	0.44	0.43	0.51
BaO	0.56	0.50	0.26	0.33	0.24	0.28	0.30	0.45	0.31	0.31
Oxide Total (%)	99.7	99.8	99.7	99.9	99.4	99.7	99.8	99.6	99.8	99.7
As	–	–	0.006	–	0.001	–	–	–	–	0.002
Au	–	–	–	–	0.002	–	–	–	–	–
Ce	0.020	–	0.024	–	0.015	–	–	–	–	0.038
Cl	0.047	0.027	0.036	0.022	0.073	0.046	0.031	0.060	0.015	0.039
Co	–	–	–	–	–	–	–	–	–	0.006
Cr	0.004	–	0.007	0.008	0.014	0.018	0.009	0.025	0.020	0.018
Cs	–	–	–	–	–	–	–	–	–	–
Cu	–	–	0.041	–	0.013	0.006	–	–	0.004	0.010
F	0.038	–	–	–	0.282	–	–	0.155	0.010	0.010
Ga	0.001	–	0.002	–	0.003	–	–	0.002	0.002	0.002
La	0.007	–	0.015	–	0.011	–	–	–	–	–
Mo	–	–	–	–	–	–	–	–	–	0.001
Nb	0.004	0.002	0.002	0.002	0.002	0.002	0.002	0.002	0.002	0.002
Ni	0.005	–	0.004	–	0.007	–	–	0.004	0.005	0.004
Pb	0.002	–	0.005	–	0.003	–	–	0.003	0.003	0.002
Rb	0.039	0.051	0.036	0.038	0.031	0.032	0.037	0.035	0.031	0.027
S	0.006	0.073	0.046	0.054	0.086	0.109	0.064	0.010	0.006	0.013
Sb	–	–	–	–	–	–	–	–	–	–
Sn	0.029	0.005	0.007	0.005	0.004	–	0.006	0.025	0.005	0.005
Sr	0.043	0.066	0.049	0.080	0.079	0.084	0.068	0.062	0.062	0.061
Th	0.003	–	0.003	–	0.003	–	–	0.002	0.002	0.002
U	0.002	–	0.002	–	–	–	–	0.001	–	–
V	0.021	–	0.009	–	0.021	–	–	0.019	0.017	0.018
W	0.001	–	0.006	–	0.001	–	–	–	–	–
Y	0.004	0.004	0.003	0.003	0.004	0.004	0.004	0.004	0.003	0.004
Zn	0.005	–	0.007	–	0.005	0.004	0.005	0.006	0.004	0.003
Zr	0.029	0.026	0.024	0.025	0.024	0.024	0.026	0.025	0.025	0.025

– element not detected.

* Pressed pellet XRF analysis

** Slab XRF analysis

Table 3.A-3. Felsic (porphyritic) dike compositions by XRF.

Sample ID	SK08-003	SK08-004	SK08-008	SK08-008	SK08-015	SK08-015	SK08-025	SK08-027	SK08-027
Depth (m)	82.50**	241.00*	110.10*	114.80**	82.50*	82.50**	75.50*	45.90**	46.00*
SiO_2	65.9	64.3	65.7	62.4	62.8	66.0	63.6	65.3	64.5
Al_2O_3	15.6	15.5	15.7	15.8	15.5	15.0	15.9	15.6	15.9
CaO	4.29	4.59	3.81	5.87	5.40	4.40	5.12	4.14	3.92
Na_2O	3.31	3.42	3.61	2.96	2.94	3.30	2.71	3.28	3.50
K_2O	5.70	5.53	5.61	6.76	4.89	5.40	7.52	6.48	6.35
MgO	1.23	1.45	1.34	1.65	2.17	1.30	1.19	1.19	1.19
FeO	2.76	3.62	2.93	3.22	4.87	3.50	2.54	2.73	3.19
TiO_2	0.43	0.53	0.42	0.52	0.56	0.55	0.53	0.40	0.50
MnO	0.05	0.06	0.06	0.05	0.11	0.06	0.07	0.06	0.09
P_2O_5	0.31	0.35	0.26	0.32	0.32	0.31	0.34	0.32	0.36
BaO	0.22	0.19	0.19	0.25	0.17	0.20	0.27	0.23	0.21
Oxide Total (%)	99.8	99.5	99.6	99.8	99.7	100.0	99.7	99.7	99.7
As	–	0.001	0.002	0.001	–	–	0.003	–	–
Au	–	–	–	–	–	–	–	–	–
Br	–	–	–	–	–	–	–	–	–
Ce	–	0.023	–	–	0.010	–	0.016	–	0.019
Cl	0.033	0.083	0.076	0.017	0.112	0.043	0.047	0.024	0.058
Co	–	–	–	–	–	–	–	–	–
Cr	–	0.003	0.003	–	0.006	–	0.006	–	0.006
Cs	–	–	–	–	–	–	–	–	–
Cu	–	0.001	0.005	0.017	0.003	–	0.002	–	–
F	–	0.148	0.073	–	0.021	–	0.073	–	0.074
Ga	–	0.002	0.002	0.003	0.002	–	0.002	0.002	0.002
La	–	–	–	–	–	–	0.008	–	0.007
Mo	–	–	–	–	–	–	–	–	–
Nb	0.001	0.002	0.002	0.002	0.001	0.002	0.002	0.002	0.002
Ni	–	0.003	0.004	0.007	0.004	–	0.003	–	0.002
Pb	–	0.005	0.007	0.007	0.004	0.009	0.004	–	0.003
Rb	0.028	0.026	0.024	0.033	0.023	0.028	0.032	0.033	0.028
S	0.078	0.034	0.103	0.033	0.029	0.036	0.019	0.083	0.045
Sb	–	–	–	–	–	–	–	–	–
Sn	–	0.003	0.002	0.006	–	–	0.006	–	0.003
Sr	0.079	0.082	0.072	0.051	0.075	0.084	0.061	0.070	0.069
Th	–	0.002	0.003	–	0.002	–	0.002	–	0.003
U	–	0.001	–	–	0.001	–	–	–	–
V	–	0.011	0.008	–	0.013	–	0.010	–	0.009
W	–	0.001	0.003	–	0.001	–	0.006	–	0.001
Y	0.003	0.002	0.002	–	0.003	0.003	0.003	–	0.002
Zn	0.004	0.006	0.007	0.003	0.007	0.006	0.003	0.003	0.003
Zr	0.019	0.022	0.019	0.020	0.016	0.024	0.021	0.021	0.022

–element not detected.
* Pressed pellet XRF analysis
** Slab XRF analysis

Table 3.A-4. Xenolith compositions by XRF.

Sample ID	SK08-004	SK08-015
Depth (m)	248.00*	84.73*
SiO_2	53.6	58.6
Al_2O_3	14.8	15.6
CaO	9.71	7.50
Na_2O	3.40	3.25
K_2O	1.91	5.00
MgO	5.15	2.28
FeO	8.86	5.47
TiO_2	0.79	0.73
MnO	0.24	0.09
P_2O_5	0.47	0.52
BaO	0.08	0.18
Oxide Total (%)	99.0	99.2
As	0.007	0.002
Au	-	-
Br	0.004	-
Ce	0.005	0.016
Cl	0.630	0.118
Co	0.000	-
Cr	0.016	0.003
Cs	-	0.013
Cu	0.010	0.003
F	0.039	0.298
Ga	0.002	0.002
La	-	0.009
Mo	-	-
Nb	0.001	0.003
Ni	0.005	0.003
Pb	0.007	0.007
Rb	0.009	0.031
S	0.103	0.069
Sb	-	-
Sn	-	0.005
Sr	0.071	0.102
Th	0.001	0.004
U	0.001	0.003
V	0.022	0.016
W	0.001	0.001
Y	0.002	0.004
Zn	0.008	0.010
Zr	0.010	0.031

- element not detected.

* Pressed pellet XRF analysis

Table 3.A-5. Mike Lake pluton compositions by XRF.

Sample ID	MLP-1	MLP-2	MLP-3	MLP-4	MLP-5
Depth (m)	Surface*	Surface*	Surface*	Surface*	Surface*
SiO_2	64.8	65.0	64.9	63.3	63.4
Al_2O_3	15.8	15.6	15.6	15.7	15.5
CaO	7.01	6.97	7.00	6.05	5.98
Na_2O	3.80	3.73	3.77	3.04	3.13
K_2O	3.72	3.75	3.72	5.23	5.17
MgO	1.63	1.59	1.59	2.19	2.05
FeO	2.06	2.08	2.08	2.94	3.09
TiO_2	0.44	0.45	0.46	0.55	0.56
MnO	0.04	0.04	0.04	0.06	0.06
P_2O_5	0.32	0.34	0.35	0.35	0.35
BaO	0.11	0.11	0.11	0.16	0.16
Oxide Total (%)	99.7	99.7	99.6	99.6	99.4
As	0.032	0.032	0.034	0.012	0.014
Au	-	-	-	-	-
Br	-	-	-	-	-
Ce	-	-	-	-	-
Cl	0.038	0.020	0.024	0.113	0.081
Co	-	-	-	-	-
Cr	0.006	0.007	0.006	0.007	0.009
Cs	-	-	-	-	-
Cu	0.000	0.000	0.000	0.002	0.001
F	0.082	0.009	0.050	0.123	0.176
Ga	0.002	0.003	0.002	0.002	0.002
La	-	-	-	-	-
Mo	0.001	0.001	0.001	-	0.000
Nb	0.002	0.002	0.002	0.002	0.002
Ni	0.003	0.004	0.004	0.004	0.004
Pb	0.003	0.003	0.003	0.005	0.006
Rb	0.015	0.015	0.016	0.020	0.022
S	0.012	0.012	0.012	0.013	0.006
Sb	-	-	-	-	-
Sn	0.004	0.004	0.003	0.003	0.004
Sr	0.066	0.066	0.067	0.072	0.071
Th	0.003	0.003	0.003	0.003	0.003
U	0.001	0.000	0.001	0.000	0.000
V	0.010	0.009	0.009	0.011	0.013
W	0.001	-	-	-	0.001
Y	0.003	0.003	0.003	0.003	0.003
Zn	0.003	0.003	0.004	0.005	0.006
Zr	0.015	0.015	0.015	0.012	0.015

- element not detected.

* Pressed pellet XRF analysis

Table 3.A-6. Calc-silicate hornfels analyses by XRF.

Sample ID	SK07-001	SK08-004	SK08-004	SK08-004	SK08-011	SK08-011
Depth	106.34	92.97	225.00	225.00	110.64	111.50
SiO_2	57.0	86.1	65.5	81.9	67.4	69.7
Al_2O_3	14.2	6.89	9.59	7.65	13.7	3.85
CaO	9.49	0.75	7.56	2.19	11.0	20.0
Na_2O	0.83	0.30	1.24	1.26	2.00	0.60
K_2O	8.10	5.21	3.66	1.73	0.13	0.35
MgO	2.91	-	5.50	1.94	1.32	1.32
FeO	5.74	-	4.42	2.25	2.56	2.98
TiO_2	0.68	0.45	1.19	0.55	1.56	0.31
MnO	-	-	0.08	0.04	0.10	0.26
P_2O_5	0.22	-	0.34	0.18	-	0.32
BaO	0.61	0.20	0.24	0.17	0.04	0.04
Oxide Total (%)	99.8	99.9	99.3	99.9	99.8	99.7
As	0.009	-	-	-	-	-
Br	-	-	-	-	-	-
Ce	-	0.079	-	-	-	0.014
Cl	0.048	-	0.053	0.086	-	0.029
Cr	-	-	-	0.004	-	-
Cs	-	-	-	-	-	-
Cu	-	-	0.003	-	-	-
F	-	-	0.385	-	-	-
Ga	-	-	-	0.001	-	-
Nb	-	-	0.003	0.001	-	0.001
Ni	-	-	-	0.003	-	0.003
Pb	-	-	-	-	-	-
Rb	0.041	0.020	0.015	0.009	-	0.003
S	0.019	-	0.201	0.044	0.038	0.215
Sb	-	-	-	-	-	-
Sn	0.077	-	-	-	-	-
Sr	0.045	0.017	0.022	0.020	0.050	0.029
V	-	-	-	-	-	-
Y	0.004	-	0.003	0.001	-	-
Zn	-	0.010	0.006	0.004	-	0.003
Zr	-	0.002	0.031	0.009	0.033	0.004

Table 3.A-7. Miscellaneous metamorphic rock analyses by XRF.

	Grit		Black Hornfels
Sample ID	SK08-011	SK08-011	SK08-004
Depth	101.10	101.12	92.97
SiO2	79.0	78.1	81.3
Al2O3	5.13	5.33	8.05
CaO	7.95	8.06	2.18
Na2O	1.75	1.78	1.23
K2O	0.14	0.18	2.41
MgO	1.23	1.37	1.83
FeO	2.90	3.11	1.79
TiO2	1.14	1.16	0.51
MnO	0.09	0.09	-
P2O5	0.20	0.23	-
BaO	-	-	0.15
Oxide Total (%)	99.5	99.4	99.4
As	-	-	-
Br	0.003	0.003	-
Ce	-	-	-
Cl	0.398	0.409	-
Cr	0.010	0.011	-
Cs	0.006	0.015	-
Cu	-	-	-
F	-	-	-
Ga	0.000	-	-
Nb	0.002	0.002	-
Ni	-	-	-
Pb	0.002	-	-
Rb	0.001	0.001	0.013
S	0.004	0.051	0.469
Sb	-	-	-
Sn	0.007	0.006	-
Sr	0.011	0.012	0.023
V	0.014	0.013	0.033
Y	0.003	0.001	-
Zn	0.003	0.004	-
Zr	0.011	0.011	0.009

Table 3.A-8. Clinopyroxene compositions by EMPA.

Sample ID	Depth (m)	SiO_2	Al_2O_3	CaO	MgO	FeO	MnO	Total	%Hd	%Jo	%Di
SK05-001	375.00	54.3	0.37	25.6	15.5	4.04	0.10	100.1	12.7	0.3	87.0
		54.6	0.72	25.4	15.3	4.10	0.08	100.3	13.1	0.3	86.7
		54.4	0.39	25.6	15.3	4.32	0.27	100.3	13.6	0.9	85.5
		54.4	0.39	25.4	15.5	4.50	0.13	100.4	14.0	0.4	85.6
SK05-002	84.00	50.3	0.48	23.3	6.33	18.0	0.75	99.2	59.8	2.5	37.6
		50.6	0.22	23.1	5.65	19.4	0.69	99.8	64.3	2.3	33.3
		51.2	0.40	23.8	6.74	17.8	0.75	100.7	58.2	2.5	39.3
		50.5	0.18	23.4	5.07	19.0	0.67	98.8	66.2	2.4	31.4
		50.3	0.30	23.4	4.75	19.8	0.80	99.5	68.0	2.8	29.2
		51.0	0.13	23.5	4.88	20.2	0.88	100.6	67.8	3.0	29.2
		50.2	0.52	22.9	6.61	16.9	0.37	97.5	58.1	1.3	40.6
		51.4	0.41	23.9	6.92	16.5	1.07	100.2	55.1	3.6	41.2
		50.7	0.64	23.1	6.20	18.8	0.65	100.3	61.6	2.2	36.3
SK05-002	87.00	51.7	1.38	24.2	12.3	9.38	0.13	99.4	29.9	0.4	69.7
		50.0	0.08	23.7	6.08	19.3	0.63	99.9	62.7	2.1	35.2
		49.4	0.25	23.2	5.85	20.1	0.81	99.6	64.1	2.6	33.3
		49.4	0.33	23.4	5.51	20.2	0.82	99.8	65.5	2.7	31.8
		48.5	5.37	22.4	4.59	17.9	0.78	99.8	66.6	3.0	30.5
		48.3	0.53	23.0	6.33	19.2	0.79	98.4	61.4	2.5	36.1
		48.5	0.30	23.2	5.60	20.3	0.68	98.5	65.6	2.2	32.2
		48.7	0.28	23.1	5.70	19.9	0.64	98.5	64.8	2.1	33.0
		48.6	0.30	23.2	6.39	19.5	0.54	98.6	62.0	1.7	36.2
		48.1	0.37	22.3	5.08	19.0	0.59	95.6	66.3	2.1	31.6
		49.3	1.68	21.6	5.08	18.9	0.39	97.0	66.6	1.4	32.0
		48.0	1.05	22.6	5.49	19.3	0.72	97.4	64.7	2.5	32.8
		48.6	1.18	22.6	5.38	18.8	0.65	97.5	64.8	2.3	33.0
		49.2	0.53	24.1	7.06	16.1	0.72	98.0	54.8	2.5	42.7
		49.2	0.26	23.4	6.21	18.8	0.64	98.6	61.6	2.1	36.3
		50.1	0.61	23.8	7.98	15.2	0.55	98.2	50.6	1.9	47.5
SK07-001	Surface	48.7	0.08	23.5	5.36	19.4	0.56	97.6	65.7	1.9	32.3
		48.3	0.31	23.4	4.04	21.3	0.49	98.0	73.4	1.7	24.9
		48.7	0.18	23.7	5.27	19.6	0.44	98.1	66.6	1.5	31.9
		49.0	0.15	23.6	5.15	20.6	0.49	99.1	68.0	1.6	30.4
		49.7	0.14	23.4	6.13	18.2	0.53	98.1	61.4	1.8	36.8
		49.7	0.13	23.3	5.57	19.0	0.50	98.4	64.6	1.7	33.7
		48.6	0.46	23.3	3.54	22.3	0.63	98.7	76.2	2.2	21.6
		47.1	0.13	23.3	4.64	21.2	0.56	97.0	70.5	1.9	27.6
		47.6	0.21	23.8	4.78	20.2	0.37	97.3	69.5	1.3	29.3
		47.9	0.32	23.1	4.44	21.2	0.52	97.5	71.6	1.8	26.7
		47.8	0.13	23.5	5.12	20.3	0.55	97.7	67.8	1.8	30.4
		48.2	0.18	23.6	5.05	20.2	0.62	97.9	67.7	2.1	30.2
		49.2	0.16	23.6	5.37	20.2	0.53	99.0	66.6	1.8	31.6
		47.9	0.20	23.4	5.35	18.5	0.57	96.1	64.6	2.0	33.4

		48.0	0.18	23.3	5.24	20.4	0.33	97.5	67.8	1.1	31.1
		48.2	0.19	23.8	5.07	19.7	0.52	97.5	67.3	1.8	30.9
		48.1	0.23	23.5	4.30	21.4	0.43	97.9	72.5	1.5	26.0
		48.4	0.11	23.6	4.38	21.4	0.39	98.3	72.3	1.3	26.4
		48.8	0.10	23.3	5.00	21.2	0.64	99.0	68.9	2.1	29.0
		49.6	0.07	23.9	6.02	18.9	0.43	98.9	62.9	1.4	35.6
SK07-001	3.00	48.8	0.25	23.4	3.88	22.4	0.59	99.3	74.9	2.0	23.1
		50.3	0.09	23.5	5.25	19.9	0.33	99.4	67.2	1.1	31.7
		49.8	0.14	23.2	5.01	20.7	0.64	99.7	68.3	2.2	29.5
		49.7	0.09	23.5	5.47	21.1	0.50	100.2	67.3	1.6	31.1
		50.3	0.13	23.7	6.04	20.1	0.36	100.8	64.3	1.2	34.5
		50.2	0.11	23.6	5.85	19.1	0.41	99.5	63.8	1.4	34.8
		49.7	0.09	23.4	5.16	21.4	0.48	100.2	68.8	1.6	29.6
		50.6	0.14	23.7	6.14	19.8	0.54	101.1	63.3	1.7	35.0
		48.2	0.10	23.2	5.19	21.4	0.59	98.9	68.5	1.9	29.6
		48.3	0.18	23.5	4.80	22.0	0.57	99.3	70.6	1.9	27.5
		49.1	0.21	23.2	4.67	22.3	0.61	100.0	71.4	2.0	26.7
		49.6	0.16	23.2	5.05	21.4	0.54	100.2	69.2	1.8	29.1
		48.3	0.07	23.0	5.24	20.7	0.53	97.9	67.6	1.8	30.6
		48.8	0.22	23.5	7.21	18.6	0.38	98.9	58.5	1.2	40.3
		48.2	0.12	23.4	5.27	21.3	0.74	99.1	67.7	2.4	29.9
SK07-001	41.00	50.2	0.18	22.4	4.66	21.1	0.31	99.1	71.0	1.1	27.9
		50.4	0.23	23.2	3.77	21.5	0.43	99.6	75.0	1.5	23.5
		50.8	0.18	23.1	4.12	21.0	0.43	99.6	72.9	1.5	25.6
		49.8	0.21	23.1	3.31	22.8	0.41	99.8	78.3	1.4	20.3
		48.9	0.14	22.8	4.21	21.7	0.36	98.4	73.4	1.2	25.4
		49.9	0.31	22.7	4.92	20.6	0.40	99.0	69.2	1.4	29.4
		49.5	0.21	23.0	3.45	23.2	0.71	99.8	77.1	2.4	20.5
		46.6	0.28	22.3	4.61	21.8	0.64	96.5	71.1	2.1	26.8
		47.6	0.08	22.5	5.15	21.5	0.43	97.4	69.1	1.4	29.5
		47.6	0.25	22.6	4.65	22.1	0.45	97.8	71.6	1.5	26.9
		49.9	0.31	23.0	3.02	22.5	0.53	99.5	79.2	1.9	18.9
		49.3	0.17	22.9	3.77	22.9	0.53	99.7	75.9	1.8	22.3
		50.0	0.40	22.8	3.26	23.0	0.74	100.4	77.8	2.5	19.7
		50.1	0.21	23.2	2.97	24.4	0.64	101.7	80.4	2.1	17.5
		49.0	0.07	22.7	3.90	22.0	0.42	98.2	74.9	1.4	23.7
		51.1	0.09	23.3	5.23	19.2	0.60	99.6	65.9	2.1	32.1
SK07-001	43.00	49.5	0.29	23.1	3.44	21.3	0.75	98.3	75.5	2.7	21.8
		49.9	0.47	23.2	3.48	21.6	0.66	99.4	75.9	2.3	21.8
		49.8	0.19	22.7	3.02	23.4	0.64	99.7	79.5	2.2	18.3
		49.7	0.28	23.1	3.37	22.7	0.64	99.8	77.3	2.2	20.5
		50.1	0.03	23.1	4.13	20.8	0.46	98.7	72.7	1.6	25.7
		50.5	0.10	23.2	4.34	20.3	0.54	98.9	71.0	1.9	27.1
		50.0	0.09	23.3	3.60	22.8	0.61	100.4	76.4	2.1	21.5
		48.3	0.23	23.0	1.65	24.6	0.87	98.6	86.5	3.1	10.4
		50.0	0.22	23.3	3.41	21.2	0.55	98.7	76.1	2.0	21.9
		50.2	0.12	23.3	4.43	22.1	0.57	100.9	72.3	1.9	25.8

SK08-003	11.58	47.8	0.09	23.3	8.27	15.9	0.33	95.7	51.4	1.1	47.5
		47.9	0.17	23.4	8.45	16.0	0.34	96.2	50.9	1.1	48.0
		48.2	0.17	23.3	8.71	15.8	0.25	96.5	50.0	0.8	49.2
		48.4	0.09	23.2	8.28	16.8	0.33	97.1	52.7	1.1	46.2
		50.0	0.23	23.2	8.86	15.2	0.42	98.0	48.4	1.4	50.3
		50.0	0.18	23.3	8.29	17.2	0.29	99.4	53.4	0.9	45.7
		47.9	0.13	23.3	8.33	16.0	0.31	96.1	51.3	1.0	47.6
SK08-003	27.50	46.8	0.08	22.8	6.06	19.5	0.40	95.7	63.6	1.3	35.1
		47.4	0.80	23.1	5.72	19.2	0.39	96.6	64.4	1.3	34.3
		45.7	1.11	22.7	3.85	22.1	0.71	96.2	74.5	2.4	23.1
		46.6	1.09	22.8	3.57	23.0	0.72	97.8	76.4	2.4	21.1
		49.1	0.09	23.1	6.42	19.1	0.55	98.4	61.4	1.8	36.8
		49.5	0.13	23.2	6.46	19.6	0.67	99.6	61.7	2.1	36.2
		48.3	0.33	22.8	5.31	20.6	0.65	97.9	67.1	2.1	30.8
		49.0	0.18	22.7	5.18	20.8	0.66	98.5	67.7	2.2	30.1
		49.8	0.09	22.7	5.72	20.3	0.61	99.3	65.3	2.0	32.7
SK08-003	52.50	47.2	0.33	24.1	5.58	20.4	0.44	98.0	66.2	1.5	32.3
		47.0	0.36	22.4	5.48	19.8	0.47	95.5	65.9	1.6	32.5
		47.2	0.33	22.6	5.38	19.9	0.46	95.8	66.4	1.6	32.0
SK08-003	66.10	50.1	0.09	23.7	4.27	20.6	0.51	99.3	71.7	1.8	26.5
		49.8	0.11	23.2	2.84	23.5	0.52	100.0	80.8	1.8	17.4
		50.3	0.22	23.4	3.73	22.2	0.59	100.4	75.4	2.0	22.5
		50.6	0.08	23.7	4.74	21.3	0.45	100.9	70.5	1.5	28.0
		49.9	0.04	23.4	2.81	24.2	0.75	101.1	80.8	2.5	16.7
		50.4	0.23	23.3	2.37	24.8	0.82	101.9	83.0	2.8	14.2
		49.5	-0.04	23.5	5.05	20.1	0.35	98.4	68.2	1.2	30.6
		49.3	0.13	23.8	4.24	22.6	0.60	100.6	73.5	2.0	24.6
		48.4	0.10	23.5	4.32	20.3	0.47	97.1	71.3	1.7	27.0
		48.4	0.11	23.7	4.43	20.9	0.60	98.2	71.1	2.1	26.8
		49.0	0.14	23.8	4.17	21.6	0.46	99.1	73.2	1.6	25.2
		48.9	0.17	23.6	4.30	21.8	0.55	99.2	72.6	1.8	25.5
		49.3	0.21	23.5	4.29	21.5	0.67	99.5	72.1	2.3	25.6
		49.6	0.24	23.9	4.45	20.6	0.71	99.6	70.4	2.5	27.1
		50.5	0.26	24.0	5.50	19.8	0.55	100.6	65.7	1.8	32.5
		50.0	0.25	23.6	3.88	22.9	0.49	101.1	75.6	1.6	22.8
		48.8	0.11	23.3	2.40	24.0	0.71	99.3	82.7	2.5	14.8
		49.2	0.15	23.3	2.56	24.0	0.63	99.9	82.1	2.2	15.7
		49.2	0.13	23.3	2.94	24.2	0.59	100.4	80.6	2.0	17.5
		49.9	0.08	23.5	3.05	23.6	0.65	100.7	79.5	2.2	18.3
		49.8	0.06	23.6	3.05	24.0	0.60	101.0	79.8	2.0	18.2
		49.8	0.12	23.3	2.94	24.8	0.63	101.6	80.8	2.1	17.1
		48.3	0.17	23.6	4.31	20.1	0.66	97.1	70.6	2.3	27.1
		48.5	0.33	23.8	6.04	18.8	0.43	97.9	62.7	1.5	35.8
		48.5	0.06	23.6	4.75	20.5	0.44	97.9	69.7	1.5	28.8
		47.9	0.47	23.3	3.58	22.4	0.82	98.4	75.6	2.8	21.6
		48.2	0.04	23.6	4.47	22.2	0.65	99.2	72.0	2.1	25.8
SK08-004	188.50	49.1	0.06	22.5	4.57	20.2	0.64	97.0	69.7	2.2	28.1

		50.1	0.10	22.7	5.25	19.2	0.36	97.7	66.4	1.3	32.3
		50.1	0.12	23.0	5.30	19.3	0.53	98.3	65.9	1.8	32.2
		49.4	0.11	23.0	5.94	18.1	0.49	97.0	62.0	1.7	36.3
		50.0	0.10	23.4	5.44	18.4	0.50	97.7	64.3	1.8	33.9
		49.8	0.07	22.9	4.43	20.1	0.52	97.8	70.5	1.9	27.7
		50.1	0.07	23.0	5.17	19.5	0.61	98.5	66.5	2.1	31.4
		48.1	0.35	22.9	3.12	22.0	0.71	97.1	77.8	2.5	19.7
		48.9	0.10	22.7	4.84	20.8	0.57	97.9	69.3	1.9	28.8
		50.1	0.11	22.0	4.87	19.5	0.47	97.1	68.1	1.7	30.3
		49.5	0.10	23.1	4.72	19.7	0.58	97.7	68.7	2.1	29.3
		49.9	0.38	22.5	4.53	20.3	0.64	98.3	70.0	2.2	27.8
		50.5	0.11	23.2	5.07	19.5	0.57	98.9	67.0	2.0	31.0
SK08-004	72.40	48.7	0.10	22.5	2.80	23.5	0.62	98.3	80.7	2.2	17.1
		48.7	0.11	22.6	2.80	23.5	0.63	98.4	80.7	2.2	17.1
		49.1	0.09	22.7	3.13	23.0	0.72	98.7	78.5	2.5	19.1
		49.0	0.07	22.8	2.91	23.5	0.61	98.9	80.2	2.1	17.7
		48.0	0.23	22.8	5.48	20.2	0.43	97.0	66.4	1.4	32.2
		48.2	0.17	23.1	4.97	21.1	0.45	98.0	69.4	1.5	29.1
		48.7	0.27	22.6	5.47	21.1	0.33	98.5	67.6	1.1	31.3
		49.0	0.23	22.2	5.13	22.1	0.50	99.2	69.6	1.6	28.8
		49.3	0.31	22.7	4.14	22.3	0.86	99.6	73.0	2.9	24.2
		49.0	0.29	22.8	4.32	22.6	0.76	99.7	72.7	2.5	24.8
		47.4	0.19	22.8	4.02	22.1	0.76	97.4	73.6	2.6	23.8
		48.9	0.27	22.8	3.72	22.5	0.91	99.1	74.9	3.1	22.1
		49.8	0.25	22.8	3.83	23.2	0.71	100.5	75.4	2.4	22.2
SK08-005	110.10	47.8	0.11	22.8	5.64	20.8	0.44	97.6	66.5	1.4	32.1
		48.1	0.16	22.9	5.72	20.7	0.42	98.0	66.0	1.4	32.6
		49.5	0.06	22.9	5.43	19.8	0.57	98.4	65.9	1.9	32.1
		49.8	0.11	22.9	5.95	21.0	0.41	100.1	65.5	1.3	33.2
		48.4	0.11	23.3	7.85	17.1	0.37	97.2	54.3	1.2	44.5
		49.2	0.07	23.5	7.98	17.5	0.48	98.6	54.3	1.5	44.2
		50.1	0.10	23.3	7.62	17.3	0.45	98.8	55.1	1.5	43.4
SK08-005	20.50	45.5	0.66	22.5	4.00	21.8	0.84	95.4	73.2	2.9	23.9
		48.3	0.68	22.7	3.89	22.6	0.70	98.9	74.8	2.3	22.9
SK08-005	28.20	48.2	0.24	22.2	5.05	21.1	0.64	97.5	68.6	2.1	29.3
		48.8	0.23	22.2	4.65	21.8	0.65	98.3	70.9	2.2	26.9
		48.0	0.14	22.3	4.84	20.4	0.68	96.4	68.7	2.3	29.0
		47.9	0.13	22.4	4.47	21.4	0.59	96.9	71.4	2.0	26.6
		47.7	0.12	22.1	4.95	22.0	0.53	97.5	70.2	1.7	28.1
		48.1	0.18	22.6	4.36	22.1	0.63	98.1	72.5	2.1	25.5
		49.5	0.24	22.7	4.58	20.8	0.77	98.6	70.0	2.6	27.4
		46.6	0.17	22.6	4.86	20.4	0.40	95.1	69.2	1.4	29.4
		46.9	0.29	22.1	5.22	20.1	0.65	95.3	66.9	2.2	30.9
		47.7	0.25	22.5	4.44	21.9	0.89	97.6	71.3	2.9	25.8
SK08-005	62.00	47.7	0.41	22.5	3.30	24.5	0.84	99.2	78.4	2.7	18.8
		49.4	0.10	22.7	3.43	23.1	0.92	99.7	76.6	3.1	20.3
SK08-005	64.80	48.4	0.21	23.3	3.56	21.5	0.57	97.6	75.7	2.0	22.3

		49.0	0.11	23.4	4.88	20.9	0.62	98.9	69.2	2.1	28.7
		48.5	0.14	23.5	3.77	23.3	0.50	99.8	76.4	1.7	22.0
		49.8	0.15	23.7	4.95	22.2	0.33	101.1	70.8	1.1	28.2
		49.5	0.25	23.7	3.86	21.0	0.67	99.0	73.5	2.4	24.1
		50.1	0.09	23.8	4.57	21.3	0.46	100.3	71.2	1.5	27.3
		50.0	0.24	23.5	4.03	22.0	0.70	100.4	73.6	2.4	24.0
		50.4	0.13	23.6	4.97	21.6	0.58	101.4	69.6	1.9	28.5
		48.3	0.28	23.2	3.85	20.8	0.50	97.0	73.8	1.8	24.4
		48.0	0.18	23.4	3.44	21.8	0.55	97.3	76.5	1.9	21.5
		48.9	0.18	23.3	4.71	21.0	0.43	98.5	70.4	1.5	28.1
		48.7	0.21	23.5	3.83	22.4	0.42	99.1	75.6	1.4	23.0
		48.5	1.12	21.2	4.28	21.9	0.51	97.5	72.8	1.7	25.4
		48.2	0.10	23.3	4.58	20.9	0.56	97.6	70.5	1.9	27.6
		48.8	0.13	23.4	4.96	20.2	0.57	98.1	68.2	2.0	29.8
		47.9	0.16	23.1	3.90	23.3	0.51	98.8	75.7	1.7	22.6
SK08-006	120.81	52.5	3.66	21.8	3.95	17.0	0.63	99.6	68.9	2.6	28.5
		50.3	0.08	23.9	5.50	19.3	0.71	99.8	64.8	2.4	32.8
		50.3	0.12	23.7	5.48	19.8	0.62	100.1	65.6	2.1	32.3
		50.9	0.10	23.9	6.00	18.9	0.38	100.2	63.1	1.3	35.6
		50.8	0.09	23.8	5.98	19.0	0.81	100.4	62.3	2.7	35.0
		50.7	0.26	23.5	4.97	20.6	0.53	100.6	68.7	1.8	29.5
		50.6	0.11	23.8	5.28	20.3	0.51	100.6	67.2	1.7	31.1
		50.5	0.20	24.0	4.98	20.6	0.47	100.7	68.7	1.6	29.7
		50.4	0.18	23.7	5.27	19.8	0.53	99.9	66.6	1.8	31.6
		50.7	0.16	23.9	6.52	18.2	0.40	99.9	60.2	1.3	38.5
		50.8	0.08	23.7	5.85	19.3	0.45	100.2	63.9	1.5	34.5
		50.0	0.10	23.4	4.52	22.2	0.53	100.7	72.1	1.8	26.2
		50.7	0.15	23.7	5.66	19.9	0.30	100.4	65.7	1.0	33.3
		50.8	0.04	24.0	6.21	18.4	0.90	100.4	60.6	3.0	36.4
		50.8	0.10	23.5	5.58	21.0	0.38	101.3	67.0	1.2	31.8
SK08-007	11.58	51.3	0.10	23.2	6.66	19.3	0.48	101.0	60.9	1.5	37.6
		51.6	0.30	23.1	6.48	19.0	0.69	101.2	60.8	2.2	36.9
		51.8	0.14	23.2	6.75	18.1	0.33	100.2	59.4	1.1	39.5
		51.8	0.69	23.5	8.73	15.6	0.38	100.7	49.5	1.2	49.3
		51.5	0.15	22.9	6.04	20.0	0.40	100.9	64.2	1.3	34.6
		51.7	0.17	23.3	7.25	18.1	0.47	101.0	57.5	1.5	41.0
		50.8	0.17	22.9	5.09	20.4	0.41	99.8	68.3	1.4	30.4
		50.7	0.30	22.9	5.73	20.3	0.34	100.2	65.7	1.1	33.1
		50.6	0.21	22.9	5.79	20.7	0.27	100.6	66.2	0.9	32.9
		51.0	0.28	22.9	5.10	20.9	0.51	100.8	68.5	1.7	29.8
		49.6	0.20	23.0	5.38	21.1	0.35	99.6	67.9	1.1	30.9
		50.6	0.12	22.8	6.51	19.6	0.34	99.9	62.1	1.1	36.8
		51.4	0.17	23.0	6.43	19.7	0.57	101.3	62.0	1.8	36.1
		51.0	0.18	23.2	6.49	18.2	0.48	99.4	60.1	1.6	38.3
		49.9	0.11	23.1	5.78	20.7	0.71	100.3	65.2	2.3	32.5
		51.6	0.11	23.2	6.66	19.2	0.34	101.0	61.1	1.1	37.8
		48.4	0.15	22.8	5.43	20.9	0.51	98.2	67.2	1.7	31.1

		49.9	0.11	23.0	6.54	19.2	0.50	99.3	61.2	1.6	37.1
		51.0	0.11	23.0	6.20	19.9	0.37	100.6	63.5	1.2	35.3
		48.9	0.06	23.6	4.79	19.1	0.74	97.2	67.2	2.7	30.1
		49.3	0.16	23.6	6.06	18.2	0.77	98.0	61.1	2.6	36.3
		49.3	0.14	23.6	5.91	19.0	0.51	98.5	63.3	1.7	35.0
		49.5	0.06	23.3	5.92	19.6	0.33	98.7	64.3	1.1	34.6
SK08-007	42.00	49.1	0.18	22.5	3.23	21.2	0.65	97.0	76.8	2.4	20.8
		49.4	0.12	22.8	4.03	20.2	0.66	97.2	72.0	2.4	25.6
		48.7	0.29	22.3	2.49	23.1	0.60	97.4	82.1	2.2	15.8
		48.4	0.18	22.2	1.89	24.0	1.01	97.7	84.5	3.6	11.9
		49.9	0.10	22.9	5.75	17.7	0.67	97.0	61.8	2.4	35.8
		49.7	0.14	23.0	5.31	19.0	0.44	97.6	65.7	1.5	32.8
		50.3	0.10	23.0	5.98	18.3	0.57	98.3	62.0	2.0	36.0
		48.7	0.09	22.2	2.86	22.6	0.82	97.3	79.3	2.9	17.8
SK08-007	62.40	48.7	0.40	23.4	7.05	18.5	0.35	98.4	58.9	1.1	40.0
		48.8	0.37	23.5	6.98	18.9	0.38	99.0	59.6	1.2	39.2
SK08-007	7.90	50.9	0.14	23.9	9.54	13.9	0.50	98.9	44.2	1.6	54.2
		50.7	0.11	23.7	9.30	15.0	0.48	99.3	46.8	1.5	51.7
SK08-008	122.20	50.6	0.13	23.5	6.26	19.1	0.46	100.1	62.2	1.5	36.3
		50.4	0.20	23.2	6.34	19.0	0.40	99.5	61.9	1.3	36.8
		50.7	0.25	23.4	6.37	19.9	0.40	100.9	62.9	1.3	35.9
		49.4	0.19	23.4	7.03	18.7	0.30	99.0	59.3	1.0	39.7
		49.9	0.18	23.4	7.26	18.7	0.38	99.8	58.4	1.2	40.4
		51.9	1.11	22.5	7.15	16.8	0.65	100.1	55.6	2.2	42.2
		51.6	0.21	23.2	7.28	17.8	0.38	100.5	57.2	1.2	41.6
		51.5	0.51	23.2	7.65	16.7	0.62	100.1	53.9	2.0	44.1
		49.6	0.19	23.1	6.34	19.6	0.39	99.2	62.6	1.3	36.2
		51.1	0.25	23.6	8.74	15.9	0.40	100.0	49.8	1.3	48.9
SK08-009	49.60	50.2	0.17	23.6	4.80	21.0	0.53	100.3	69.8	1.8	28.4
		50.9	0.38	23.7	4.78	20.7	0.51	100.9	69.6	1.7	28.7
		50.1	0.35	23.6	4.26	22.2	0.78	101.4	72.6	2.6	24.8
		49.1	0.32	24.5	3.91	21.4	0.67	99.9	73.7	2.3	24.0
		50.1	0.18	23.4	3.14	22.6	1.04	100.5	77.2	3.6	19.2
		49.4	0.23	23.2	4.17	23.0	0.55	100.6	74.2	1.8	24.0
		49.8	0.23	23.3	5.23	22.0	0.52	101.1	69.0	1.7	29.3
		50.8	0.17	23.6	4.64	22.1	0.50	101.8	71.6	1.6	26.8
SK08-009	54.00	48.1	0.18	22.8	5.01	21.6	0.51	98.2	69.6	1.7	28.7
		48.7	0.10	22.6	5.02	21.9	0.52	98.8	69.8	1.7	28.6
		50.4	0.11	22.9	5.36	21.0	0.48	100.2	67.6	1.6	30.8
		50.4	0.22	22.8	4.33	22.4	0.53	100.6	73.1	1.7	25.2
		47.7	0.15	22.8	5.24	21.1	0.38	97.4	68.5	1.2	30.3
		47.9	0.14	22.7	5.59	20.8	0.30	97.4	66.9	1.0	32.1
		51.9	0.56	23.4	8.91	15.3	0.18	100.3	48.9	0.6	50.6
		50.4	0.26	22.7	4.43	21.8	0.82	100.4	71.4	2.7	25.9
		47.9	0.24	22.4	3.47	23.8	0.41	98.3	78.3	1.4	20.3
		48.0	0.23	22.7	3.93	23.5	0.57	98.9	75.6	1.9	22.5
		50.2	0.20	23.0	4.01	22.5	0.46	100.4	74.7	1.6	23.7

		50.6	0.16	22.8	4.08	22.7	0.58	101.0	74.3	1.9	23.8
		50.3	0.17	22.9	3.62	23.4	0.57	101.1	76.9	1.9	21.2
		47.0	0.14	23.0	4.37	21.6	0.62	96.7	72.0	2.1	26.0
		49.2	0.67	22.8	3.16	22.7	1.08	99.6	77.2	3.7	19.1
		49.5	0.16	22.8	3.62	22.4	1.24	99.7	74.4	4.2	21.5
		48.3	0.16	22.9	4.44	22.3	0.80	98.9	71.9	2.6	25.5
		49.2	0.15	22.8	4.22	23.4	0.48	100.3	74.5	1.5	23.9
		49.3	0.25	22.5	3.44	24.3	0.59	100.3	78.3	1.9	19.8
		49.1	0.16	22.6	3.99	24.0	0.44	100.3	76.1	1.4	22.5
		50.3	0.14	22.8	4.39	22.5	0.80	101.0	72.3	2.6	25.1
		46.8	0.15	22.5	5.18	20.6	0.47	95.7	68.0	1.6	30.5
		50.2	0.13	22.7	4.04	22.9	0.61	100.6	74.6	2.0	23.4
SK08-010	43.70	46.8	0.38	22.4	3.68	23.2	0.75	97.2	76.0	2.5	21.5
		47.1	0.34	22.3	3.65	23.8	0.76	98.0	76.6	2.5	20.9
		47.5	0.36	22.6	3.48	23.2	0.88	98.0	76.6	2.9	20.5
		49.0	0.20	22.6	4.07	23.4	0.56	99.8	75.0	1.8	23.2
		50.0	0.31	22.0	4.98	22.0	0.50	99.8	70.1	1.6	28.3
		49.8	0.16	22.7	3.96	23.6	0.64	100.9	75.4	2.1	22.5
		46.6	0.41	22.6	3.66	23.2	1.00	97.4	75.5	3.3	21.2
		49.3	0.15	22.7	4.51	22.1	0.52	99.3	72.1	1.7	26.2
		49.6	0.24	22.8	4.69	21.9	0.55	99.9	71.1	1.8	27.1
		48.8	0.30	22.6	3.18	24.3	1.03	100.2	78.3	3.4	18.3
		48.2	0.16	22.7	4.71	22.5	0.47	98.7	71.7	1.5	26.8
SK08-011	42.75	48.2	0.08	21.9	5.36	20.8	0.50	96.8	67.4	1.6	31.0
		48.3	0.16	22.7	4.73	20.9	0.61	97.4	69.8	2.1	28.1
		47.6	0.14	22.5	4.82	22.0	0.43	97.5	70.9	1.4	27.7
		48.1	0.10	22.8	5.63	20.0	0.67	97.3	65.2	2.2	32.6
		49.4	0.10	22.7	5.73	19.8	0.62	98.3	64.6	2.0	33.3
		49.4	0.35	22.6	6.05	19.7	0.48	98.7	63.7	1.6	34.8
		50.4	0.05	22.9	5.77	20.3	0.52	99.9	65.2	1.7	33.1
SK08-011	67.50	47.4	0.14	22.6	4.46	21.3	0.48	96.4	71.6	1.6	26.7
		47.1	0.13	23.9	4.64	21.7	0.45	97.9	71.3	1.5	27.2
		48.9	0.10	22.8	4.49	23.3	0.37	100.0	73.6	1.2	25.2
		48.9	0.15	22.9	5.48	20.1	0.63	98.1	65.9	2.1	32.0
		48.3	0.09	22.9	5.50	20.9	0.60	98.3	66.7	1.9	31.3
		49.1	0.09	23.1	5.36	20.4	0.63	98.6	66.7	2.1	31.3
		48.3	0.11	22.5	4.92	21.8	0.48	98.1	70.2	1.6	28.2
		48.5	0.09	22.6	4.96	22.7	0.34	99.2	71.2	1.1	27.7
		49.7	0.14	22.6	5.13	21.7	0.51	99.7	69.2	1.6	29.2
SK08-011	76.50	50.5	0.12	24.2	6.07	19.5	0.49	100.9	63.3	1.6	35.1
SK08-013	111.50	48.7	0.11	22.9	4.93	20.7	0.46	97.7	69.1	1.5	29.3
		48.6	0.14	22.7	5.61	21.1	0.61	98.8	66.5	1.9	31.5
		48.9	0.03	22.7	4.53	22.2	0.60	98.9	71.9	2.0	26.2
		49.4	0.11	22.8	6.10	20.0	0.70	99.1	63.3	2.2	34.5
SK08-013	208.00	49.3	0.13	23.1	6.33	18.6	0.58	98.0	61.0	1.9	37.1
		49.4	0.37	23.0	6.39	18.5	0.49	98.1	60.9	1.6	37.5
		49.5	0.29	23.3	6.41	18.4	0.58	98.6	60.5	1.9	37.5

		50.1	0.25	23.2	7.20	18.7	0.53	100.0	58.3	1.7	40.1
		47.3	0.29	23.0	5.02	20.9	0.66	97.3	68.5	2.2	29.3
SK08-016	51.50	48.6	0.12	22.6	5.93	20.5	0.49	98.2	65.0	1.6	33.5
		47.8	0.06	22.5	6.38	19.2	0.31	96.3	62.2	1.0	36.8
		49.1	0.15	22.9	6.77	19.4	0.40	98.7	60.9	1.3	37.8
		50.5	0.15	22.8	5.78	19.8	0.38	99.4	64.9	1.3	33.8
		50.8	0.10	23.1	6.23	19.2	0.40	99.8	62.5	1.3	36.2
		51.3	0.30	22.7	5.87	19.6	0.37	100.1	64.4	1.2	34.4
		50.6	0.17	23.0	6.31	19.7	0.53	100.3	62.6	1.7	35.7
SK08-017	98.50	47.1	0.52	22.4	3.56	23.7	0.63	98.0	77.3	2.1	20.7
		47.1	0.59	22.7	3.60	23.6	0.72	98.3	76.8	2.4	20.9
		47.7	0.60	22.7	3.57	23.5	0.66	98.7	76.9	2.2	20.9
		46.1	0.13	22.5	2.73	23.7	0.87	96.0	80.5	3.0	16.5
		46.1	0.18	22.5	2.86	23.8	0.72	96.2	80.4	2.4	17.2
		48.2	0.32	22.5	2.93	24.3	0.76	99.1	80.2	2.5	17.3
		47.4	0.78	22.5	3.09	23.8	0.60	98.2	79.6	2.0	18.4
SK08-018	32.20	50.9	0.09	23.8	5.48	19.9	0.45	100.6	66.1	1.5	32.4
		50.8	0.10	23.8	5.53	20.4	0.41	101.0	66.5	1.4	32.1
		51.1	0.12	24.0	5.58	20.0	0.47	101.3	65.8	1.6	32.7
		48.4	0.16	23.5	5.35	20.0	0.63	98.0	66.3	2.1	31.6
		50.3	0.18	23.4	4.37	21.4	0.48	100.1	72.1	1.6	26.3
		50.4	0.14	23.8	5.48	19.9	0.61	100.2	65.7	2.0	32.2
		50.7	0.15	23.9	4.90	20.5	0.50	100.7	69.0	1.7	29.3
		50.6	0.09	24.0	5.23	20.4	0.48	100.8	67.5	1.6	30.8
		50.8	0.10	23.9	5.22	20.0	0.42	100.4	67.2	1.4	31.3
		50.9	0.05	23.8	4.90	20.6	0.47	100.7	69.0	1.6	29.3
		50.5	0.15	23.6	4.20	22.0	0.35	100.9	73.8	1.2	25.1
		50.3	0.18	23.6	4.29	22.2	0.51	101.1	73.1	1.7	25.2
SK08-019	114.50	51.9	1.41	24.1	12.2	9.18	0.14	98.8	29.6	0.5	69.9
		52.5	2.06	24.0	12.2	9.09	0.15	100.0	29.4	0.5	70.1
		53.1	2.00	23.4	12.2	8.99	0.28	100.0	28.9	0.9	70.2
		50.7	0.41	24.0	11.9	10.9	0.19	98.0	33.7	0.6	65.7
		52.8	2.30	23.6	10.8	10.7	0.04	100.2	35.7	0.1	64.2
SK08-019	44.50	52.2	0.59	25.1	11.9	9.53	0.19	99.5	30.9	0.6	68.5
		52.2	0.26	25.3	12.2	9.92	0.16	100.0	31.2	0.5	68.2
		52.6	0.72	25.1	12.4	9.47	0.04	100.3	30.0	0.1	69.9
		51.2	0.28	26.0	11.5	10.6	0.10	99.7	34.0	0.3	65.7
		53.6	0.75	25.2	12.0	9.38	0.09	101.0	30.5	0.3	69.3
		52.7	0.95	25.2	12.2	9.12	0.09	100.3	29.4	0.3	70.3
		53.0	0.22	25.0	11.7	10.8	0.13	100.9	34.1	0.4	65.5
		53.4	0.46	25.1	11.3	10.6	0.22	101.1	34.2	0.7	65.1
SK08-019	70.10	49.2	0.35	23.1	2.53	22.5	0.70	98.3	81.2	2.5	16.3
		49.6	0.14	23.1	2.82	22.1	0.97	98.7	78.6	3.5	17.9
		50.0	0.17	23.2	4.18	20.7	0.48	98.7	72.3	1.7	26.0
		49.8	0.28	23.6	4.53	20.2	0.41	98.8	70.4	1.4	28.1
		49.6	0.27	23.3	4.31	19.8	0.59	97.9	70.5	2.1	27.3
		49.4	0.51	23.1	3.38	21.0	0.63	98.0	75.9	2.3	21.8

		48.7	0.55	23.1	3.32	21.6	0.84	98.0	76.1	3.0	20.9
		49.5	0.26	23.1	4.44	20.4	0.39	98.1	71.1	1.4	27.5
		51.0	0.14	23.6	5.72	19.5	0.35	100.3	64.8	1.2	34.0
		51.2	0.11	23.8	5.38	20.1	0.56	101.1	66.4	1.9	31.7
		51.3	0.17	23.7	4.77	21.1	0.58	101.7	69.9	1.9	28.1
		50.7	0.21	23.7	5.06	19.9	0.57	100.2	67.5	1.9	30.6
		50.7	0.43	24.0	4.08	20.7	0.95	100.8	71.6	3.3	25.1
		51.0	0.18	23.8	4.65	21.1	0.46	101.3	70.7	1.6	27.7
		50.9	0.40	23.9	4.52	21.1	0.69	101.5	70.6	2.3	27.0
		50.8	0.57	23.8	4.22	21.3	0.94	101.6	71.5	3.2	25.3
SK08-021	63.22	46.9	0.17	22.7	3.79	23.6	0.52	97.7	76.5	1.7	21.8
		47.9	0.17	22.6	3.60	23.2	0.69	98.2	76.5	2.3	21.1
		45.8	0.47	22.6	3.84	22.1	0.77	95.6	74.3	2.6	23.0
		46.8	0.29	22.7	3.15	23.9	0.66	97.5	79.2	2.2	18.6
		48.7	0.24	22.7	3.44	23.2	0.86	99.1	76.8	2.9	20.3
		49.8	0.14	22.8	3.10	23.5	0.81	100.1	78.8	2.7	18.5
		47.6	0.14	22.5	3.23	23.5	0.86	97.9	78.0	2.9	19.1
		48.5	0.16	22.7	3.35	23.3	0.70	98.7	77.7	2.4	19.9
		49.1	0.18	22.9	3.26	23.3	0.90	99.6	77.6	3.0	19.4
		49.8	0.38	22.8	3.29	22.5	0.90	99.7	76.9	3.1	20.0
SK08-022	40.02	48.1	0.07	22.8	5.38	20.7	0.68	97.7	66.8	2.2	31.0
		50.8	0.32	22.7	5.35	19.3	0.67	99.2	65.3	2.3	32.4
		50.2	0.17	22.4	5.59	21.4	0.37	100.1	67.4	1.2	31.4
		50.8	0.20	22.1	6.45	20.2	0.46	100.2	62.8	1.4	35.8
		50.5	0.34	22.6	4.30	21.8	0.70	100.3	72.3	2.3	25.4
		47.2	0.22	22.6	3.44	22.9	0.62	97.0	77.2	2.1	20.6
		47.6	0.06	22.9	3.93	22.9	0.62	98.0	75.0	2.1	22.9
		50.4	0.19	22.9	6.40	18.2	0.69	98.8	60.0	2.3	37.6
		50.2	0.13	22.6	4.70	21.2	0.54	99.4	70.4	1.8	27.8
		49.6	0.19	22.6	4.70	22.7	0.61	100.5	71.6	2.0	26.4
		51.7	0.10	22.2	4.55	21.2	0.76	100.5	70.4	2.6	27.0
		51.0	0.11	22.8	5.51	20.8	0.46	100.7	66.9	1.5	31.6
		50.4	0.21	22.8	4.17	22.7	0.63	101.0	73.8	2.1	24.1
		50.8	0.17	22.8	5.95	21.0	0.52	101.2	65.3	1.6	33.0
		46.0	0.44	22.5	3.06	24.0	0.75	96.7	79.4	2.5	18.1
		46.9	0.23	22.5	4.48	22.0	0.61	96.7	71.9	2.0	26.1
		47.4	0.27	22.7	3.83	23.1	0.85	98.1	75.0	2.8	22.2
		50.2	0.23	23.0	5.36	20.0	0.79	99.6	65.9	2.6	31.4
		50.4	0.25	22.7	4.84	21.1	0.67	99.9	69.4	2.2	28.4
		51.0	0.17	23.0	6.37	19.1	0.40	100.1	62.0	1.3	36.7
		50.2	0.43	22.9	4.01	22.4	0.71	100.6	74.0	2.4	23.6
		48.5	0.28	22.7	4.03	23.3	0.76	99.5	74.5	2.5	23.0
		49.7	0.32	23.0	4.13	22.3	0.64	100.1	73.6	2.1	24.3
		49.0	0.08	22.9	5.06	22.8	0.48	100.4	70.6	1.5	27.9
		47.2	0.39	22.6	4.14	23.0	0.71	98.1	74.0	2.3	23.7
		47.2	0.41	22.7	3.90	23.3	0.67	98.2	75.4	2.2	22.5
		48.4	0.31	22.8	4.41	22.9	0.71	99.6	72.7	2.3	25.0

		47.4	0.14	22.5	2.92	24.9	0.51	98.4	81.3	1.7	17.0
		47.8	0.12	22.6	3.73	24.0	0.55	98.9	76.9	1.8	21.3
		45.5	0.31	22.7	3.84	22.4	0.56	95.3	75.2	1.9	22.9
		46.5	0.12	22.8	5.88	19.7	0.41	95.4	64.4	1.4	34.3
		48.3	0.19	22.9	6.64	18.1	0.73	96.9	59.0	2.4	38.6
		46.9	0.30	22.6	3.90	22.8	0.74	97.2	74.7	2.5	22.8
		47.8	0.08	22.9	6.05	19.8	0.46	97.1	63.8	1.5	34.7
		48.2	0.07	22.8	6.02	19.9	0.57	97.7	63.8	1.9	34.3
SK08-024	7.00	49.5	0.26	23.5	3.92	20.7	0.95	98.8	72.2	3.4	24.4
		49.8	0.79	23.8	5.54	19.0	0.56	99.4	64.5	1.9	33.6
		49.7	0.32	23.6	4.89	20.8	0.79	100.1	68.6	2.6	28.8
		50.5	0.26	23.7	4.76	20.1	0.82	100.1	68.3	2.8	28.9
		50.0	0.72	23.8	5.33	19.6	0.80	100.2	65.5	2.7	31.8
		50.4	0.29	23.7	4.68	21.1	0.62	100.7	70.2	2.1	27.8
		50.8	0.16	23.7	6.75	17.8	0.35	99.6	59.0	1.2	39.8
		51.2	0.10	24.0	6.83	17.5	0.44	100.0	58.0	1.5	40.5
		50.7	0.16	23.8	5.77	19.1	0.47	100.0	64.0	1.6	34.5
		50.6	0.17	23.9	5.80	19.7	0.54	100.8	64.4	1.8	33.8
		51.5	0.12	23.9	6.25	19.2	0.46	101.3	62.3	1.5	36.2
		50.2	0.61	23.7	6.56	17.5	0.36	98.9	59.2	1.2	39.6
		49.7	0.33	23.5	4.63	19.9	0.75	98.9	68.8	2.6	28.5
		50.1	0.30	23.4	4.30	21.5	0.82	100.4	71.6	2.8	25.6
		50.5	0.40	23.6	5.15	20.6	0.63	100.9	67.7	2.1	30.2
		50.0	0.32	23.7	4.30	21.8	0.86	101.0	71.9	2.9	25.2
		50.7	0.12	23.8	6.09	18.3	0.43	99.4	61.8	1.5	36.7
		50.0	0.12	23.7	3.96	21.5	0.80	100.1	73.2	2.8	24.1
		51.1	0.07	24.0	5.99	19.0	0.46	100.6	63.1	1.5	35.4
		51.0	0.17	24.1	6.08	18.9	0.49	100.7	62.5	1.6	35.9
SK08-025	21.40	48.3	0.31	22.4	3.40	22.9	0.55	97.8	77.6	1.9	20.5
		48.8	0.41	22.6	5.90	20.0	0.46	98.1	64.5	1.5	34.0
		48.3	0.39	22.5	3.41	23.0	0.73	98.2	77.1	2.5	20.4
		49.1	0.39	22.5	4.09	22.5	0.65	99.2	73.9	2.2	23.9
		49.9	0.34	22.7	4.60	21.3	0.65	99.5	70.7	2.2	27.1
		47.3	0.33	21.8	5.05	20.2	0.52	95.1	67.9	1.8	30.3
SK08-026	34.00	48.8	0.21	23.4	5.05	21.0	0.26	98.7	69.4	0.9	29.7
		49.0	0.16	23.5	4.15	21.8	0.52	99.1	73.3	1.8	24.9
		49.9	0.12	23.4	6.08	19.5	0.29	99.4	63.6	1.0	35.4
		50.0	0.04	23.6	6.02	20.1	0.21	100.0	64.7	0.7	34.6
		49.2	0.18	23.4	4.08	22.5	0.67	100.1	73.9	2.2	23.9
		49.2	0.20	23.6	4.79	20.8	0.53	99.1	69.6	1.8	28.6
		49.6	0.10	23.6	5.36	20.4	0.58	99.6	66.8	1.9	31.3
		49.0	0.11	23.6	4.66	22.0	0.49	99.9	71.4	1.6	27.0
		49.1	0.29	23.2	4.50	22.3	0.43	99.9	72.5	1.4	26.1
		49.5	0.28	23.4	4.63	21.7	0.41	100.0	71.5	1.4	27.1
		49.4	0.09	23.9	6.75	19.0	0.40	99.5	60.5	1.3	38.2
		49.7	0.12	23.6	5.20	20.7	0.69	100.0	67.5	2.3	30.2
		49.8	0.16	23.7	5.02	20.9	0.51	100.1	68.9	1.7	29.4

		49.6	0.09	23.5	4.82	21.7	0.62	100.3	70.1	2.0	27.8
		49.8	0.04	23.6	5.41	21.1	0.38	100.4	67.8	1.2	31.0
		49.9	0.06	23.6	4.92	21.2	0.38	100.1	69.9	1.3	28.9
		50.4	0.17	23.7	4.78	21.0	0.41	100.5	70.2	1.4	28.5
		50.0	0.11	23.6	4.65	21.6	0.69	100.7	70.6	2.3	27.1
		50.3	0.09	23.8	4.38	22.2	0.53	101.3	72.7	1.8	25.5
		49.8	0.21	23.6	4.43	22.9	0.51	101.4	73.1	1.6	25.2
SK08-027	15.50	50.1	0.14	24.1	13.2	8.46	0.14	96.1	26.3	0.4	73.2
		50.1	0.24	24.4	13.2	8.61	0.11	96.6	26.7	0.4	73.0
		49.9	0.18	24.3	13.2	9.10	0.15	96.9	27.7	0.5	71.8
		50.9	0.14	24.2	13.1	9.05	0.13	97.6	27.8	0.4	71.8
		49.6	0.23	24.3	13.0	8.63	0.23	96.1	26.9	0.7	72.4
		50.1	0.17	24.3	13.2	8.97	0.34	97.0	27.4	1.1	71.6
		51.0	0.20	24.3	13.0	9.56	0.21	98.2	29.0	0.7	70.3
		50.0	0.46	23.7	10.9	12.8	0.31	98.1	39.3	1.0	59.7
		50.8	0.23	23.8	9.65	14.4	0.27	99.1	45.2	0.8	54.0
		52.0	0.52	23.7	8.69	14.0	0.32	99.2	47.0	1.1	51.9
		51.8	0.81	23.6	9.34	13.5	0.30	99.3	44.2	1.0	54.8
SK08-027	37.00	50.3	0.09	23.9	5.88	18.7	0.38	99.3	63.2	1.3	35.5
		50.6	0.03	23.9	5.61	19.9	0.30	100.3	65.9	1.0	33.1
		49.7	0.05	24.0	4.98	21.0	0.54	100.3	69.0	1.8	29.2
		50.3	0.18	23.4	3.91	22.1	0.52	100.4	74.7	1.8	23.6
		51.3	0.07	23.9	5.76	19.9	0.37	101.3	65.2	1.2	33.6
		50.8	0.11	24.0	6.31	17.9	0.63	99.8	60.1	2.1	37.7
		51.1	0.16	24.1	6.76	17.5	0.85	100.5	57.6	2.8	39.6
		51.2	0.13	24.0	6.63	18.0	0.57	100.5	59.2	1.9	38.9
		51.2	0.10	24.1	6.64	17.8	0.72	100.6	58.6	2.4	39.0
		51.3	0.13	24.1	6.73	18.0	0.57	100.8	58.9	1.9	39.2
		51.4	0.09	24.0	6.81	18.1	0.61	101.0	58.7	2.0	39.3
Homestake Trench		48.4	0.12	21.8	4.77	20.4	0.66	96.2	69.0	2.3	28.8
(Surface)		48.1	0.06	22.8	5.49	20.0	0.53	97.0	66.0	1.8	32.2
		49.9	0.14	22.2	5.30	19.3	0.43	97.3	66.1	1.5	32.4
		48.4	0.05	22.7	4.91	21.2	0.59	97.9	69.4	1.9	28.6
		49.0	0.12	22.5	5.41	20.6	0.59	98.3	66.9	1.9	31.2
		49.7	0.09	22.8	4.21	21.8	0.57	99.1	72.9	1.9	25.1
		49.8	0.10	22.5	5.79	18.8	0.40	97.5	63.7	1.4	34.9
		49.1	0.10	22.8	6.76	18.4	0.43	97.5	59.5	1.4	39.1
		50.0	0.09	22.9	6.53	19.4	0.26	99.2	62.0	0.8	37.2

Hd: Hedenbergite ($CaFeSi_2O_6$)

Jo: Johannsenite ($CaMnSi_2O_6$)

Di: Diopside ($CaMgSi_2O_6$)

Table 3.A-9. Garnet compositions by EMPA.

Sample ID	Depth (m)	SiO_2	Al_2O_3	CaO	MgO	FeO	Total	%Ad	%Al+Sp	%Gr
SK05-002	84.00	38.5	16.8	34.6	0.07	8.39	98.4	24.0	2.6	73.2
		38.4	17.2	34.3	0.06	8.34	98.3	22.2	3.9	73.7
		38.5	17.2	34.1	0.08	7.99	97.9	22.1	3.4	74.2
		38.4	16.6	34.0	0.02	9.19	98.2	25.1	3.5	71.4
		38.3	16.5	34.6	0.01	8.63	98.0	24.7	2.7	72.6
		38.3	16.0	34.6	0.03	9.63	98.5	27.2	3.1	69.7
		38.7	15.7	34.4	0.07	9.54	98.4	24.9	2.5	72.5
		38.9	16.4	34.5	0.05	8.65	98.5	25.3	2.6	72.0
		38.8	17.0	34.7	0.05	7.85	98.4	23.1	2.4	74.4
		38.7	16.7	34.7	0.05	8.16	98.3	24.0	2.4	73.5
SK05-002	87.00	37.8	16.4	34.4	0.03	8.45	97.1	24.8	2.3	72.7
		37.6	16.7	34.6	0.11	8.68	97.6	24.4	2.8	72.5
		37.9	16.3	34.2	0.05	8.76	97.2	25.5	2.6	71.7
		37.7	16.7	34.5	0.05	8.53	97.5	23.6	3.3	73.0
		37.7	16.4	34.8	0.04	8.41	97.4	25.0	2.3	72.6
		37.1	16.6	34.6	0.06	8.57	96.9	24.0	3.0	72.8
		37.0	16.3	34.4	0.04	8.73	96.4	24.8	2.9	72.2
SK08-003	66.10	38.2	17.2	35.7	0.06	7.64	98.8	19.7	3.5	76.6
		37.7	17.2	35.6	0.08	8.07	98.7	19.6	4.4	75.7
		38.0	17.7	35.6	0.06	7.58	98.9	17.9	4.8	77.2
		37.6	17.4	35.6	0.09	8.79	99.4	19.2	5.7	74.8
		38.2	17.2	35.6	0.08	7.85	99.0	19.8	3.8	76.1
		37.9	16.1	35.5	0.08	9.29	98.8	24.5	3.9	71.4
		38.3	16.7	35.5	0.09	8.80	99.3	22.1	3.9	73.7
		37.8	17.1	35.5	0.10	8.31	98.8	20.1	4.8	74.9
		38.2	17.4	35.5	0.08	7.93	99.1	19.0	4.5	76.2
		38.1	17.6	35.5	0.03	8.25	99.4	18.4	5.2	76.3
		38.1	17.6	35.3	0.06	8.26	99.3	18.3	5.7	75.9
		38.0	17.8	35.6	0.06	8.35	99.7	17.9	5.6	76.3
		38.4	17.5	35.4	0.08	8.51	100.0	19.3	5.2	75.3
		38.2	17.9	35.4	0.11	7.58	99.2	17.4	4.9	77.4
		38.4	17.6	35.3	0.09	7.89	99.3	18.7	4.7	76.3
		38.3	17.6	35.4	0.07	7.92	99.3	18.6	4.9	76.3
		38.1	17.8	35.4	0.08	8.22	99.6	17.7	5.9	76.1
		38.7	17.6	35.3	0.06	8.46	100.1	19.3	5.1	75.4
		37.4	17.2	35.4	0.08	7.68	97.8	19.0	4.2	76.5
		37.5	17.1	35.8	0.10	7.84	98.3	19.6	4.0	76.2
		37.8	17.2	35.8	0.07	8.04	98.8	19.9	4.1	75.8
		37.9	17.3	35.9	0.07	8.14	99.2	19.7	4.3	75.8
		38.0	17.3	35.8	0.06	8.44	99.5	19.9	4.7	75.3
		37.8	17.3	35.8	0.10	8.56	99.5	19.8	5.1	74.8
SK08-007	11.58	37.2	11.4	32.9	0.07	14.4	95.9	43.5	3.0	53.4
		37.2	10.9	33.4	0.04	16.3	97.8	46.4	3.9	49.6
		37.4	7.66	33.5	0.04	19.3	97.9	61.5	2.0	36.5

		35.5	7.94	33.4	0.04	17.0	93.9	58.5	1.4	40.0
		37.1	5.47	33.4	0.03	21.3	97.3	71.9	1.1	26.9
		37.3	6.20	33.3	0.02	20.7	97.5	68.4	1.4	30.2
		36.7	7.28	33.7	0.01	19.9	97.5	63.0	2.1	34.9
		37.4	7.82	33.6	0.03	18.9	97.8	60.7	1.8	37.4
		37.5	10.5	33.9	0.03	16.8	98.7	48.5	3.4	48.0
		38.6	14.3	34.3	0.00	12.0	99.3	32.4	3.9	63.6
		39.0	14.0	34.1	0.00	12.0	99.1	34.0	3.3	62.7
		38.0	12.4	34.0	0.00	14.5	99.0	40.2	4.0	55.8
		38.0	12.4	34.1	0.01	14.3	98.8	40.4	3.5	56.1
		38.5	13.9	34.2	0.00	12.0	98.5	34.0	3.3	62.7
		38.9	14.1	34.1	0.02	12.2	99.4	33.6	3.8	62.5
		38.5	15.3	34.1	0.02	11.1	99.0	28.1	4.7	67.2
		38.5	14.3	34.0	0.02	12.7	99.5	32.5	4.9	62.6
		37.7	12.9	33.9	0.02	14.0	98.5	38.0	4.2	57.7
		37.8	11.7	33.7	0.00	15.1	98.3	43.2	3.7	53.1
		38.9	17.9	34.6	0.07	7.50	99.0	17.5	4.4	77.9
		38.8	16.2	34.4	0.03	9.96	99.4	24.4	4.9	70.7
		38.1	10.6	34.0	0.03	16.7	99.3	48.6	3.2	48.2
		37.9	10.6	34.0	0.03	16.7	99.2	48.2	3.3	48.4
		38.1	12.6	34.0	0.01	13.9	98.6	39.2	3.7	57.1
		38.9	14.1	33.9	0.03	12.2	99.1	33.5	3.7	62.7
		38.4	12.3	34.1	0.04	15.2	100.0	41.4	4.0	54.5
		38.5	13.4	34.0	0.06	13.4	99.4	36.2	4.2	59.5
		38.3	12.9	34.1	0.05	13.2	98.5	38.1	3.1	58.6
		38.6	12.5	33.9	0.02	14.4	99.4	40.3	3.7	55.9
SK08-007	42.00	36.4	9.90	33.2	0.15	15.2	94.8	49.7	2.1	47.9
		37.5	14.2	33.3	0.00	10.4	95.4	30.5	3.2	66.3
		37.0	13.2	33.0	0.01	12.1	95.3	34.7	3.9	61.3
		37.2	12.3	33.0	0.05	12.9	95.4	39.2	3.1	57.6
		37.6	14.6	33.2	0.01	10.6	96.1	29.3	4.4	66.3
		37.4	12.9	33.3	0.03	13.5	97.1	37.2	4.5	58.2
		37.0	11.0	32.9	0.06	14.3	95.3	45.0	2.4	52.4
		37.8	17.1	33.3	0.06	7.74	96.1	18.3	4.7	76.7
		38.0	19.9	34.5	0.11	4.18	96.7	7.6	4.9	87.2
		38.5	19.0	34.5	0.09	5.16	97.3	11.9	4.1	83.7
		38.7	19.6	34.5	0.06	4.79	97.7	9.8	4.7	85.3
SK08-024	7.00	36.3	2.49	33.9	0.02	23.9	96.5	86.8	0.3	12.9
		36.7	5.96	34.3	0.02	20.1	97.1	69.4	0.8	29.8
		36.9	8.49	34.4	0.02	17.6	97.4	57.3	1.6	41.1
		35.9	1.55	34.0	0.05	25.3	96.8	91.7	0.2	8.1
		36.8	6.98	34.4	0.04	19.1	97.3	64.5	1.1	34.3
		37.3	8.59	34.8	0.05	16.9	97.6	57.1	1.0	41.8
		37.2	8.16	34.2	0.03	18.0	97.7	59.0	1.4	39.5
		35.7	0.38	33.6	0.05	27.1	96.8	97.9	0.1	2.0
		36.4	5.30	33.8	0.05	21.9	97.4	72.6	1.3	26.0
		37.1	6.93	34.3	0.02	19.8	98.1	65.0	1.5	33.6

		37.2	7.10	34.3	0.00	19.5	98.2	64.2	1.4	34.4
		37.1	7.28	34.4	0.07	19.2	98.1	63.3	1.4	35.1
		37.6	10.3	35.1	0.07	15.6	98.7	49.6	1.7	48.6
		37.7	10.4	34.9	0.08	15.9	99.0	49.2	2.1	48.5
SK08-027	37.00	36.9	16.9	34.7	0.00	9.40	98.0	20.1	7.1	72.8
		37.0	15.5	34.3	0.03	11.1	97.8	26.3	6.7	67.1
		37.1	13.7	34.4	0.04	13.1	98.4	34.1	5.1	60.7
		37.4	13.9	34.6	0.02	12.6	98.5	33.2	4.8	62.0
		37.3	13.3	35.0	0.02	13.7	99.4	36.1	4.6	59.3
		36.6	14.5	35.0	0.04	11.9	98.1	30.0	5.2	64.7
		36.8	13.6	34.6	0.02	13.1	98.1	34.4	5.0	60.6
		37.1	15.0	34.2	0.00	11.6	97.9	28.4	6.3	65.3
		37.0	14.5	34.4	0.03	12.4	98.3	30.3	5.8	63.8
		37.4	15.3	34.7	0.06	11.2	98.7	27.3	5.3	67.2
		37.5	14.7	35.1	0.04	11.4	98.7	30.1	4.5	65.2
		37.4	16.8	35.2	0.03	9.40	98.8	21.1	6.4	72.4

Ad: Andradite ($Ca_3Fe_2Si_3O_{12}$)

Al+Sp: Almandine ($Fe_3Al_2(SiO_4)_3$) + spessartine ($Mn^{2+}{}_3Al_2(SiO_4)_3$)

Gr: Grossular ($Ca_3Al_2(SiO_4)_3$)

Table 3.A.10. Scapolite compositions by EMPA.

Sample ID	Depth (m)	SiO_2	Al_2O_3	CaO	Na_2O	K_2O	CO_2	Cl	-O=Cl	Total	%Me
SK05-002	84.00	51.6	25.2	12.6	6.00	1.22	2.47	1.89	0.43	101.4	50.9
		51.9	24.8	11.5	7.04	1.16	2.26	2.25	0.51	101.4	44.9
		51.7	25.1	11.7	6.52	1.23	2.30	2.17	0.49	101.2	46.8
		52.0	24.9	11.7	6.78	1.32	2.31	2.26	0.51	101.7	45.6
		52.2	24.9	11.7	6.86	1.29	2.31	2.24	0.50	102.0	45.5
		51.2	24.9	12.5	6.24	1.10	2.47	1.94	0.44	100.8	50.2
		51.8	24.7	12.0	6.43	1.17	2.36	2.14	0.48	101.1	48.2
		50.9	25.3	12.3	6.44	1.02	2.42	1.84	0.42	100.7	48.9
		51.3	25.3	12.6	6.29	1.31	2.48	2.00	0.45	101.8	49.6
		52.1	25.0	11.9	6.45	1.27	2.35	2.25	0.51	101.8	47.3
SK05-002	87.00	50.4	24.0	11.1	7.03	1.33	2.19	2.37	0.54	99.1	44.2
		50.0	23.9	11.7	6.76	1.18	2.30	2.08	0.47	98.4	46.3
		49.9	24.0	11.1	7.15	1.25	2.19	2.19	0.49	98.3	43.7
		51.0	23.2	10.7	6.28	0.88	2.10	1.78	0.40	96.3	46.8
		52.3	24.4	11.0	7.13	1.28	2.17	2.42	0.55	101.3	43.3
		51.8	24.6	11.6	6.70	1.29	2.29	2.32	0.52	101.1	46.0
		52.0	24.7	11.2	6.78	1.36	2.21	2.30	0.52	101.1	44.9
		51.6	24.7	11.1	7.49	0.86	2.19	2.18	0.49	100.6	43.5
		50.0	23.2	12.4	6.65	0.93	2.45	1.89	0.43	97.9	50.5
		50.8	23.5	10.7	6.46	0.84	2.11	1.91	0.43	96.8	47.0
		50.5	24.3	11.6	7.10	1.26	2.29	2.16	0.49	99.7	44.5
		50.4	24.2	11.8	6.79	1.25	2.32	2.20	0.50	99.4	46.4
SK07-001	3.00	50.6	24.3	11.4	6.92	1.36	2.25	2.26	0.51	99.6	44.9
		50.5	24.5	11.7	7.08	1.20	2.30	2.21	0.50	99.9	45.4
		50.2	24.2	11.6	6.88	1.30	2.28	2.32	0.52	99.3	45.9
		50.9	24.4	11.8	6.85	1.38	2.32	2.09	0.47	100.2	45.8
		50.7	24.4	11.9	6.90	1.19	2.34	2.13	0.48	100.0	46.0
		50.3	24.1	11.4	7.03	1.26	2.25	2.30	0.52	99.1	44.6
		51.2	24.9	12.2	6.77	1.12	2.41	1.93	0.43	100.9	47.8
		51.6	24.7	11.5	6.97	1.33	2.26	2.21	0.50	101.0	45.3
		51.4	24.7	11.8	6.99	1.16	2.33	2.11	0.48	101.0	45.9
		51.1	24.8	11.6	6.98	1.22	2.28	2.19	0.49	100.6	45.3
		49.1	24.3	12.1	6.77	1.15	2.39	2.04	0.46	98.3	47.7
		49.4	24.2	11.8	6.66	1.20	2.32	2.07	0.47	98.1	47.2
		49.4	24.5	12.1	6.66	1.31	2.39	2.00	0.45	98.8	47.5
		49.7	24.3	11.5	7.06	1.14	2.26	2.04	0.46	98.4	44.9
		51.9	24.9	11.7	6.81	1.31	2.31	2.17	0.49	101.6	45.7
		52.4	24.7	11.5	7.03	1.34	2.27	2.22	0.50	102.1	44.5
		51.6	24.9	12.1	6.67	1.26	2.38	2.13	0.48	101.5	47.3
		48.7	24.3	11.5	6.97	1.14	2.26	2.13	0.48	97.4	45.8
		48.1	24.2	11.7	6.93	1.17	2.30	2.12	0.48	96.9	45.9
		50.3	23.9	10.7	7.90	1.07	2.10	2.50	0.56	99.0	41.3
		51.2	24.3	10.9	7.79	0.95	2.15	2.35	0.53	100.1	42.3
		49.8	25.0	13.3	5.52	1.17	2.62	1.69	0.38	99.5	54.3

		49.5	25.1	13.1	5.93	1.21	2.59	1.70	0.38	99.6	52.2
SK07-001	41.00	51.6	24.5	11.7	6.33	1.18	2.31	2.15	0.48	100.3	47.8
		53.1	24.4	10.3	7.17	1.26	2.03	2.41	0.54	101.1	42.2
		52.4	24.7	11.1	6.93	1.24	2.18	2.31	0.52	101.4	44.6
		52.3	24.9	11.6	6.20	1.17	2.29	2.06	0.46	101.0	48.2
		52.3	25.2	11.9	6.08	1.13	2.35	1.90	0.43	101.4	49.3
		51.0	24.8	11.9	6.14	1.11	2.35	1.90	0.43	99.7	49.5
		50.3	24.5	11.8	6.02	1.17	2.32	1.98	0.45	98.6	49.4
		52.4	24.6	11.1	6.67	1.06	2.19	2.14	0.48	100.7	45.7
		50.9	24.9	12.5	6.00	1.09	2.46	1.81	0.41	100.1	51.1
		51.5	23.2	10.0	7.64	0.96	1.97	2.29	0.52	98.0	40.3
		50.3	23.5	10.6	7.61	1.18	2.08	2.21	0.50	98.0	41.1
		49.9	24.0	11.8	6.80	1.16	2.33	2.01	0.45	98.5	46.2
SK07-001	43.00	51.8	24.5	11.1	7.32	1.09	2.20	2.28	0.51	100.9	43.4
		50.8	24.7	11.3	6.65	1.18	2.23	2.17	0.49	99.6	47.1
		52.2	24.3	10.4	7.92	1.14	2.06	2.11	0.48	100.6	40.5
SK07-001	Surface	50.4	22.8	10.7	5.89	0.97	2.10	1.78	0.40	95.0	47.5
		50.5	23.3	11.0	6.02	0.87	2.17	1.70	0.38	96.0	48.4
SK08-003	66.10	54.3	23.6	9.73	7.13	0.96	1.92	1.95	0.44	100.1	41.1
		55.9	24.1	8.92	8.16	0.88	1.76	2.61	0.59	102.9	35.8
		54.6	24.6	9.82	8.30	1.10	1.93	2.54	0.57	103.4	37.8
		49.3	22.9	11.3	6.27	0.96	2.23	1.64	0.37	95.0	50.6
		51.2	23.6	10.4	7.07	0.70	2.06	2.13	0.48	97.7	44.1
		52.9	25.0	11.6	7.03	1.07	2.29	2.09	0.47	102.5	45.6
		52.2	25.4	12.4	7.00	0.90	2.44	1.84	0.41	102.7	47.7
		53.0	23.0	10.9	6.40	0.83	2.14	1.89	0.43	98.5	46.8
		49.2	23.2	10.6	6.16	0.73	2.08	1.88	0.42	94.2	47.7
		49.9	23.4	9.04	6.63	0.68	1.78	1.92	0.43	93.8	55.3
		54.7	24.5	10.3	7.90	0.94	2.03	2.31	0.52	103.3	40.0
		53.9	24.7	10.5	7.96	0.91	2.07	2.26	0.51	102.9	40.7
		50.3	24.8	13.1	5.84	0.88	2.59	1.77	0.40	99.7	54.5
		57.4	22.9	8.33	8.24	0.91	1.64	2.49	0.56	102.5	34.6
		55.4	23.6	8.60	8.44	0.86	1.69	2.80	0.63	102.0	34.3
		55.3	23.8	8.89	8.74	1.00	1.75	2.57	0.58	102.7	34.1
		51.8	25.4	13.5	5.86	1.15	2.65	1.84	0.42	102.5	52.9
		52.1	23.5	9.70	8.10	1.00	1.91	2.31	0.52	99.2	38.5
		53.1	23.8	9.78	8.03	1.08	1.93	2.54	0.57	100.8	38.0
		52.2	24.5	11.1	7.57	0.92	2.18	2.12	0.48	101.0	42.9
SK08-003	101.50	45.3	22.5	13.2	4.33	1.10	2.59	1.77	0.40	91.1	59.4
		48.4	22.5	12.3	4.88	1.21	2.42	2.13	0.48	94.3	54.9
		48.1	22.1	12.3	4.35	0.88	2.42	1.63	0.37	92.1	59.3
		46.4	22.3	12.1	4.81	1.14	2.39	2.04	0.46	91.7	54.9
		46.2	22.3	12.5	4.82	1.04	2.45	1.94	0.44	91.6	55.9
SK08-004	72.40	51.1	21.8	10.8	5.32	1.08	2.12	2.23	0.50	94.9	50.3
		50.8	22.0	10.8	5.42	0.96	2.12	2.41	0.54	94.9	49.9
		48.2	22.5	12.0	5.27	0.87	2.36	1.90	0.43	93.5	53.5
SK08-004	188.50	54.9	22.9	8.17	8.10	0.63	1.61	2.31	0.52	99.2	35.7

		55.5	23.5	8.84	7.28	0.86	1.74	2.15	0.49	100.3	38.9
		54.6	23.8	8.68	8.91	1.04	1.71	2.35	0.53	101.5	33.6
		54.7	23.9	8.81	9.04	1.05	1.73	2.53	0.57	102.3	33.2
		54.6	23.9	8.70	8.75	1.25	1.71	2.58	0.58	102.1	33.6
		52.9	22.8	9.26	6.70	0.79	1.83	2.05	0.46	96.8	42.0
		53.1	23.4	9.53	7.61	0.84	1.88	2.23	0.50	99.1	38.9
		52.5	23.7	9.76	8.48	0.93	1.92	2.41	0.54	100.2	37.5
		52.6	22.9	8.14	8.39	1.18	1.60	2.68	0.60	98.1	33.2
		52.6	23.0	8.32	8.65	1.22	1.64	2.58	0.58	98.6	33.2
SK08-005	20.50	51.7	20.7	8.38	6.58	0.74	1.65	2.96	0.67	93.3	40.2
		51.7	21.1	9.05	6.67	0.89	1.78	2.79	0.63	94.6	41.5
		48.0	22.1	11.7	5.41	0.92	2.30	2.26	0.51	93.1	52.1
		47.5	22.8	12.8	4.87	1.06	2.52	1.98	0.45	93.9	56.5
		46.6	22.8	12.9	4.56	1.06	2.55	1.88	0.42	92.9	58.2
SK08-005	28.20	47.1	20.6	11.2	5.86	1.14	2.20	2.02	0.45	90.5	48.2
		51.4	23.2	12.3	4.66	0.99	2.41	2.23	0.50	97.6	56.3
SK08-005	64.80	48.0	24.4	12.5	6.55	1.06	2.46	1.85	0.42	97.2	49.1
		47.8	25.5	13.7	6.02	1.02	2.70	1.51	0.34	98.6	53.6
		48.8	24.4	12.3	6.61	0.86	2.41	1.62	0.37	97.3	49.1
		48.2	24.6	12.3	6.52	1.15	2.43	1.96	0.44	97.6	48.9
		48.4	24.9	12.6	6.44	1.02	2.47	1.81	0.41	98.0	49.6
		48.3	25.1	12.6	5.96	1.02	2.48	1.54	0.35	97.4	51.2
		48.0	23.5	11.2	7.18	1.10	2.21	2.09	0.47	95.8	44.0
		48.9	23.6	11.4	6.94	1.09	2.25	1.90	0.43	96.6	45.0
		49.2	24.0	11.0	7.48	1.10	2.17	2.12	0.48	97.6	42.8
		48.6	24.2	11.9	6.75	0.99	2.34	1.70	0.38	96.7	47.0
		51.0	24.6	11.6	7.03	1.12	2.29	1.98	0.45	100.1	45.3
		50.9	24.7	11.5	7.01	1.20	2.27	2.16	0.49	100.3	45.2
		51.0	24.9	11.9	6.81	1.24	2.34	2.06	0.46	100.7	46.4
SK08-005	110.10	46.2	21.4	11.5	5.25	1.13	2.26	2.32	0.52	90.5	51.3
SK08-006	120.81	55.0	23.9	10.1	5.93	0.80	1.98	1.96	0.44	100.0	47.2
		52.5	24.3	11.1	6.55	0.83	2.19	2.11	0.48	100.1	48.8
		49.9	26.7	14.0	4.96	1.24	2.76	1.63	0.37	101.5	58.5
		54.2	24.2	11.1	5.79	0.70	2.19	1.57	0.35	100.1	50.3
		50.8	25.6	12.0	6.86	0.89	2.36	2.11	0.48	101.0	47.7
		51.5	25.9	12.7	6.69	1.17	2.49	1.84	0.42	102.7	49.5
		55.3	23.6	9.05	9.27	0.98	1.78	2.65	0.60	103.2	33.6
		55.3	24.0	9.17	8.83	0.79	1.81	2.50	0.56	102.9	35.5
		55.1	24.2	10.0	7.79	0.75	1.97	2.34	0.53	102.6	40.1
		56.3	23.9	8.06	8.93	0.67	1.59	2.76	0.62	102.8	33.7
		52.2	25.0	11.5	6.13	1.09	2.27	2.01	0.45	100.7	49.1
		52.5	25.0	11.3	6.64	1.04	2.23	1.94	0.44	101.1	47.6
SK08-007	11.58	51.6	22.1	10.2	5.68	0.76	2.01	2.02	0.45	94.9	48.1
		50.9	22.7	11.2	5.26	0.92	2.21	1.89	0.43	95.5	51.1
		49.8	22.9	12.7	4.85	1.19	2.50	2.16	0.49	96.6	55.7
		54.8	21.0	8.25	6.70	1.14	1.63	2.94	0.66	97.1	38.6
		52.3	21.9	10.1	5.87	1.09	1.99	2.50	0.56	96.3	46.5

		51.6	22.3	11.1	5.04	1.27	2.18	2.16	0.49	96.1	51.1
		51.2	22.5	11.7	4.67	1.49	2.30	2.25	0.51	96.6	53.5
		51.2	22.1	12.0	4.63	1.46	2.36	2.15	0.49	96.4	54.4
		51.1	22.5	12.6	4.41	1.19	2.48	1.75	0.39	96.5	57.2
		50.9	22.1	11.2	5.19	1.29	2.22	2.17	0.49	95.7	51.0
		52.4	22.7	10.8	5.60	0.99	2.14	2.28	0.51	97.5	49.6
		52.0	22.1	11.1	5.46	1.08	2.18	2.28	0.51	96.7	49.6
		51.7	22.4	11.0	5.44	0.93	2.17	2.32	0.52	96.5	50.4
		51.5	22.7	11.9	5.31	1.02	2.34	2.01	0.45	97.2	52.3
		50.6	22.8	11.9	5.26	0.91	2.34	2.09	0.47	96.4	53.4
SK08-007	41.90	54.1	23.8	10.4	5.91	0.95	2.05	1.76	0.40	99.4	46.8
		54.0	24.4	10.2	8.17	1.07	2.02	2.45	0.55	102.9	39.0
		54.4	24.4	9.90	7.78	1.08	1.95	2.38	0.54	102.4	39.5
		53.3	24.5	10.5	7.81	1.08	2.07	2.30	0.52	102.1	40.2
		51.7	24.3	10.5	7.84	1.06	2.07	2.15	0.48	100.1	40.7
		51.4	24.5	11.1	7.44	0.98	2.20	2.03	0.46	100.1	43.3
		52.4	24.5	10.3	7.89	1.06	2.03	2.14	0.48	100.8	40.6
		51.1	24.8	10.9	7.29	0.91	2.16	1.86	0.42	99.5	44.0
		53.1	25.1	11.0	7.58	1.22	2.17	2.26	0.51	103.0	42.4
		52.2	25.1	12.2	7.05	1.06	2.40	1.86	0.42	102.3	46.2
		52.9	25.2	11.4	7.41	1.07	2.24	2.28	0.51	103.0	43.9
		52.4	25.3	11.8	7.11	1.05	2.32	2.06	0.46	102.5	45.5
		52.2	25.4	11.8	7.14	1.07	2.32	1.98	0.45	102.3	45.9
SK08-007	42.00	52.7	24.0	10.3	7.65	0.99	2.03	2.11	0.47	100.3	40.8
		52.5	24.2	10.5	7.74	0.90	2.08	2.09	0.47	100.6	40.7
		52.5	24.4	11.0	6.94	1.00	2.16	2.14	0.48	100.6	44.3
		52.6	24.5	10.8	7.52	0.94	2.12	1.99	0.45	100.9	42.2
		52.8	23.9	10.2	7.70	1.21	2.02	2.31	0.52	100.6	40.6
		49.9	24.2	11.3	7.15	0.99	2.22	1.78	0.40	97.9	44.3
		51.2	24.6	10.8	6.99	1.04	2.13	1.90	0.43	99.1	43.7
		51.0	24.7	10.9	6.96	1.10	2.14	2.08	0.47	99.3	43.9
		49.9	24.8	11.0	6.86	0.96	2.16	1.97	0.44	98.0	44.7
		51.5	24.8	10.0	7.77	1.45	1.96	2.37	0.53	100.4	38.9
		51.1	25.0	11.0	6.97	0.96	2.17	1.99	0.45	99.6	44.6
		51.3	25.2	11.6	7.06	0.90	2.28	1.90	0.43	100.7	45.7
SK08-007	62.40	46.2	22.0	11.3	5.13	1.08	2.23	2.25	0.51	90.7	51.6
		52.1	20.9	9.82	5.73	0.83	1.93	2.41	0.54	94.3	46.5
		51.5	21.2	9.39	5.86	0.95	1.85	2.43	0.55	93.7	44.9
		51.5	21.6	9.70	6.32	0.90	1.91	2.73	0.61	95.3	43.9
SK08-008	67.30	50.8	23.5	9.66	8.24	1.05	1.90	2.36	0.53	98.0	37.4
		50.3	22.2	11.0	5.60	1.05	2.16	2.49	0.56	95.3	49.4
		50.1	22.3	10.9	5.36	1.14	2.14	2.48	0.56	95.0	50.2
		48.6	22.0	10.8	5.43	1.15	2.13	2.45	0.55	93.1	49.1
		48.4	21.9	10.8	5.60	1.16	2.13	2.33	0.53	92.9	48.8
SK08-008	122.20	50.0	22.8	12.0	5.02	1.06	2.37	2.19	0.49	96.0	53.8
		50.0	22.7	11.2	5.58	1.06	2.21	2.34	0.53	95.7	49.8
		49.1	23.1	11.7	5.10	0.94	2.31	2.15	0.48	94.8	53.1

		49.0	22.2	10.9	5.43	1.19	2.16	2.41	0.54	93.9	49.4
		54.8	21.4	8.21	6.95	1.25	1.62	3.39	0.76	98.3	37.3
		54.4	21.4	8.84	6.71	1.13	1.74	2.94	0.66	97.9	40.1
		53.6	21.5	9.16	6.50	0.85	1.80	2.35	0.53	96.3	42.1
		53.1	21.0	8.30	6.46	1.13	1.64	3.17	0.71	95.5	39.5
		51.5	21.3	8.48	6.54	0.98	1.67	2.98	0.67	94.2	39.9
		51.2	22.4	11.9	4.82	1.17	2.34	2.14	0.48	96.4	54.0
		50.3	22.6	11.6	5.24	1.07	2.28	2.01	0.45	95.5	51.8
		49.1	23.1	12.2	4.91	1.11	2.40	2.12	0.48	95.3	54.6
		48.9	22.5	11.6	4.98	1.12	2.29	2.05	0.46	93.8	53.3
		47.5	22.4	12.5	4.49	1.07	2.47	1.80	0.41	92.6	57.0
SK08-009	49.60	47.8	22.6	10.6	6.83	0.87	2.08	1.63	0.37	92.8	44.5
		47.9	23.2	10.7	7.31	0.81	2.10	1.84	0.42	94.3	43.0
		53.6	24.7	11.4	7.73	0.94	2.25	2.18	0.49	103.3	42.9
		53.0	25.5	11.9	6.97	1.03	2.34	2.06	0.46	103.1	46.2
		52.4	25.6	12.2	6.60	0.99	2.40	1.91	0.43	102.4	48.7
		51.9	25.7	12.3	6.60	0.92	2.43	1.78	0.40	102.0	49.2
		51.9	24.9	11.5	6.74	1.15	2.27	2.02	0.46	101.0	46.6
		53.0	25.0	11.2	7.55	1.06	2.22	2.35	0.53	102.9	43.2
		52.3	25.1	11.6	6.89	1.16	2.28	2.03	0.46	101.8	46.3
		52.4	25.1	12.0	6.98	1.03	2.37	2.01	0.45	102.4	46.9
SK08-010	43.70	52.6	23.1	10.1	7.12	0.80	1.98	1.92	0.43	98.0	42.9
		55.5	24.8	10.2	7.55	1.12	2.00	2.33	0.52	104.0	41.1
		54.4	24.9	10.5	7.30	1.19	2.06	2.58	0.58	103.6	41.7
		54.7	25.0	10.5	7.51	1.05	2.07	2.39	0.54	103.7	41.7
		54.9	25.0	10.6	7.65	1.14	2.09	2.41	0.54	104.3	41.2
		54.7	25.1	10.7	7.73	0.98	2.11	2.51	0.56	104.5	41.7
		54.6	25.2	11.1	7.34	1.04	2.19	2.47	0.56	104.5	43.4
		53.8	25.4	11.5	7.10	1.08	2.27	2.41	0.54	104.1	45.3
		53.8	25.5	11.5	6.84	1.02	2.26	2.21	0.50	103.6	46.2
		52.3	21.8	10.1	5.83	1.20	1.98	2.60	0.59	96.4	45.2
		51.1	22.4	10.9	5.51	1.19	2.15	2.45	0.55	96.2	48.9
		51.0	21.9	9.9	5.83	1.34	1.94	2.80	0.63	95.3	45.1
		51.0	21.6	10.0	5.56	1.20	1.96	2.52	0.57	94.4	46.5
		49.4	21.4	9.78	5.79	1.20	1.93	2.61	0.59	92.8	45.0
SK08-011	67.50	49.6	21.7	11.0	5.33	1.17	2.16	2.40	0.54	93.9	50.1
		49.4	21.5	10.5	5.67	1.22	2.06	2.34	0.53	93.1	47.1
		49.1	21.7	11.1	5.47	1.24	2.18	2.28	0.51	93.6	50.1
		48.5	21.7	11.0	5.42	1.19	2.17	2.50	0.56	93.0	49.6
SK08-011	76.50	53.2	22.8	9.01	7.86	0.88	1.77	2.33	0.52	98.4	41.1
		53.0	24.6	11.3	6.35	0.81	2.22	1.60	0.36	100.2	48.3
		52.6	25.7	12.3	6.78	1.30	2.43	1.83	0.41	103.3	47.4
SK08-013	111.50	50.9	21.7	11.1	5.35	1.17	2.18	2.23	0.50	95.1	49.8
		50.0	21.7	11.5	4.89	1.49	2.27	2.34	0.53	94.8	52.3
		49.8	21.8	11.2	5.17	1.16	2.21	2.24	0.50	94.1	51.3
		49.7	21.8	11.2	5.03	1.20	2.21	2.12	0.48	93.7	51.8
		48.9	21.2	11.3	5.17	1.37	2.23	2.21	0.50	92.9	51.0

		49.9	21.4	10.8	5.69	0.95	2.13	2.27	0.51	93.6	49.0
		49.7	21.4	10.6	5.71	1.04	2.09	2.42	0.55	93.5	48.0
		49.0	21.3	11.1	5.92	0.97	2.19	2.40	0.54	93.4	48.4
SK08-013	208.00	53.4	24.9	11.0	7.55	1.00	2.16	2.34	0.53	102.8	42.5
		53.4	25.4	11.4	7.72	1.06	2.24	2.18	0.49	103.9	42.8
		52.9	25.4	11.6	7.80	0.73	2.28	2.31	0.52	103.5	43.6
		52.4	25.5	11.7	7.16	1.08	2.31	2.05	0.46	102.7	45.0
		52.9	24.8	11.4	7.63	1.18	2.24	2.36	0.53	103.1	43.2
		52.8	24.8	11.6	7.08	1.11	2.28	2.10	0.47	102.2	45.5
		53.2	25.1	11.1	7.71	1.08	2.18	2.31	0.52	103.2	42.7
		52.5	25.3	12.0	6.64	1.04	2.36	2.08	0.47	102.3	47.8
		53.7	24.6	11.2	7.64	1.11	2.20	2.23	0.50	103.1	42.5
		54.6	24.9	10.8	7.33	1.15	2.13	2.46	0.55	103.9	42.4
		53.5	25.0	11.2	7.31	1.20	2.22	2.39	0.54	103.4	43.6
		52.7	25.6	11.9	7.35	1.11	2.35	1.98	0.45	103.4	45.4
		52.6	25.6	11.7	7.28	1.07	2.30	2.20	0.49	103.2	45.3
		52.7	25.6	11.8	7.36	1.17	2.33	2.26	0.51	103.7	44.7
		52.6	25.6	12.2	6.91	0.90	2.41	1.99	0.45	103.1	47.9
		53.1	25.8	11.2	7.48	0.88	2.22	2.30	0.52	103.6	44.0
		54.7	24.2	10.5	7.42	0.97	2.07	2.27	0.51	102.6	42.2
		53.7	24.9	11.0	7.38	0.92	2.17	2.19	0.49	102.8	43.2
		47.6	21.9	11.9	4.86	0.97	2.34	1.99	0.45	92.0	54.6
		46.7	22.4	12.3	4.71	1.08	2.43	2.12	0.48	92.2	55.8
		46.1	22.2	12.3	4.83	1.21	2.43	1.93	0.44	91.4	55.1
		51.9	21.6	9.70	5.75	1.00	1.91	2.50	0.56	94.9	45.9
		51.3	21.6	10.3	5.84	1.05	2.03	2.54	0.57	95.3	47.3
		50.3	21.5	10.2	5.65	0.98	2.00	2.43	0.55	93.6	47.2
SK08-018	32.20	51.4	24.9	12.3	6.53	0.94	2.43	1.66	0.37	100.6	49.1
		55.0	24.1	8.78	8.72	1.13	1.73	2.93	0.66	103.1	33.9
		54.5	24.2	9.07	8.58	1.04	1.79	2.61	0.59	102.4	35.1
		55.0	24.6	8.56	8.16	1.00	1.69	2.52	0.57	102.1	34.9
		55.0	24.0	8.92	8.47	1.19	1.76	2.81	0.63	102.8	34.3
		55.2	24.1	8.91	8.98	1.10	1.75	2.82	0.64	103.5	34.1
SK08-019	44.50	50.8	25.8	13.0	6.16	1.32	2.56	2.08	0.47	102.3	50.8
		50.4	26.0	12.9	6.27	1.27	2.53	2.11	0.48	101.9	50.2
		51.5	25.5	11.7	7.01	1.12	2.30	2.35	0.53	102.0	45.3
		51.3	25.6	12.7	6.34	1.20	2.50	2.06	0.46	102.1	49.8
		52.8	25.3	12.1	6.67	1.10	2.38	2.10	0.47	102.9	48.3
		52.2	25.3	12.9	6.30	1.36	2.53	2.10	0.47	103.1	49.5
		52.3	25.5	12.7	6.33	1.26	2.50	2.11	0.48	103.1	49.6
		51.8	25.9	13.4	5.80	1.13	2.63	1.99	0.45	103.1	53.1
		52.4	25.0	12.0	6.69	1.33	2.37	2.14	0.48	102.5	47.1
		51.6	25.2	12.4	6.84	1.18	2.44	2.02	0.46	102.1	47.5
		52.3	25.3	12.1	6.28	1.34	2.38	2.17	0.49	102.3	48.2
		52.1	25.4	12.4	6.66	1.17	2.45	1.85	0.42	102.5	47.7
SK08-019	114.50	50.5	22.4	11.9	5.02	1.18	2.34	2.05	0.46	95.9	53.4
		50.0	22.5	12.0	5.13	1.22	2.36	2.06	0.46	95.7	53.0

		49.2	22.3	12.0	5.18	1.18	2.36	2.22	0.50	94.9	53.2
		48.2	22.1	12.2	4.93	1.13	2.41	2.15	0.48	93.5	54.6
SK08-020	20.45	54.5	25.1	10.8	7.62	0.76	2.13	2.14	0.48	103.5	43.4
		52.2	25.3	12.2	6.41	1.12	2.40	1.84	0.41	101.9	48.7
		56.3	24.4	9.14	9.02	1.08	1.80	2.71	0.61	105.0	34.5
SK08-021	63.22	47.7	22.2	12.3	4.89	1.04	2.43	2.17	0.49	93.2	55.4
		47.3	22.4	12.9	4.56	0.92	2.54	1.86	0.42	92.9	58.3
		46.2	21.8	12.6	4.79	0.93	2.49	1.71	0.38	90.9	57.1
		49.1	22.6	12.4	4.74	1.06	2.44	2.06	0.46	94.8	55.9
		48.9	22.6	12.7	4.61	1.19	2.50	2.06	0.46	95.0	56.6
		48.9	22.7	12.7	4.68	1.13	2.51	1.90	0.43	95.0	56.7
		48.6	22.5	12.9	4.52	1.04	2.54	1.98	0.45	94.5	58.1
		49.2	22.6	12.1	4.63	1.34	2.38	2.08	0.47	94.8	55.1
		48.9	22.8	12.1	4.70	1.33	2.37	2.01	0.45	94.6	54.5
SK08-022	40.02	51.9	22.0	11.3	5.24	1.13	2.23	2.30	0.52	96.6	51.3
		50.1	20.9	9.31	5.80	0.76	1.83	2.53	0.57	91.7	45.5
		52.0	21.5	9.80	6.05	1.00	1.93	2.34	0.53	95.1	44.9
		51.9	22.1	10.7	5.34	1.23	2.11	2.38	0.54	96.3	48.5
		51.3	22.0	10.9	5.44	1.12	2.15	2.09	0.47	95.5	50.0
		50.8	22.1	11.1	5.47	1.09	2.18	2.35	0.53	95.5	49.8
		50.7	22.3	11.6	5.33	1.01	2.28	2.14	0.48	95.8	52.1
		50.2	22.6	12.0	5.16	0.96	2.36	2.08	0.47	95.8	53.7
		50.1	21.8	10.7	5.35	1.21	2.11	2.44	0.55	94.3	49.4
		48.8	21.6	10.3	5.48	1.16	2.02	2.61	0.59	92.6	48.2
SK08-024	7.00	55.1	23.6	9.46	8.36	1.10	1.86	2.55	0.57	102.6	36.7
		54.7	23.7	9.40	8.20	1.03	1.85	2.52	0.57	102.0	37.1
		54.7	24.1	9.36	8.27	1.08	1.84	2.85	0.64	102.9	36.8
		54.1	24.1	9.79	8.12	1.04	1.93	2.35	0.53	101.9	38.5
		54.5	24.3	9.92	8.29	0.85	1.95	2.48	0.56	102.8	38.6
		54.4	24.5	9.78	8.55	0.73	1.93	2.62	0.59	103.1	37.6
		54.9	24.0	9.79	7.92	1.04	1.93	2.48	0.56	102.6	39.5
		52.3	23.8	10.1	7.69	0.75	1.99	2.32	0.52	99.5	41.3
		51.8	25.0	12.4	6.36	1.06	2.45	1.92	0.43	101.5	49.8
		51.6	25.5	12.4	6.33	1.12	2.45	2.04	0.46	101.9	49.8
		50.9	26.2	13.4	6.22	1.02	2.64	1.96	0.44	102.8	52.1
		56.7	23.0	7.23	8.83	1.15	1.42	3.22	0.72	102.3	30.2
		56.4	23.4	7.45	9.41	1.07	1.47	3.21	0.72	103.2	28.7
		51.0	25.3	11.8	6.58	0.82	2.33	2.05	0.46	100.4	47.9
		51.4	25.6	12.5	6.46	1.00	2.47	1.84	0.42	101.7	49.8
SK08-025	21.40	49.1	21.4	11.2	5.19	1.15	2.21	2.31	0.52	93.1	51.4
		47.0	21.4	11.1	5.24	1.20	2.18	2.34	0.53	90.9	50.5
		50.8	21.2	9.00	6.30	0.88	1.77	2.77	0.63	93.4	42.1
		50.4	20.7	8.90	5.99	0.76	1.75	2.49	0.56	91.5	43.4
		49.9	22.1	11.2	5.39	1.02	2.20	2.28	0.51	94.6	50.3
		49.4	22.0	11.0	5.66	1.06	2.17	2.22	0.50	94.0	49.1
		50.4	21.2	9.43	6.07	1.13	1.86	2.73	0.62	93.4	43.9
		50.0	21.5	9.65	6.15	1.16	1.90	2.76	0.62	93.7	43.8

		48.8	21.3	10.2	5.94	1.07	2.00	2.42	0.55	92.3	46.0
		48.2	21.6	10.8	5.76	1.09	2.13	2.45	0.55	92.6	48.0
SK08-026	34.00	50.0	24.7	12.9	6.01	1.28	2.54	1.94	0.44	99.8	51.2
		50.5	25.0	13.2	5.92	1.25	2.61	1.97	0.44	100.9	52.3
		50.0	25.0	13.0	6.09	1.27	2.57	2.00	0.45	100.4	51.4
		50.3	25.1	13.3	6.00	1.17	2.61	1.89	0.43	100.8	52.4
		50.7	25.3	12.9	5.97	1.24	2.53	1.83	0.41	100.9	51.5
		51.0	25.5	12.9	6.09	1.20	2.55	1.95	0.44	101.7	50.6
		50.7	24.9	12.9	6.25	1.15	2.55	1.70	0.38	100.6	50.6
		51.1	25.0	12.6	6.07	1.32	2.49	2.02	0.45	101.0	50.5
		50.3	25.1	13.4	5.93	1.06	2.63	1.65	0.37	100.4	52.7
		49.8	25.2	13.3	5.82	1.07	2.63	1.63	0.37	99.9	53.2
		50.7	25.2	13.1	5.97	1.10	2.58	1.68	0.38	100.7	52.2
		50.6	25.4	12.9	6.05	1.11	2.54	1.84	0.41	100.9	51.3
		50.7	25.3	13.8	5.68	1.10	2.72	1.77	0.40	101.4	54.5
		50.7	25.3	13.2	5.76	1.22	2.61	1.90	0.43	101.1	52.6
		51.1	25.4	13.4	5.60	1.12	2.63	1.80	0.41	101.4	53.8
		50.9	25.4	13.9	5.76	1.17	2.73	1.77	0.40	102.0	54.2
		50.6	25.7	13.9	5.63	1.05	2.74	1.65	0.37	101.7	55.0
		50.8	24.7	13.2	5.51	1.23	2.60	2.01	0.45	100.6	53.1
		51.2	24.9	13.0	5.85	1.21	2.56	1.92	0.43	101.1	52.2
		51.2	25.0	13.0	6.23	1.16	2.55	1.87	0.42	101.3	50.8
		51.5	25.0	12.7	5.93	1.12	2.51	1.80	0.41	101.0	51.3
		51.5	25.2	13.3	5.46	1.27	2.62	1.83	0.41	101.6	54.2
		51.4	25.4	13.1	5.72	1.26	2.57	1.84	0.41	101.6	52.7
SK08-027	37.00	55.8	24.2	9.18	9.14	0.98	1.81	2.82	0.63	104.6	34.2
		56.1	22.5	7.57	9.27	1.18	1.49	3.12	0.70	102.0	29.6
		56.3	22.6	7.55	9.13	1.09	1.49	3.09	0.70	101.9	30.2
		56.5	22.8	7.35	9.51	1.25	1.45	3.02	0.68	102.5	28.2
		56.8	23.0	7.50	9.28	1.11	1.48	3.06	0.69	102.9	29.1
SK08-043	9.50	52.2	22.8	9.86	7.02	0.96	1.94	1.98	0.45	97.1	42.4
		54.2	24.0	10.3	7.93	1.27	2.04	2.52	0.57	102.9	39.5
		54.2	24.3	10.4	8.37	1.16	2.05	2.27	0.51	103.2	39.0
		56.8	25.0	9.51	6.95	1.17	1.87	2.28	0.51	104.0	40.5
		50.3	22.7	10.5	6.04	0.93	2.06	2.19	0.49	95.1	46.8
		56.7	24.9	10.5	6.92	1.05	2.08	2.23	0.50	104.9	43.4
		57.0	25.6	10.6	6.93	1.24	2.10	2.54	0.57	106.6	43.7

Me: meionite ($Ca_4Al_6Si_6O_{24}CO_3$) scapolite group end-member.

Table 3.A-11. Amphibole compositions by EMPA.

Sample ID	Depth (m)	SiO_2	Al_2O_3	CaO	K_2O	Na_2O	MgO	FeO	MnO	TiO_2	Cl	-O=Cl	Totals	Mineral name*
SK08-003	66.10	48.5	0.47	11.7	0.09	0.06	4.50	30.3	0.78	0.19	0.04	0.01	96.5	Fe-Hornblende
		48.5	0.51	12.0	0.06	0.19	5.83	26.9	0.66	0.24	0.02	0.00	94.8	Fe-Hornblende
		45.2	1.61	11.7	0.06	0.16	6.38	26.9	0.60	0.19	0.05	0.01	92.9	Fe-Actinolite
		45.7	1.80	11.9	0.10	0.22	5.79	26.9	0.39	0.24	0.05	0.01	93.1	Fe-Hornblende
		46.3	0.40	19.4	0.02	0.08	5.81	21.0	0.46	0.05	0.00	0.00	93.5	Fe-Hornblende
		47.2	2.78	12.4	0.22	0.38	4.54	27.2	0.34	0.07	0.17	0.04	95.2	Fe-Hornblende
SK08-005	64.80	45.2	4.27	12.0	0.24	0.48	4.94	27.4	0.31	0.15	0.07	0.02	95.0	Fe-Actinolite
		46.7	3.15	11.8	0.20	0.31	4.90	27.6	0.46	0.05	0.09	0.02	95.3	Fe-Hornblende
		47.0	2.46	11.4	0.13	0.41	4.51	29.3	0.57	0.02	0.07	0.02	95.8	Fe-Hornblende
SK08-007	42.00	40.6	9.27	11.3	1.24	0.89	1.82	30.8	0.27	0.38	0.67	0.15	97.0	Fe-Edenite
		40.1	10.1	11.2	1.09	1.09	1.58	28.6	0.24	0.38	0.56	0.13	94.8	Fe-Edenite
		40.4	8.95	11.2	1.22	0.85	1.72	29.1	0.32	0.38	0.72	0.15	94.7	Fe-Edenite
		43.4	11.9	11.0	1.13	2.19	1.39	25.2	0.28	0.07	0.49	0.11	96.9	Fe-Edenite
		37.1	11.8	11.2	2.13	1.07	1.97	28.1	0.25	0.12	1.81	0.41	95.2	Fe-Pargasite
		39.6	10.6	11.3	1.25	1.15	2.51	28.5	0.33	0.26	0.63	0.14	96.0	Fe-Pargasite
		39.4	10.3	11.2	1.39	1.01	2.09	28.8	0.29	0.22	0.90	0.20	95.3	Fe-Edenite
		36.9	12.3	11.2	2.16	1.11	1.44	28.4	0.20	0.00	1.57	0.35	94.9	Fe-Pargasite
		37.5	11.9	11.3	1.49	1.27	1.29	28.7	0.25	0.02	0.92	0.21	94.4	Fe-Pargasite
		38.5	11.1	11.4	1.62	1.14	1.33	28.9	0.26	0.14	1.04	0.23	95.1	Fe-Pargasite
SK08-008	67.30	48.1	2.78	12.1	0.15	0.34	7.04	24.4	0.45	0.29	0.07	0.02	95.7	Fe-Hornblende
		48.0	2.00	11.9	0.14	0.15	7.03	24.8	0.39	0.02	0.06	0.01	94.5	Fe-Hornblende
SK08-009	54.00	33.1	12.6	10.6	2.61	1.01	1.51	29.4	0.25	0.38	1.95	0.44	92.9	Fe-Pargasite
		34.0	12.0	10.8	2.77	1.03	1.56	30.6	0.25	0.26	2.49	0.56	95.2	Fe-Pargasite
		35.2	12.2	10.9	3.03	1.00	1.59	30.4	0.32	0.07	2.38	0.54	96.7	Fe-Pargasite
		33.4	12.1	10.7	2.63	1.01	1.65	29.6	0.29	0.14	2.22	0.50	93.2	Fe-Pargasite
		34.2	12.1	10.7	2.70	1.19	1.53	30.6	0.08	0.29	2.32	0.52	95.1	Fe-Pargasite
		34.6	12.1	10.8	2.62	0.86	1.67	29.0	0.25	0.29	1.78	0.40	93.6	Fe-Pargasite
		35.1	11.7	10.7	2.48	1.19	1.42	31.0	0.25	0.17	2.17	0.49	95.7	Fe-Pargasite
		34.6	12.1	10.8	2.91	1.01	1.60	28.5	0.17	0.05	2.08	0.47	93.4	Fe-Pargasite
		35.2	12.2	10.8	2.37	0.95	1.84	28.8	0.19	0.38	1.86	0.42	94.2	Fe-Pargasite
		34.8	11.9	11.0	2.49	1.09	1.81	27.8	0.30	0.19	1.63	0.37	92.7	Fe-Pargasite
		35.5	12.3	11.1	2.71	1.19	1.59	28.9	0.05	0.02	2.19	0.47	94.9	Fe-Pargasite
		36.7	12.2	11.1	2.62	1.04	1.92	29.8	0.30	0.17	1.86	0.42	97.2	Fe-Pargasite
		36.9	12.5	11.0	2.45	0.99	1.78	28.1	0.28	0.14	1.76	0.40	95.5	Fe-Pargasite
		42.2	3.50	11.2	0.47	0.41	4.43	28.5	0.25	0.00	0.23	0.05	91.1	Fe-Actinolite
		31.4	11.3	10.2	2.45	1.16	1.56	30.6	0.15	0.21	2.16	0.49	90.6	Fe-Pargasite
		34.4	12.1	10.8	2.67	1.07	1.60	30.4	0.00	0.38	2.07	0.47	95.2	Fe-Pargasite
SK08-013	208.00	46.1	1.78	11.9	0.09	0.38	10.2	23.6	0.36	0.00	0.05	0.01	94.5	Fe-Actinolite
SK08-016	51.50	48.4	0.85	11.5	0.05	0.11	8.23	24.5	0.47	0.00	0.08	0.02	94.2	Fe-Hornblende
SK08-019	70.10	43.3	7.02	11.7	0.77	0.83	5.40	25.0	0.27	0.00	0.33	0.07	94.5	Fe-Actinolite
		41.6	6.42	11.6	0.64	0.78	5.67	25.0	0.26	0.00	0.20	0.05	92.1	Fe-Actinolite
		43.0	5.09	11.6	0.64	0.59	5.62	25.7	0.31	0.00	0.36	0.08	92.8	Fe-Actinolite
		43.6	4.79	11.5	0.42	0.61	6.00	25.0	0.25	0.00	0.26	0.06	92.4	Fe-Actinolite
		44.1	4.73	11.5	0.62	0.57	5.19	27.0	0.31	0.00	0.38	0.08	94.3	Fe-Actinolite
		39.9	8.89	11.7	0.99	1.04	4.31	25.7	0.19	0.02	0.41	0.09	93.0	Fe-Edenite
		41.0	7.20	11.2	0.97	0.97	4.55	25.7	0.38	0.32	0.50	0.11	92.6	Fe-Edenite
SK08-022	40.02	49.8	2.11	13.3	0.13	0.21	5.88	24.0	0.47	0.19	0.07	0.02	96.2	Fe-Hornblende
		49.6	2.35	11.4	0.15	0.21	6.22	24.8	0.47	0.34	0.08	0.02	95.6	Fe-Hornblende
		51.2	4.74	11.5	0.14	0.40	4.22	21.6	0.23	0.07	0.06	0.01	94.1	Fe-Hornblende
SK08-024	7.00	48.3	3.44	12.3	0.24	0.35	6.24	26.7	0.47	0.00	0.09	0.02	98.0	Fe-Actinolite
SK08-043	9.50	48.5	1.72	12.1	0.16	0.22	7.81	23.8	0.48	0.22	0.07	0.01	94.9	Fe-Hornblende
		46.2	2.60	11.7	0.29	0.30	5.40	28.0	0.39	0.17	0.06	0.01	95.1	Fe-Actinolite
		50.1	2.92	12.0	0.15	0.28	6.69	24.2	0.34	0.29	0.03	0.01	97.0	Fe-Hornblende
		50.3	1.97	11.9	0.13	0.20	6.45	24.8	0.56	0.29	0.07	0.02	96.7	Fe-Hornblende

*Classification based on the nomenclature of Leake et al., 1997.

4. Structural Geology and Ore Body Morphology

4.1. Introduction

Structural geology plays a major role in the formation and preservation of an ore body by these and other mechanisms: (1) fluid pathways (commonly contacts and (or) faults); (2) structural traps for fluids; and (3) disruption of the ore body by post-mineralization dikes and faults. All of these are important in the Mike Lake skarn system and none have been addressed by previous workers. The structure of the Skarn Ridge area and morphology of the Skarn Ridge ore body presented here is based on a compilation of surface mapping, drill core logging, and examination of the two in 3D with Vulcan™ and Leapfrog™ software. Because we did not drill oriented core, lithological unit orientations must be determined by connecting known units between drill holes and then correlating the units to the surface geological map. As several geologists logged the core and worked on the surface geologic map, assembling all the observations into a coherent body was a non-trivial task aided in many cases by geochemical analyses of the core samples.

4.2. Methods

Fieldwork for this project was conducted from May-August 2008. During that time I logged several kilometers of drill core and helped make a detailed (1:5,000 scale) surface map of Skarn Ridge and the surrounding area (Figure 3.1). Sub-surface geological modeling was conducted using two different 3D modeling software packages: Vulcan™ (by Maptek™, Lakewood, Colorado) and Leapfrog™ (by AranzGeo™, New Zealand). All drill hole data was compiled into a master database, which included collar

location (X, Y, Z), orientation (azimuth, dip), total drill hole depth (TD), lithology, assays, and mineral composition (clinopyroxene, garnet, scapolite, and arsenopyrite) data from this study. This database was imported into both software programs where each was used to model different aspects of the geology. I used Vulcan™ to plot, hand-digitize, and connect drill hole data to create 3D shapes and surfaces (also called 'solids' or 'triangulations') for some key geologic features. The features I modeled include topography, a dike, mafic sills, a lithologic contact (the black hornfels/skarn contact), and a fault (SAM's Fault). All other contacts and structures were either too complex to model at the same resolution or could easily be compartmentalized within the framework of my 3D model. I used Leapfrog™ to composite assay data into 2 meter intervals and then interpolate the assay data to create 'grade shells' for Au, Cu, W, and other elements. Grade interpolation was conducted using standard geological modeling parameters (Baojun et al., 2009), including a 'clip transformed value distribution', which allowed all assay values to be included in the calculations. Variogram parameters included a spheroidal model, sill = 1, range = 75 m, nugget = 0.3, and constant drift (ordinary Kriging). A structural trend (defined by the local dip of bedding) was superimposed on the variogram to 'force' the elongation of grade shells to trend with the observed geology and mineralization controls. Leapfrog™ grade shells and mineral compositional data were superimposed on my Vulcan™ 3D geology model in order to better assess ore distribution by lithology, ore controls, and zoning relationships in this complex skarn system.

4.3. This Study

Extensive talus cover and lack of outcrop makes most of the unit contacts on the surface tentative; units encountered at the tops of drill holes are generally used to determine bedrock at drill hole sites. Unit orientations are also mostly uncertain except at the rare outcrops (Figure 3.1). Significant map features include a body of marble on the west side of Skarn Ridge, black hornfels on the east side, dikes of variable orientations suggested by float patterns, and both NW-SE and NNE-SSW oriented folds indicated by bedding/foliation measurements and rare outcrop-scale fold axes.

In drill core, the most consistently identified lithologic features were the various felsic dikes and the contact between calc-silicate rocks and the underlying black siliceous hornfels. This typically sharp contact is present 100-150 meters below the surface near the top of Skarn Ridge, but the distance tapers downslope. The 'main' felsic porphyritic dike near the top of Skarn Ridge is the most straightforward geologic feature: it occurs as a near-vertical body 10-12 meters wide, striking approximately E-W (Figure 3.1). Although little altered and lacking Au-Cu mineralization, the dike itself does not appear to offset lithologic units or mineralization. Additional dikes of the same generation occur on Skarn Ridge in areas that were drilled less extensively (Figure 3.1).

In contrast, the extensively altered mafic sills were the least consistently identified unit on Skarn Ridge. They exhibit a tabular to undulatory morphology that is broadly concordant with, but also appears to shallowly cut across the enclosing rock (Figure 4.1). There are at least two sills; the upper sill is thicker and more continuous than the lower sill, although drilling may not have gone deep enough to determine the true extent of the

lower sill. They both taper up-dip (to the north) and generally thicken down-dip (to the south and southwest). In the east, the upper sill appears to exploit the skarn-black hornfels contact, however it diverges from this contact to the west (Figure 4.1). Both sills are cut (but not offset) by porphyritic and green dikes (Figure 4.2).

Reconstruction of the altered mafic sills reveals that Skarn Ridge is approximately bisected by a N-S striking, steeply-east-dipping (~015°, 85° E) normal fault, "SAM's fault" (Figure 4.1). The fault displaces the sill such that the eastern half is approximately 80 meters (260 feet) lower than its western half. The surface expression of SAM's fault is minimal in terms of apparent offset (< 10 meters), however it does occupy the main drainage in the drilled area and several geological features terminate at its trace (Figure 3.1). It causes only a slight apparent left-lateral offset in the only major E-W striking porphyritic dike on Skarn Ridge, as well as major vertical displacement of mafic sills and all metamorphic units that can only be seen in subsurface drill core examination. This fault was not noted during mapping in the summer of 2008; however, it must be present to account for the geometries observed immediately to the east and west of its inferred location and in the subsurface. SAM's fault clearly cuts across the ore body and mineralization (Figure 4.3 A). The cross-cutting relationships indicate that post-ore normal faulting is the last significant structural event to take place on Skarn Ridge.

The black, siliceous hornfels is positively distinguishable from overlying calc-silicate-bearing rocks. Lack of any indicators of shear at the contact with the overlying rocks makes it likely that the contact is depositional and was originally horizontal. Thus, the present (non-horizontal) orientation of this contact presumably reveals details of the

broad-scale folds and faults that are present here. From a geological modeling perspective, this stratigraphic boundary is important because it is accurately identified in most core logs, and therefore a relatively simple and unambiguous surface to model. In addition, most drill holes reached this contact, as it defines the bottom of significant mineralization (Table 4.1). That is, drilling at a given site was stopped only after the drill reached this horizon.

I modeled the top of the black hornfels by placing a point on each drill hole trace to mark the top of the unit, and then I connected all of the points with a 3D triangulation mesh. The top of the unit sits approximately 120 meters below the surface at its deepest point (just north of the main porphyritic dike). This distance gradually tapers downdip and downslope until it reaches the main drainage south of Skarn Ridge where it crops out again intermittently (Figure 3.1). Figure 4.3 shows contours of the top of the black hornfels with a 15 m contour interval, using the 3D triangulation mesh as a base.

The structure contour map (Figure 4.4) shows that the upper contact of the black hornfels unit—and, by inference, the surrounding region—is complexly folded and cut by the same steeply-dipping normal fault identified as cutting the mafic sills. East of the normal fault the structure contours identify a major west-plunging antiform with a nearly E-W axis and a less well-defined, west-plunging syncline approximately 120 meters to the north (Figure 4.4). West of the normal fault the situation is considerably more complicated. An east-plunging anticline apparently bifurcates into an east and a southeast-plunging anticline. South of the anticline a series of south to south-southwest

plunging folds, each spaced about 70 meters apart, dominates the structure contours (Figure 4.4).

The overall structural pattern, observed by combining surficial and sub-surficial geology (Figure 3.1) shows that both approximately E-W striking and N-S trending fold axes are present in the region. Dikes apparently cut across the fold axes and display no evidence of folding.

4.4. Ore Body Morphology

The Skarn Ridge ore body is defined by high concentrations of Au and Cu in a lithologically and structurally controlled package. The focus of mineralization is in the NW corner of Skarn Ridge where the general shape of the ore body resembles a crude U-shape that opens toward the southeast in plan view (Figure 4.3 A). In section view (looking east), its folded appearance mimics the shape of the anticline observed at the upper contact of the black hornfels. The ore body displays strong vertical continuity from the surface to near the base of the skarn unit (top of the black hornfels), below which the grade becomes spotty and discontinuous (Figure 4.3 B). Low to trace concentrations of base metals and pathfinder elements extend throughout and beyond the drilled area (as observed during field mapping). Neither the dikes nor the Mike Lake pluton are mineralized; both sets of dikes (porphyritic and green) clearly cut across mineralization with sharp, abrupt contacts (Tables 4.2 and 4.3). Vertically continuous mineralization in skarn and calc-silicate hornfels is observed for 120 meters (true thickness) in the NW corner of the drilling area, but it diminishes to the south and east (Figure 4.3 B); there is no information to the north and west due to the lack of drilling in

this area. Laterally continuous mineralization continues to the east and south for approximately 500 meters (Figure 4.3 A). Mineralization will be discussed in detail in Chapter 5.

4.5. Discussion

The structural complexity of Skarn Ridge is not fully obvious from the surface. Detailed examination of the sub-surface geology, by both structure contours in the top of the black hornfels (Figure 4.4) and by cross sections (Figure 4.2), reveals at least two generations of folding and at least two generations of faulting (one occupied by dikes). The major NNE-trending post-ore normal fault that bisects Skarn Ridge displaces the ore body down to the east by ~100 m, as shown by assay contours.

The oldest structures include two sets of folds; one with NNE-trending fold axes, which are overprinted by folds with WNW-oriented axes. The latter dominate the subsurface structural fabric of Skarn Ridge. Presumably these indicate two different collisional events with stresses oriented roughly perpendicular to each other (producing so-called 'egg-crate' folding). Structural complexity at Mike Lake is likely related to the northeasterly-directed compression from the Mesozoic thrust event that produced the Robert Service, Tombstone, and Dawson thrust faults and associated regional deformation (Figure 2.4).

The shape of the ore body, based on assay contours, appears to be mostly controlled by the stratigraphy. Ore is confined to the calc-silicate lithologies, which crop out on Skarn Ridge and are bounded below by the siliceous black hornfels. As a result, the shape of the ore body broadly mimics the orientation of the rock layers. Although the

ore is not concentrated at the top of an anticline, the overall shape is elongated to the WNW, subparallel to the fold axes. The concentration of ore in the northwest quadrant of Skarn Ridge seems to be a combination of both one large-scale marble front (Figure 3.1) and several small-scale individual marble fronts created by the complexly interlayered skarn and calc-silicate hornfels units.

Felsic porphyritic dikes cut across Skarn Ridge in two main orientations, ~030° and ~090°. Their presence indicates local extension sometime post-ore, as there is no obvious displacement of the ore body. It is possible that the orientations represent a conjugate set of fractures that are oriented roughly parallel to the two generations of fold axes, NNE and WNW, and that the axes provided planes of weakness to accommodate the minor extension.

Finally, SAM's fault is the youngest structural feature present. Its orientation roughly parallels the NNE trending fold axes, which are a likely plane of weakness. In this context, the absence of more such normal faults in the study area is strikingly odd. Perhaps there are more, but with less noticeable offsets. The 'normal' sense of slip on this fault and offset of dikes and ore indicates that extension took place again after magmatism. The timing of this extension is not well constrained and could have been any time after the mid-Cretaceous, based on the observed cross-cutting relationships.

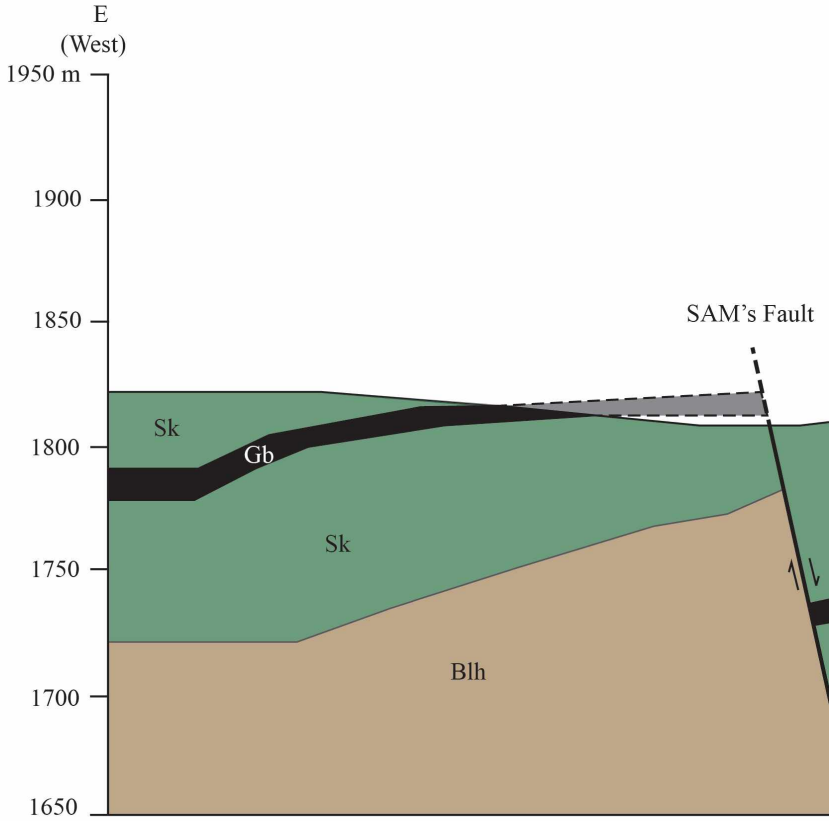

Figure 4.1. Displacement of mafic sill (Gb) along SAM's fault.
Simplified view of the geology along the E-E' cross section line (Figure 3.2).

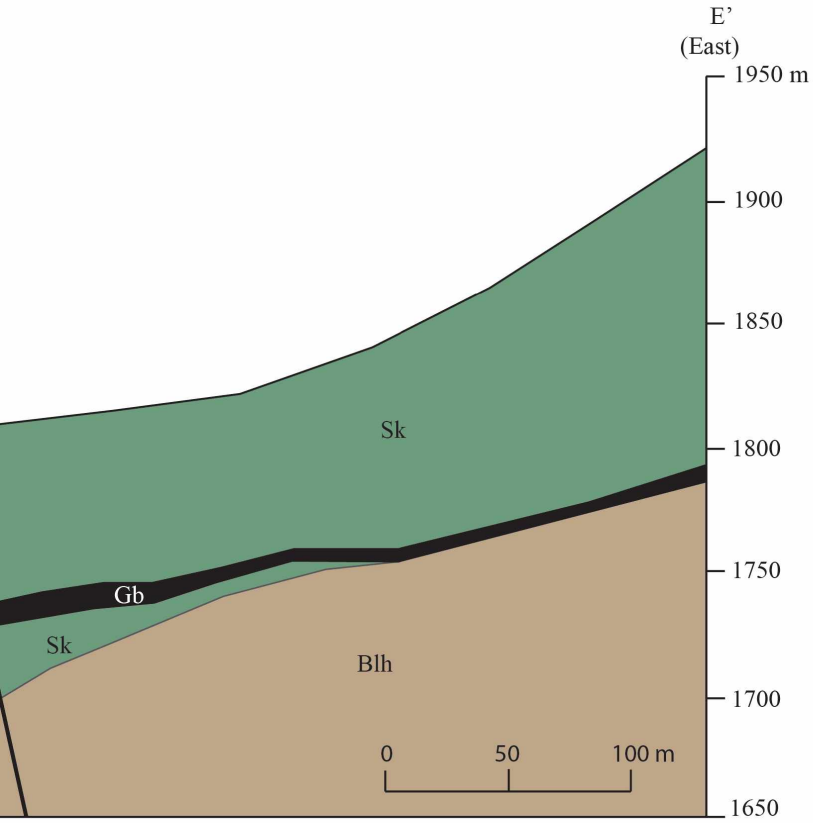
E'
(East)
1950 m
1900
1850
1800
1750
1700
1650
Sk
Gb
Sk
Blh
0
50
100 m

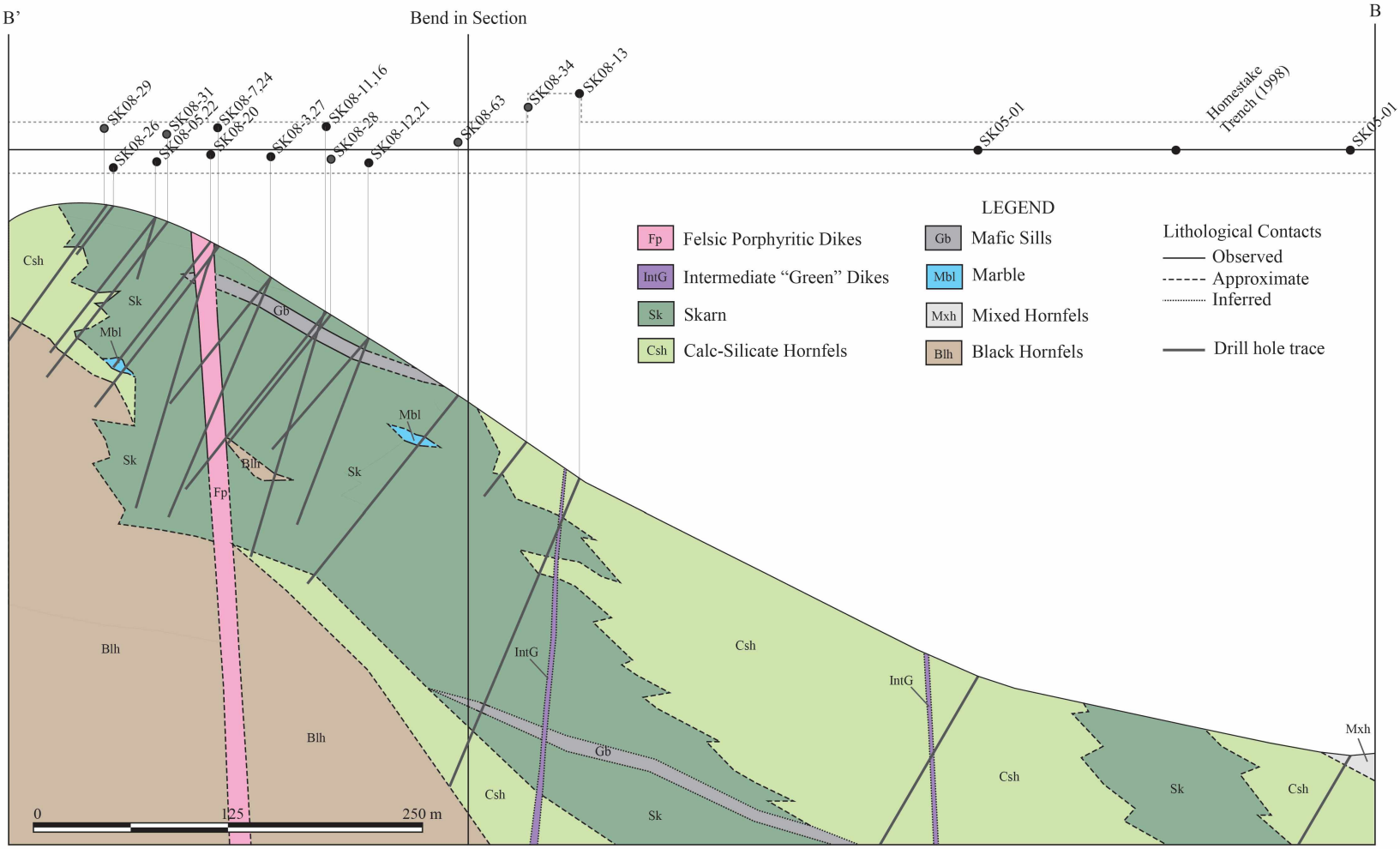

Figure 4.2. General geology along cross section B'-B.
Mafic sills are cut by younger felsic and intermediate dikes. For cross section reference map, see Figure 3.2.

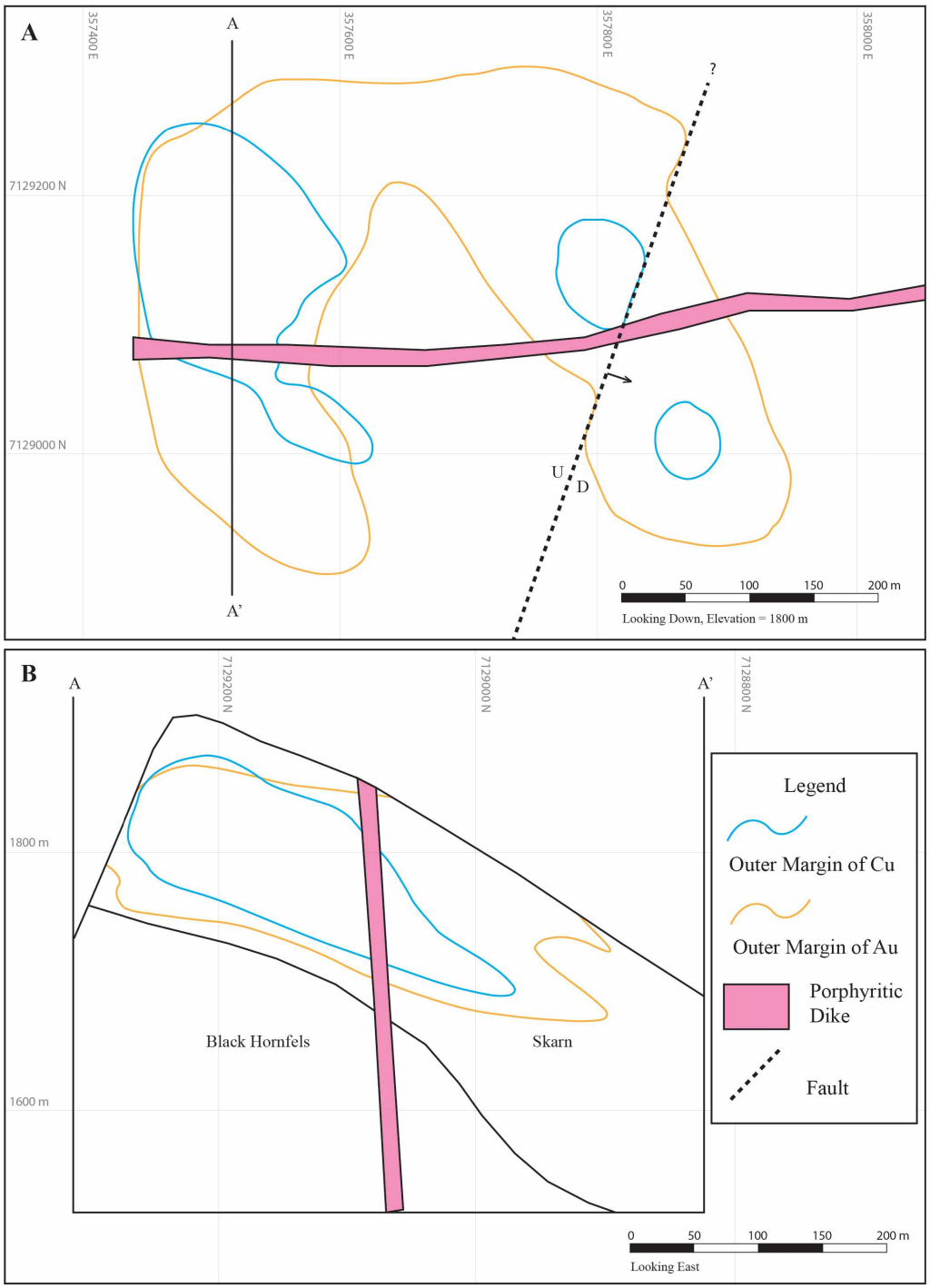

Figure 4.3. Ore body morphology based on low-grade Au and Cu grade shells.
A: the main porphyritic dike and SAM's Fault both cut across mineralization. B: a section view of line A-A' from plan view (A) above.

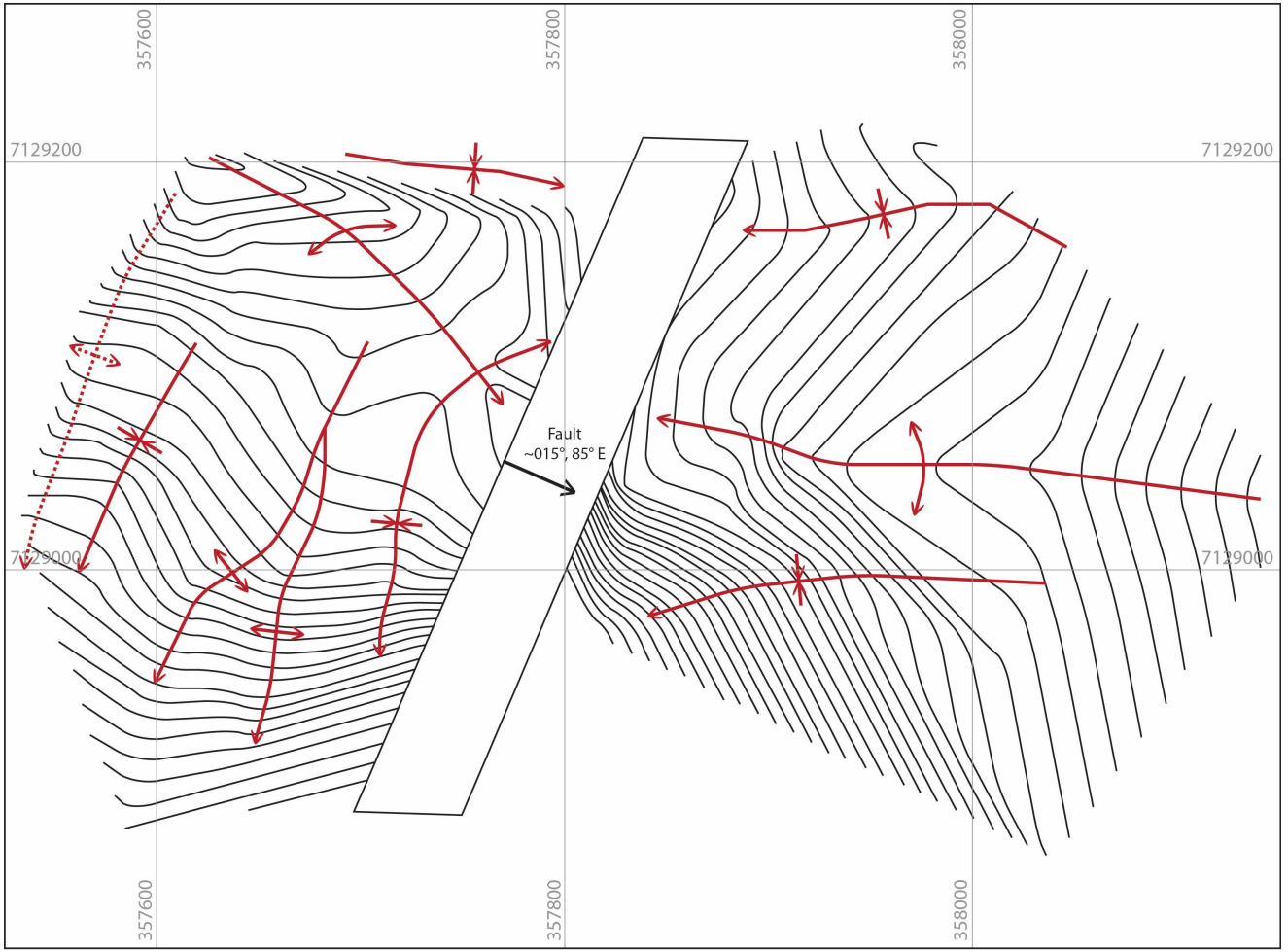

Figure 4.4. Structure contour map of the top of the black hornfels unit.
Roughly perpendicular fold axes illustrate the complexity of folding that is not apparent from the surface geology. For location reference, see Figure 3.2.

Table 4.1. Grade distribution across the skarn-hornfels contact.
Gold concentrations are listed as: BDL = below detection limit; L = low; M = moderate.

Hole ID	Thickness		Parts per Million						
(SK08-)	(m)	Lithology	Au	Ag	As	Bi	Cu	W	Zn
003	2.00	Skarn	M	7	6890	340	BDL	60	170
	2.00	Skarn	BDL	1	1740	BDL	140	BDL	80
	2.00	Skarn	L	BDL	650	20	160	120	60
	1.00	Skarn	BDL	BDL	310	BDL	270	50	100
	2.00	Hornfels	BDL	BDL	80	BDL	280	BDL	50
	2.00	Hornfels	BDL	BDL	BDL	BDL	60	BDL	50
	2.00	Hornfels	BDL	BDL	BDL	BDL	40	BDL	60
007	2.00	Skarn	L	3	410	30	1210	BDL	150
	2.00	Skarn	L	BDL	300	20	460	BDL	110
	2.00	Skarn	BDL	3	240	BDL	700	1820	120
	2.00	Skarn	L	8	2920	20	3770	420	190
	2.00	Hornfels	L	2	680	BDL	720	BDL	90
	2.00	Hornfels	BDL	4	370	BDL	BDL	BDL	100
	2.02	Hornfels	BDL	2	BDL	BDL	110	BDL	40
	2.14	Hornfels	BDL	BDL	BDL	BDL	90	BDL	20
025	2.85	Skarn	L	BDL	150	20	410	BDL	80
	2.31	Skarn	L	1	830	50	730	BDL	110
	2.17	Skarn	L	BDL	1120	70	380	BDL	100
	1.44	Skarn	M	1	12650	330	BDL	BDL	100
	2.94	Hornfels	BDL	BDL	1200	BDL	110	BDL	100
	1.44	Hornfels	L	BDL	1240	20	190	BDL	100
	1.54	Hornfels	L	BDL	370	BDL	180	BDL	120
042	2.99	Skarn	L	2	160	60	680	BDL	160
	2.06	Skarn	L	1	200	30	BDL	BDL	110
	1.28	Skarn	L	3	160	40	400	BDL	120
	2.96	Hornfels	L	3	60	BDL	40	BDL	130
	3.00	Hornfels	BDL	1	BDL	BDL	30	BDL	170
	2.98	Hornfels	BDL	BDL	BDL	BDL	20	BDL	150
051	3.01	Skarn	M	1	23900	140	40	70	40
	2.99	Skarn	L	BDL	1760	BDL	BDL	BDL	50
	2.52	Skarn	L	BDL	8360	20	BDL	BDL	50
	0.96	Hornfels	BDL	1	1410	BDL	80	BDL	60
	3.03	Hornfels	BDL	BDL	90	BDL	40	BDL	80
	3.00	Hornfels	BDL	BDL	BDL	BDL	30	BDL	30

Table 4.2. Grade distribution in and around felsic porphyritic dikes.
Gold concentrations are listed as: BDL = below detection limit; L = low; and H = high.

Hole ID	Depth (m)			Parts per Million						
(SK08-)	From	To	Lithology	Au	Ag	As	Bi	Cu	W	Zn
003	68.00	70.00	Skarn	L	2	5760	150	940	<50	110
	70.00	73.00	Skarn	L	2	4210	50	630	<50	110
	73.00	75.00	Felsic Porphyritic Dike	BDL	<1	<50	<20	50	<50	30
	75.00	78.00	Felsic Porphyritic Dike	BDL	<1	<50	<20	30	<50	40
	78.00	81.00	Felsic Porphyritic Dike	BDL	<1	<50	<20	30	<50	40
	81.00	84.00	Felsic Porphyritic Dike	BDL	<1	<50	<20	20	<50	30
	84.00	87.00	Felsic Porphyritic Dike	BDL	<1	<50	<20	<10	<50	30
	87.00	90.00	Felsic Porphyritic Dike	BDL	<1	<50	<20	<10	<50	30
	90.00	92.00	Felsic Porphyritic Dike	BDL	<1	<50	<20	10	<50	30
	92.00	93.18	Felsic Porphyritic Dike	BDL	<1	540	<20	20	<50	<20
	93.18	94.00	Skarn	H	9	18050	70	3740	<50	150
	94.00	96.00	Skarn	L	6	36800	20	4970	<50	210
	96.00	98.00	Skarn	L	3	28800	30	1820	<50	140
039	34.00	35.97	Skarn	H	9	3090	460	3940	<50	260
	35.97	38.27	Skarn	L	5	190	90	520	<50	100
	38.27	41.00	Felsic Porphyritic Dike	L	<1	90	<20	20	<50	60
	41.00	44.00	Felsic Porphyritic Dike	BDL	1	<50	<20	10	<50	50
	47.72	50.72	Felsic Porphyritic Dike	BDL	<1	<50	<20	10	<50	50
	50.72	53.72	Felsic Porphyritic Dike	BDL	3	60	<20	290	<50	120
	53.72	56.72	Skarn & Hornfels	L	1	<50	<20	170	<50	110
	56.72	58.50	Skarn & Hornfels	BDL	4	<50	<20	120	<50	90

Table 4.3. Grade distribution in and around the green dikes.
Gold concentrations are listed as: BDL = below detection limit; L = low; H = high.

Hole ID	Depth (m)			Parts per Million						
(SK08-)	From	To	Lithology	Au	Ag	As	Bi	Cu	W	Zn
009	65.00	66.82	Skarn & Hornfels	L	1	1140	<20	70	<50	100
	66.82	68.84	Skarn & Hornfels	L	2	1210	70	620	<50	120
	68.84	69.31	Green Dike	BDL	1	160	<20	50	<50	60
	69.31	71.20	Skarn & Hornfels	L	1	1770	120	240	<50	80
	71.20	73.00	Skarn & Hornfels	L	1	410	20	20	<50	100
011	41.00	43.00	Skarn	L	1	3690	50	1470	90	90
	43.00	44.05	Skarn	L	1	3450	100	830	<50	60
	44.05	44.80	Green Dike	L	<1	540	<20	150	<50	<20
	44.80	46.00	Skarn	L	1	2160	100	1470	<50	70
	46.00	48.00	Skarn	L	2	1420	150	1340	<50	80
016	48.03	50.04	Skarn	BDL	1	2940	20	790	<50	120
	50.04	52.22	Skarn	L	5	1070	80	3470	<50	200
	52.22	53.26	Green Dike	BDL	1	2020	30	400	<50	70
	53.26	55.73	Skarn	L	7	3120	180	1790	<50	120
	55.73	57.50	Skarn	L	3	3720	80	2210	660	130
021	25.74	27.92	Skarn	L	<1	1340	60	30	<50	110
	27.92	30.14	Skarn	L	<1	1060	<20	60	<50	100
	30.14	30.92	Green Dike	L	<1	<50	<20	30	<50	30
	30.92	32.61	Skarn	H	8	17850	920	3450	<50	130
	32.61	34.59	Skarn	H	11	4070	570	4650	680	170

4.6. References

Baojun, W., Bin, S., and Zhen S., 2009, A simple approach to 3D geological modeling and visualization: Bulletin of Engineering Geology and the Environment, v. 68, p. 559-565.

5. Mineralization

5.1. Introduction

The Skarn Ridge ore body is defined by high concentrations of gold, bismuth, and copper, ± tungsten, hosted in a lithologically complex and structurally controlled package. Ore, in the sense of mineralized rock that *could* be mined for a profit (depending on metal prices, infrastructure, etc.) is largely restricted to skarn. However on Skarn Ridge not *all* skarn is ore and not all ore is in skarn.

The lithological package on Skarn Ridge can be broadly divided into two types: 'ore' and 'barren' (including weakly mineralized rocks that are not considered to be ore). Figure 5.1 shows that ore-bearing lithologies include skarn, calc-silicate hornfels, and a mixture of the two rock types, while barren (and weakly mineralized) lithologies include all other metamorphic and igneous rocks. It is clear that the black hornfels, grit, and marble have very slight enrichments in Cu, though they rarely contain Au or W above detection limits. Mafic sills are anomalous in Au and Cu but not in W. Green dikes are anomalous in Au and Cu, and have noticeable enrichments in W, but the porphyritic dikes are marginally anomalous in Cu and are consistently below detection limits for W and Au. Besides the rare occurrences of W in the green dikes (e.g., SK08-054, 73.40-75.02 m), all other notable W occurrences are in skarn and calc-silicate hornfels. Generalizations can also be made regarding the textures and mineralogy of ore versus barren rock. Ore-bearing rocks tend to be dominated by medium- coarse-grained calc-

silicate minerals; barren lithologies (except for igneous rocks) tend to be fine-grained with variable compositions (quartz- to biotite-rich) but are generally calc-silicate poor.

A geologist attempting to accurately classify the rock types at Skarn Ridge faces many challenges; consequently rock types (as reported in drill logs) are not always accurate. All metamorphic rocks on Skarn Ridge are complexly interlayered; to what extent this complexity is due to original sedimentary bedding versus metamorphic intercalation is not known. Compounding this is the overprint of metasomatism, which created a real (and apparent) compositional variability that was difficult to resolve in the field. The interlayered nature of skarn and calc-silicate hornfels combined with the low-resolution core logging (minimum logging interval = 1 meter) led to lumping of these units over assay intervals (typically ~ 2 m) depending on which unit appeared to be present in greater abundance.

There are essentially two end members of 'skarn' (as logged) at Mike Lake: the first is 'true' skarn (inferred marble protolith), the second is variably metasomatized calc-silicate hornfels (calcareous siltstone protolith). The rocks present span the complete range. In some cases, however, it is simply unclear whether a given calc-silicate rock was originally marble versus hornfels. Where scapolite is abundant, I am reasonably certain that the protolith was marble, as scapolitic marble is common in the area, and scapolitic hornfels is not. Similarly, fine-grained calc-silicate hornfels is easily distinguishable from coarser-grained skarn (marble protolith rocks). But in the absence of scapolite and/or fine-grained calc-silicate hornfels, for a given green rock it is

uncertain precisely what the protolith was; it could have been any combination of skarn and (or) calc-silicate hornfels. Rocks fitting into this spectrum were logged as the dominant rock type to the nearest meter, either as 'skarn', 'mixed skarn + calc-silicate hornfels', or as 'calc-silicate hornfels'. At this resolution, rare 2 cm wide skarn veins cutting calc-silicate hornfels would not change the classification from hornfels to skarn, but could have an enormous effect on the metal grades reported for a given lithology. Such a classification scheme does not show the spatial distribution of skarn well, but more detailed (hence, accurate) logging schemes cause different problems.

The most common ore minerals on Skarn Ridge are (in decreasing order of abundance) pyrrhotite, chalcopyrite, arsenopyrite, sphalerite, cubanite, native bismuth, gold (electrum), scheelite, galena, marcasite, the telluride minerals hedleyite and hessite, and Ni-Sb-(S) minerals (nisbite, breithauptite, and ullmannite). Neither pyrite nor bismuthinite are apparently present *anywhere* on Skarn Ridge, attesting to the low sulfidation state of the system. Styles of mineralization include patchy and net-textured replacements of skarn, patchy replacements of calc-silicate hornfels and mafic sills, 'skarn' veins, metallic sulfide veins (including veinlets and stringer veins), disseminations, and rare semi-massive replacements (Figure 5.2).

The purpose of this chapter is to describe the distribution of ore minerals at Mike Lake, both between the different rock types and within the Skarn Ridge area. This work leans heavily on reflected light petrography (as confirmed by the electron microprobe), and on the large data set of rock analyses from drill core. I ultimately attempted to

understand and show the complex ore geometries using Vulcan™ and Leapfrog™ 3D modeling software.

5.2. Mineral Textures and Occurrences

5.2.1. Pyrrhotite and Marcasite

Pyrrhotite ($Fe_{1-x}S$) is ubiquitous, occurring in all units except for the Mike Lake pluton and felsic porphyritic dikes. It is present as both hexagonal (high temperature, non-magnetic) and monoclinic (low temperature, magnetic) varieties. To distinguish between the two, I used a 1:10 dilution of magnetic colloid "ferrofluid" in turpentine and an eyedropper to transfer 1-2 drops onto each thin section; the magnetic particles are attracted to monoclinic pyrrhotite, revealing the two types that were otherwise indistinguishable (Figure 5.3). Monoclinic pyrrhotite is most abundant (~70% of all pyrrhotite) in the samples I looked at and it commonly replaces hexagonal pyrrhotite along grain boundaries or other planes of weakness (Figure 5.3 A). Supergene marcasite, where present, preferentially replaces the monoclinic variety (Figure 5.3 B). Less than 10% of all thin sections I examined displayed supergene marcasite.

In skarn and calc-silicate hornfels, pyrrhotite occurs as patchy replacements, veins and veinlets, and as rare semi-massive replacements of clinopyroxene and calcite. In black hornfels, pyrrhotite tends to occur as disseminations, blebs, and discontinuous stringer veinlets. Mafic sills are the only igneous rocks that contain pyrrhotite; it is present in veins and as coarse disseminations throughout the sills where it is most commonly observed as a product of the breakdown of primary biotite. The breakdown

products include secondary biotite and rutile, and the pyrrhotite often replaces altered groundmass. Less commonly, it occurs with scapolite + calcite + clinopyroxene.

5.2.2. Chalcopyrite

Chalcopyrite ($CuFeS_2$) is almost as common as pyrrhotite and it occurs in the same lithological units, although it is significantly less abundant than pyrrhotite in black hornfels and mafic sills. In skarn, chalcopyrite is most frequently present as patchy and net-textured replacements of clinopyroxene and less commonly as veins or veinlets. Net-textured replacements occur in scapolite-rich (> 30% by volume) skarn where mineralization (chalcopyrite and/or pyrrhotite) directly replaces interstitial clinopyroxene and leaves the abundant scapolite unaffected. The resulting appearance is a honeycomb or net-textured mineralization style. Alternatively, in scapolite-poor skarn, sulfide replacements often appear coarse and patchy.

Another important chalcopyrite occurrence is as 'skarn veins'. Skarn veins are narrow zones (typically 2-3 cm wide) of chalcopyrite + clinopyroxene + calcite, which cut across otherwise barren skarn and/or calc-silicate hornfels (Figure 5.2 C). Other minerals that occur in skarn veins include pyrrhotite, native bismuth, and gold. Core intervals containing skarn veins yield much higher gold and copper values in the veins than in the surrounding rock, based on re-examining the core with assay results in hand.

Despite the strong assay correlation between silver and copper (see ahead), the Ag concentration in chalcopyrite is below detection by microprobe analysis (ca. 0.05 wt %) in one sample (SK08-011, 76.50 m, Table 5.1) although appreciably present in another

sample (SK08-005, 15.75 m). Silver might be present as micro-inclusions of a Cu-Ag-S mineral in SK08-011 (76.50 m), or the particular grains analyzed might not have been representative, or sample might not have been representative. In contrast, the elements Bi, As, and Sb are not present above detection levels in the grains analyzed (Table 5.1). Cubanite and sphalerite are also intimately associated with chalcopyrite, as described ahead.

5.2.3. Cubanite

Cubanite ($CuFe_2S_3$) is only present as exsolved grains in chalcopyrite, and never as isolated grains. The optical properties of cubanite (as observed in reflected light) are quite similar to chalcopyrite, hence the distinction between them is subtle (cubanite is slightly more pink than chalcopyrite and anisotropism is more distinct). Cubanite takes on an elongate lath-shaped and (occasionally) triangular form inside of some chalcopyrite crystals (Figure 5.4 A, B). The mineral is best observed under nearly crossed polars, where cubanite displays more intense anisotropism. The abundance and distribution of cubanite is not fully known since it was only confirmed in one thin section (SK08-019, 77.20 m) and it is easy to overlook.

At high temperatures a solid solution phase exists in the Cu-Fe-Zn-S system ("*iss*" – intermediate solid solution), which, on cooling, turns into chalcopyrite with exsolved cubanite ± sphalerite (Craig and Kullerud, 1969). Hence the presence of cubanite indicates that chalcopyrite formed at a relatively high temperature. Chalcopyrite lacking cubanite either formed at a lower temperature or started off with a composition very close

to $CuFeS_2$. It is quite likely that the apparent variable presence of cubanite indicates chalcopyrite was deposited (or re-deposited) at several different temperatures.

5.2.4. Sphalerite

Sphalerite (ZnS) occurs as a minor ore mineral with two styles of mineralization: 1) as sphalerite "stars" in chalcopyrite and cubanite (Figure 5.4 C); and 2) as subhedral individual crystals up to 500 μm, typically with pyrrhotite ± chalcopyrite ± arsenopyrite ± native bismuth clots. The first style of mineralization (star sphalerite) is generally regarded as an exsolution product of the Cu-Fe-Zn-S system; as high temperature mixtures ("*iss*") begin to cool, sphalerite components un-mix (Marignac, 1989). Not all chalcopyrite at Skarn Ridge contains sphalerite stars. The only observed cubanite occurrences do contain sphalerite stars, and the stars cross-cut cubanite-chalcopyrite mineral boundaries (Figure 5.4 C). The exsolution timing implied by this relationship is *iss*→ chalcopyrite + cubanite→ chalcopyrite + cubanite + sphalerite.

I analyzed sphalerite compositions (Chapter 6) in conjunction with arsenopyrite for the purpose of determining thermal zoning (geothermometry) of the assemblage arsenopyrite + pyrrhotite ± sphalerite or Bi^0 (native bismuth). Based on 47 microprobe analyses the sphalerite is quite iron-rich (average 13.2 wt % Fe, max = 17.2%, min = 12.3%), consistent with a pyrrhotite-bearing assemblage lacking pyrite. I made no attempt to analyze sphalerite stars.

5.2.5. Native Bismuth

Native bismuth was only locally identified in drill core, but is commonly seen in polished thin section, in close association and/or intergrown with gold (Figure 5.5). I have only rarely seen native bismuth without nearby (within 1 mm) gold. In drill core, Bi^0 stands out due to its high reflectivity and considerable softness. Individual grains are typically 0.5 to 5 mm long, anhedral, and have blob-shaped, rounded (never angular) grain boundaries with Au and (or) Te-bearing minerals (hedleyite or hessite). The most common style of occurrence is patchy replacement of clinopyroxene, although native bismuth is locally present in veins and rarely in complex assemblages that include sulfides and bismuth tellurides (described ahead).

5.2.6. Gold

Gold is typically present as free grains, 20-150 μm, and is spatially associated with native bismuth in polished section (Figure 5.4). Gold fineness (1000 × wt% Au/(wt% Au + wt % Ag)) determined by EMPA is 745 to 780, meaning that the "gold" grains contain approximately 25% Ag and are compositionally closer to electrum than pure gold. In most cases gold directly replaces clinopyroxene in skarn; it is not particularly associated with any other ore minerals besides native bismuth. Like native bismuth, gold tends to occur as anhedral blobs with rounded grain boundaries. In rare cases, gold is present in complex ore assemblages. I found only one case (out of hundreds of grains) where fine-grained gold is encapsulated in arsenopyrite, SK08-011-77.50 m (Figure 5.5).

5.2.7. Arsenopyrite

Arsenopyrite (generally described as FeAsS, but actually (Fe,Co,Ni) As_{1+x} S_{1-x}) is widely distributed throughout the deposit, though it is most abundant in skarn, calc-silicate hornfels, and the mafic sills. Based on numerous microprobe analyses, at Mike Lake the atomic percent As varies from 32.8 to 35.4, i.e., the arsenopyrite is mostly As-rich and S-poor relative to the theoretical value of 33.33 atomic percent As. Based on 6 mm XRF analysis of 17 large arsenopyrite grains, Mike Lake arsenopyrite contains 0.14 -2.0% Co and 0.02-0.57% Ni, with Co typically 3-4 times as abundant as Ni. That is, Co is an important component which I did not analyze by microprobe.

Arsenopyrite occurs as patchy replacements, isolated euhedral crystals, disseminations, veinlets, and as an accessory mineral in sulfide veins. Coarse-to-massive arsenopyrite often occurs with calcite rhombs (up to 2 cm) and euhedral scheelite crystals (± axinite) as a vein-filling assemblage. Gold can be in the general vicinity of arsenopyrite, but shows no systematic association (Figure 5.5 D, F).

5.2.8. Scheelite

Scheelite ($CaWO_4$) is most often identified in core from the northwestern part of Skarn Ridge. Scheelite is best identified with shortwave ultraviolet light, as it fluoresces light blue. It was noted in core logs where detected by UV light, but otherwise it is inferred to be the mineral responsible for elevated tungsten assays – even though not always observed in tungsten-bearing core intervals. It is possible that wolframite ($(Fe,Mn)WO_4$) is the responsible mineral in such cases, although I have never identified

it in thin section or hand specimen. Scheelite is almost exclusively present in skarn or mixed skarn/calc-silicate hornfels, but nearly half of the assays of green dikes yielded anomalous (70-680 ppm) tungsten. Elevated tungsten assays occur over short intervals (typically <2 meters) and are often not continuous over any length of core.

Scheelite typically occurs as pale yellow crystals, often euhedral, with pyramidal terminations, up to 2 cm long, in coarse-grained aggregates of calcite ± arsenopyrite ± axinite ± amphibole ± apatite. Veins and veinlets containing scheelite, as well as fine disseminations, are also present. Overall, scheelite appears to be part of a late mineralization stage, based on the observation that scheelite-bearing veins cut across prograde mineralized skarn. In addition, the occurrence of scheelite with axinite in dikes that cut (post-date) gold mineralization indicates scheelite deposition is a separate and younger mineralizing event.

5.2.9. Galena

Galena (PbS) is a rare mineral on Skarn Ridge. It was never recognized during core logging and rarely seen in reflected light petrography, but its presence was confirmed by EMPA. Most Pb assays are <100 ppm. Galena is most often observed in complex ore assemblages (Figure 5.6). Microprobe analyses reveal that Skarn Ridge galena can contain up to 5.4 wt. % Se and lacks detectable Ag.

5.2.10. Tellurides and Complex Ore Assemblages

Hedleyite (Bi_7Te_3) and hessite (Ag_2Te) occur almost exclusively in the form of *complex assemblage clots*, intermingled mixtures of sulfide, telluride, and native metal

minerals that include galena, pyrrhotite, native bismuth, gold, and minor chalcopyrite (Figure 5.6). These assemblages typically fill angular spaces between adjacent arsenopyrite crystals; they tarnish readily after polishing (Figure 5.6 B-D). These assemblages are relatively rare in the samples I examined; about 50% of them occur in coarse-grained axinite with nearby amphibole, while the remaining 50% occur in the clinopyroxene-dominated prograde silicate assemblage.

Hedleyite and hessite can occur as bite-shaped replacements in native Bi. Although hedleyite, hessite, and native Bi have similar hardnesses, the higher reflectivity and brighter white color of the tellurides distinguish them from native Bi in reflected light. Individual grains are 5-20 μm across and always anhedral, often with rounded grain boundaries adjacent to Bi^0.

5.2.11. Ni-Sb-(S) Minerals

Ullmannite (NiSbS), breithauptite (NiSb), and nisbite ($NiSb_2$) occur in trace quantities in skarn and calc-silicate hornfels. Confirmed observations of these minerals are exceptionally rare in reflected light, but they were unquestionably identified using semi-quantitative microprobe analysis (EDS). In polished section, nisbite and ullmannite are difficult to tell apart; they are both white, have similar hardnesses (5 and 5.5, respectively), and display weak anisotropism (Figure 5.7 A). In contrast, breithauptite is easily distinguished from the others by its light copper-red-violet color, distinct anisotropism, and distinct pleochroism (Figure 5.7 B, C). Grain sizes for all Ni-Sb-(S)

minerals do not exceed 25 μm, which also contributes to the challenge of identifying them with a petrographic microscope.

5.3. Metals and Metal Associations

I used drill core assay values to determine correlation coefficients for 26 elements against Au, Cu, and W (Table 5.2). Assay techniques are described in Chapter 3. Correlation coefficients were calculated in three separate batches, using different cut-offs for each element. For Au and Cu, only those assay values ≥ 10 times the detection limit were used in the calculations (cutoffs of 0.1 ppm and 100 ppm, respectively). For W, a cutoff of 200 ppm was determined to be sufficient since the detection limit was 50 ppm, and using a cutoff of 500 ppm would have greatly truncated the dataset. All of these correlation coefficients are based on 6^{th} order polynomial trend lines.

The most important ore element correlations are Au with Bi ($R^2 = 0.74$) and Cu with Ag ($R^2 = 0.94$). The latter relationship seemingly requires that chalcopyrite contain Ag in solid solution. The average Cu:Au ratio of 453 (Figure 5.8 A) gives a silver concentration in chalcopyrite of ~ 0.08% – confirmed by microprobe analysis in a single sample, SK08-005-15.75 m (Table 5.1). In contrast, the mineral association of Bi and Au is extremely common at Mike Lake and results in a strong Au-Bi correlation (Figure 5.8 B, Table 5.2). The only other strong correlation is between Cu and Zn ($R^2 = 0.49$). Sphalerite occurs both as 'star' exsolution grains in chalcopyrite and as isolated grains commonly present near chalcopyrite, causing the correlation.

In sum, the assay correlations show that Au and Cu share moderate-to-strong associations with Zn, Ag, and Bi, weak associations with S and Co, and have essentially no association with W (Table 5.2). In contrast, the strongest relationships observed with W are weak to moderate (R^2 = 0.21 to 0.35) and occur with Co, As, Mg, Ni, and S; correlations with Au, Bi, and Cu are very weak to weak at best ($R^2 \leq 0.11$).

The moderate correlation of W and As agrees with the frequent occurrence of scheelite with arsenopyrite, typically in veins or clots containing axinite. The very strong (R^2 = 0.8) to strong (R^2 = 0.56) correlations of As with Co and Ni, respectively (Table 5.3), are consistent with the elevated concentrations of Co and Ni in arsenopyrite (as determined by 6 mm XRF). They also indicate that the vast bulk of the cobalt at Mike Like is present in solid solution in arsenopyrite, while some of the Ni is present in other minerals. Thus, the W-As-Co-Ni correlations (Table 5.2) are consistent with the observed mineralogical and mineral compositional data.

Other element pairs with moderately strong correlations ($0.62 < R^2 > 0.4$, Table 5.3) include Ag-Zn, Sb-As, and those involving elements primarily in silicate minerals, e.g., Ca-Al, Fe-Ca, Ca-Mn, Mg-Al, Mg-Fe, Ti-Mg and Ti-V. The Ag-Zn relationship is a secondary one, as both elements are present in chalcopyrite. The Sb-As correlation is probably due to trace amounts of Sb in arsenopyrite.

5.4. Spatial Distribution of Ore

The shape of the ore body is such that Au and Cu are concentrated in the north and west quadrants of Skarn Ridge (Figure 5.9). Au and Cu assay values taper to the east

and south, lending to a broadly U-shaped ore zone, open to the south and southeast. Au and Bi assay contours display similar shapes and distributions (Figure 5.9), as do Cu and Ag (Figure 5.10), and W and As (Figure 5.11). In particular, the bulk of the higher assay values for Au, Bi, Ag, and Cu are present north of the E-W felsic dike and west of the fault. This is especially true for Cu and Ag, and for Au and Bi at lower elevations. None of these four elements display patterns suggesting a zoning around the E-W felsic dike.

Tungsten does not appear to follow the same distribution as the other elements; rather, the W values are broadly symmetrical around the E-W felsic dike, especially at the 1750 and 1700 m elevations and the far western part of the 1800 m elevation (Figure 5.11). The outline of higher As concentrations (Figure 5.11) is intermediate between that of W and the other four metals: neither entirely symmetric nor asymmetric around the E-W felsic dike.

5.5. Discussion

The elemental correlations observed (Tables 5.2 and 5.3) are largely compatible with the petrographic associations and mineral compositions observed at Mike Lake. For example, Au and Bi typically occur together in polished section and correlate strongly in assays. Although I have found no evidence for Au-Bi minerals (e.g., maldonite – Au_2Bi or johnsonite – $AuBi_5S_4$), the strong spatial and assay correlation of Au with Bi leads me to suspect much or all the gold might have originally been precipitated as maldonite (+ Bi^0). If this was the case, the original maldonite decomposed (with addition of Ag) to form electrum + native bismuth. This hypothetical reaction occurred prior to retrograde

alteration, as there is no association of the mixed Bi and Au-Ag grains with lower-temperature phases.

The average Bi:Au ratio at Mike Lake is approximately 200 (Figure 5.8 B), considerably higher than that seen in typical plutonic-related gold deposits (e.g., Fort Knox, Bi:Au ~20; Pogo, Bi:Au ~5 (Flanigan et al., 2000)). At the Nixon Fork Au skarn in south-central Alaska, the Bi:Au ratio of primary ore (unoxidized skarn) is approximately 15 (Newberry et al., 2010). In contrast, the Bi:Au ratio at the Buckhorn Au skarn, NW Washington State, varies from less than 2 to more than 1000 (Deal et al., 2012). The approximately constant Bi:Au ratio at Mike Like implies that the two metals have not been remobilized (by way of extensive retrograde alteration, for example); the very high ratio might reflect the unusually low fS_2 conditions at Mike Lake, for which all of the bismuth is present in sulfur-absent minerals. Furthermore, the presence of nickel-antimonide (i.e., sulfur-absent) minerals reaffirms that the Skarn Ridge system has a very low sulfidation state.

The extremely strong Ag-Cu correlation at Mike Lake (Cu:Ag = 453) essentially requires that the chalcopyrite consistently contains about 0.08% Ag. I found such a concentration (0.09 ± 0.06%, Table 5.1) in one chalcopyrite grain from Mike Lake, but was unable to find similar concentrations in six different chalcopyrite grains from a different sample. Chalcopyrite with Ag concentrations of 0.026-0.056 wt. % has been identified from the Izok Lake VMS deposit (Harris et al., 1984), a deposit at which a similarly very strong correlation between Cu and Ag is observed. That Cu:Ag ratio at

that deposit (890:1) requires an average Ag concentration in the chalcopyrite of 0.04%. If such variation is typical, then the chalcopyrite at Mike Lake would be expected to contain approximately 0.1-0.04% Ag, the latter being below detection with the conditions I employed. In sum, the bulk of silver at Mike Lake is most likely present as solid solution in chalcopyrite.

The variable presence of star sphalerite (exsolution "inclusions") in chalcopyrite indicates that chalcopyrite deposition (and re-deposition) took place over a broad range of temperatures – some too low for significant ZnS solid solution. This could also account for the apparently variable Ag content in the chalcopyrite, solid solution for any element being more widespread at higher than lower temperatures.

At least four lines of evidence indicate that the bulk of tungsten deposition at Mike Like post-dated and is unrelated to Au-Cu deposition. First, the lack of correlation of Au and W (Table 5.2) is striking, especially because both gold and prograde scheelite are commonly concentrated on the outer fringes of calcic skarn (Newberry, 1982; Meinert, 1989). Secondly, anomalous tungsten values are present in the 'green dikes', which lack gold and appear to cut across (post-date) Au-mineralized skarn. Tungsten values above the detection limit (50 ppm) were not reported from porphyry dikes; however, this unusually high detection limit (~ 25 times background for normal rocks; Taylor and McLennan, 1985), does not preclude the presence of anomalous tungsten in these dikes. My XRF analyses indicates that both green and felsic dikes at Mike Like contain 30-60 ppm W. Third, the common association of scheelite with axinite (the latter

is seen as an alteration product in all the igneous rocks except the Rubble Lake pluton) indicates that a younger axinite-scheelite event overprinted rocks at Skarn Ridge. Finally, the distribution of higher tungsten values at Skarn ridge, symmetric about the E-W felsic dike (Figure 5.11), suggests that fluids responsible for tungsten deposition accompanied the felsic dikes.

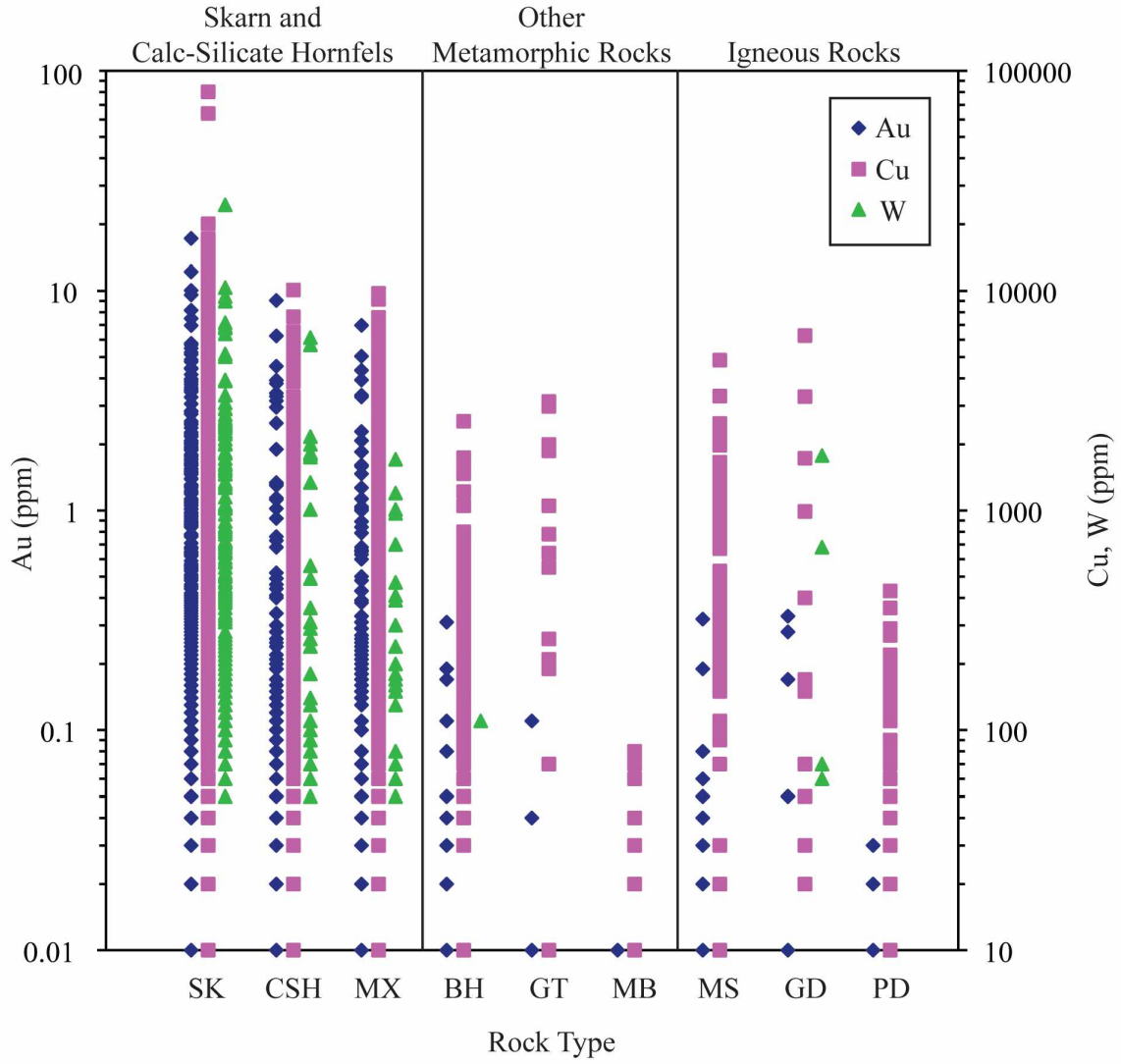

Figure 5.1. Au, Cu, and W assays by rock type.
SK = skarn, CSH = calc-silicate hornfels, MX = mixed skarn +calc-silicate hornfels, BH = black hornfels, GT = grit, MB = marble, MS = mafic sills, GD = green dikes, PD = porphyritic dikes.

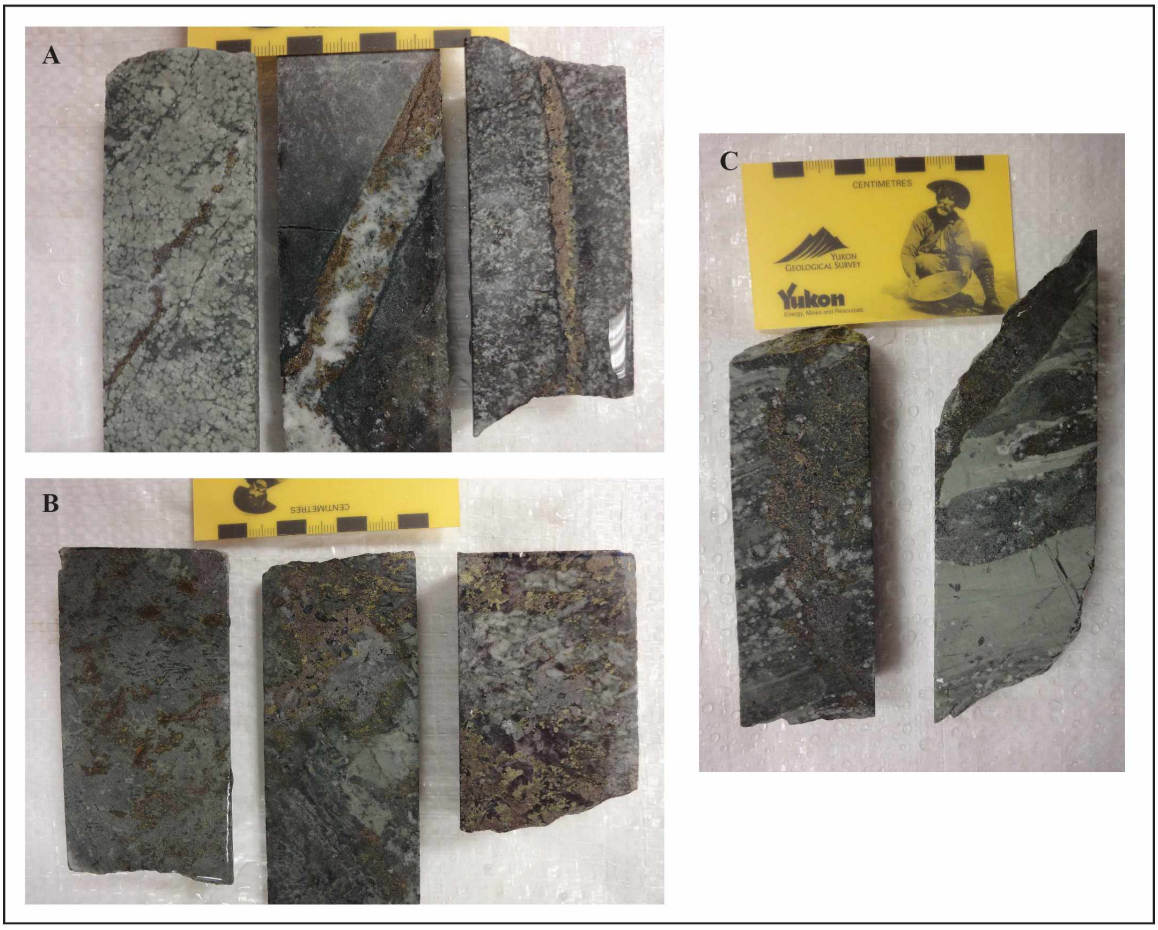

Figure 5.2. Styles of mineralization.
A: sulfide-rich veins in skarn (far left) and mafic sills (middle and right). B: replacement-style mineralization in skarn. C: Skarn veins cut across calc-silicate hornfels. In each case, minerals present include chalcopyrite and pyrrhotite, with traces of Au and native bismuth.

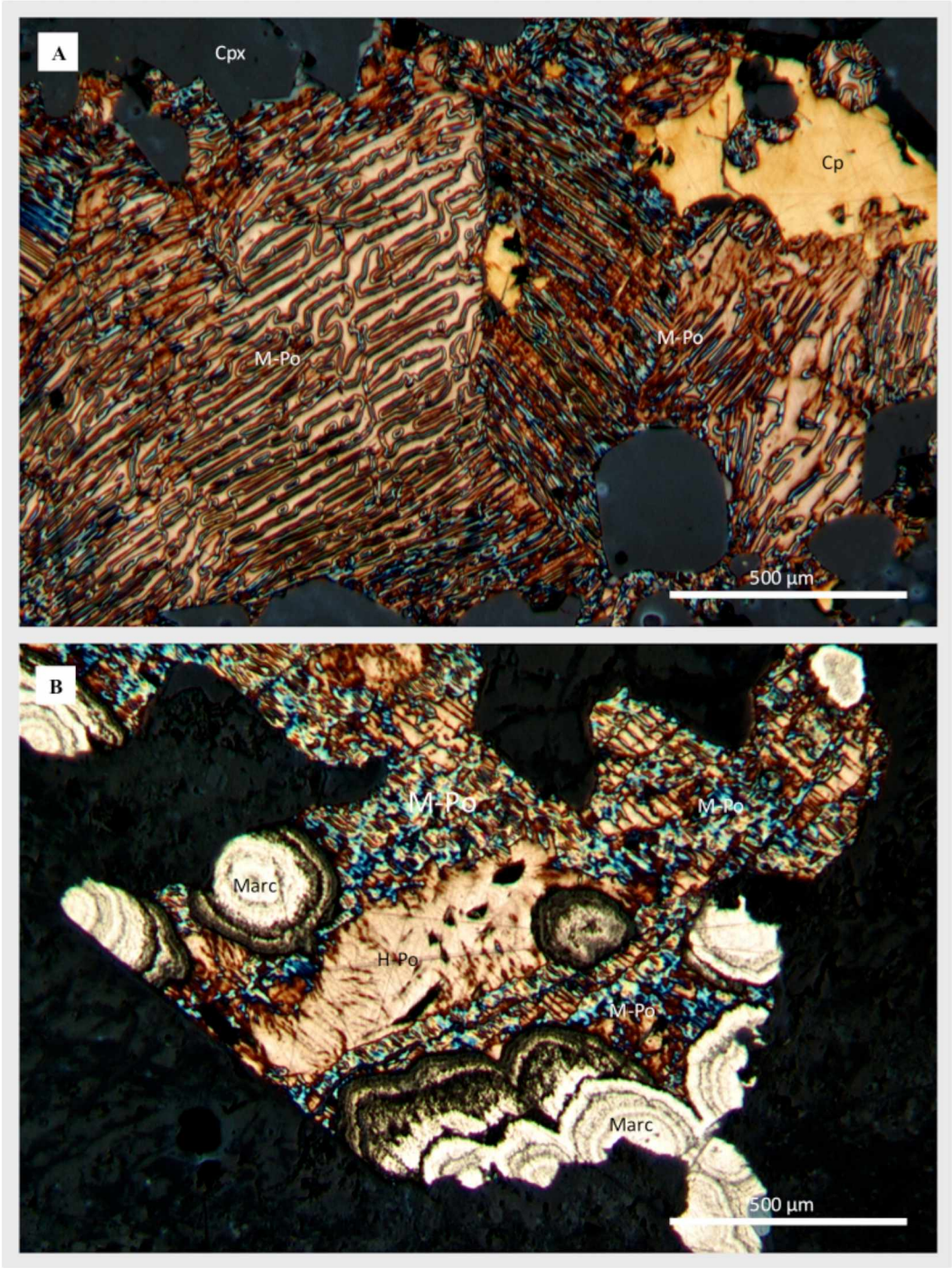

Figure 5.3. Pyrrhotite and marcasite relationships in thin section (reflected light).
A: monoclinic pyrrhotite (M-Po) is revealed in the presence of "ferrofluid". B: low temperature M-Po replaces high temperature hexagonal pyrrhotite (H-Po); supergene marcasite (Marc) replaces M-Po.

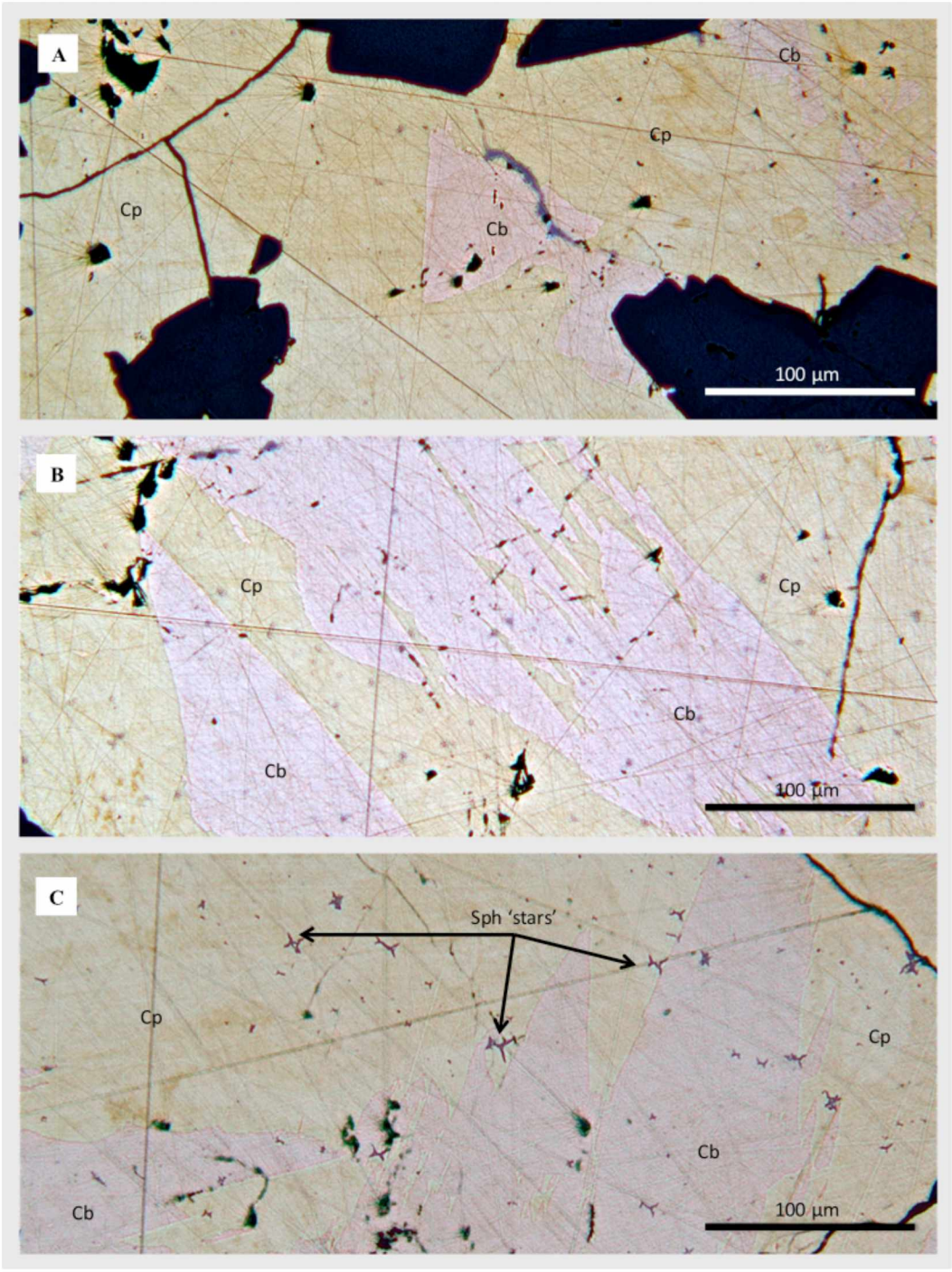

Figure 5.4. Chalcopyrite-cubanite relationships in thin section (reflected light).
A: triangular cubanite (Cb) in chalcopyrite (Cp). B: the more typical cubanite laths. C: sphalerite (Sph) stars cut across cubanite-chalcopyrite mineral boundaries indicating late exsolution.

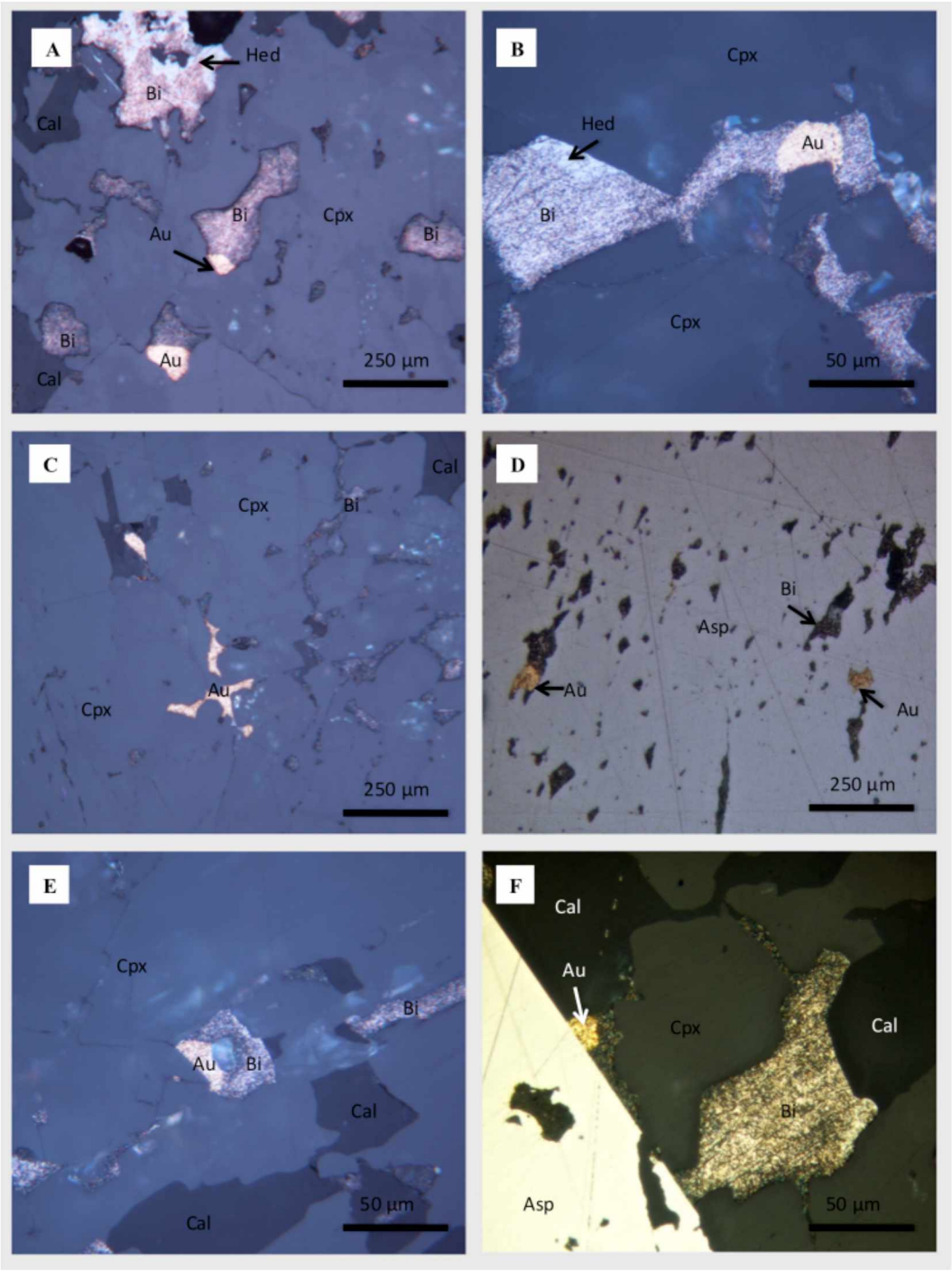

Figure 5.5. Gold (Au) and native bismuth (Bi) relationships in thin section (reflected light). See text for descriptions. Other minerals present include arsenopyrite (Asp), calcite (Cal), clinopyroxene (Cpx), and hedleyite (Hed).

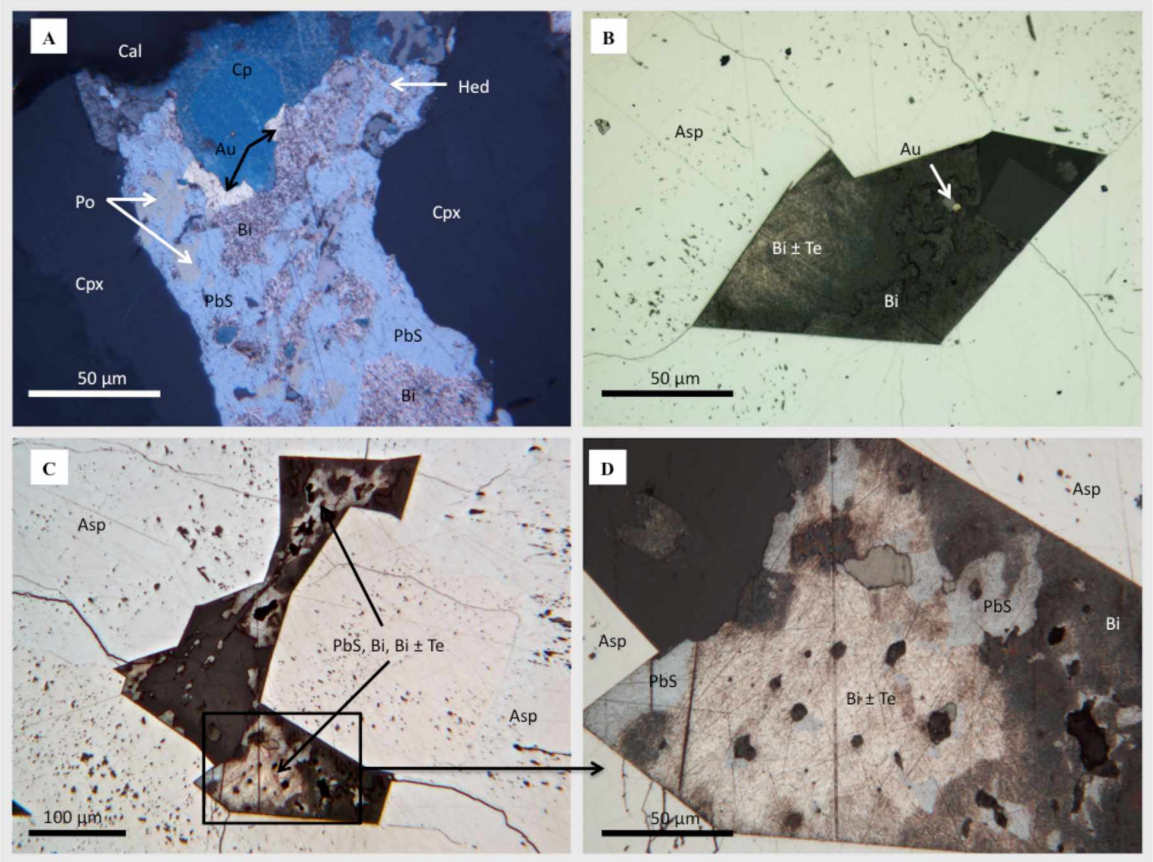

Figure 5.6. Complex ore assemblages in thin section (reflected light).
A: assemblage containing sulfides, tellurides, and native metals in clinopyroxene skarn. The bluish hue is from residual carbon coating the sample for microprobe analysis. B-D: angular void-filling bismuth telluride (Bi-Te) assemblages more typical of axinite-arsenopyrite zones.

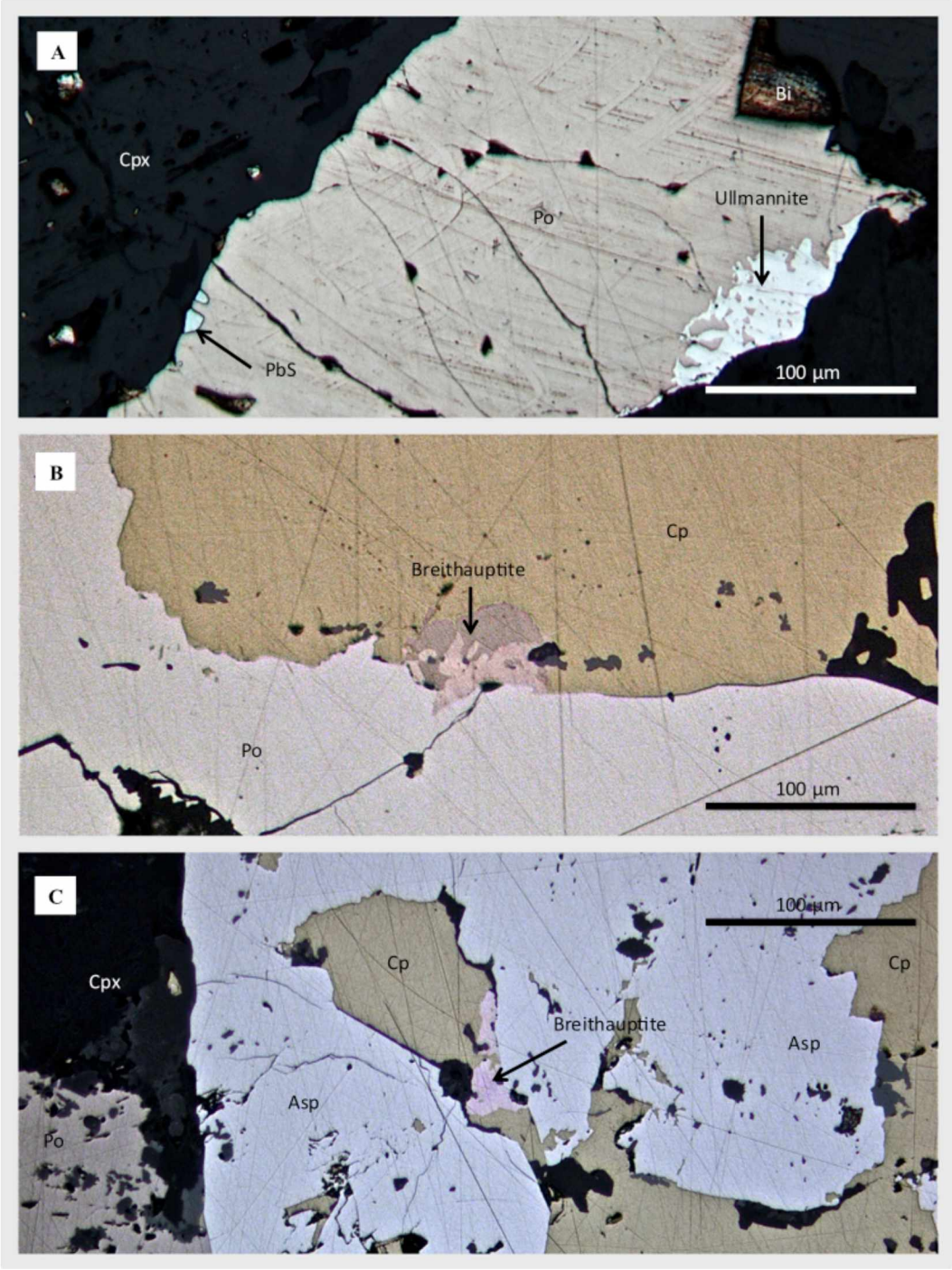

Figure 5.7. Nickel-antimony ± sulfur minerals in thin section (reflected light).
See text for descriptions. Other minerals present include pyrrhotite (Po), arsenopyrite (Asp), galena (PbS), chalcopyrite (Cp), and clinopyroxene (Cpx).

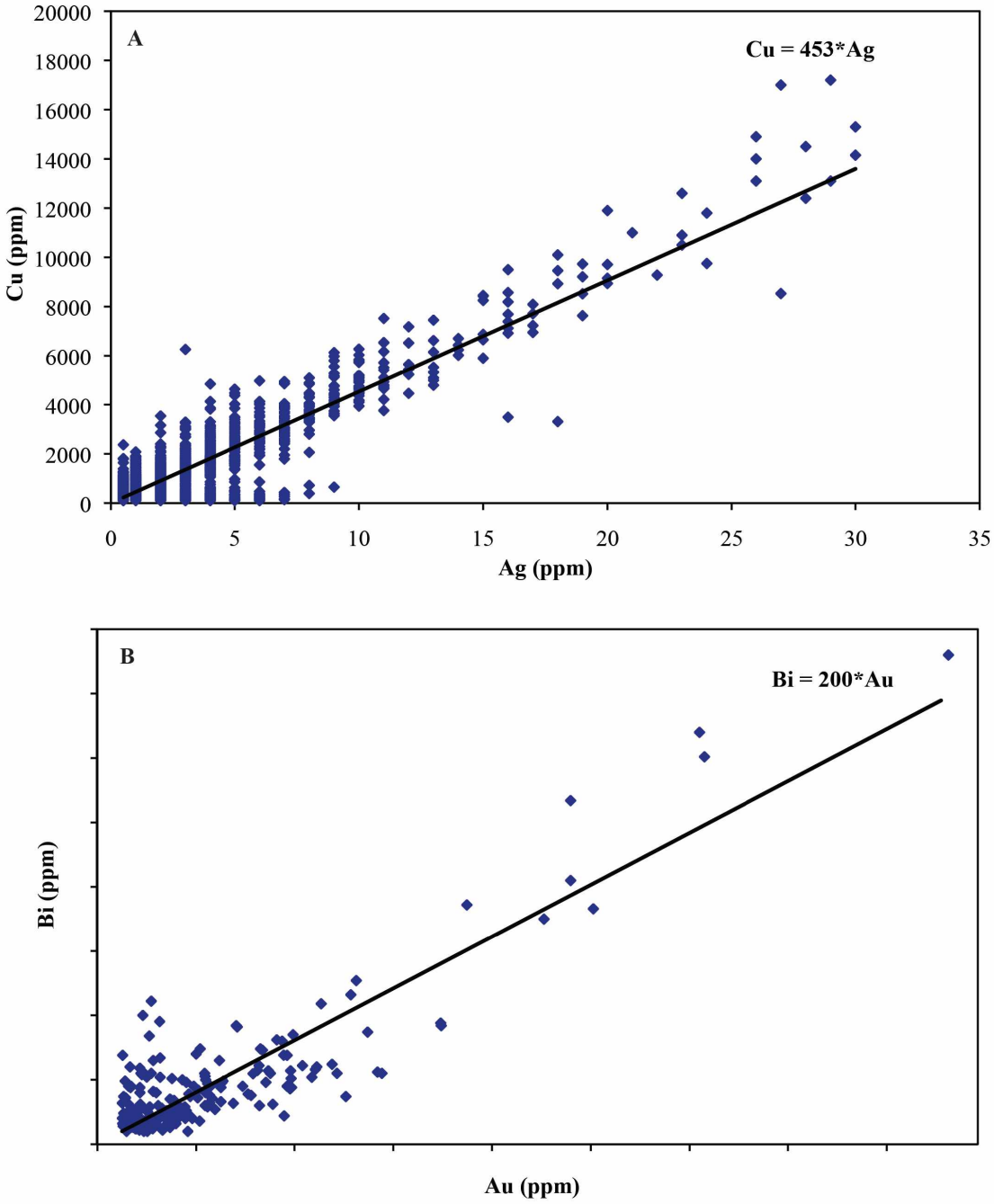

Figure 5.8. Significant assay correlations for selected ore elements.
Gold values are omitted in compliance with the confidentiality agreement.

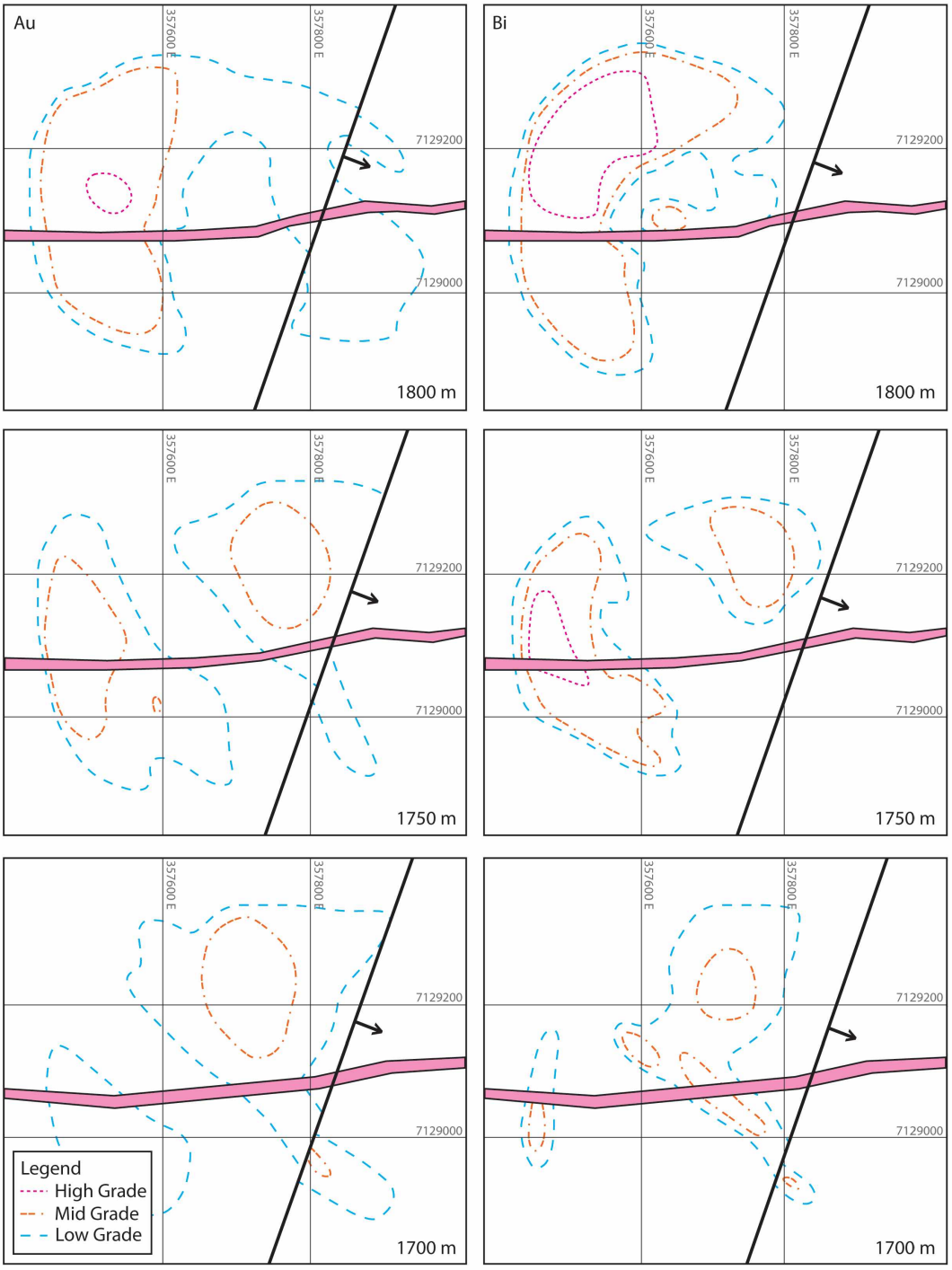

Figure 5.9. Assay contours by depth for gold and bismuth.
SAM's fault (bold black line with dip arrow pointing east) and main felsic dike (pink east-west structure) are included for reference. See text for contour construction. For location map, see Figure 3.2.

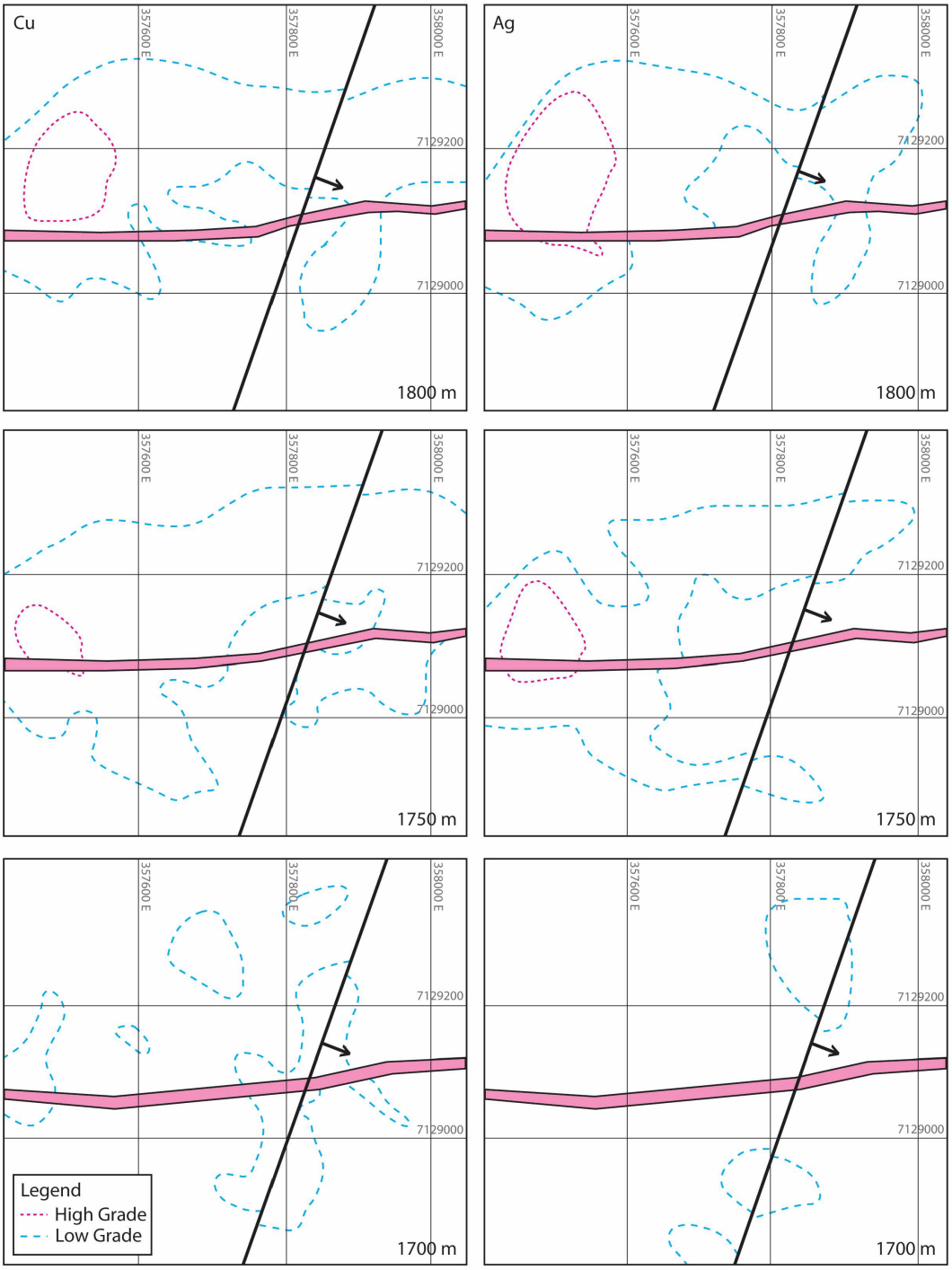

Figure 5.10. Assay contours by depth for copper and silver.
SAM's fault (bold black line with dip arrow pointing east) and main felsic dike (pink east-west structure) are included for reference. For location map, see Figure 3.2.

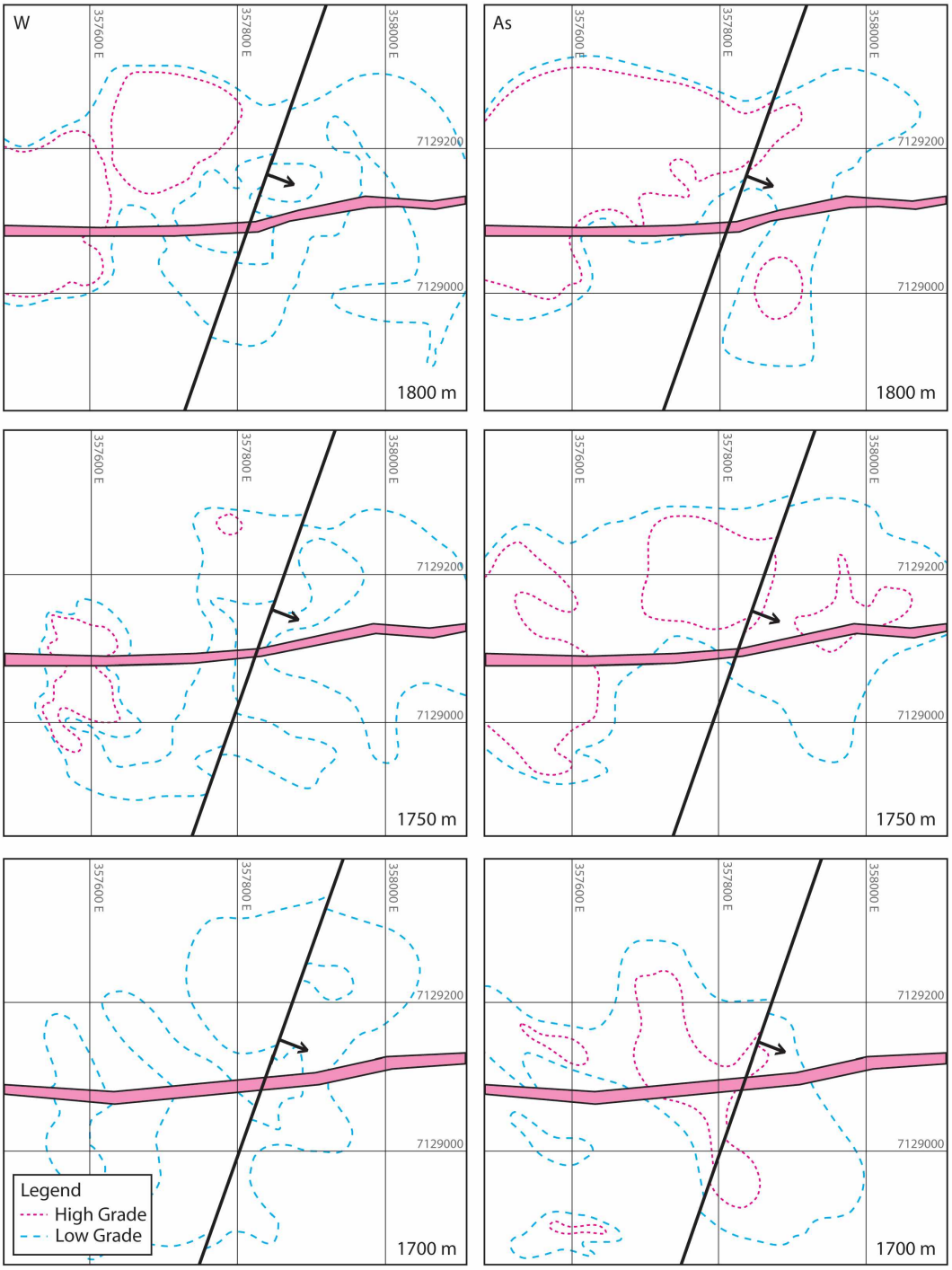

Figure 5.11. Assay contours by depth for tungsten and arsenic.
SAM's fault (bold black line with dip arrow pointing east) and main felsic dike (pink east-west structure) are included for reference. For location map, see Figure 3.2.

Table 5.1 Chalcopyrite compositions by EMPA.

Sample ID	Grain #	n	% Ag	% Bi	% As	% Sb
SK08-011-76.5	1	8	0.02 ± 0.0	-	0.01 ± 0.0	-
SK08-011-76.5	2	3	0.03 ± 0.0	-	-	-
SK08-011-76.5	3	3	-	-	-	-
SK08-011-76.5	4	3	0.03 ± 0.0	-	-	0.01 ± 0.0
SK08-011-76.5	5	3	0.01 ± 0.0	-	-	-
SK08-011-76.5	6	3	0.01 ± 0.0	0.02 ± 0.1	0.01 ± 0.0	-
SK08-005-15.75	1	5	0.09 ± 0.1	-	-	-

Table 5.2. R^2 values for significant Au, Cu, and W correlations.
All pass t- and F- tests for statistical significance at alpha = 0.05 (6^{th} order polynomials).

Au		Cu		W	
Bi	0.74	Ag	0.94	Co	0.35
Ag	0.24	Zn	0.49	As	0.31
Cu	0.23	Bi	0.20	Mg	0.24
Zn	0.17	Co	0.20	Ni	0.22
Sb	0.12	S	0.18	S	0.21
	-	Fe	0.16	Sr	0.2
	-	As	0.14	Ti	0.18
	-	Au	0.14	Sb	0.17
	-		-	P	0.16
	-		-	Cr	0.15
	-		-	V	0.14

Table 5.3. R^2 values for linear correlations between non-ore elements.

	As	Ca	Fe	K	Mg	Mn	Na	Ni	S	Sb	Ti	V	Zn
Ag	-	-	-	-	-	-	-	-	0.25	-	-	0.19	0.6
Al	-	0.5	0.3	-	0.4	0.25	0.50	-	-	-	0.34	-	-
As	-	-	-	-	-	-	-	0.5	0.30	0.5	-	-	-
Ba	-	-	-	0.90	-	-	-	-	-	-	0.20	0.24	-
Bi	-	-	-	-	-	-	-	-	-	0.2	-	-	-
Ca	-	-	0.4	-	0.3	0.40	0.21	-	-	-	-	-	-
Co	0.80	-	-	-	-	-	-	0.6	0.21	0.3	-	-	-
Cr	-	0.3	0.2	-	0.3	-	-	-	-	-	0.35	0.30	-
Fe	-	-	-	-	0.4	0.37	-	-	0.14	-	0.14	0.13	0.2
K	-	-	-	-	0.1	-	-	-	-	-	0.21	0.25	-
Mg	-	-	-	-	-	0.15	0.24	-	-	-	0.47	0.43	-
Ni	-	-	-	-	-	-	-	-	0.13	0.2	-	-	-

- indicates R^2 <0.1

5.6. References

Craig, J.R., and Kullerud, G., 1969, The Cu-Zn-S System: Carnegie Institute of Washington, Year Book, v. 67, p. 177-179.

Deal, M.L., Newberry, R.J., Willard, R., Ellis, J., and Cooper, P., 2012, Zoning and origins of the Buckhorn gold skarn deposit, northeast Washington: 2012 Arctic International Mining Symposium, Fairbanks Alaska, Abstracts with Program, p. 10-11.

Flanigan, B., Freeman, C., Newberry, R.J., McCoy, D., and Hart, C., 2000, Exploration models for mid- and Late Cretaceous intrusion-related gold deposits in Alaska and the Yukon Territory, Canada *in* Cluer, J.K., Price, J.G., Struhsacker, E.M., Hardyman, R.F., and Morris, C.L., eds., Geology and Ore Deposits 2000: The Great Basin and Beyond: Geological Society of Nevada Symposium Proceedings, May 15-18, 2000, p. 591-614.

Harris, D.C., Cabri, L.J., and Nobiling, R., 1984, Silver-bearing chalcopyrite, a principal source of silver in the Izok Lake massive-sulfide deposit: confirmation by electron and proton microprobe analyses: Canadian Mineralogist, v. 22, p. 493-498.

Marignac, C., 1989, Sphalerite stars in chalcopyrite: are they always the result of an unmixing process?, Mineralium Deposita, v. 24, p. 176-182.

Meinert, L.D., 1989, Gold skarn deposits – geology and exploration criteria *in* Groves, D., Keays, R., and Ramsay, R., eds., Proceedings of Gold '88: Economic Geology Monograph #6, p.537-552.

Newberry, R.J., 1982, Tungsten-bearing skarns of the Sierra Nevada. I. The Pine Creek Mine, California: Economic Geology, v. 77, p. 823-844.

Newberry, R.J., Mrozek, S.A., Perttu, B.K., Broman, B., Wagner, K., and Lessard, R., 2010, Yet still ANOTHER look at the Nixon Fork Au-Cu-Ag Skarn, SW Alaska: Alaska Miners Association Spring Meeting, Abstracts with Program, p. 12-15.

Taylor S.R., and McLennan, S.M., 1985, The Continental Crust: Its Composition and Evolution. Blackwell Scientific Publishers, Oxford, England, 312 pp.

6. Zoning

6.1. Introduction

Zoning is an important feature of skarn deposits that occurs in both igneous and metasomatic rocks and on many different scales. On the deposit scale, there is often a prograde mineralogical zoning *away* from the hydrothermal fluid source/conduit, consisting of garnet → garnet + clinopyroxene → clinopyroxene → (± wollastonite) → marble (in the original marble host), and ± garnet ±clinopyroxene and calcic plagioclase in the igneous host (Einaudi et al., 1981). Mineral compositional zoning also occurs, with higher Mg in skarn minerals closer to the fluid source and higher Fe and Mn farther from the source (e.g., Meinert, 1992). One would further anticipate zoning in the Cl contents of Cl-bearing skarn minerals (e.g., scapolite) as the hydrothermal fluid evolves with space and time. Ore minerals also commonly show patterns related to skarn silicate zoning, e.g., gold grades are typically higher in skarn with greater distance from the fluid source (Ray et al., 1990) and tungsten grades in prograde skarn increase towards the marble front (Newberry, 1982; Newberry, 1998). An understanding of these patterns is important for exploration success, since they can indicate the direction towards ore in the skarn system.

At Skarn Ridge, deposit-scale mineralogical zoning is not recognizable without compositional data. There is very little garnet; whatever garnet is present occurs as widely spaced individual crystals that do not form a distinct 'zone'. Also garnet does not appear to be proximal to any single dike/group of dikes, and there is no other indication

of zoning (i.e., no endoskarn alteration) around any of the dikes on Skarn Ridge. Instead, the prograde skarn assemblage at Mike Lake is dominated by clinopyroxene and scapolite. In some skarns it may be possible to visually estimate clinopyroxene composition by the intensity of its color and hence, determine the direction of zoning. However at Skarn Ridge there is enough dark green amphibole (actinolite, hornblende) and colorless scapolite intergrown with clinopyroxene to make this estimation problematic. In addition, the lack of an obvious endoskarn and significant garnet zone make determination of zoning patterns virtually impossible without compositional data.

Through compositional data (described ahead), several styles of zoning are observed for the Skarn Ridge deposit. These include: deposit-scale skarn compositional zoning for garnet, clinopyroxene, scapolite, and amphiboles; metal zoning for Au and Cu; and thermal zoning as determined by arsenopyrite (± sphalerite ± native Bi) geothermometry. Garnet and amphibole analyses are few due to their scarcity in the deposit and the lack of available samples for this study. Thus, these zoning patterns are difficult to discern. Compositional zoning patterns for clinopyroxene and scapolite are more straightforward based on several hundred microprobe analyses distributed over much of the skarn. Gold distribution and concentration appears to partly mimic clinopyroxene and scapolite compositional zoning, as does copper. Arsenopyrite major element compositions determined for geothermometry show a complex pattern due to variations in cobalt contents.

6.2. Methods

Silicate (clinopyroxene, garnet, scapolite, amphiboles, biotite), sulfide (arsenopyrite, sphalerite, galena, etc.), and native metal minerals (Au, Bi, Ag, Te, etc.) were analyzed by electron microprobe using standard-calibrated routines as described in Chapter 3. I performed all quantitative microprobe analyses with a Cameca SX-50 microprobe equipped with four wavelength dispersive spectrometers (WDS). All data were collected in three separate batches over a two-year period, and a secondary standard was employed to ensure consistency of the data acquired from each analytical session. Semi-quantitative analyses were performed with the same instrument using energy dispersive spectrometry (EDS).

I compiled all data into a database and plotted it using Vulcan™ and Leapfrog™ 3D modeling software. Cross sections were 'cut' in Vulcan™ and digitized in Adobe Illustrator™. The location of cross section lines (Figure 3.2) was based primarily on data availability.

I calculated endowment zoning for Au, Cu, and W by: Endowment = $\sum$ (assay ppm $\times$ interval width) for an entire drill hole. This results in point values representing the total contained metal value for each drill hole. Endowment is different from the assay contours presented in Chapter 5. Assay contours represent a slice through an interpolated 3D shape that encompasses all assays above a certain threshold, at a specific elevation (Z). The shape of the assay contours will change with depth, as they represent the 'real' shape of the grade distribution that is dependent on Z. Contours of endowment points are

independent of Z, as there is no vertical change in endowment (it is the sum of all grades represented by a single point). The point locations for endowment values are best presented in plan view, where each point represents the midpoint of the mineralized interval within each drill hole, projected to the surface. (Usually this 'centroid' was located approximately half way down the drill hole, but in rare cases this point was adjusted to more accurately represent the midpoint of mineralization). This approach to presenting the data gives a more realistic sense of the spatial distribution of each metal, since the bulk of the endowment (as visible in cross section) is not concentrated at the surface, and the drill holes are not vertical. That is: using the drill hole collar would not be the best approximation for the location of the endowment.

6.3. Clinopyroxene Zoning

Although pyroxene compositions vary within a single thin section, generally the standard deviation is 3-4 mole % hedenbergite (Hd) for > 10 good microprobe analyses. The exception is where both 'metamorphic' and 'metasomatic' pyroxenes are present (Chapter 3); typically these compositions define a bimodal population. In such cases, I averaged only the higher-iron (metasomatic) pyroxene compositions.

A plan map of these compositions, projected from drill hole locations to the surface (Figure 6.1) is not easily interpreted. Although the pyroxenes with highest % Hd are mostly located in the NW corner (higher-Au grade area), an isolated point well to the south also has this combination. The data are too irregular to be contoured. I interpret

this to the fact that vertical pyroxene compositional zoning (which cannot be shown on this plan map) is also critically important.

Average % Hd in skarn pyroxene values plotted along drill hole traces in cross-section, however (Figure 6.2), show a well-defined vertical and horizontal zonation. Low-Fe clinopyroxene (Hd < 70) + garnet defines the center of the zonation pattern, with % Hd increasing around this zone (both 'up' and 'down'), updip, and towards the marble front (Figure 6.2). Maximum % Hd values occur close to the marble front, in the deeper and westernmost parts of each cross-section.

The overall zoning pattern suggests that fluids came up from the south or southeast and traveled updip between the skarn/black hornfels contact and the upper mafic sill. Where the sill stopped the zoning pattern shows fluid flowed more westerly than 'up'. This zoning seems to completely ignore (predate?) both sets of dikes, and to some extent, the mafic sills as well. I suspect that clinopyroxenes with analyses of Hd < 60% have a major metamorphic component (i.e., the likely protolith was a calc-silicate hornfels with Mg supplied by the host rock), and as a result they do not fit with the skarn zoning pattern. These data are plotted on the cross section, but are ignored in drawing the pyroxene compositional contours.

6.4. Scapolite Zoning

Maximum % Cl values in scapolite increase from south to north but also increase 'up' from the lower hornfels contact (Figure 6.3). The patterns are more complicated than I anticipated, perhaps because the % Cl in a scapolite reflects temperature, Cl

content of the fluid, and major element composition of the scapolite (Na/Na+Ca). The pattern is consistent with % Hd in pyroxene, however, in that it suggests fluid flowed generally 'up' and to the northwest.

6.5. Thermal Zoning

Sulfide deposition temperatures were estimated by determining the composition of arsenopyrite in the presence of pyrrhotite + native bismuth (fS_2 buffer), using the geothermometry method of Scott (1983). Unfortunately (in retrospect) only four out of eleven arsenopyrite grains meticulously analyzed for As, Fe, and S also contain sufficiently low quantities of cobalt (Co < 0.5%) that they are considered reliable for temperature estimation (Scott, 1983). The distribution of most reliable calculated temperatures (Figure 6.4) shows that the highest temperatures are generally 'deeper' and to the SE, consistent with the fluid flow generally 'up' and to the NW. The paucity of reliable data inhibits further comment. The cobalt contents of arsenopyrite do broadly decrease away from the mafic sills (Figure 6.4), suggesting that the sills were the source for the anomalous cobalt.

6.6. Gold Endowment Zoning

Gold is distributed such that the highest endowment values occur in the northwestern-most portion of Skarn Ridge, north of the main porphyritic dike, immediately east of the marble front. The lowest values form a trough-like body oriented NW-SE across the center of the drilled area (Figure 6.5) and higher values flank this zone. If gold is mostly precipitated 'distal' to the fluid flow path then the shape of the

lowest endowment region represents the fluid source direction. Overall, endowment values increase to the WNW, suggesting a fluid-flow direction from the southeast.

6.7. Copper Endowment Zoning

Copper endowment (Figure 6.5) shows a similar pattern to gold distribution in that the highest values occur in the northwest corner of the drilled area, north of the main porphyritic dike. Similarly, the lowest values form a belt that extends toward the high values in the WNW. This pattern is also consistent with fluid flow from the southeast.

6.8. Tungsten Endowment Zoning

Tungsten shows a completely different zoning pattern compared to gold and copper (Figure 6.5). Although the highest W values are also in the NW quadrant of Skarn Ridge, their distribution is not the same. Mainly, the highest W values are 'islands' surrounded by lower values that diminish outward in all directions. There is no sense of a central low-grade zone with endowment increasing around it. Further, unlike gold and copper, the highest W values occur on both sides of the main porphyritic dike, rather than being confined to the north side of it.

6.9. Discussion

Several zoning patterns are observed through analysis of different minerals, mineral assemblages, and metals. Zoning patterns for clinopyroxene composition, gold endowment, and copper endowment are broadly similar in that they show enrichment in the northwest part of Skarn Ridge (Figures 6.1, 6.5). Tungsten endowment also shows maximum values in the same general area as gold and copper, however the distribution

pattern is quite different. In cross-section, patterns of %Cl in scapolite analyses show a general increase 'up' and to the northwest. Apparent thermal zoning based on arsenopyrite geothermometry yields inconclusive results due to a lack of reliable (low cobalt) data but can be viewed as similar to the pyroxene compositional pattern. The overall patterns displayed by clinopyroxene, gold, and copper indicate that the predominant fluid-flow direction was updip from SE to NW. The highest Au and Cu endowment values coincide with the highest mol % Hd on the most distal fringe of the skarn, adjacent to the marble front (Figures 6.1, 6.5).

The center of fluid flow, as indicated by the central 'low' in gold and copper endowment, does not correspond to any obvious mapped structure on Skarn Ridge (Figure 6.5 A and B), nor do the highest endowment values. That is, despite their abundance on Skarn Ridge, anticline hinges do not appear to be structural traps or pathways for mineralizing fluids, as seen by the lack of correlation of fold hinges and endowment zoning (Figure 6.5). Instead, the apparent fluid-flow directions as seen on the N-S cross-sections (Figure 6.2) located on the west side of SAM's fault (Figure 3.1), were up-dip and to the north. On the plan map, however, and especially east of SAM's fault, the apparent fluid flow direction was from SE to NW, across unit layering and dip directions. I am not sure how to reconcile the apparent plan and section zoning. However, the highest Au and Cu values are immediately adjacent to the main marble front.

Clinopyroxene compositions display an apparently straightforward zoning pattern

in cross-section only if three points that are not likely metasomatic (mol % Hd < 60), are ignored. This demonstrates the importance of being able to distinguish between truly metasomatic minerals (those formed exclusively by addition of components to a pure marble protolith) versus those formed by a combination of metasomatism and isochemical metamorphism (i.e., some of the components already present in the protolith). Only the former yield information readily useful for creating vectors of metasomatic fluid flow, and hence guides to ore mineralization. Tungsten endowment zoning shows a pattern unlike gold and copper, which is not surprising considering the observed mineralogical relationships (Chapter 3) and the W assay contours presented in Chapter 5. This feature again points to the likelihood that much of the scheelite was (re?)-deposited after the bulk of Au and Cu.

The total lack of Au and Cu endowment symmetry around the E-W felsic dike (Figure 6.5) indicates that the felsic dike had nothing to do with Cu and Au deposition. The virtual lack of alteration in the felsic dike indicates it was intruded after the bulk of skarn formation. In contrast, the greater degree of W endowment symmetry around the E-W felsic dike (combined with the common occurrence of axinite both with scheelite and in the felsic dike) suggests that the felsic dike was a major fluid conduit during the deposition or re-deposition of scheelite in the Skarn Ridge area.

Arsenopyrite compositional geothermometry requires establishing both the fS_2 and arsenopyrite composition from coexisting mineral assemblages. Because the first several arsenopyrite grains I analyzed contained negligible cobalt (as indicated by EDS

examination) I both did not add cobalt to my analytical routine for arsenopyrite and assumed that all the Mike Lake arsenopyrites were low in cobalt. After establishing a very strong As-Co relationship in the assays (Chapter 5), I re-analyzed large Mike Like arsenopyrite crystals by 6 mm XRF and determined many contained cobalt in excess of 0.5%. These higher-cobalt arsenopyrites yield Fe-As-S compositions that cannot be reliably used for geothermometry, as established by Scott (1983). Hence, the apparently bizarre temperature distribution pattern (Figure 6.4) is due to mostly unreliable temperature estimates. The few reliable data (those from low-Co arsenopyrite), however, yield a spatial pattern consistent with the pyroxene compositional zoning.

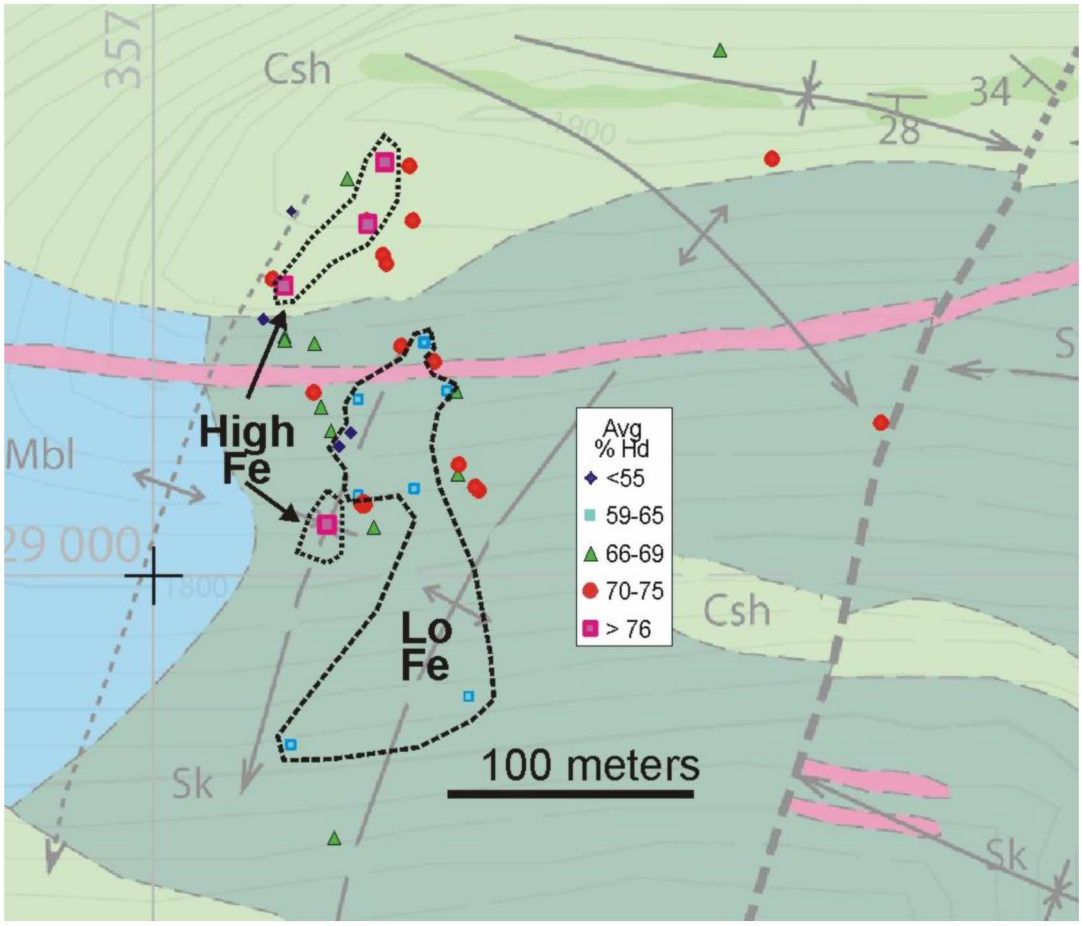

Figure 6.1. Spatial distribution of average %Hedenbergite (%Hd) in clinopyroxene. Points are superimposed on the geologic map of Figure 3.1. The '+' in the center-left is the intersection of UTMs 7,192,000 N and 357,500 E, zone 11, NAD 83. Samples from SK05-01 and SK05-02 are 250-500 meters south of the map; these yielded low-%Hd pyroxenes and are omitted so the complex spatial patterns in the areas of abundant data can be seen. Hand-drawn contours identify areas with especially high- and low-Fe clinopyroxenes.

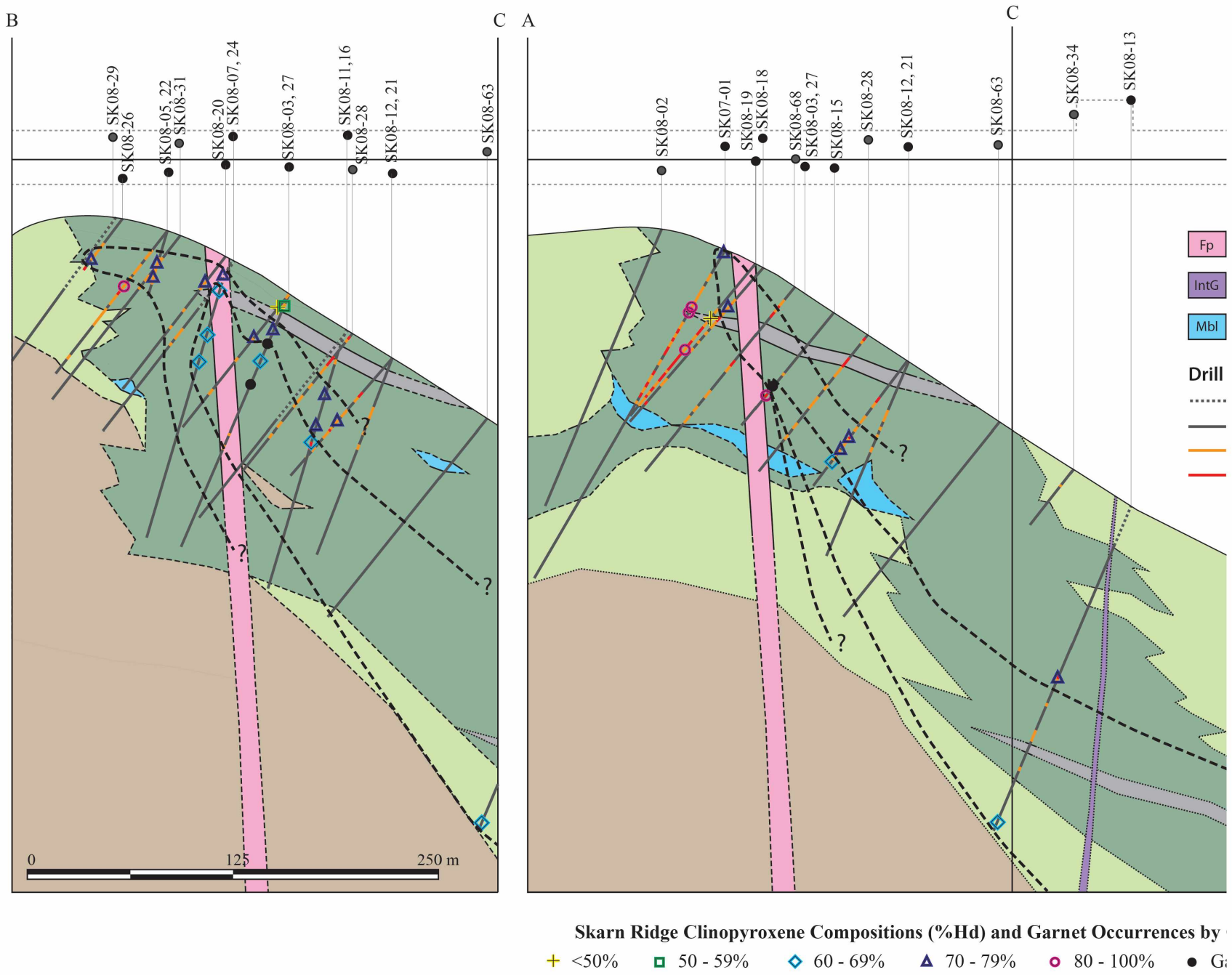

Figure 6.2. Clinopyroxene zoning (%Hd) along cross-sections A-C-A' and B-C.
Although shown as cut by the zoning, the felsic porphyry dike actually cuts across the skarn (and hence the clinopyroxene zoning). Cross section location is on I
felsic dike are actually in skarn immediately outside of the dike.

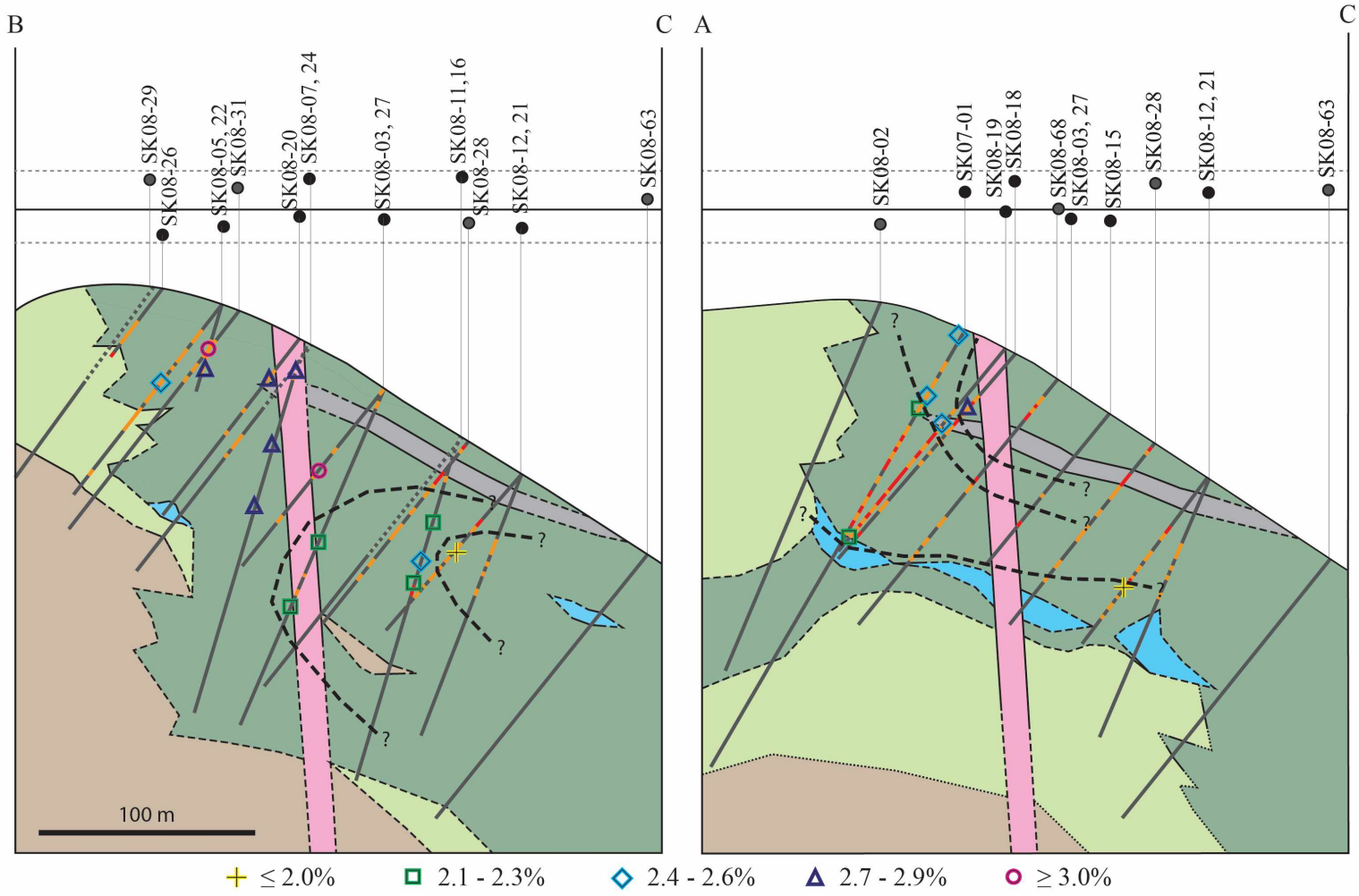

Figure 6.3. Percent Cl in Skarn Ridge scapolite.
Data are superimposed on the geologic cross-sections of Figure 6.2. The values generally increase to the NW and 'up'.

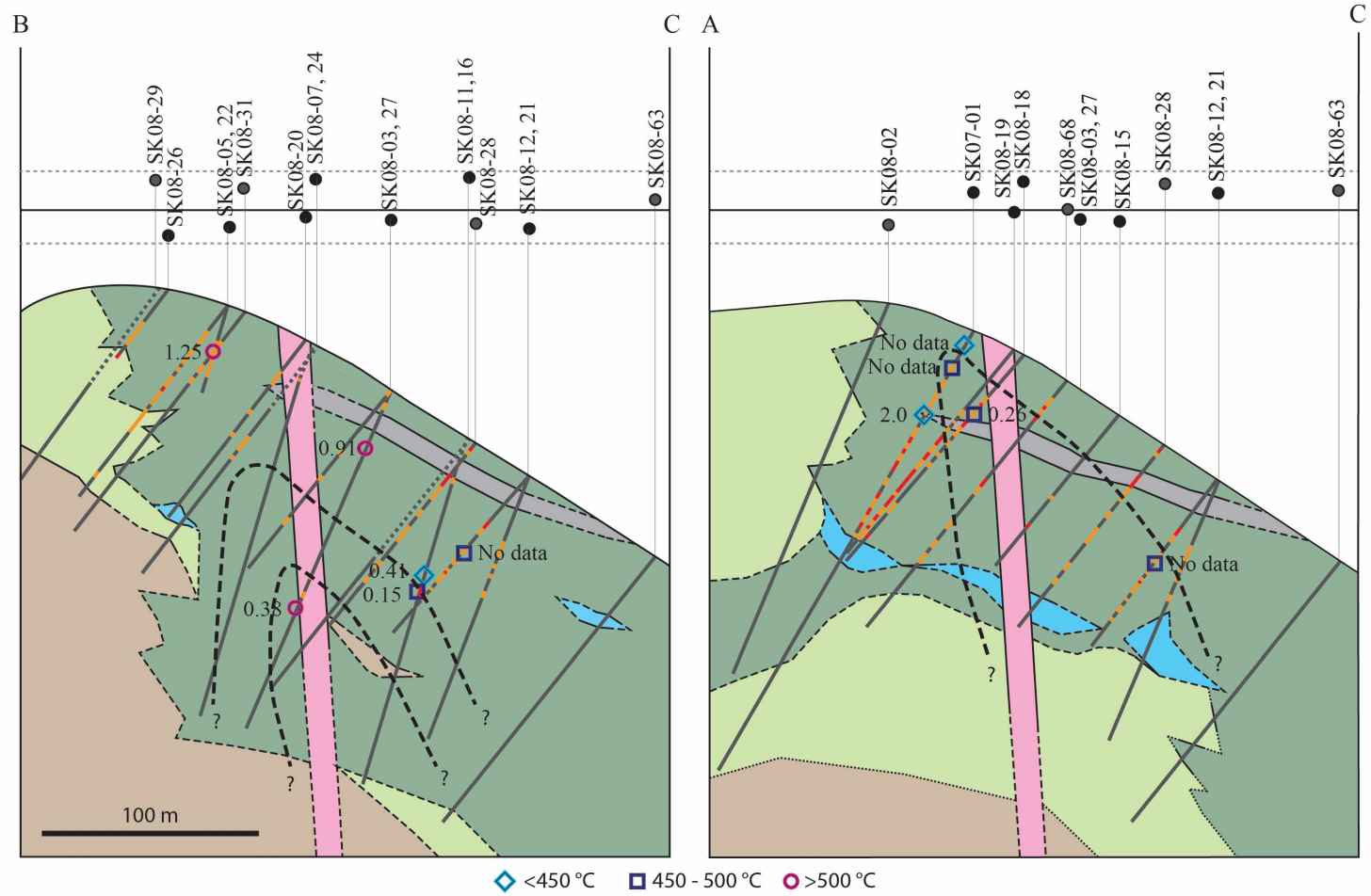

Figure 6.4. Thermal zoning illustrated by arsenopyrite geothermometry.
Cobalt (wt. %) in arsenopyrite values are plotted along drill hole traces; symbol type indicates calculated temperature group, based on the fS_2-T isopleths of Scott (1983). Only those arsenopyrite grains with Co < 0.5% are likely to yield reliable temperature. For cross section reference, see Figure 3.2.

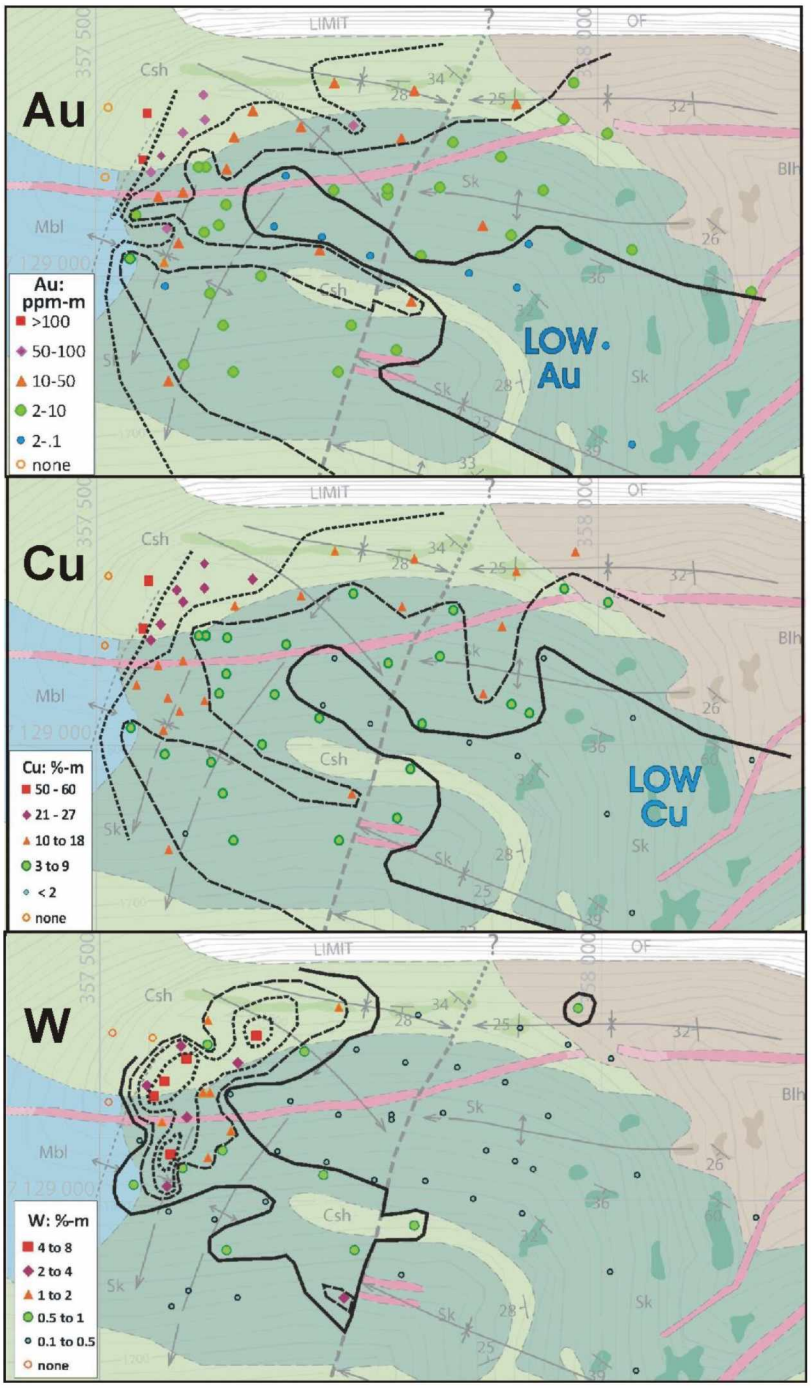

Figure 6.5. Au, Cu, and W endowment.
Endowment is superimposed on the geologic map of Figure 3.1 and calculated as described in text. Cu and Au show similar 'bullet shaped' patterns increasing towards the WNW, whereas W endowment shows a different pattern, partly symmetric around the felsic dike. Hand-drawn contours separate the different endowment range symbols.

6.10. References

Einaudi, M.T., Meinert, L.D., and Newberry, R.J., 1981, Skarn Deposits: Economic Geology, 75th Anniversary Volume, p. 317-391.

Meinert, L.D., 1992, Skarns and skarn deposits: Geoscience Canada, v. 19, p. 145-162.

Newberry, R.J., 1982, Tungsten-bearing skarns of the Sierra Nevada. I. The Pine Creek Mine, California: Economic Geology, v. 77, p. 823-844.

Newberry, R.J., 1998, W- and Sn-Skarn deposits: a 1998 Status Report *in* D.R. Lentz, ed., Mineralized Intrusion-Related Skarn Systems: Mineralogical Association of Canada Short Course, v. 26, p. 289-335.

Ray, G.E., Ettlinger, A.D., and Meinert, L.D., 1990, Gold skarns: Their distribution, characteristics, and problems in classification: British Columbia Geological Survey Geological Fieldwork 1989, Paper 1990-1, p. 237-246.

Scott, S.D., 1983, Chemical behavior of sphalerite and arsenopyrite in hydrothermal and metamorphic environments: Mineralogical Magazine, v. 47, p. 427-435.

7. Radiometric Dating

7.1. Introduction

Direct dating of skarn deposits by the $^{40}Ar/^{39}Ar$ geochronology method is unconventional due to the typical lack of abundant K-bearing minerals. As a result, relative dating techniques (dating potassium minerals in associated igneous rocks and establishing cross-cutting relationships) are traditionally applied to bracket the age of skarns. A few recent studies have reported variable success from directly dating skarn minerals, including: garnet by U-Pb (Meinert et al., 2001), phlogopite by $^{40}Ar/^{39}Ar$ (Beuchat, 2003), and actinolite and hornblende by U-Pb (Mueller et al., 2004). In this study, I use both direct and relative dating methods to determine the age of the Skarn Ridge deposit and the overall timing of geological events. Igneous units dated include the Mike Lake pluton (biotite and hornblende) and a mafic sill (biotite). In addition, I dated the skarn using hornblende and scapolite.

Though not commonly used for geochronological studies, scapolite has been successfully dated by the K-Ar method (MacIntyre, 1966) and the $^{40}Ar/^{39}Ar$ method (Reddy et al., 1997; Kendrick and Phillips, 2009). Potential problems with scapolite are: (1) it has a wide range of compositions and typically contains insufficient potassium for K-Ar or $^{40}Ar/^{39}Ar$ dating, and (2) argon retention behavior and closure temperature are not well understood. At Skarn Ridge, scapolite is invariably present throughout the deposit with K_2O concentrations of 1.5-4.0%; perfectly adequate for $^{40}Ar/^{39}Ar$ dating.

This study demonstrates the use of scapolite as a geochronometer and provides a novel way to directly date skarn deposits.

Scapolite is a tectosilicate with solid solution between marialite ($Na_4Al_3Si_9O_{24}Cl$) and meionite ($Ca_4Al_6Si_6O_{24}CO_3$), although compositionally pure end-members have not been identified in nature (Pan, 1998). Scapolite solid solution is analogous to the Na-Ca solid solution in the plagioclase series, and as such, the chemical formulae are often written to emphasize this similarity: $3NaAlSi_3O_8 \bullet NaCl$ (marialite) and $3CaAl_2Si_2O_8 \bullet CaCO_3$ (meionite) (Pan, 1998). Argon diffusion rates in scapolite are not well constrained. Based on scapolite behavior in a regional metamorphic setting, Kendrick and Phillips (2009) felt that argon retentivity should be similar to that of plagioclase feldspar (based on structural similarities).

7.2. Methods

A total of eight samples were dated in this study (Figure 7.1 and Table 7.1). All samples were prepared and analyzed by $^{40}Ar/^{39}Ar$ geochronology at the Geochronology Laboratory at the University of Alaska Fairbanks (UAF). Each sample was crushed, washed, and sieved and suitable grains were manually selected for dating. The monitor mineral MMhb-1 (Samson and Alexander, 1987) with an age of 513.9 Ma (Lanphere and Dalrymple, 2000) was used to monitor neutron flux and calculate the irradiation parameter, J. The samples and standards were wrapped in aluminum foil and loaded into aluminum cans of 2.5 cm diameter and 6 cm height. The samples were irradiated in position 5c of the uranium-enriched research reactor of McMaster University in

Hamilton, Ontario, Canada for 10 hours (30 megawatt-hours). Mineral grains were loaded into 2 mm diameter holes in a copper tray and incremental step-heating analyses were conducted according to the schedules presented in Table 7.A-1. The mass spectrometer, model VG-3600, is equipped with an ultra-high vacuum extraction line and an 8-watt argon-ion laser, as described in detail by Layer (2000).

Quantitative microprobe analyses were conducted for comparison with mass-spectrometry derived values for some geochronology samples (scapolite, hornblende, and biotite). In addition, the remaining scapolite separate from Scap #1 was formed into a pressed pellet for quantitative XRF analysis. Data obtained from both XRF and microprobe studies were used to establish the acceptable range of Ca/K and Cl/K values for Skarn Ridge scapolite and for comparison to argon isotope proxies measured by mass spectrometry. Microprobe and XRF methods are discussed in detail in Chapter 3.

7.3. Results

Biotite from a mafic sill produced the oldest ages for all rocks on Skarn Ridge: integrated ages of 226.3 ± 0.9 Ma and 248.3 ± 1.2 Ma for two subsamples of the same separate (Figure 7.2. A and B). The spectra do not exhibit plateaus; rather they have a saddle shape, or "pseudo plateau", with 2-4 intermediate steps of younger ages surrounded by steps of older ages on both sides. Biotite A has a weakly developed saddle comprised of three steps with a weighted mean age of 202.9 ± 3.7 Ma. Biotite B has a well-developed saddle comprised of four steps with a weighted mean age of 238.0 ± 4.8 Ma. The samples do not form an isochron, indicating a complex thermal history.

Three different samples of scapolite were dated. Due to the lack of available data on scapolite as a geochronometer, five step-heating experiments were performed on the first sample (Scap #1A-1E) in order to assess the mineral's behavior and response to the laser. This sample of scapolite was a colorless, transparent mineral that did not couple well with the argon-ion laser used in the UAF laboratory. This behavior made it difficult to fuse or extract all the gas from the sample. For all laser runs in this study, the laser beam was defocused to cover the whole mineral (~2 mm spot size). To try to ensure that most of the gas was released from these clear minerals, the laser was refocused to smaller spot sizes at maximum laser power (9000 mW). These are reported as different laser powers (e.g. 9001, 9002 mW) in Table 7.A-1.

The age spectra from the five runs show variable behavior, especially at the low temperature steps (Figure 7.3). At higher temperatures, the ages all are similar at about 100 Ma. Ca/K and Cl/K spectra show complex, low-temperature release behavior similar to the associated age spectra. Initial steps have elevated Ca/K values and significantly reduced Cl/K values, suggesting release from a high-Ca, low-Cl mineral less retentive of argon than scapolite, perhaps calcite. The compositional range of Skarn Ridge scapolite is defined by 363 quantitative microprobe analyses: Ca/K = 8.8 ± 1.0, Cl/K = 2.8 ± 0.3, and K_2O = 1.1 ± 0.1 (Chapter 3). From these values, a "scapolite" Ca/Cl ratio would be about 3.1. I show Ca/Cl versus age for step-heat fractions in Figure 7.4, and on that figure identify a cluster of fractions with similar Ca/Cl ratios and similar ages. This cluster corresponds to the higher temperature fractions that display Ca/K and Cl/K ratios

similar to those determined for scapolite by microprobe and XRF analyses. For these 13 high temperature fractions, the Ca/K ratios vary from 8.2 to 15.8, and the Cl/K ratios vary from 2.7 to 3.0. The weighted average Ca/Cl ratio is 3.40 ± 0.06. This is slightly higher than the microprobe results, implying that there is probably still a hint of calcite even in these 'scapolite' steps.

For each scapolite run, the highest temperature steps were used and constitute the majority of gas release. For run A, the last three steps constitute 58% of gas release; for B, 2 steps, 50%; for C, 2 steps, 91%; for D, 3 steps, 89% and for E, 3 steps, 58%. Combined results for all 13 Scap #1 fractions yield a weighted mean age of 98.6 ± 0.4 Ma, (Figure 7.3). Therefore I interpret the age spectra to reflect two (or more) mineral phases, and I only used the heating steps with 'scapolite' composition to calculate ages. Also, all Scap #1 isochron plots show more than one population, and as a result isochrons did not provide an age correlative to the plateau age.

Two additional samples of skarn scapolite, Scap #2 and Scap #3, yield ages of 100.4 ± 0.7 Ma and 97.1 ± 0.5 Ma, respectively (Figure 7.5 A and B). In an effort to try to remove the "calcite" contamination seen in Scap #1, these samples were treated with acetic acid (post crushing and sieving). The spectra display flat plateaus with little to no argon loss or gain in the initial steps and a smaller proportion of calcite. These samples were also opaque (likely due to fluid inclusions), unlike the transparent Scap #1 sample. Scap #2 plateau consists of 9 fractions accounting for 97.9% of argon released, while the Scap #3 plateau consists of 7 fractions/steps accounting for 97.0% of argon released.

Both samples isochron well, which adds confidence to the plateau age estimates (Figure 7.6).

The skarn hornblende age spectrum steps up from 82.8 ± 2.7 Ma to 90.5 ± 1.2 Ma (Figure 7.7). Statistically, this satisfies the criteria for a plateau, however "stepping-up" behavior makes a complex thermal history likely. Additionally, the Ca/K and Cl/K values in the initial low-temperature release steps are incompatible with skarn hornblende compositions (Ca/K = 9.8, Cl/K = 0.6), as determined by microprobe analysis (Chapter 3) indicating that this is not a pure hornblende and may have been altered.

Hornblende and biotite from the Mike Lake pluton were dated separately and yield ages of 88.0 ± 1.1 Ma and 89.1 ± 0.8 Ma, respectively (Figure 7.8 A and B). Biotite yields a flat plateau based on 6 steps and 98.3% of all argon released. Ca/K and Cl/K spectra are flat and correspond well with compositions determined by microprobe (e.g., Cl/K ~ 0.09). Hornblende also yields a flat plateau based on 6 steps and 96.6% argon release. Ca/K and Cl/K spectra show more complex behavior than biotite from this sample in both low- and high-temperature release steps. However, Ca/K of ~ 12 and Cl/K ~ 0.6 from the Ar spectra match the ratios determined by microprobe analyses (~12 and ~ 0.7, respectively).

7.4. Discussion

Three types of patterns are observed in the Skarn Ridge age spectra: (1) flat plateaus, (2) stepping-up, and (3) saddles. Each shape provides valuable information about the thermal history of each sample and reflects differences in how the various

minerals respond to re-heating events. Spectra with flat plateaus are interpreted to have had a single cooling event and a straightforward thermal history (no argon loss or gain). While it is conceivable that such spectra represent minerals that have completely reset by losing or gaining Ar, such is unlikely. The second type of pattern, a stepping-up pattern, is one in which the age (and fraction of argon released) increases with each progressive heating step. This is most likely due to radiogenic argon loss from the least retentive phases of the mineral, which is typically caused by a reheating or alteration event. As the laser temperature increases with each step in the heating process, radiogenic argon is released from the more retentive mineral structure. The age of a sample with this type of spectrum is most accurately determined from the final step, and is a minimum age at best. The third type of age spectrum pattern is the saddle, which appears as younger ages surrounded by older ages in a broad 'U' or saddle shape. This pattern is interpreted to indicate the presence of excess argon and a complex thermal history. The apparently older ages are caused by excess argon or argon recoil from parts of the crystal lattice (McDougall and Harrison, 1999), however, from both the highest- and lowest-temperature fractions. That is, the anomalous behavior occurs in what is supposed to be the most retentive part of the grain. Biotite is known to be prone to such behavior, although exactly why this happens is not known (McDougall and Harrison, 1999). In such cases the 'most reliable age is derived from what is not normally considered the best part of the Ar-release spectrum.

A problematic consideration relates to the heating schedules employed and the response of each sample to the laser. Heating schedules for scapolite varied from 6 to 11 steps and the laser power applied at each step also varied (Table 7.A-1). It is also not certain that all the Ar from the East Skarn Ridge scapolite samples was released, as these never fused. However, ages from the "correct" Ca/K and Cl/K phases can provide information on the age of the mineral.

A final consideration for evaluating age spectra is that different minerals are more (or less) susceptible to thermal reset and to exhibiting a particular type of reset behavior, depending on the crystal structure. The phyllosilicate structure of biotite is notorious for being non-retentive with respect to argon and has a low closure temperature of approximately 250-350 °C (depending on the cooling rate) that makes it easily reset in hydrothermal settings (Dalmeyer, 1978; Layer et al., 1987). The inosilicate structure of hornblende is more retentive of argon; it has a higher closure temperature and is generally less susceptible to reset. However, alteration of either mineral by chlorite makes the mineral more susceptible to Ar loss, both during the alteration event and during the cooling period following the alteration event.

Scapolite behavior as a geochronometer is poorly understood; very few studies exist on the mineral and most focus on its behavior in regional metamorphic settings rather than contact metamorphic-hydrothermal environments. One would predict (based on its tectosilicate structure) that scapolite is expected to have Ar-retentivity similar to K-

feldspar. However, this study demonstrates that scapolite may be more retentive than K-feldspar, and perhaps a better choice for dating in a hydrothermal setting.

The problems of radiometric age versus true age of formation are best illustrated by the Mike Lake pluton hornblende and biotite data (Figure 7.8). Cretaceous plutonic rocks—e.g., plutons of the Sierra Nevada, California—invariably yield radiometric ages such that the zircon U-Pb age is about 1 Ma older than the hornblende Ar-Ar plateau age from the same rock, which is in turn about 2 Ma older than the biotite Ar-Ar age (Evernden and Kistler, 1970; Stern et al., 1981; duBray and Dellinger, 1988). Such an age pattern is in agreement with the known age retention temperatures and the typical rates of pluton cooling. For the Mike Lake pluton sample, hornblende yielded an age of 88.0 ± 1.1 and biotite 89.1 ± 0.8 Ma. Statistically these ages are indistinguishable, but typically they wouldn't be: the biotite age would be approximately 2 Ma younger.

The petrographic characteristics of these Mike Lake pluton minerals differ slightly: the hornblende displays minor chloritization and some magmatic intergrowths with clinopyroxene; the biotite displays neither. Both of these features could make the Mike Lake hornblende slightly more susceptible to Ar loss during the weak chlorite alteration episode that presumably took place in the waning stages of cooling, approximately at the biotite Ar retention temperature. Or, conceivably the biotite gained Ar during cooling and its radiometric age is anomalously old. Both spectra look straightforward (Figure 7.8). The most obvious difference in their Ar spectra is the variability in Ca/K and Cl/K ratios for the hornblende at high and low-temperature

heating steps. This behavior (not exhibited by the biotite) implies that the hornblende – not the biotite – has been slightly reset.

The skarn hornblende Ar spectrum (Figure 7.7) seems to show a simple stepping-up age pattern, but the complex Ca/K and Cl/K ratio patterns belie a simple interpretation. The Cl/K ratios in the hornblende vary from < 0.1 to > 0.4 and the Ca/K from < 1 to > 8, implying that the sample contained multiple phases and (or) underwent severe chemical alteration. And in either case the hornblende would be considerably less Ar-retentive than normal. More alarmingly, there is no known source of heating at the lower-temperature fraction age of 83 Ma. Something allowed this hornblende to continue losing Ar even after the Rubble Lake plutonic biotite and hornblende reached their age retention temperature. The highest-temperature fraction age (90.5 Ma) is truly a minimum age for formation of the skarn hornblende.

Oddly enough, the scapolite samples show little evidence for thermal resets, even though their tectosilicate structure is expected to be less retentive of Ar than the sheet or chain silicate structures of biotite and hornblende. The East Skarn Ridge scapolite Ar spectra are complicated due to a small amount of adhering calcite and its clear nature (and thus difficult heat absorption). However, significant portions of the argon release indicate that a pure scapolite phase was dated. Of note is that at nearly the same location (Figure 7.1), the mafic sill biotite has had its Ar redistributed and the skarn hornblende sample has been extensively modified, but the two scapolite samples exhibit only minor signs of Ar loss. The sample with the younger age (Figure 7.5 B) does show evidence for

both Ar gain and Ar loss in the lower-temperature fractions, compatible with more reset than the sample with the older age. Particularly if this apparently younger scapolite has been reset, it exhibits such by radically different behavior than that of the skarn hornblende; perhaps assumptions concerning Ar retention in scapolite should be re-assessed.

It is possible that the Rubble Lake pluton is physically closest to the location of the skarn hornblende sample (as shown diagrammatically in Figure 7.1) and this might account for the apparently greater degree of reset in the hornblende than the nearby scapolite samples. An additional possibility is that thermal resets are (in this setting) really *hydro*thermal resets, and the lack of alteration in the scapolite, combined with some chloritization of the hornblende, makes scapolite apparently more Ar-retentive than the hornblende in this setting.

In sum, the radiometric age spectra do not provide a crystal-clear picture of the absolute ages of skarn formation and subsequent alteration; however, they are most compatible with a model of skarn formation considerably before intrusion of the nearby Mike Lake pluton (Figure 7.8). The mafic sills are at least 125 Ma older than any other rock dated from Skarn Ridge; they are likely Triassic and are temporally unrelated to any of the skarn-forming events. Whether they are early, middle, or late Triassic cannot be claimed with much certainty. The mafic magma that intruded the Paleozoic sedimentary package likely produced little (if any) alteration in the host rocks, given its small size and

extent. However, it apparently acted as a plumbing system for future skarn-forming fluids, as indicated by its extensive, high-temperature alteration (Chapters 3 and 4).

Figure 7.9 illustrates a summary of geologic events based on age determinations by geochronology. Skarn formation began as early as 100 Ma as evidenced by scapolite ages of 100.4 ± 0.7 to 96.7 ± 1.0 Ma. The age differences between the oldest and two youngest scapolite samples are statistically significant; however, almost certainly they do not indicate two different pulses of scapolite formation. More likely they display variable degrees of age reset with a minimum age of ~100 Ma.

The skarn hornblende yields a much younger minimum age of 90.5 ± 1.2 Ma, approximately 10 Ma younger than the oldest scapolite age. The "stepping-up" pattern of the age spectra indicates that the oldest (highest-temperature) fraction yields the best estimate of the minimum age. However, could this amphibole have lacked sufficient retentivity to have lost 10 Ma worth of Ar? The obvious possibilities are either (a) the retrograde event documented by the hornblende is considerably younger than and unrelated to the prograde event recorded by the scapolites, or (b) the skarn hornblende has undergone considerable Ar loss. Given the youngest apparent age for this hornblende of 83 Ma (Figure 7.7), at least 5 Ma younger than the pluton likely responsible for the thermal reset, a bizarre Ar loss seems at least plausible.

Biotite and hornblende from the Mike Lake pluton yielded the youngest radiometric ages of this study; more than 10 Ma younger than the oldest skarn scapolite. Thus, almost certainly, the Mike Lake pluton was unrelated to formation of the nearby

Mike Lake skarn. Finally, based on drill core observations summarized in Chapter 3, the undated green dikes intruded during or slightly after skarn formation. The porphyritic dikes intruded after the green dikes and clearly after the skarn formed. The presence of axinite alteration in both of these dikes, however, indicates that an additional hydrothermal system was superimposed on the region. The lack of axinite in the Mike Lake pluton makes this intrusive body an unlikely source; at most the Mike Lake pluton was associated with minor propylitic-style alteration.

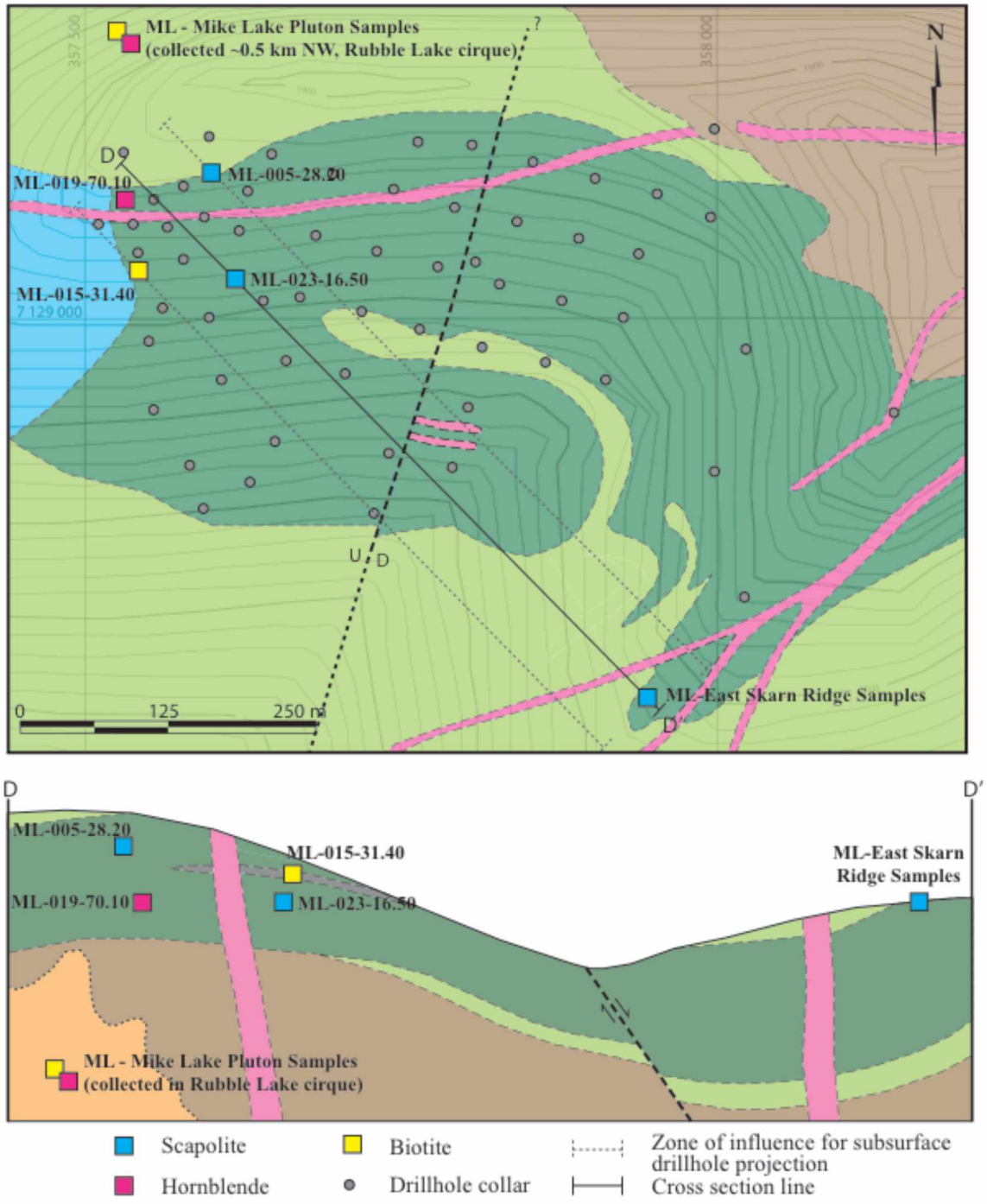

Figure 7.1. Location map and cross section for geochronology samples.
The location of cross section D-D' can also be found in Figure 3.2. Location of Mike Lake pluton samples is shown schematically, actual sample location is not in the cross-section. Hypothetical pluton underlies 'D' to account for thermal resets.

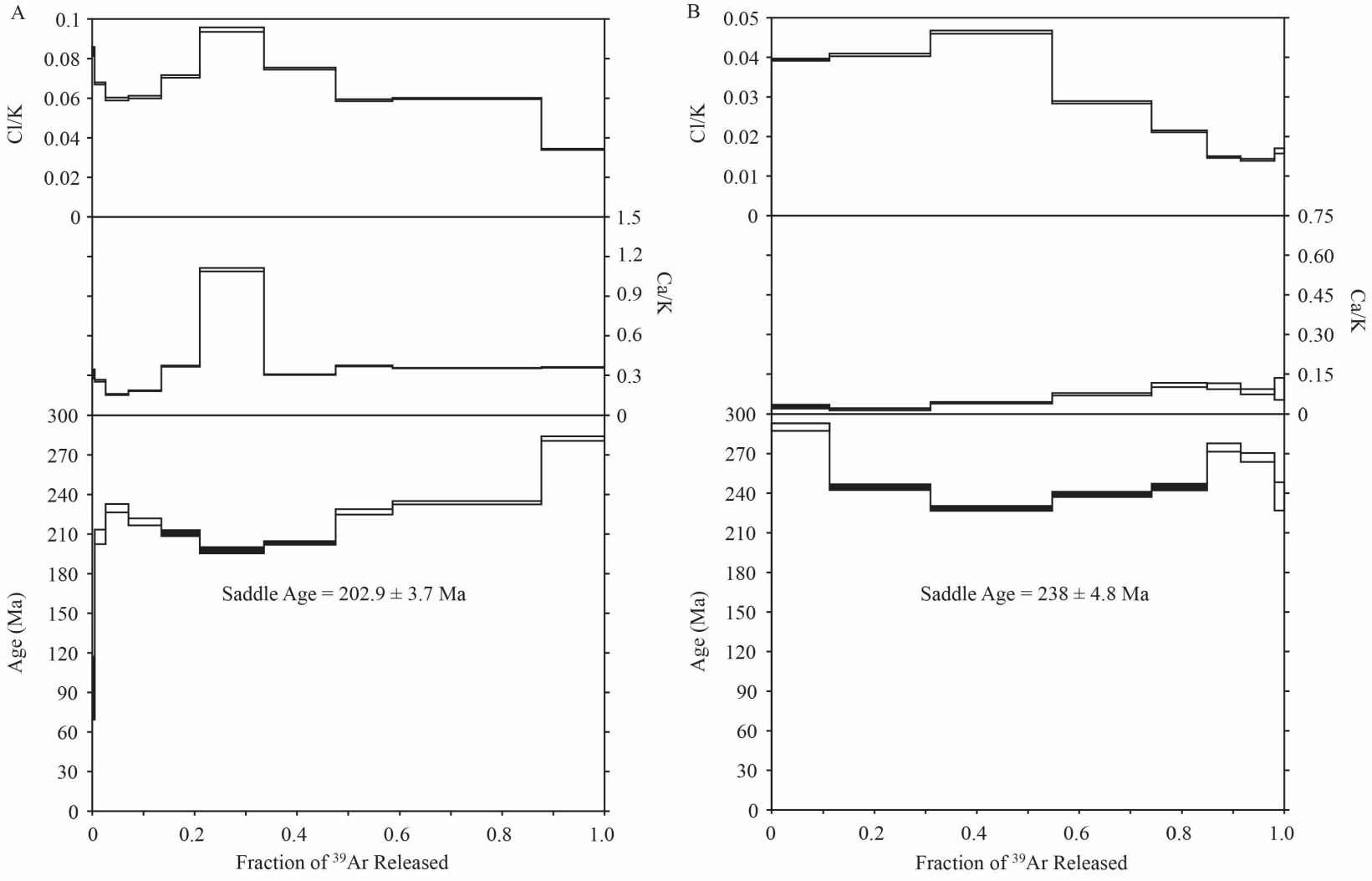

Figure 7.2. Age spectra for biotite from mafic sill sample ML-015-31.40.

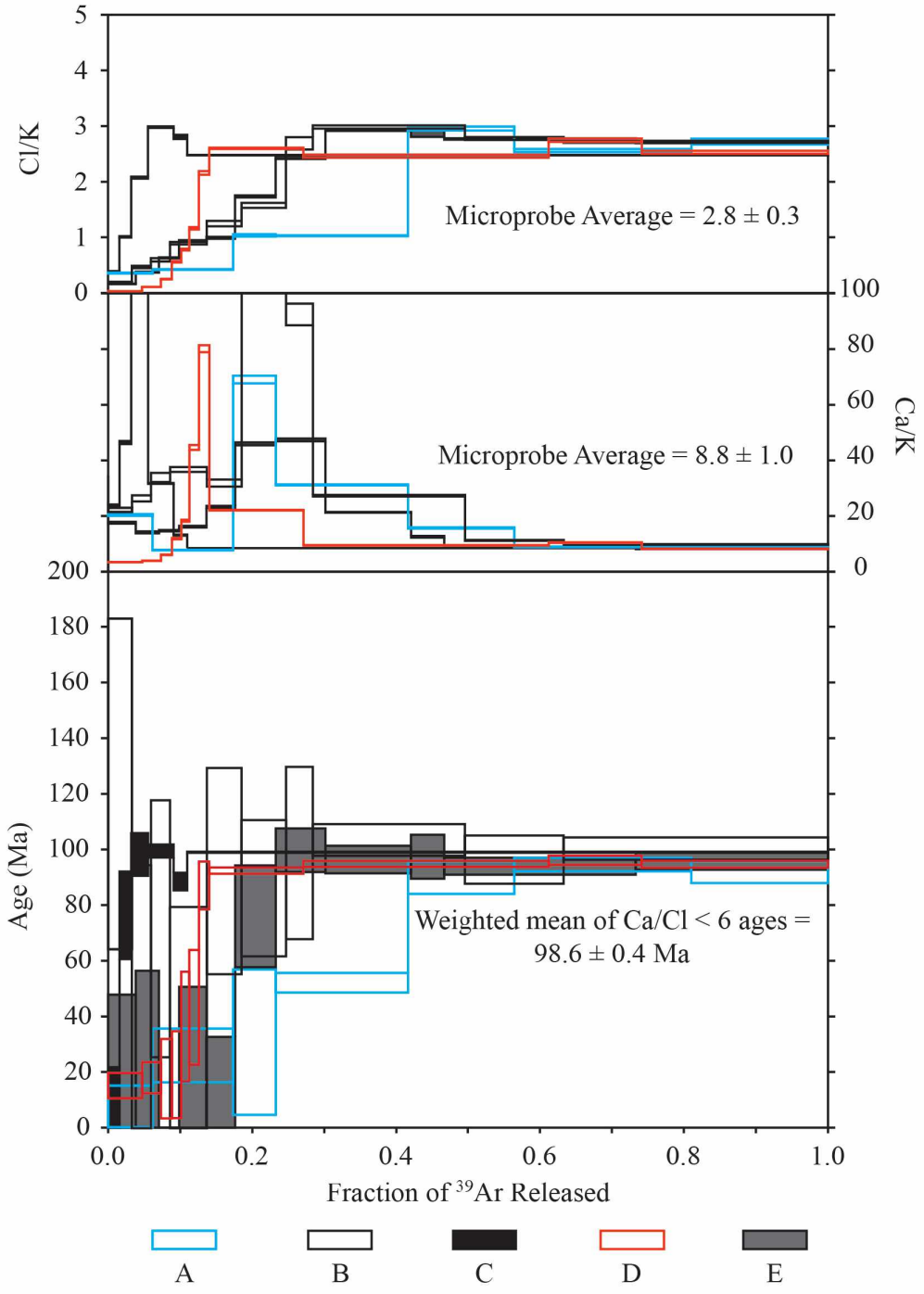

Figure 7.3. Age spectra for skarn scapolite from East Skarn Ridge. Five (A to E) splits of this sample were separately analyzed.

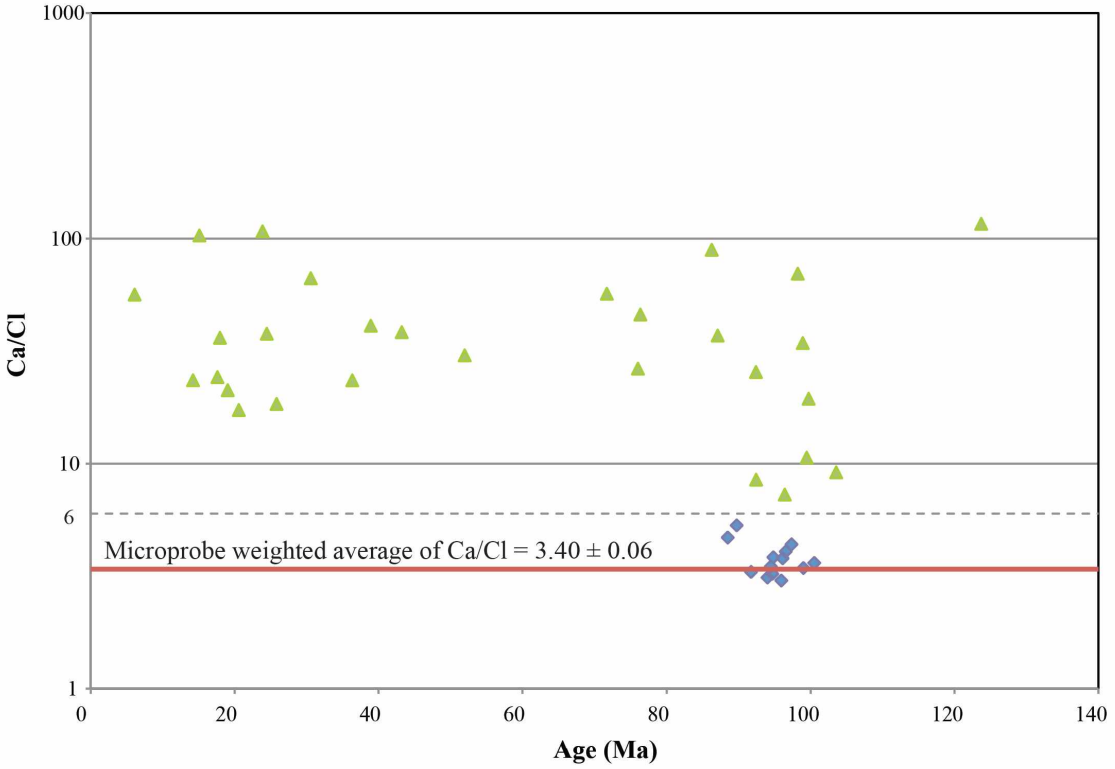

Figure 7.4. Ca/Cl versus age for scapolite step-heat fractions.
The cluster of points with Ca/Cl < 6 corresponds to the higher temperature fractions with Ca/K and Cl/K ratios similar to average microprobe values.

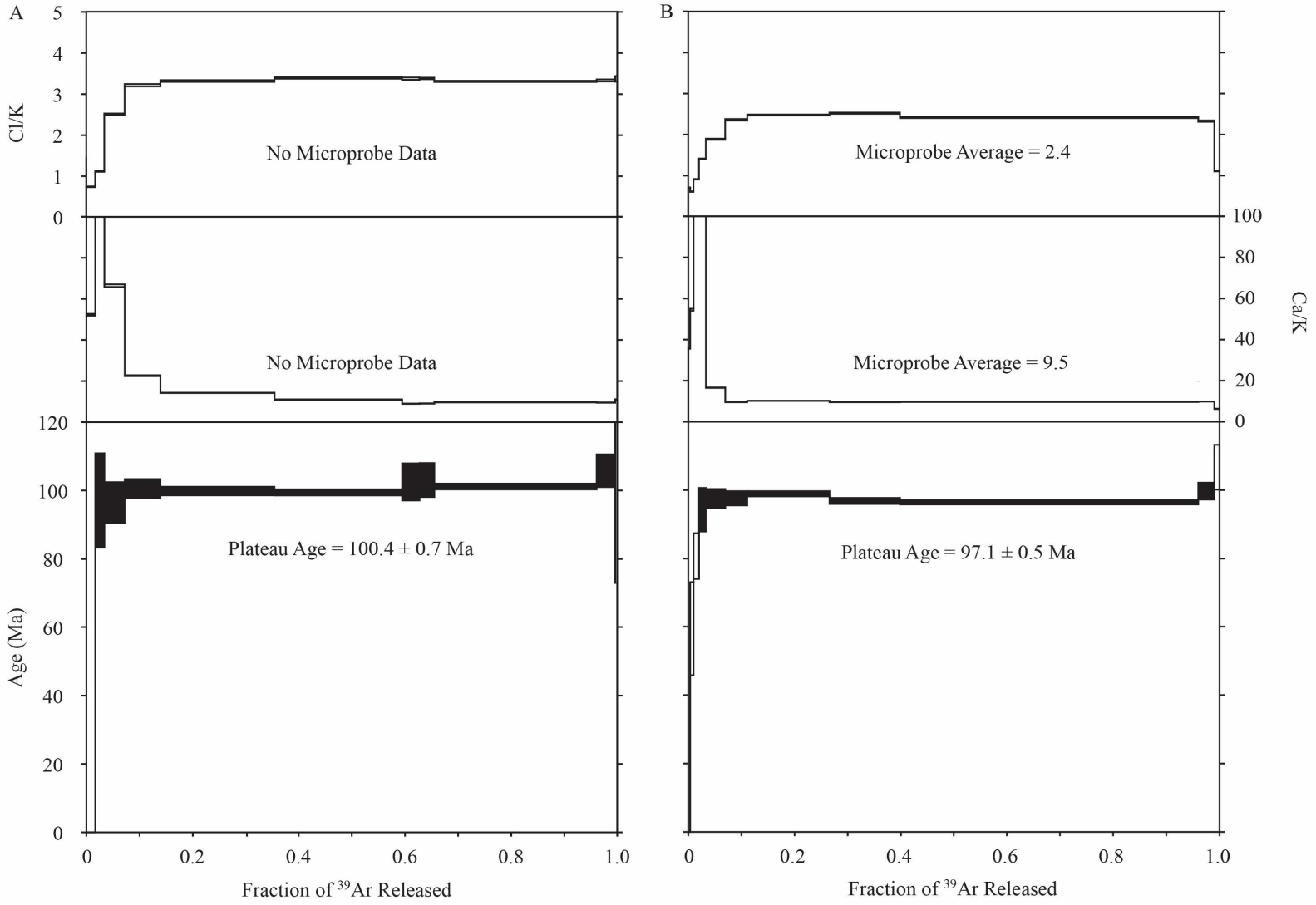

Figure 7.5. Age spectra for skarn scapolite samples ML-023-16.50 (A), and ML-005-28.20 (B).

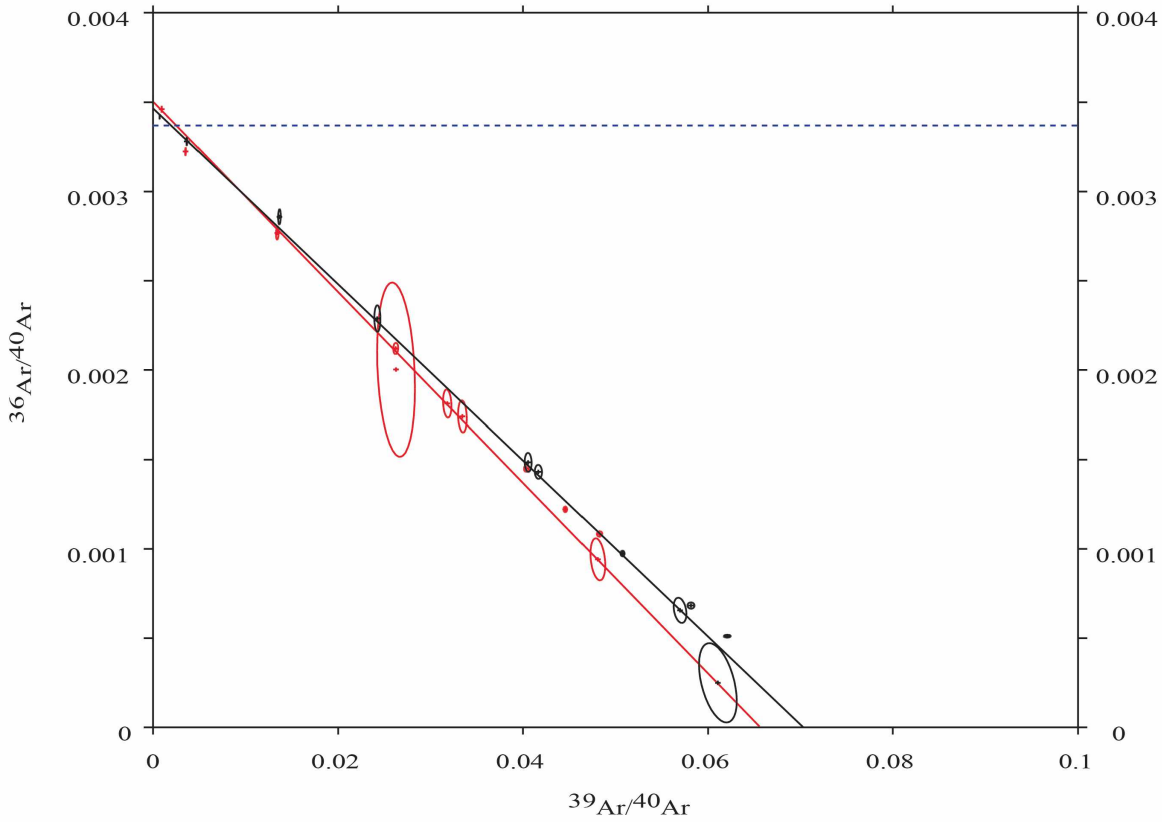

Figure 7.6. Isochron plot for Scap #2 (red) and Scap #3 (black).

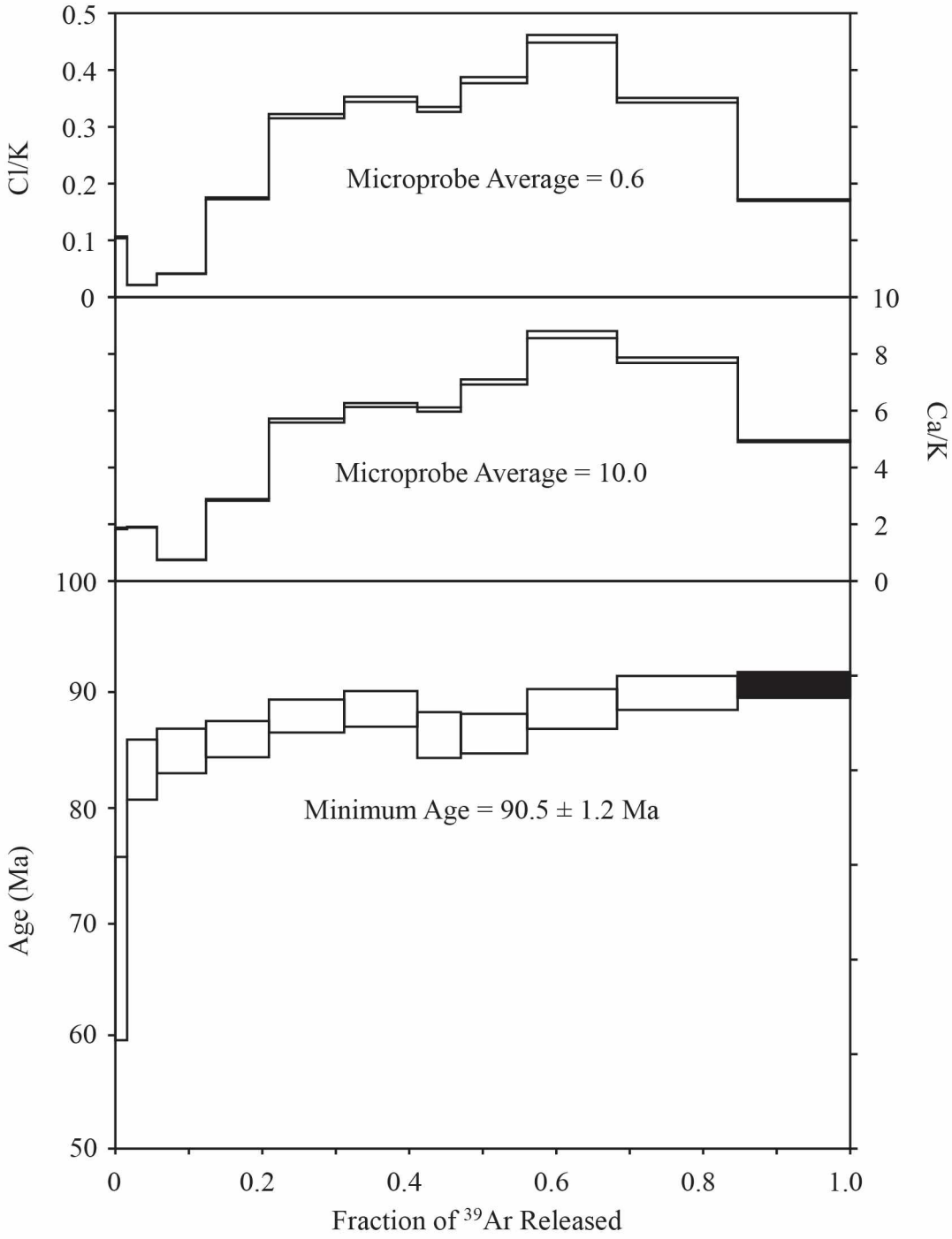

Figure 7.7. Age spectrum for skarn hornblende from sample ML-019-70.10.

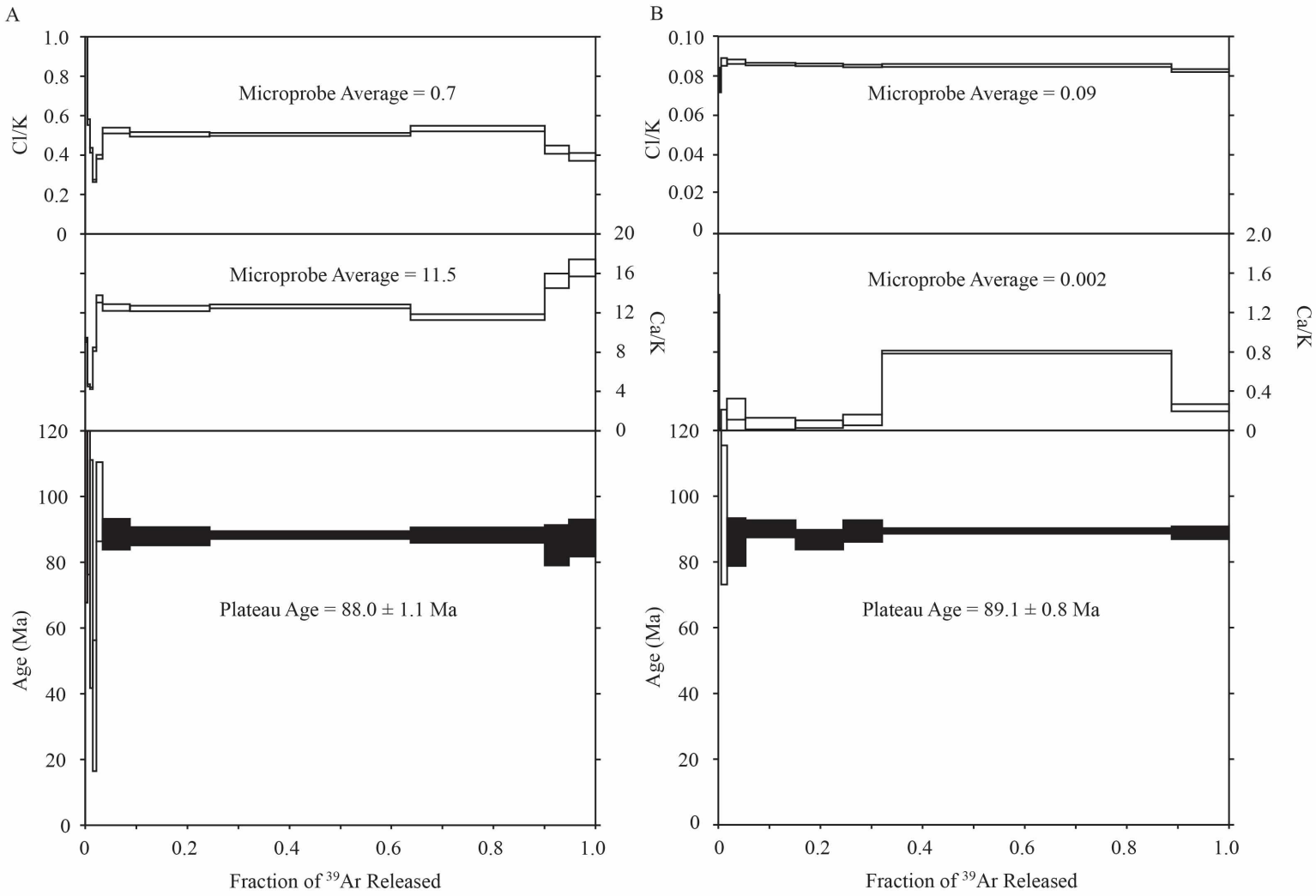

Figure 7.8. Age spectra for samples from the Mike Lake pluton. Spectrum A is from hornblende and spectrum B is from biotite.

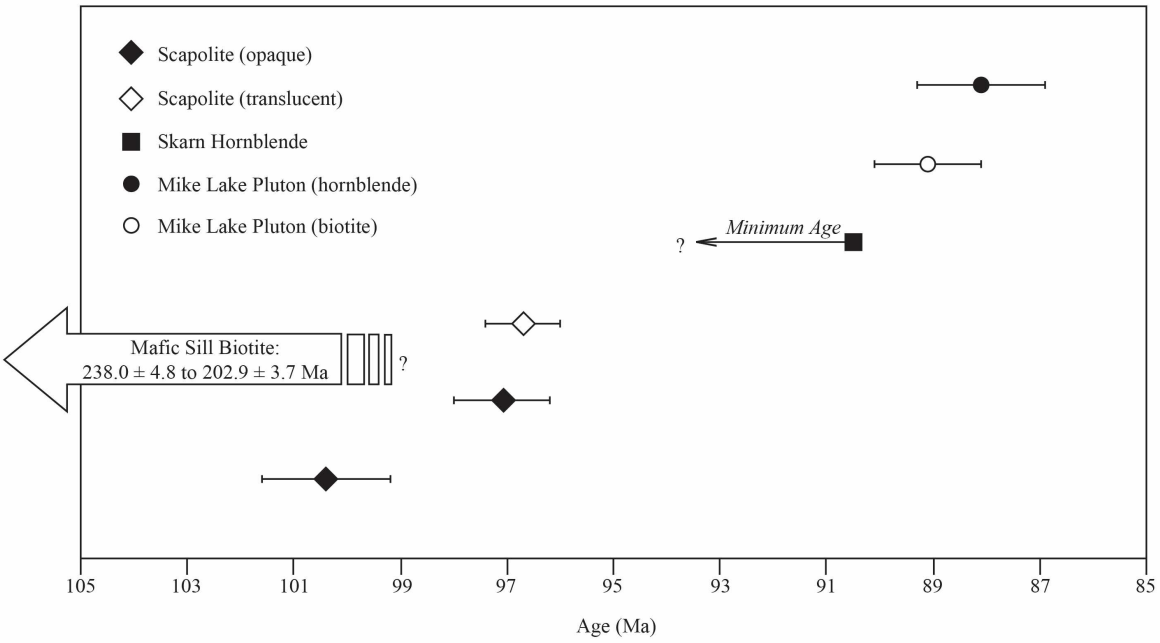

Figure 7.9. Ages and error for lithological units dated by $^{40}Ar/^{39}Ar$ geochronology.

Table 7.1. Sample scheme for $^{40}Ar/^{39}Ar$ geochronology.

Sample ID	Mineral	Context	Notes
ML-East Skarn Ridge	Scapolite	Skarn	Subcrop; coarse-grained aggregate; no acetic acid pre-treatment.
ML-005-28.20	Scapolite	Skarn	Drill core; Acetic acid pre-treatment.
ML-023-16.50	Scapolite	Skarn	Drill core; Acetic acid pre-treatment.
ML-019-70.10	Hornblende	Skarn	Drill core; Retrograde skarn.
ML-015-31.40 (x2)	Biotite	Mafic Sill	Drill core; Least-altered sample from center of sill; two runs.
ML-MLP-HBL	Hornblende	Mike Lake Pluton	Subcrop; Least-altered sample from Rubble Lake Cirque.
ML-MLP-BIO	Biotite	Mike Lake Pluton	Subcrop; Least-altered sample from Rubble Lake Cirque.

7.5. References

Beuchat, S., 2003, Geochronological, structural, isotopes and fluid inclusion constraints of the polymetallic Domo de Yauli district, Peru, Genève, Terre & Environnement, v. 41, 130 p.

Dalmeyer, R.D., 1978, $^{40}Ar/^{39}Ar$ incremental-release ages of hornblende and biotite from Grenville basement rocks within the Indian Head Range complex, southwest Newfoundland: their bearing on Late Proterozoic-Early Paleozoic thermal history: Canadian Journal of Earth Sciences, v. 15, p. 1374-1379.

duBray, E., and Dellinger, D.A., 1988, Potassium-argon ages for plutons in the eastern and southern Sierra Nevada Batholith, California: U.S. Geological Survey Bulletin, v. 1799, 10 p.

Evernden, J.F., and Kistler, R.W., 1970, Chronology of emplacement of Mesozoic batholithic complexes in California and western Nevada: U.S. Geological Survey Professional Paper 623, 42 p.

Kendrick, M.A., and Phillips, D., 2009, New constraints on the release of noble gases during in vacuo crushing and application to scapolite Br-Cl-I and $^{40}Ar/^{39}Ar$ age determinations: Geochimica et Cosmochimica Acta, v. 73, p. 5673-5692.

Lanphere, M.A., and Dalrymple, G.B., 2000, First-principles calibration of ^{38}Ar tracers: Implications for the ages of $^{40}Ar/^{39}Ar$ fluence monitors: U.S. Geological Survey Professional Paper 1621, 10 p.

Layer, P., 2000, Argon-40/argon-39 age of the El'gygytgyn impact event, Chukotka, Russia: Meteorics & Planetary Science, v 35, p. 591-599.

Layer, P.W., Hall, C.M., and York, D., 1987, The deviation of $^{40}Ar/^{39}Ar$ age spectra of single grains of hornblende and biotite by laser step heating: Geophysical Research Letters, v. 14, p. 757-760.

MacIntyre, R.M., 1966, Studies of Potassium-Argon Dating: Unpublished Ph.D. thesis, Toronto, Ontario, The University of Toronto, 191 p.

McDougall, I., and Harrison, T.M., 1999, Geochronology and Thermochronology by the $^{40}Ar/^{39}Ar$ Method: Oxford University Press, New York.

Meinert, L.D., Nicolescu, S., Mortensen, J.K., and Cornell, D.H., 2001, U-Pb dating of hydrothermal garnet from skarn deposits; implications for petrogenesis and ore deposits: Geological Society of America, Abstracts with Programs, v. 33, p. 130.

Mueller, A.G., Nemchin, A.A., and Frei, R., 2004, The Nevoria Gold Skarn Deposit, Southern Cross Greenstone Belt, Western Australia: II. Pressure-Temperature-Time Path and Relationship to Postorogenic Granites: Economic Geology, v. 99, p. 453-478.

Pan, Y., 1998, Scapolite in skarn deposits: petrogenetic and geochemical significance *in* D.R. Lentz, ed., Mineralized Intrusion Related Skarn Systems, Mineralogical Association of Canada Short Course Series, v. 26, p. 169-209.

Reddy, S.M., Kelley, S.P., and Lochlann, M., 1997, A microstructural and argon laserprobe study of shear zone development at the western margin of the Nanga Parbat-Haramosh Massif, western Himalaya: Contributions in Mineralogy and Petrology, v. 128, p. 16-29.

Samson, S.D., and Alexander, E.C., 1987, Calibration of the interlaboratory $^{40}Ar/^{39}Ar$ dating standard, MMhb1: Chemical Geology, v. 66, p. 27-34.

Stern, T.W., Bateman, P.C., Morgan, B.A., Newell, M.F., and Peck, D.L., 1981, Isotopic U-Pb ages of zircon from the granitoids of the central Sierra Nevada: U.S. Geological Survey Professional Paper 1185, 17 p.

7.6. Appendix

Table 7.A-1. $^{40}Ar/^{39}Ar$ step heating data for all geochronology samples.

ML-East Skarn Ridge, Skarn Scapolite #1A
Weighted average of J from standards = 3.411e-03± 1.051e-05

Laser Power	^{39}Ar	$^{40}Ar/^{39}Ar$	$^{37}Ar/^{39}Ar$	$^{36}Ar/^{39}Ar$	^{40}Ar				$^{40*}Ar/^{39}K$	Age (Ma)
(mW)	Cumulative	Measured	Measured	Measured	% Atm.	Ca/K	Cl/K	Ca/Cl		
400	0.062	352 ± 5.0	11.0 ± 0.17	1.19 ± 0.02	100	20.4 ± 0.31	0.36 ± 0.01	56.6 ± 1.29	-0.12 ± 2.5	-0.74 ± 16
1200	0.173	167 ± 2.0	4.24 ± 0.05	0.551 ± 0.01	97.5	7.81 ± 0.09	0.42 ± 0.01	18.4 ± 0.32	4.23 ± 1.6	25.8 ± 10
2000	0.233	213 ± 4.1	36.7 ± 0.72	0.714 ± 0.02	97.7	69.1 ± 1.4	1.04 ± 0.02	66.7 ± 1.90	5.01 ± 4.3	30.6 ± 26
3500	0.416	51.2 ± 0.30	16.8 ± 0.10	0.149 ± 0.00	83.4	31.2 ± 0.19	1.03 ± 0.01	30.3 ± 0.28	8.57 ± 0.59	52.0 ± 3.6
5000	**0.565**	**31.8 ± 0.39**	**8.52 ± 0.11**	**0.060 ± 0.00**	**53.2**	**15.7 ± 0.21**	**2.96 ± 0.04**	**5.32 ± 0.10**	**14.9 ± 0.99**	**89.7 ± 5.8**
9000	**0.810**	**20.0 ± 0.20**	**4.86 ± 0.05**	**0.016 ± 0.00**	**21.6**	**8.94 ± 0.09**	**2.56 ± 0.03**	**3.49 ± 0.05**	**15.8 ± 0.42**	**94.5 ± 2.4**
9001	**1.000**	**25.7 ± 0.50**	**4.89 ± 0.10**	**0.037 ± 0.00**	**40.7**	**9.00 ± 0.18**	**2.72 ± 0.05**	**3.30 ± 0.09**	**15.3 ± 0.66**	**91.7 ± 3.9**
Integrated		77.1 ± 0.36	9.84 ± 0.05	0.225 ± 0.00	85.4	18.2 ± 0.09	1.90 ± 0.01	9.55 ± 0.07	11.3 ± 0.43	68.4 ± 2.5

ML-East Skarn Ridge, Skarn Scapolite #1B
Weighted average of J from standards = 3.411e-03 ± 1.051e-05

Laser Power	^{39}Ar	$^{40}Ar/^{39}Ar$	$^{37}Ar/^{39}Ar$	$^{36}Ar/^{39}Ar$	^{40}Ar				$^{40*}Ar/^{39}K$	Age (Ma)
(mW)	Cumulative	Measured	Measured	Measured	% Atm.	Ca/K	Cl/K	Ca/Cl		
300	0.033	704 ± 21	12.0 ± 0.39	2.32 ± 0.08	97.1	22.2 ± 0.73	0.191 ± 0.01	116 ± 6.19	20.8 ± 10	124 ± 59
700	0.059	447 ± 18	14.2 ± 0.59	1.51 ± 0.08	99.8	26.4 ± 1.1	0.468 ± 0.02	56.4 ± 3.48	0.994 ± 14	6.10 ± 88
1100	0.086	344 ± 16	18.2 ± 0.87	1.13 ± 0.06	96.6	33.9 ± 1.6	0.595 ± 0.03	56.9 ± 3.98	11.9 ± 7.8	71.7 ± 46
1600	0.137	440 ± 10	19.8 ± 0.46	1.47 ± 0.04	98.6	36.8 ± 0.88	0.896 ± 0.02	41.0 ± 1.40	6.40 ± 6.7	38.9 ± 41
2000	0.185	335 ± 13	17.2 ± 0.67	1.09 ± 0.05	95.5	31.9 ± 1.3	1.25 ± 0.05	25.6 ± 1.41	15.4 ± 6.3	92.4 ± 37
3000	0.247	188 ± 5.1	72.6 ± 1.96	0.612 ± 0.02	92.8	140 ± 4.0	1.57 ± 0.05	89.3 ± 3.60	14.4 ± 4.2	86.3 ± 24
4000	0.284	100 ± 4.0	48.7 ± 1.97	0.299 ± 0.02	84.1	92.5 ± 3.9	2.69 ± 0.11	34.4 ± 2.01	16.5 ± 5.3	98.9 ± 31
6000	0.496	26.1 ± 0.26	14.7 ± 0.15	0.034 ± 0.00	34.2	27.3 ± 0.28	2.99 ± 0.03	9.16 ± 0.13	17.3 ± 0.98	104 ± 5.7
9000	**0.633**	**23.3 ± 0.23**	**6.13 ± 0.09**	**0.026 ± 0.00**	**31.2**	**11.3 ± 0.16**	**2.78 ± 0.03**	**4.07 ± 0.07**	**16.1 ± 1.5**	**96.5 ± 8.7**
9001	**1.000**	**21.2 ± 0.15**	**5.35 ± 0.05**	**0.017 ± 0.00**	**21.0**	**9.85 ± 0.10**	**2.72 ± 0.02**	**3.62 ± 0.04**	**16.8 ± 0.69**	**101 ± 4.0**
Integrated		115 ± 0.59	15.5 ± 0.08	0.342 ± 0.00	86.6	28.8 ± 0.16	2.35 ± 0.01	12.3 ± 0.09	15.6 ± 0.88	93.8 ± 5.1

ML-East Skarn Ridge, Skarn Scapolite #1C

Weighted average of J from standards = 3.411e-03 ± 1.051e-05

Laser Power (mW)	^{39}Ar Cumulative	$^{40}Ar/^{39}Ar$ Measured	$^{37}Ar/^{39}Ar$ Measured	$^{36}Ar/^{39}Ar$ Measured	^{40}Ar % Atm.	Ca/K	Cl/K	Ca/Cl	$^{40*}Ar/^{39}K$	Age (Ma)
800	0.016	459 ± 3.5	12.9 ± 0.14	1.56 ± 0.02	100	23.9 ± 0.26	0.388 ± 0.00	61.6 ± 0.89	-0.030 ± 3.5	-0.18 ± 22
2000	0.032	349 ± 4.1	24.9 ± 0.29	1.14 ± 0.01	96.4	46.5 ± 0.54	1.01 ± 0.01	46.0 ± 0.77	12.7 ± 2.7	76.3 ± 16
4000	0.055	152 ± 1.1	74.8 ± 0.54	0.482 ± 0.00	89.8	145 ± 1.1	2.07 ± 0.02	69.9 ± 0.79	16.4 ± 1.3	98.2 ± 7.7
6000	0.091	32.0 ± 0.13	17.1 ± 0.08	0.057 ± 0.00	48.7	31.8 ± 0.15	2.98 ± 0.01	10.7 ± 0.07	16.6 ± 0.40	99.5 ± 2.3
9000	**0.110**	**21.5 ± 0.28**	**7.15 ± 0.10**	**0.025 ± 0.00**	**31.7**	**13.2 ± 0.19**	**2.81 ± 0.04**	**4.70 ± 0.09**	**14.7 ± 0.54**	**88.5 ± 3.1**
9001	**1.000**	**18.1 ± 0.03**	**4.63 ± 0.00**	**0.007 ± 0.00**	**8.71**	**8.52 ± 0.00**	**2.48 ± 0.00**	**3.44 ± 0.01**	**16.6 ± 0.03**	**99.0 ± 0.2**
Integrated		34.4 ± 0.05	7.31 ± 0.01	0.064 ± 0.00	53.1	13.5 ± 0.02	2.44 ± 0.00	5.54 ± 0.01	16.2 ± 0.08	96.9 ± 0.6

ML-East Skarn Ridge, Skarn Scapolite #1D

Weighted average of J from standards = 3.411e-03 ± 1.051e-05

Laser Power (mW)	^{39}Ar Cumulative	$^{40}Ar/^{39}Ar$ Measured	$^{37}Ar/^{39}Ar$ Measured	$^{36}Ar/^{39}Ar$ Measured	^{40}Ar % Atm.	Ca/K	Cl/K	Ca/Cl	$^{40*}Ar/^{39}K$	Age (Ma)
300	0.047	90.0 ± 0.59	1.89 ± 0.02	0.297 ± 0.00	97.3	3.47 ± 0.03	0.034 ± 0.00	103 ± 1.76	2.46 ± 0.74	15.1 ± 4.5
700	0.073	133 ± 1.1	2.14 ± 0.02	0.442 ± 0.00	97.8	3.93 ± 0.04	0.108 ± 0.00	36.3 ± 0.49	2.93 ± 0.92	18.0 ± 5.6
1100	0.089	207 ± 3.0	3.31 ± 0.06	0.693 ± 0.01	98.6	6.08 ± 0.11	0.251 ± 0.00	24.3 ± 0.59	2.88 ± 2.3	17.6 ± 14
1600	0.102	221 ± 3.8	6.44 ± 0.12	0.738 ± 0.01	98.6	11.9 ± 0.23	0.560 ± 0.01	21.2 ± 0.56	3.11 ± 2.6	19.0 ± 16
2000	0.113	240 ± 4.4	9.92 ± 0.19	0.796 ± 0.02	97.5	18.3 ± 0.35	0.781 ± 0.02	23.5 ± 0.64	5.97 ± 3.3	36.4 ± 20
3000	0.126	243 ± 4.6	23.9 ± 0.46	0.807 ± 0.02	97.1	44.7 ± 0.88	1.16 ± 0.02	38.4 ± 1.05	7.11 ± 3.4	43.2 ± 21
4000	0.140	92.8 ± 1.4	42.4 ± 0.64	0.278 ± 0.01	84.8	80.1 ± 1.2	2.16 ± 0.03	37.1 ± 0.80	14.5 ± 1.5	87.1 ± 8.6
6000	0.271	26.1 ± 0.11	11.9 ± 0.05	0.040 ± 0.00	41.4	22.1 ± 0.10	2.60 ± 0.01	8.50 ± 0.05	15.4 ± 0.19	92.4 ± 1.1
9000	**0.612**	**17.0 ± 0.18**	**5.13 ± 0.06**	**0.005 ± 0.00**	**7.07**	**9.45 ± 0.11**	**2.46 ± 0.03**	**3.84 ± 0.06**	**15.8 ± 0.18**	**94.8 ± 1.1**
9001	**0.742**	**20.9 ± 0.24**	**5.66 ± 0.05**	**0.018 ± 0.00**	**23.3**	**10.4 ± 0.10**	**2.75 ± 0.03**	**3.80 ± 0.05**	**16.0 ± 0.28**	**96.1 ± 1.7**
9002	**1.000**	**17.0 ± 0.19**	**4.45 ± 0.05**	**0.005 ± 0.00**	**7.24**	**8.19 ± 0.09**	**2.53 ± 0.03**	**3.24 ± 0.05**	**15.8 ± 0.21**	**94.7 ± 1.2**
Integrated		37.4 ± 0.15	6.53 ± 0.03	0.080 ± 0.00	62.1	12.0 ± 0.06	2.26 ± 0.01	5.33 ± 0.04	14.2 ± 0.13	85.4 ± 0.8

ML-East Skarn Ridge, Skarn Scapolite #1E

Weighted average of J from standards = 3.411e-03 ± 1.051e-05

Laser Power (mW)	^{39}Ar Cumulative	$^{40}Ar/^{39}Ar$ Measured	$^{37}Ar/^{39}Ar$ Measured	$^{36}Ar/^{39}Ar$ Measured	^{40}Ar % Atm.	Ca/K	Cl/K	Ca/Cl	$^{40*}Ar/^{39}K$	Age (Ma)
300	0.038	444 ± 7.7	9.54 ± 0.17	1.49 ± 0.03	99.1	17.6 ± 0.32	0.163 ± 0.00	108 ± 3.16	3.91 ± 3.9	23.9 ± 24
700	0.071	350 ± 8.4	7.69 ± 0.19	1.17 ± 0.03	98.9	14.2 ± 0.35	0.375 ± 0.01	37.8 ± 1.33	4.00 ± 5.3	24.5 ± 32
1100	0.099	339 ± 4.7	7.99 ± 0.14	1.17 ± 0.02	102	14.7 ± 0.26	0.630 ± 0.01	23.4 ± 0.55	-7.46 ± 5.2	-46.5 ± 33
1600	0.137	393 ± 6.0	8.77 ± 0.15	1.32 ± 0.03	99.1	16.2 ± 0.29	0.935 ± 0.01	17.3 ± 0.41	3.36 ± 4.9	20.6 ± 30
2000	0.176	285 ± 4.6	12.6 ± 0.22	0.962 ± 0.02	99.2	23.3 ± 0.40	0.991 ± 0.02	23.5 ± 0.57	2.32 ± 3.0	14.2 ± 18
3000	0.233	256 ± 2.7	24.6 ± 0.27	0.831 ± 0.01	95.2	45.9 ± 0.52	1.74 ± 0.02	26.5 ± 0.41	12.6 ± 3.1	76.0 ± 18
4000	0.302	76.2 ± 0.79	25.3 ± 0.27	0.209 ± 0.00	78.5	47.4 ± 0.52	2.44 ± 0.03	19.4 ± 0.29	16.7 ± 1.3	99.7 ± 7.8
6000	0.420	42.7 ± 0.23	11.5 ± 0.07	0.094 ± 0.00	62.6	21.4 ± 0.13	2.93 ± 0.02	7.29 ± 0.06	16.1 ± 0.85	96.4 ± 5.0
9000	**0.467**	**26.9 ± 0.63**	**6.02 ± 0.16**	**0.038 ± 0.00**	**39.9**	**12.6 ± 0.30**	**2.87 ± 0.06**	**4.38 ± 0.14**	**16.3 ± 1.4**	**97.4 ± 7.9**
9001	**0.733**	**20.1 ± 0.09**	**4.69 ± 0.02**	**0.016 ± 0.00**	**22.1**	**8.63 ± 0.04**	**2.77 ± 0.01**	**3.12 ± 0.02**	**15.7 ± 0.52**	**94.0 ± 3.0**
9002	**1.000**	**19.4 ± 0.09**	**4.45 ± 0.02**	**0.013 ± 0.00**	**17.8**	**8.19 ± 0.05**	**2.71 ± 0.01**	**3.03 ± 0.02**	**16.0 ± 0.55**	**95.9 ± 3.3**
Integrated		101 ± 0.27	8.96 ± 0.03	0.299 ± 0.00	86.9	16.5 ± 0.05	2.32 ± 0.01	7.14 ± 0.03	13.3 ± 0.46	79.8 ± 2.8

ML-005-28.20, Skarn Scapolite #2

Weighted average of J from standards = 4.016e-03 ± 1.200e-05

Laser Power (mW)	^{39}Ar Cumulative	$^{40}Ar/^{39}Ar$ Measured	$^{37}Ar/^{39}Ar$ Measured	$^{36}Ar/^{39}Ar$ Measured	^{40}Ar % Atm.	Ca/K	Cl/K	$^{40*}Ar/^{39}K$	Age (Ma)
300	0.004	1380 ± 9.4	19.2 ± 0.14	4.72 ± 0.04	101	35.8 ± 0.27	0.707 ± 0.01	-14.6 ± 6.1	-109.1 ± 47
500	0.010	268 ± 2.4	29.1 ± 0.26	0.886 ± 0.01	96.9	54.5 ± 0.50	0.613 ± 0.01	8.34 ± 1.9	59.5 ± 14
750	0.020	70.4 ± 0.55	56.2 ± 0.40	0.217 ± 0.00	84.5	107 ± 0.79	0.913 ± 0.01	11.4 ± 0.97	80.7 ± 6.7
1000	0.033	38.8 ± 0.35	86.6 ± 0.73	0.113 ± 0.00	67.6	169 ± 1.52	1.41 ± 0.01	13.4 ± 0.93	94.3 ± 6.4
1500	0.070	24.5 ± 0.18	8.96 ± 0.06	0.039 ± 0.00	43.9	16.5 ± 0.11	1.89 ± 0.01	13.8 ± 0.40	97.6 ± 2.8
2000	0.111	23.9 ± 0.19	5.18 ± 0.04	0.036 ± 0.00	42.3	9.54 ± 0.06	2.36 ± 0.02	13.8 ± 0.30	97.6 ± 2.1
2500	0.266	19.7 ± 0.08	5.53 ± 0.03	0.021 ± 0.00	28.8	10.2 ± 0.05	2.48 ± 0.01	14.0 ± 0.11	98.9 ± 0.8
3000	0.398	17.2 ± 0.11	5.18 ± 0.03	0.013 ± 0.00	20.2	9.55 ± 0.05	2.52 ± 0.02	13.7 ± 0.13	96.8 ± 0.9
5000	0.960	16.1 ± 0.10	5.27 ± 0.05	0.010 ± 0.00	15.1	9.70 ± 0.10	2.42 ± 0.01	13.7 ± 0.09	96.5 ± 0.7
9000	0.990	17.5 ± 0.13	5.34 ± 0.03	0.013 ± 0.00	19.4	9.83 ± 0.06	2.33 ± 0.02	14.2 ± 0.36	99.7 ± 2.5
9001	1.000	16.4 ± 0.09	3.40 ± 0.04	0.005 ± 0.00	7.38	6.26 ± 0.07	1.11 ± 0.01	15.2 ± 0.96	106.7 ± 6.6
Integrated		25.0 ± 0.09	7.27 ± 0.03	0.041 ± 0.00	45.7	13.4 ± 0.06	2.36 ± 0.01	13.6 ± 0.07	96.0 ± 0.6

ML-023-16.50, Skarn Scapolite #3

Weighted average of J from standards = 4.016e-03 ± 1.200e-05

Laser Power (mW)	^{39}Ar Cumulative	$^{40}Ar/^{39}Ar$ Measured	$^{37}Ar/^{39}Ar$ Measured	$^{36}Ar/^{39}Ar$ Measured	^{40}Ar % Atm.	Ca/K	Cl/K	$^{40*}Ar/^{39}K$	Age (Ma)
300	0.017	1039 ± 7.8	27.9 ± 0.24	3.60 ± 0.032	102	52.3 ± 0.45	0.741 ± 0.01	-22.8 ± 5.8	-173.3 ± 46
500	0.034	272 ± 2.3	59.2 ± 0.49	0.892 ± 0.008	95.1	113 ± 0.97	1.12 ± 0.01	13.8 ± 2.0	97.1 ± 14
750	0.072	72.7 ± 0.68	35.3 ± 0.32	0.211 ± 0.003	81.7	66.5 ± 0.62	2.50 ± 0.02	13.7 ± 0.87	96.5 ± 6.0
1000	0.139	37.8 ± 0.35	12.2 ± 0.12	0.083 ± 0.001	62.6	22.6 ± 0.22	3.21 ± 0.03	14.3 ± 0.40	100.6 ± 2.7
1500	0.355	24.6 ± 0.16	7.72 ± 0.05	0.038 ± 0.000	42.8	14.2 ± 0.09	3.31 ± 0.02	14.2 ± 0.18	99.8 ± 1.3
2000	0.594	20.7 ± 0.12	5.97 ± 0.04	0.024 ± 0.000	31.9	11.0 ± 0.07	3.39 ± 0.02	14.1 ± 0.13	99.5 ± 0.9
2500	0.627	29.8 ± 0.25	4.87 ± 0.04	0.053 ± 0.003	51.3	8.96 ± 0.07	3.37 ± 0.03	14.6 ± 0.79	102.5 ± 5.4
3000	0.655	31.4 ± 0.21	4.93 ± 0.03	0.058 ± 0.002	53.4	9.07 ± 0.06	3.38 ± 0.02	14.6 ± 0.73	103.1 ± 5.0
5000	0.961	22.4 ± 0.09	5.23 ± 0.02	0.029 ± 0.000	36.0	9.63 ± 0.04	3.31 ± 0.01	14.4 ± 0.12	101.2 ± 0.9
9000	0.996	20.8 ± 0.14	5.16 ± 0.04	0.021 ± 0.002	27.7	9.50 ± 0.08	3.33 ± 0.03	15.0 ± 0.70	105.8 ± 4.8
9001	1.000	38.0 ± 0.76	5.89 ± 0.15	0.077 ± 0.018	59.1	10.9 ± 0.27	3.37 ± 0.07	15.6 ± 5.4	109.6 ± 37
Integrated		47.6 ± 0.11	8.91 ± 0.02	0.12 ± 0.000	71.5	16.5 ± 0.04	3.22 ± 0.01	13.6 ± 0.14	96.2 ± 1.0

ML-019-70.10, Skarn Hornblende

Weighted average of J from standards = 4.016e-03 ± 1.200e-05

Laser Power (mW)	^{39}Ar Cumulative	$^{40}Ar/^{39}Ar$ Measured	$^{37}Ar/^{39}Ar$ Measured	$^{36}Ar/^{39}Ar$ Measured	^{40}Ar % Atm.	Ca/K	Cl/K	$^{40*}Ar/^{39}K$	Age (Ma)
500	0.016	55.0 ± 0.48	1.01 ± 0.02	0.154 ± 0.004	82.9	1.85 ± 0.03	0.105 ± 0.00	9.37 ± 1.2	66.7 ± 8.3
750	0.057	17.4 ± 0.11	1.03 ± 0.01	0.020 ± 0.001	32.8	1.90 ± 0.02	0.021 ± 0.00	11.7 ± 0.39	82.8 ± 2.7
1000	0.123	14.7 ± 0.10	0.41 ± 0.00	0.009 ± 0.001	18.7	0.747 ± 0.01	0.041 ± 0.00	11.9 ± 0.29	84.5 ± 2.0
1250	0.209	16.4 ± 0.16	1.56 ± 0.02	0.015 ± 0.001	26.1	2.86 ± 0.03	0.174 ± 0.00	12.1 ± 0.24	85.6 ± 1.6
1500	0.312	14.6 ± 0.17	3.07 ± 0.04	0.008 ± 0.000	15.4	5.65 ± 0.07	0.319 ± 0.00	12.4 ± 0.22	87.7 ± 1.5
1750	0.411	14.7 ± 0.17	3.37 ± 0.04	0.009 ± 0.001	15.3	6.20 ± 0.07	0.349 ± 0.00	12.5 ± 0.23	88.3 ± 1.6
2000	0.470	15.1 ± 0.19	3.28 ± 0.04	0.011 ± 0.001	19.7	6.04 ± 0.08	0.331 ± 0.00	12.1 ± 0.30	85.9 ± 2.1
2500	0.560	16.4 ± 0.21	3.81 ± 0.05	0.015 ± 0.001	25.9	7.01 ± 0.09	0.382 ± 0.01	12.2 ± 0.26	86.1 ± 1.8
3000	0.683	16.8 ± 0.24	4.71 ± 0.07	0.016 ± 0.001	26.0	8.68 ± 0.12	0.455 ± 0.01	12.5 ± 0.26	88.3 ± 1.8
5000	0.847	17.7 ± 0.20	4.23 ± 0.05	0.018 ± 0.000	28.2	7.78 ± 0.10	0.347 ± 0.00	12.7 ± 0.22	89.8 ± 1.5
9000	1.000	16.2 ± 0.12	2.68 ± 0.02	0.012 ± 0.000	20.8	4.93 ± 0.03	0.171 ± 0.00	12.8 ± 0.17	90.5 ± 1.2
Integrated		16.7 ± 0.06	3.09 ± 0.01	0.016 ± 0.000	26.2	5.68 ± 0.02	0.280 ± 0.00	12.4 ± 0.08	87.4 ± 0.6

ML-Rubble Lake HBL, Hornblende (Mike Lake Pluton)

Weighted average of J from standards = 4.016e-03 ± 1.200e-05

Laser Power (mW)	^{39}Ar Cumulative	$^{40}Ar/^{39}Ar$ Measured	$^{37}Ar/^{39}Ar$ Measured	$^{36}Ar/^{39}Ar$ Measured	^{40}Ar % Atm.	Ca/K	Cl/K	$^{40*}Ar/^{39}K$	Age (Ma)
500	0.004	1479 ± 25	5.03 ± 0.12	4.90 ± 0.10	98.0	9.26 ± 0.23	1.32 ± 0.03	29.9 ± 21	204.7 ± 137
750	0.009	93.0 ± 2.1	2.53 ± 0.06	0.265 ± 0.01	84.1	4.65 ± 0.11	0.567 ± 0.01	14.8 ± 4.1	104.5 ± 28
1000	0.015	40.0 ± 1.4	2.36 ± 0.06	0.100 ± 0.02	73.1	4.34 ± 0.11	0.424 ± 0.01	10.8 ± 5.0	76.4 ± 35
1250	0.022	30.1 ± 0.60	4.51 ± 0.10	0.086 ± 0.01	83.2	8.31 ± 0.19	0.269 ± 0.01	5.07 ± 2.8	36.4 ± 20
1500	0.034	27.9 ± 0.66	7.27 ± 0.20	0.049 ± 0.01	50.2	13.4 ± 0.36	0.391 ± 0.01	14.0 ± 1.8	98.4 ± 12
1750	0.088	24.3 ± 0.63	6.80 ± 0.19	0.042 ± 0.00	48.6	12.5 ± 0.34	0.524 ± 0.01	12.5 ± 0.68	88.5 ± 4.7
2000	0.244	19.1 ± 0.42	6.75 ± 0.15	0.024 ± 0.00	35.0	12.4 ± 0.28	0.505 ± 0.01	12.4 ± 0.40	87.9 ± 2.8
2500	0.638	15.4 ± 0.19	6.86 ± 0.10	0.012 ± 0.00	19.1	12.7 ± 0.19	0.505 ± 0.01	12.5 ± 0.17	88.3 ± 1.2
3000	0.901	13.9 ± 0.35	6.27 ± 0.16	0.007 ± 0.00	10.3	11.6 ± 0.30	0.534 ± 0.01	12.5 ± 0.34	88.3 ± 2.3
5000	0.948	14.6 ± 0.72	8.26 ± 0.40	0.011 ± 0.00	17.8	15.2 ± 0.74	0.427 ± 0.02	12.0 ± 0.89	85.2 ± 6.1
9000	1.000	15.2 ± 0.77	8.97 ± 0.47	0.012 ± 0.00	18.8	16.6 ± 0.87	0.391 ± 0.02	12.4 ± 0.82	87.4 ± 5.6
Integrated		23.2 ± 0.20	6.80 ± 0.07	0.038 ± 0.00	46.3	12.5 ± 0.13	0.504 ± 0.01	12.5 ± 0.18	88.3 ± 1.3

ML-Rubble Lake BIO, Biotite (Mike Lake Pluton)

Weighted average of J from standards = 4.016e-03 ± 1.200e-05

Laser Power (mW)	^{39}Ar Cumulative	$^{40}Ar/^{39}Ar$ Measured	$^{37}Ar/^{39}Ar$ Measured	$^{36}Ar/^{39}Ar$ Measured	^{40}Ar % Atm.	Ca/K	Cl/K	$^{40*}Ar/^{39}K$	Age (Ma)
300	0.001	44.4 ± 6.3	-0.429 ± 0.40	-0.019 ± 0.25	-12.4	-0.786 ± 0.73	0.037 ± 0.03	49.8 ± 73	329.1 ± 441
600	0.003	34.8 ± 2.1	-0.048 ± 0.12	0.035 ± 0.07	29.7	-0.088 ± 0.23	0.081 ± 0.01	24.5 ± 19	169.2 ± 128
900	0.006	23.3 ± 0.96	0.059 ± 0.07	-0.019 ± 0.04	-24.2	0.107 ± 0.13	0.075 ± 0.01	28.9 ± 11	198.0 ± 69
1200	0.017	18.4 ± 0.24	-0.008 ± 0.02	0.017 ± 0.01	27.4	-0.016 ± 0.04	0.083 ± 0.00	13.4 ± 3.1	94.3 ± 21
1500	0.054	13.9 ± 0.11	0.012 ± 0.01	0.006 ± 0.00	12.2	0.022 ± 0.01	0.083 ± 0.00	12.2 ± 1.1	86.1 ± 7.3
2000	0.151	13.3 ± 0.09	0.004 ± 0.00	0.002 ± 0.00	3.69	0.007 ± 0.01	0.082 ± 0.00	12.7 ± 0.38	90.1 ± 2.6
2500	0.245	13.1 ± 0.08	0.003 ± 0.00	0.003 ± 0.00	6.44	0.006 ± 0.00	0.082 ± 0.00	12.3 ± 0.44	86.8 ± 3.0
3000	0.321	13.1 ± 0.10	0.006 ± 0.00	0.002 ± 0.00	3.51	0.011 ± 0.01	0.081 ± 0.00	12.6 ± 0.48	89.4 ± 3.3
5000	0.888	13.2 ± 0.10	0.044 ± 0.00	0.002 ± 0.00	4.07	0.080 ± 0.00	0.082 ± 0.00	12.7 ± 0.12	89.4 ± 0.9
9000	1.000	13.2 ± 0.09	0.013 ± 0.00	0.002 ± 0.00	4.90	0.023 ± 0.00	0.079 ± 0.00	12.6 ± 0.28	88.9 ± 2.0
Integrated		13.4 ± 0.06	0.027 ± 0.00	0.002 ± 0.00	4.91	0.050 ± 0.00	0.081 ± 0.00	12.7 ± 0.13	89.8 ± 1.0

ML-015-31.40, Biotite #1 (Mafic Sill)

Weighted average of J from standards = 4.016e-03 ± 1.200e-05

Laser Power (mW)	^{39}Ar Cumulative	$^{40}Ar/^{39}Ar$ Measured	$^{37}Ar/^{39}Ar$ Measured	$^{36}Ar/^{39}Ar$ Measured	^{40}Ar % Atm.	Ca/K	Cl/K	$^{40*}Ar/^{39}K$	Age (Ma)
300	0.005	59.4 ± 0.82	0.169 ± 0.02	0.156 ± 0.01	77.8	0.310 ± 0.03	0.084 ± 0.00	13.2 ± 3.5	93.2 ± 24
600	0.026	40.1 ± 0.33	0.141 ± 0.00	0.033 ± 0.00	24.0	0.259 ± 0.01	0.067 ± 0.00	30.4 ± 0.85	207.9 ± 5.5
900	0.071	37.4 ± 0.37	0.085 ± 0.00	0.012 ± 0.00	9.58	0.155 ± 0.00	0.060 ± 0.00	33.8 ± 0.50	229.6 ± 3.2
1200	0.135	34.5 ± 0.34	0.100 ± 0.00	0.008 ± 0.00	6.55	0.183 ± 0.00	0.061 ± 0.00	32.2 ± 0.41	219.3 ± 2.7
1500	0.210	32.8 ± 0.26	0.201 ± 0.00	0.007 ± 0.00	5.82	0.370 ± 0.00	0.071 ± 0.00	30.9 ± 0.35	210.8 ± 2.3
2000	0.336	30.2 ± 0.35	0.600 ± 0.01	0.005 ± 0.00	4.45	1.101 ± 0.01	0.095 ± 0.00	28.8 ± 0.36	197.8 ± 2.4
2500	0.476	30.8 ± 0.17	0.166 ± 0.00	0.004 ± 0.00	3.54	0.305 ± 0.00	0.075 ± 0.00	29.7 ± 0.21	203.3 ± 1.4
3000	0.587	34.5 ± 0.28	0.202 ± 0.00	0.004 ± 0.00	3.16	0.371 ± 0.00	0.059 ± 0.00	33.4 ± 0.32	226.9 ± 2.1
5000	0.877	35.8 ± 0.19	0.193 ± 0.00	0.005 ± 0.00	3.82	0.355 ± 0.00	0.060 ± 0.00	34.4 ± 0.20	233.7 ± 1.3
9000	1.000	43.4 ± 0.24	0.196 ± 0.00	0.004 ± 0.00	2.70	0.360 ± 0.00	0.034 ± 0.00	42.2 ± 0.28	282.4 ± 1.7
Integrated		35.2 ± 0.09	0.231 ± 0.00	0.006 ± 0.00	5.30	0.423 ± 0.00	0.064 ± 0.00	33.3 ± 0.11	226.3 ± 0.9

ML-015-31.40, Biotite #2 (Mafic Sill)

Weighted average of J from standards = 4.016e-03 ± 1.200e-05

Laser Power (mW)	^{39}Ar Cumulative	$^{40}Ar/^{39}Ar$ Measured	$^{37}Ar/^{39}Ar$ Measured	$^{36}Ar/^{39}Ar$ Measured	^{40}Ar % Atm.	Ca/K	Cl/K	$^{40*}Ar/^{39}K$	Age (Ma)
600	0.112	48.6 ± 0.41	0.015 ± 0.00	0.017 ± 0.00	10.5	0.027 ± 0.01	0.039 ± 0.00	43.4 ± 0.47	290.1 ± 2.9
1000	0.310	37.4 ± 0.31	0.009 ± 0.00	0.004 ± 0.00	3.15	0.017 ± 0.00	0.041 ± 0.00	36.2 ± 0.35	244.6 ± 2.2
1500	0.547	34.6 ± 0.26	0.022 ± 0.00	0.003 ± 0.00	2.65	0.041 ± 0.00	0.046 ± 0.00	33.6 ± 0.28	228.5 ± 1.8
2000	0.742	36.4 ± 0.28	0.040 ± 0.00	0.004 ± 0.00	3.04	0.073 ± 0.00	0.029 ± 0.00	35.3 ± 0.32	239.1 ± 2.0
2500	0.849	37.4 ± 0.27	0.059 ± 0.00	0.004 ± 0.00	3.16	0.109 ± 0.01	0.021 ± 0.00	36.2 ± 0.40	244.7 ± 2.5
3000	0.915	42.8 ± 0.26	0.057 ± 0.01	0.006 ± 0.00	4.31	0.104 ± 0.01	0.015 ± 0.00	40.9 ± 0.51	274.6 ± 3.2
5000	0.981	41.8 ± 0.35	0.045 ± 0.01	0.007 ± 0.00	4.94	0.083 ± 0.01	0.014 ± 0.00	39.7 ± 0.54	267.1 ± 3.4
9000	1.000	37.1 ± 0.38	0.051 ± 0.02	0.007 ± 0.01	5.56	0.094 ± 0.04	0.016 ± 0.00	35.0 ± 1.7	237.6 ± 11
Integrated		38.4 ± 0.12	0.031 ± 0.00	0.006 ± 0.00	4.32	0.056 ± 0.00	0.034 ± 0.00	36.7 ± 0.15	248.3 ± 1.2

8. Discussion and Conclusions

In this study I have presented a wide variety of geologic, isotopic, compositional, mineralogical and mineral compositional data. In this final section I attempt to pull all the various strings together into a coherent interpretation of the ore body's origin.

The Skarn Ridge Au-Cu skarn formed in response to a number of geological events that took place between 248 and 88 Ma. A combination of reactive (and unreactive) host rocks, structural and stratigraphic conduits, and a downdip fluid source with the right timing and composition all contributed to the formation of this deposit.

Contrasting compositional layers of Paleozoic strata and the emplacement of mafic sills during the Triassic (248 to 202 Ma) formed part of the plumbing system for future hydrothermal fluids (Figure 8.1 A). Regional thrusting during the Mesozoic (Jurassic to early Cretaceous?) caused local folding and tilting of the stratigraphic package and ultimately resulted in the limestone-capped dip-slope that would become Skarn Ridge.

Hydrothermal scapolite records the first signs of hydrothermal activity, between 100 and 97 Ma (Figure 8.1 B). Based on zoning patterns from clinopyroxene and gold and copper endowment, the fluids came from the subsurface south or southeast of Skarn Ridge from an unidentified plutonic source. Bounded by the (then) marble-black hornfels contact below, and a relatively unreactive lithology (mafic sill) above (?), upward-moving fluids consumed marble and calc-silicate hornfels to make skarn. Within the marble, mafic sills acted as secondary conduits and fluid partitions, forcing fluids to

pool and travel upward along the lower sill contact. At the top of skarn ridge where the upper sill pinches out, unconfined fluids spread out and deposited the bulk of the ore (Figure 8.1 A). Coincidentally (?), the remaining metasomatic fluid components equilibrated with the host rock here at the location of the observed marble front.

Shortly (within a few Ma) after skarn formation the green dikes intruded (Figure 8.1 B). The intrusion of felsic porphyritic dikes occurred not long afterward (again, within a few Ma). Both types of dikes cut across skarn, mineralization, and mafic sills (Figure 8.2 A). Even without radiometric ages, their lower-temperature alteration, lack of mineralization, and cross-cutting relationships indicate their post-ore timing. Although potential conduits for broadly skarn-related retrograde alteration, I have seen no evidence that the dikes acted as such. Given the likely 0.5 Ma lifetime for a plutonic hydrothermal system (Cathles, 1981), the dikes intruded more than 0.5 Ma after skarn formation.

Possibly contemporaneous with porphyry dike intrusion, an apparently new hydrothermal fluid pulse introduced 'axinite alteration' as an overprint on the existing skarn and all the igneous rocks on Skarn Ridge. The fluid had both 'metasomatic' and 'retrograde' effects that resulted in the commonly observed assemblage of axinite (newly introduced) ± arsenopyrite ± scheelite (possibly remobilized) ± calcite ± amphibole (retrograde from existing skarn). I have seen absolutely no evidence for boron minerals present with prograde alteration assemblages at Mike Lake; arsenopyrite is most likely a 'main stage skarn' mineral and timing of original scheelite deposition is not clear. In other words, this later fluid pulse certainly introduced boron, and may have introduced

new tungsten and arsenic as well. XRF analyses of Skarn Ridge axinite show it contains approximately 500 ppm Sn (Chapter 3). As with other components, this Sn probably—but not necessarily—was introduced with the boron. I lack sufficient Sn analyses (exclusively my own XRF data on selected Mike Lake samples) to draw any definitive conclusions. Worldwide, however, the B-Sn-W (±As) hydrothermal suite is common (Lehmann, 1990).

The likely minimum age for this younger alteration is 91-92 Ma (Figure 8.2 A), based on $^{40}Ar/^{39}Ar$ dating of skarn amphibole (Chapter 7). The amphibole I dated did not necessarily form with the axinite alteration, but its age is so much younger than that of the skarn scapolite that it must represent either a much younger event, or re-heating by a much younger event. The axinite (± W-As-Sn) assemblage fits the bill for either.

Biotite and hornblende $^{40}Ar/^{39}Ar$ ages from the Mike Lake pluton (approximately 89 ± 1 and 88 ± 1, respectively) record the time when those minerals cooled to temperatures of approximately 300- 500°C. The slightly younger cooling age for the hornblende likely reflects argon loss during its partial chloritization (Chapter 7). These ages, coupled with the lack of high temperature (secondary biotite or endoskarn) alteration, lack of significant mineralization (although anomalous in As), and lack of late axinite alteration, indicate that this pluton is the youngest intrusion in the local area (Figure 8.2 B). Based on arsenic anomalies (Table 3.2) and weak chlorite alteration of the magmatic biotite, some hydrothermal activity was associated with this intrusion; the

effect of this on Skarn Ridge may have been additional (minor) retrograde alteration and arsenopyrite deposition, indistinguishable from earlier retrograde alteration.

At least one normal fault (SAM's Fault) post-dates skarn formation and mineralization on Skarn Ridge (Figure 8.2 B). It is not known to what extent this structure plays a role in local ore remobilization (if any), or if additional structures of this orientation exist on Skarn Ridge. However (based on cross-cutting relationships), this fault represents the youngest phase of deformation in the study area.

Major remaining questions concerning the Mike Lake skarn involve the responsible pluton: Where is it? What is it? What magmatic suite does it belong to? These are not strictly academic questions, as other (additional) gold-bearing skarns are to be expected where carbonate rocks are present roughly 0.5-1.5 kilometers from this body. The 97-100 Ma ages for hydrothermal scapolite from Skarn Ridge barely fit into the age range for 'Mayo Suite' intrusions, but the deposit is approximately 75 km west of the 'official' west edge of this suite (Figures 2.2 and 2.3). The scapolite ages are far too old for an association with the Tombstone suite—although the Mike Lake pluton is conventionally considered part of this suite, presumably due to the Cu-Au-Bi association elsewhere seen in the Tombstone area (Hart, 2004). Further, the compositions of the known plutonic rocks do not fall neatly into either the Mayo (mostly granite-granodiorite) or Tombstone (mostly quartz-poor to quartz-absent rocks). Nor does the association B-Sn-W-As seem at all characteristic of either suite. In other words, the two apparently independent, hydrothermal systems present at Skarn Ridge are not easily related to any of

the known mid-Cretaceous plutonic suites in the Yukon. Either the concept of plutonic suites needs expanding or the notion and distribution—as currently expounded (e.g., Hart et al., 2004) is too simplistic.

The geological setting of the Skarn Ridge deposit provides an ideal opportunity to review exploration strategies for this and similar targets. Foremost, the importance of understanding the zoning and igneous relationships of any skarn system cannot be underemphasized. In the case of Skarn Ridge, the early assumption that the skarn was zoned with respect to the Mike Lake pluton led to a faulty exploration strategy. I suspect this happens frequently. A good example is that of the MacTung Deposit, NWT, where the skarn is not zoned away from the adjacent 'Tungsten Suite' intrusion, but instead sits above a pluton still only known from dikes (Atkinson and Baker, 1986). At the Nixon Fork (Newberry et al., 2010) and Buckhorn (Deal et al., 2012) skarn deposits the skarns are similarly not zoned with respect to the major adjacent plutons, but rather appear to originate from deeper, 'hidden' plutons under the skarns. That is: the adjacent pluton is often not the source pluton.

Building on the zoning concepts, it is equally important to determine the ore controls so that an effective model can be developed and used to find more ore. Simply 'grid drilling' the general vicinity of a deposit (as employed at Skarn Ridge) seems an especially wasteful means of blocking out a skarn deposit. Additional exploration strategies such as airborne geophysics can be useful, but only where distribution of minerals responsible for geophysical anomalies is understood. In the case of Skarn

Ridge, although pyrrhotite is broadly skarn-associated, magnetic pyrrhotite (the lower temperature polymorph) has a completely unknown distribution.

In sum, the Mike Lake (Skarn Ridge) skarn is a small, yet important, Au-Cu deposit. Its importance lies in the fact that it is small enough and yet contains a high enough density of drilling that it can be used to better understand larger and more complex skarn systems. Additionally, it has suffered little from post-ore deformation and has experienced essentially no weathering. Finally, the virtual absence of retrograde alteration provides a unique opportunity to examine metal- and silicate- zoning patterns associated with prograde alteration alone. That said, lessons one can take from the Mike Lake skarn include: (a) an intrusion near a skarn is not necessarily responsible for it, (b) significant gold deposition can take place in skarns without significant retrograde alteration, (c) mineral compositional and metal endowment zoning can be useful tools for deciphering skarns even where the hosts are not predominantly marble, and (d) multiple skarn-forming events caused by multiple intrusions in the same general area apparently happen.

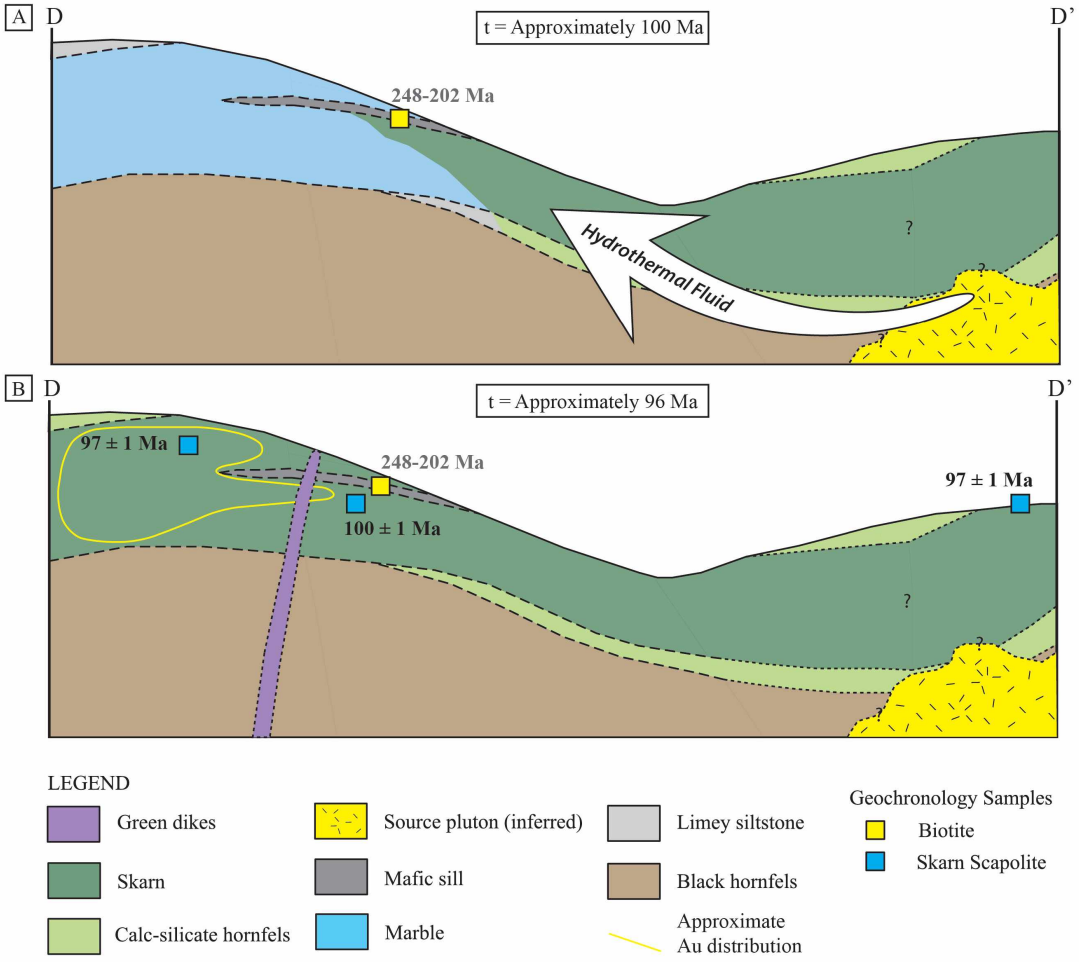

Figure 8.1. Time-slice of Skarn Ridge ore body formation from 100-96 Ma.
A: Inferred source pluton produces hydrothermal fluids that move updip, consuming marble (Rabbitkettle Formation) to make skarn. Mafic sills in the stratigraphic package form a barrier to upward fluid flow and direct fluids towards the top of Skarn Ridge. Almost certainly prograde skarn formation took place over a geologically short time (< 1 Ma). B: Based on scapolite radiometric ages, prograde skarn formation could have taken place as early as 100 Ma and was certainly completed by 96 Ma. Intrusion of green dikes occurred shortly after prograde skarn formation. For master geology legend, see Figure 3.1.

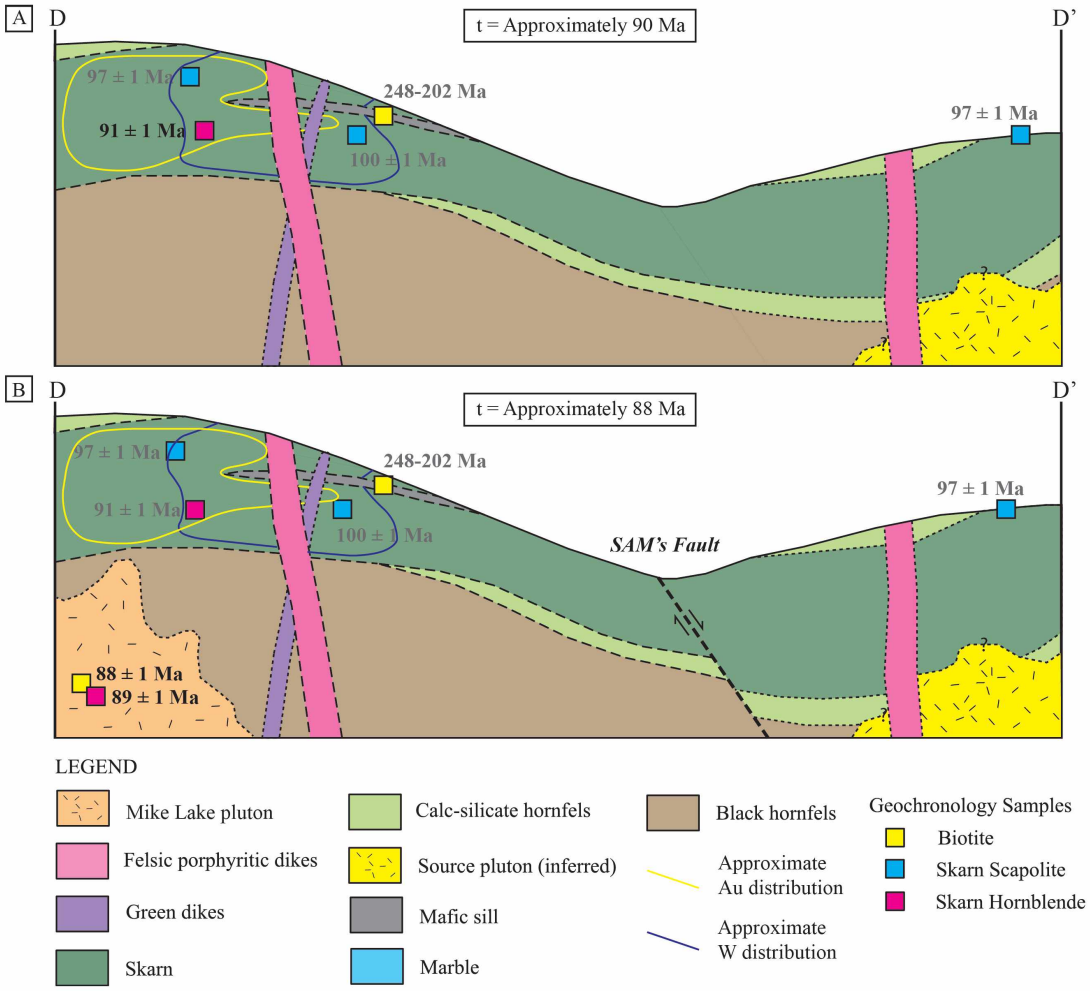

Figure 8.2. Time-slice of Skarn Ridge ore body formation from 90-88 Ma.
A: Pre-Mike Lake pluton intrusions include mafic sills, green dikes, felsic porphyritic dikes, and the inferred source pluton; gold, copper, and tungsten mineralization also pre-date the Mike Lake pluton. B: Intrusion of Mike Lake pluton at 88-89 Ma and motion along SAM's fault are the most recent geological events on Skarn Ridge. For master geology legend, see Figure 3.1.

8.1. References

Atkinson, D., and Baker, D.J., 1986, Recent developments in the geologic understanding of Mactung in J.A. Morin, ed., Mineral deposits of northern Cordillera, CIM Special Volume 37, p. 234–244.

Cathles, L.M., 1981, Fluid flow and genesis of hydrothermal ore deposits: Economic Geology 75th Anniversary Volume, p. 424-457.

Deal, M.L., Newberry, R.J., Willard, R., Ellis, J., and Cooper, P., 2012, Zoning and origins of the Buckhorn gold skarn deposit, northeast Washington: 2012 Arctic International Mining Symposium, Fairbanks Alaska, Abstracts with Program, p. 10-11.

Hart, C.J.R., 2004, Mid-Cretaceous magmatic evolution and intrusion-related metallogeny of the Tintina Gold Province, Yukon and Alaska: Unpublished Ph.D. thesis, Perth, Australia, The University of Western Australia, 198 p.

Hart, C.J.R., Goldfarb, R.J., Lewis, L.L., and Mair, J.L., 2004, The Northern Cordilleran mid-Cretaceous Plutonic Province: Ilmenite/magnetite-series granitoids and intrusion-related mineralization, Resource Geology, v. 54, p. 253-280.

Lehmann, B., 1990, Metallogeny of Tin, Lecture Notes in Earth Sciences, v. 32: Heidelberg, Springer-Verlag, 211 p.

Newberry, R.J., Mrozek, S.A., Perttu, B.K., Broman, B., Wagner, K., and Lessard, R., 2010, Yet still ANOTHER look at the Nixon Fork Au-Cu-Ag Skarn, SW Alaska: Alaska Miners Association Spring Meeting, Abstracts with Program, p. 12-15.